Offshore Power System Micro-Grid Design

by

Aaron M. MacNeill

Submitted in partial fulfilment of the requirements
for the degree of Doctor of Philosophy

at

Dalhousie University
Halifax, Nova Scotia
August 2017

This thesis is dedicated to Patrick Peters, who immigrated to Nova Scotia in the early 19th century pursuing a better life, who signed his name with an X.

Table of Contents

List of Tables

List of Figures

Abstract

Micro-grid based power systems will have a significant roll in the development of the modern renewable energy power grid. A subset of this distributed generation system involves offshore micro-grid systems. These offshore micro-grids will consist of offshore generation, power conversion, energy storage, underwater power transmission, grid interconnection, and the inclusion of either onshore or offshore loads.

Designing these systems is very different from conventional generation due to the intermittency of the renewable resources and the underwater power transmission. The intermittency of renewable resources can result in frequency fluctuations and times where there may not be any power generation. This effect can be mitigated through use of energy storage devices, grid interconnection, and power electronics. Underwater power transmission can also be a challenge due to the potentially large capacitance, and thus reactive power requirements of the underwater cable.

Studying the line parameters, harmonic propagation, developing simplified models, the power electronic conversion process, the inclusion of energy storage devices, modelling offshore generator clusters, and analyzing the economics of the micro-grid system to determine if AC or DC power transmission would be optimal are all elements required in the design and analysis of an offshore power system micro-grid.

List of Abbreviations and Symbols Used

AC	Alternating current
DC	Direct current
HVDC	High voltage direct current
kW	Kilo-watt
kWh	Kilo-watt hour
kV	Kilo-volt
MW	Mega-watt
GW	Giga-watt
MVA	Mega volt-ampere
MVAR	Mega volt-ampere reactive
VR	Voltage regulation
VSC	Voltage source converter
PWM	Pulse width modulation
THD	Total harmonic distortion
RMS	Root mean square
EPR	Ethylene propylene rubber
XLPE	Cross linked polyethylene
PE	Polyethylene
GMD	Geometric mean distance
GMR	Geometric mean radius
IEEE	Institute of electrical and electronics engineers
OERA	Ocean Energy Research Association

E	Energy
m	Mass
v	Velocity
ρ	Density of material
D	Turbine diameter, distance between conductors
P	Power
k, A	Weibull distribution parameters
$\bar{v}$	Mean velocity
Γ	Gamma function, propagation constant
C_p	Turbine efficiency coefficient
t	Time
ω	Angular electrical frequency
f	Electrical frequency
I	Electric current
V	Voltage
E	Electro motive force
N_s	Synchronous speed
P	Number of rotor poles
R	Resistance
L	Inductance
C	Capacitance
G	Conductance
X	Reactance

Z	Impedance
Y	Admittance
δ	Power angle, skin depth
ϕ	Power factor angle
s	Slip
N_R	Rotational speed of rotor
k_a	DC motor constant
Φ	Flux in DC motor along direct axis
ωm	Mechanical angular speed
T	Torque
r	Radius
F	Force
H	Magnetic field intensity
B	Magnetic flux density
E	Electric field
A	Magnetic potential
J	Current density
μ	Permeability
ε	Permittivity
ℓ	Length
ρ,ϕ,z	Cylindrical coordinates
x,y,z	Cartesian coordinates
j	Complex number

Z0	Characteristic impedance
Δx	Incremental line length
A,B,C,D	Two-port network parameters
S	Apparent power
Q	Reactive power
η	Efficiency
e	Relative error
k	Equivalent transmission line model parameter
A_0, A_N, B_N	Fourier coefficients
n	Harmonic number
α, δ, ε	Firing angles
C_{item}	Cost
β	Price per megawatt-hour of electricity
α	Cost per megavar reactive power
$\alpha_{AC}, \beta_{AC}, \gamma_{AC}$	AC cable cost coefficients
ψ_{DC}, σ_{DC}	DC cable cost coefficients
€	Euro
CAD	Canadian dollar
d	Distance to shore
h	Vertical length of offshore grid
w	Width of offshore grid

Acknowledgements

I would firstly like to thank Dr. El-Hawary for all of his support and guidance throughout my Graduate program.

I would like to thank Dr. William Phillips and Dr. Timothy Little for serving on my supervisory committee.

I would like to again thank Dr. El-Hawary, the ECED department, the Faculty of Engineering, and the Government of Nova Scotia for their financial support throughout this degree.

Finally, I would like to thank my family for their love and support throughout all my years as a Graduate student.

Chapter 1: Introduction

Micro-grid systems will play a large role in the future power system. This is due to the demand for renewable energy production. Many renewable energy turbines are required to replace current fossil fuel production. This necessitates a power grid with very distributed power generation. A subset of this is offshore micro-grids. This chapter provides a brief overview of offshore power generation. This offshore energy is supplied from two different varieties of natural resources, wind and marine energy. Marine energy incorporates several forms of energy. These include tidal energy, wave energy, or temperature gradient energy as examples. These two generic forms of offshore energy, and their applications in the world thus far, will be presented and discussed. This chapter concludes with the objectives and contributions of this thesis.

1.1 Offshore Wind Energy

Europe is the current world leader in offshore wind generation. Offshore wind farms first began being constructed in Denmark in 1991 [1]. Since then there have been many wind farms installed in Europe. Listed below are the world's largest offshore wind farms currently in commission as of 2016 [2,3,4,5,6].

- London Array, with a capacity of 630MW, 175 turbines, in the UK, commissioned in 2012
- Gwynt y Mor, with a capacity of 576MW, 140 turbines, in the UK, commissioned in 2015

- Greater Gabbard, with a capacity of 504MW, 140 turbines, in the UK, commissioned in 2012
- Anholt, with a capacity of 400MW, 111 turbines, in Denmark, commissioned in 2013
- Bard Offshore 1, with a capacity of 400MW, 80 turbines, in Germany, commissioned in 2013

There are many other offshore wind farms that are currently generating electricity. Figure 1-1 below is an example of an offshore wind farm, the London Array.

Figure 1-1: London Array Offshore Wind Farm [7]

Currently in North America there are no major offshore wind generation sites. The offshore wind generation technology is still in its planning and testing stages. In the world, as of 2012, there is 4.5GW of offshore wind power capacity, with another 4.7GW under

construction, and 30.4GW in the planning stages [8]. As of 2012 there was a total wind generation capacity of 283GW [8]. This includes both onshore and offshore wind generation. Offshore wind generation is a small percentage of this but is expanding. In Europe, as of 2017, there is a total of 3589 grid connected turbines installed in 81 wind farms in 10 European countries [9]. There has been a 39% increase in the offshore generation capacity from 2015 [9]. The average turbine generation capacity is 4.8MW [9]. The average water depth for the turbines is 29.2m with an average distance from shore of 43.5km [9]. Figure 1-2 and 1-3 below represents the cumulative offshore wind capacity in Europe and the average distance to shore and average water depth of all European installed, under construction, and planned offshore wind turbines respectively as of 2012.

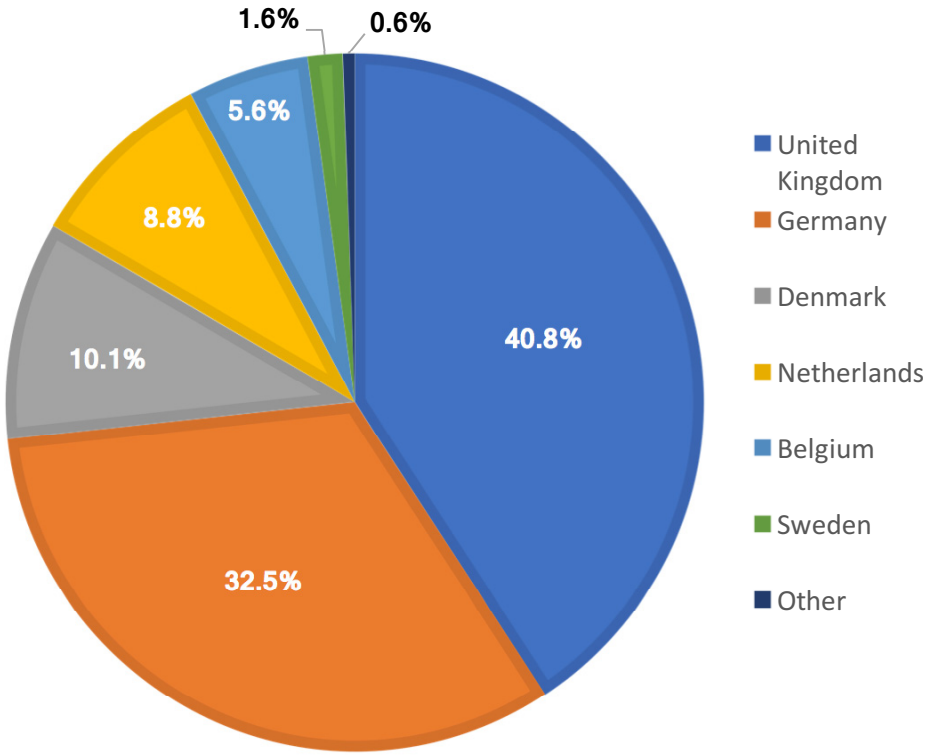

Figure 1-2: Cumulative Offshore Wind Capacity in Europe [9]

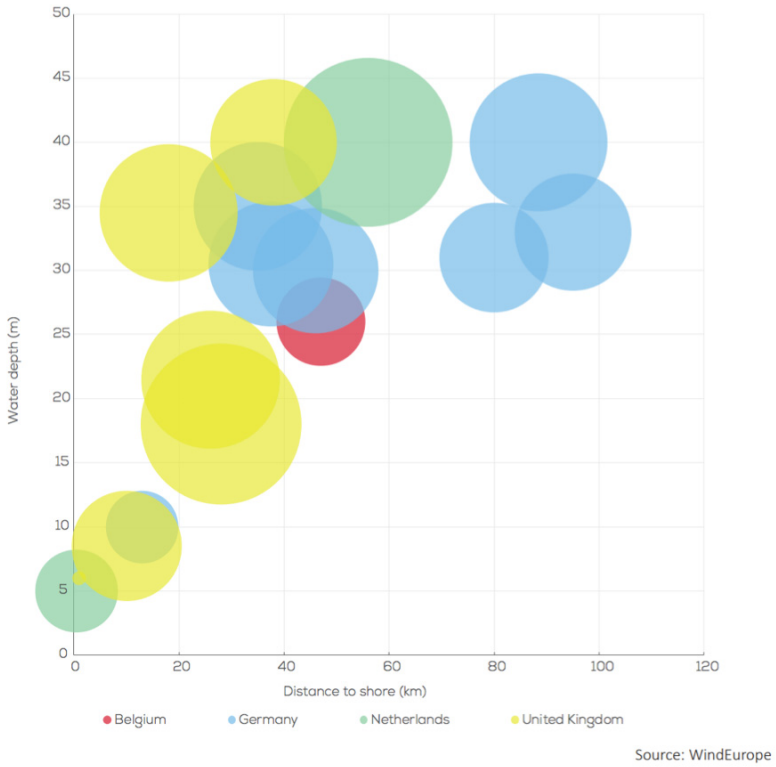

Figure 1-3: Average Water Depth and Distance to Shore of Offshore Wind Turbines [9]

As of 2015, there is currently 8GW of offshore wind generation capacity in Europe [10]. This figure is projected to triple to 23.5GW by the year 2020 [10].

There are drawbacks associated with constructing offshore wind farms. Conventional issues with wind power generation include the following [1,11]:

- Variable wind speeds
- Gear box complexity
- Geographical location
- Induction machines/variable frequency

For offshore wind farms there are additional issues, which include the following [1,11]:

- Cost of offshore construction
- Cost of offshore maintenance
- Underwater power transmission
- Weather severity
- Wildlife and visual pollution issues

Despite these difficulties, there are benefits to building offshore wind farms as opposed to onshore wind farms. The benefits include the following:

- 5-10MW turbines can be used as opposed to 1-3MW turbines. This is due to the higher wind speeds offshore [1,9]
- Wind blows more predictably offshore. This makes the wind source more reliable, providing 3000+ hours per year of power production as opposed to 2000-2300 hours per year onshore [1,11].
- A lot of high population density areas exist along the coastal regions [1].
- No visual impact [11]

1.2 Marine Energy

The two main sources of marine energy extraction are tidal currents and waves [1,12]. While there are other sources of marine energy such as ocean currents, temperature differentials, biomass, and salinity differentials, they are not currently commonly used [12]. The Bay of Fundy, in Nova Scotia, Canada, is a very promising source of tidal energy [13]. In North America, the marine power generation is still in prototype stages. In Europe, there

have been successfully grid connected marine energy generators. In Europe, as of 2013, ocean going devices have a capacity of over 10MW [14]. The largest marine power generation systems operating as of 2016 are listed below [15]:

- Sihwa Lake, South Korea, 254MW, commissioned in 2011
- Rance, France, 240MW, commissioned in 1966
- Annapolis Royal, Canada, 20MW, commissioned in 1984

The largest marine generation sites are represented by tidal barrage based generation. Wave based generation has not been constructed as of yet on a large scale. The technology is still in the research, development, and testing phases [16].

1.2.1 Tidal Energy

When discussing tidal energy, there are two main forms that must be discussed. These are the tidal streams or currents and the tidal barrage. Both of these forms of tidal energy are caused by the same tidal phenomena, however the means of extracting this energy are different.

1.2.1.1 Tidal Stream

A tidal stream turbine and generator is one that is placed in the flow path of water. This form of tidal energy extraction is analogous to wind turbines that are underwater. The first large-scale grid connected tidal stream generator was installed in Northern Ireland in April 2008. It generates 1.2MW of electricity. Figure 1-4 below is a picture of this tidal SeaGen tidal stream generator.

Figure 1-4: SeaGen Tidal Stream Turbine [17]

1.2.1.2 Tidal Barrage

A tidal barrage turbine and generator is created when the flow of tidal waters is impeded by a structure and the water is forced to cross this barrier. This energy is generated in a very similar way as in hydroelectric power plants. Figure 1-5 below shows an example of what a tidal barrage energy generation would encompass.

Figure 1-5: Tidal Barrage Power Plant in Rance, France [18]

1.2.2 Wave Energy

Wave energy is created from harnessing the up and down motion of the waves on the surface of a body of water. The waves are created primarily from the wind passing over the surface of the water. This technology is still in development and testing stages [16].

1.3 Benefits and Drawbacks

Drawbacks to generating tidal or wave power include the following:

- There is a difference in time between when the tides occur and when power demand is high. [12,13]
- Due to this difference, means of energy storage may be required. [13]

- Regions to extract tide or wave energy are in harsh environments. The harsher the tides or waves the more energy can be extracted. [19]
- Maintenance and construction issues since the installations are offshore. [8]
- Underwater power transmission. [8,12,13]
- Installations may coincide with weaker sections of the power grid. [8]
- Variable speed generators would be required. [8,12,13]
- Wildlife concerns. [13]
- Human activity such as transportation and fisheries.
- Maintenance due to the installation being in a harsh environment. [8,13]

Despite these numerous difficulties, there are benefits to using tide or wave energy as a medium of power generation. These benefits are as follows:

- Tides are predictable [13]
- Large potential generating capacity [13]
- Potential to be interconnected with offshore wind system

1.4 Thesis Objectives

The objectives of this thesis are to develop a design methodology for an offshore micro-grid power system. This involves: the analysis of underwater power transmission, the various methods of power transmission, the use of power electronics and how generated harmonics will propagate through an underwater transmission line. This thesis additionally investigates how an offshore cluster of generators will affect a small onshore power system. Energy storage techniques are reviewed and briefly discussed. A methodology to

determine economically whether AC or DC power transmission should be applied for any given offshore power installation. These components will, together, yield a design methodology that can be applied to a community that has an offshore renewable power resource.

1.5 Thesis Contribution

The contributions of this thesis include the offshore power system micro-grid design methodology framework development, the analysis of underwater power cable line parameters and their power transmission performance. This thesis also discusses the development of short and medium line models for underwater cables for use in power flow or transient analysis, as well as the analysis of how modern power electronic sources and their generated harmonics will propagate through an underwater power cable for various configurations of power conversion is analyzed. Various economic models are developed and analyzed to find the threshold distance where underwater DC power transmission is favorable over AC transmission and these economic models are used to choose an optimal cable geometry. Offshore cluster generation and the effect it has on onshore power grids is analyzed. Finally, the development and creation of models and performing numerical analysis for these models has been performed with the results and limitations being outlined.

1.6 Thesis Outline

The work in this thesis is organized as follows:

Chapter 1 presents an overview of current offshore power installations in the world and the most common forms of offshore power that are used.

Chapter 2 presents an overview of what the various offshore renewable generation profiles would be and the technology that is used to extract this power. Electrical models of these devices are detailed and their limitations of applicability.

Chapter 3 presents the analysis of underwater power cable line parameters for the various methods of underwater power transmission. These line parameters are used to observe the steady state power delivery performance of the transmission line. The resultant magnetic fields surrounding these cables are simulated. Simplified models of these cables are created and their limitations determined. These models are used to allow for simplified transient analysis and power flow analysis. Finally, the harmonic propagation for various kinds of underwater power cables have been analyzed.

Chapter 4 presents the analysis of modern power electronic devices that may be used for an offshore power installation. These devices produce harmonics, and the analysis of the harmonic propagation through underwater transmission lines is discussed. This analysis is performed for all the various power conversion topologies that may practically exist.

Chapter 5 presents an economic analysis of an offshore power system. The decision of using AC or DC power transmission is explored in detail to find at what transmission line length it is preferable to use DC transmission over AC. Several models to analyze this have

been developed. The economic models are also used to determine what geometry of cable is most economic to use.

Chapter 6 presents the analysis of an offshore cluster of generation and how this offshore generation will affect an onshore power grid. This also accounts for the inclusion of potential offshore loads. Discussion on how energy storage could be applied to a micro-grid to smooth the generation profile.

Chapter 7 presents a case study that utilized all of the tools developed in the previous chapters. This case study looks at a local offshore generation site in Nova Scotia, Canada.

Chapter 8 presents the conclusions of this thesis and provides suggestions for future work in this field of study.

Appendix A presents the various models that were used for the IEEE 14 bus simulation in Chapter 6. This chapter shows all of the models used and their corresponding equations.

Chapter 2: Review of Offshore Energy Availability and Extraction

This chapter provides an overview of the energy availability in offshore wind and marine resources, turbine configurations used to extract this energy will be summarized, and the various generators and their electrical models, which are used for renewable energy sources, will also be summarized.

2.1 Introduction

To harness offshore energy, a location must be chosen such that power can be reliably generated. Renewable energy mediums such as wind and marine are, by their nature, intermittent. A location that provides consistent high-speed air or water flow is desirable. As will be developed in subsequent sections, the power available is proportional to the density of the substance turning the turbine and to the cube of the velocity of the medium. To harness this energy a turbine is used to convert the kinetic energy of the flowing substance, water or air, into rotational mechanical energy. This rotational energy is then transformed into electrical energy through use of a generator. There are various options for turbine configurations and generator selection. These will be discussed and summarized in subsequent sections.

2.2 Energy Availability

The theoretically available energy that can be harnessed from offshore wind and marine energy sources can be determined by studying the kinetic energy passing through a given surface area. The kinetic energy is expressed as follows:

$$E = \frac{1}{2}mv^2 \tag{2.1}$$

In the case of wind and tidal energy, there is a mass flow rate. There is a certain mass of air or water passing through a given surface area every second. This mass flow rate can be defined as follows:

$$\frac{dm}{dt} = \rho\pi\left(\frac{D}{2}\right)^2 v \tag{2.2}$$

Where ρ is the density of a fluid passing through the surface area, D is the diameter of the assumed circular cross sectional area, and v is the velocity of the fluid. The available power can thus be expressed as follows:

$$P_o = \frac{1}{2}\frac{dm}{dt}v^2 \tag{2.3}$$

Substituting equation (2.2) into (2.3) results in the following equation for the theoretical power that can be extracted from offshore power installations.

$$P_o = \frac{\pi}{8}\rho D^2 v^3 \tag{2.4}$$

It can be observed that the potential output power varies by the cube of the velocity. Also worth noting is that the approximate density of air and seawater are 1.29kg/m^3 and 1020kg/m^3 respectively. Tidal streams are typically much slower than wind. If the theoretical extracted power for turbines in wind and water flow were the same, and the diameter of the cross-sectional area was the same for each, the ratio of wind speed to water speed can be determined as follows:

$$\frac{v_{wind}}{v_{water}} \cong 9.24 \tag{2.5}$$

This ratio shows what the velocity difference between the two mediums must be to achieve the same theoretical power with identical turbines. In other words, because of the density difference, the wind speed must be 9.24 times faster than the tidal stream speed to produce the same power given the same cross sectional area. Another way to view this could be to look at the case where the wind and water flow velocity is equivalent as well as the output power. This results in the following requirement:

$$\frac{D_{wind}}{D_{water}} \cong 28.12 \tag{2.6}$$

This result implies that the diameter of a wind turbine must be approximately 28 times larger than a tidal turbine to produce the same theoretical output power if the flow rates are equivalent. Equations (2.5) and (2.6) demonstrate the following points:

- Tidal energy has a greater energy potential.
- Tidal turbines can be smaller than wind to harness the same amount of power.
- Tidal flows are powerful, as such, it will be difficult to have a tidal turbine installed and not have it washed away.

In reality, the energy extracted from the tides or wind is much different from the equation (2.4) derived above [11]. The actual energy that can be extracted is related to the type of turbine used, and efficiency of the generator. The Lanchester-Betz's linear momentum theory proposes that the maximum energy extraction from a wind or tidal turbine is 16/27 or approximately 60% of this total energy assuming an ideal turbine [11]. In practice the energy extracted is in the range of 40% due to the use of non-ideal turbines. This can be thought of qualitatively as being an efficiency factor. Equation (2.4) above will then become the following:

$$P_o = C_p \frac{\pi}{8} \rho D^2 v^3 \tag{2.7}$$

Where C_p is the efficiency factor of the turbine.

2.2.1 Offshore Wind Energy Availability

The expected power to be extracted from offshore wind can be evaluated by studying the probability density function for wind speed. For offshore wind, a Weibull probability density function can be used to describe the wind speed distribution [11].

The wind velocity probability density function can then be described as [11]:

$$p(v) = \frac{k}{A}\left(\frac{v}{A}\right)^{k-1} e^{-\left(\frac{v}{A}\right)^k}, v \geq 0, A > 0, k > 0 \tag{2.8}$$

Where, v is the wind velocity, k is a shaping parameter, and A is a scaling parameter. An example of a Weibull distribution can be seen below in Figure 2-1.

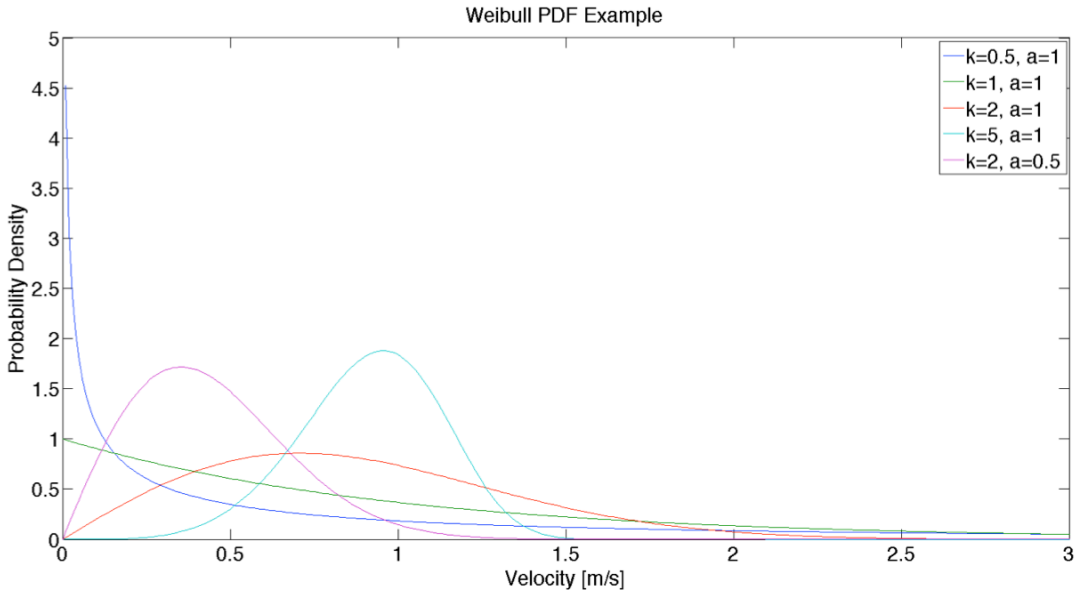

Figure 2-1: Weibull Distribution Example

The mean wind speed can be determined to be as follows [11]:

$$\bar{v} = A\Gamma\left(1 + \frac{1}{k}\right) \tag{2.9}$$

From this, the expected output power from an offshore wind turbine can be evaluated to be as follows [11]:

$$E\langle P_o \rangle = C_p \frac{\pi}{8} \rho D^2 A^3 \Gamma\left(1 + \frac{3}{k}\right) \tag{2.10}$$

A case-by-case is required in the specific area where the wind turbines are installed to determine this probability density function parameters *A* and *k*. As discussed in the previous chapter, for offshore wind turbines, the wind speed is more consistent than it is onshore.

2.2.2 Tidal Energy Availability

The tidal current velocity can be modeled by studying the periodicity of the tides. The tides on Earth are caused by the gravitational pull of the moon. The tides can be accurately predicted by solving the harmonic current equation [20]:

$$v(t) = v_0 + \sum v_a \cos\left(\frac{2\pi t}{T_a} + \rho_A\right) \tag{2.11}$$

There are six principal components that are used for this equation. These terms are listed as follows [20]:

- Principal lunar semi-diurnal constituent with a period of 12.4206 hrs
- Principal solar semi-diurnal constituent with a period of 12 hrs
- Lunar quarter diurnal with a period of 6.2103 hrs
- Lunar diurnal constituent with a period of 25.82 hrs

- Lunisolar diurnal constituent with a period of 23.93 hrs
- Lunisolar semi-diurnal constituent with a period of 11.965 hrs

These six components represent a simplified tidal model. The model of the tides can be further approximated by the Airy wave theory as follows [20]:

$$v(t) = v_0 + v_A \cos\left(\frac{2\pi t}{T_A} + \rho_A\right) \tag{2.12}$$

Where v_0 is a constant tidal velocity, v_A is the amplitude of the oscillating component of the tidal velocity, T_A is the oscillation period, and ρ_A is the phase shift. This can allow for an approximation of the instantaneous power generated. This can be approximated by the following equation [20]:

$$P_0(t) = C_p \frac{\pi}{8} \rho D^2 \left[v_0 + v_A \cos\left(\frac{2\pi t}{T_A} + \rho_A\right)\right]^3 \tag{2.13}$$

The tide velocity can be predicted by using these equations, the more terms used, the better the approximation. This ability to predict the tides makes tidal power a more reliable source of energy than wind power.

2.3 Energy Extraction

In the above sections, the maximum available energy was determined for offshore resources. The term C_p was introduced representing the efficiency of a turbine. This value is a scalar that represents how efficiently the prime mover and turbine converts kinetic energy into rotational mechanical energy from the offshore energy resource. Turbines are the energy harvesting devices that transfer the rotational mechanical energy to a generator. The generator then converts that mechanical energy into electrical energy. There are

numerous turbine designs available for use each having their own efficiency coefficient, C_p. The choice of which turbine to use depends on the offshore power installation site.

2.3.1 Tidal Turbines

The choice of generator and turbine for tidal power applications is important for maximizing the amount of extracted renewable energy. For tidal generation sites, the available head is low and continuously changing [13]. This implies a requirement of a high volume discharge of water from the turbine, further implying the necessity of a large cross sectional area of the turbine [13]. The environment in which these tidal turbines exist can cause great stress on the mechanical equipment [13]. This is due to the periodic nature of the tides, frequent starting and stopping of the turbines, and reversal of the tides [13]. Similar to wind farms, the quantity of turbines to be installed for a major tidal development can be quite high, in the order of hundreds of turbines. The turbines are subject to corrosive seawater and sea life. This necessitates the choice of appropriate materials and protection of the turbine and generator. There are four types of turbines that can be suitable for use in a tidal power installation. These turbines include the following: Kaplan, Tubular, Bulb, and Straight-flow turbines [13]. These are axial-flow and high specific speed turbines, which are ideal for tidal power generation [13]. For tidal generation, the bulb and straight-flow turbine configurations are most desirable to be used.

2.3.1.1 Kaplan Turbine

The Kaplan turbine is a vertical axis turbine, for application in tidal power generation. For this turbine configuration, water falls onto the top of the turbine. This means that this

turbine is not placed in line with the water flow. There can be additional losses incurred by directing the water to the turbine blades. Relatively deeper water would be required for an appropriate application of the Kaplan turbine. Figure 2-2 below shows a typical Kaplan turbine configuration.

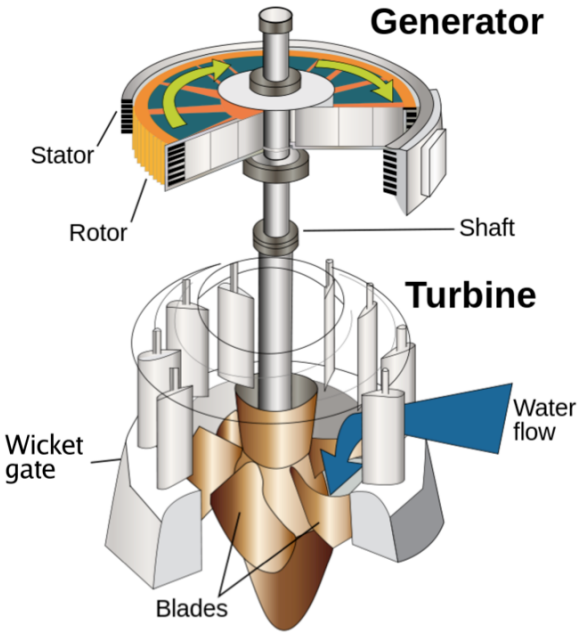

Figure 2-2: Kaplan Turbine [21]

2.3.1.2 Tubular Turbine

The tubular turbine can be used in shallower water since it is not a vertical axis turbine. This turbine is placed in the water flow. The generator is on a platform that is not in the flow of water, and the mechanical energy is transmitted to the generator through a driveshaft. A drawback to this configuration is that the driveshaft to the generator can be quite long. This results in critical speed limitations and significant torsion on the drive. Figure 2-3 below shows a typical tubular turbine configuration.

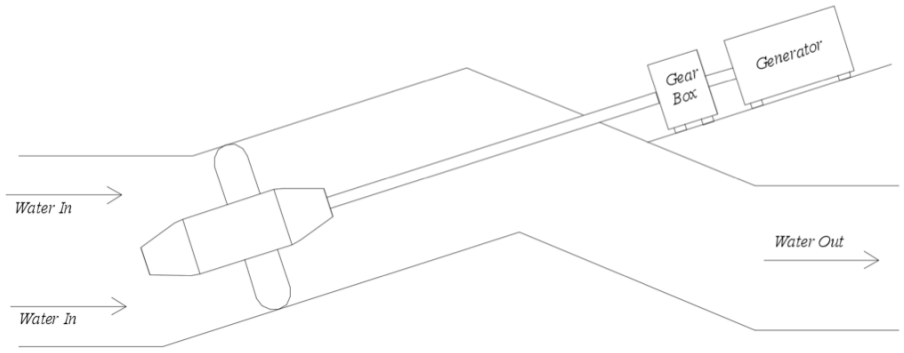

Figure 2-3: Tubular Turbine [22]

2.3.1.3 Bulb Turbine

This turbine configuration is used for straight water passages. It is similar to the tubular turbine; however, the generator in this case is attached to the turbine in a bulb that is in the flow of the water. This configuration does not require a long driveshaft. The turbine, generator, and wicket gates are included in a single assembly. The bulb turbine can be utilized in lower head applications with higher specific speeds. Difficulties of applying this generator are that it operates at low speeds, which means that the generator typically encapsulates a larger diameter, which can narrow the water pathway. Figure 2-4 below shows a typical bulb turbine configuration.

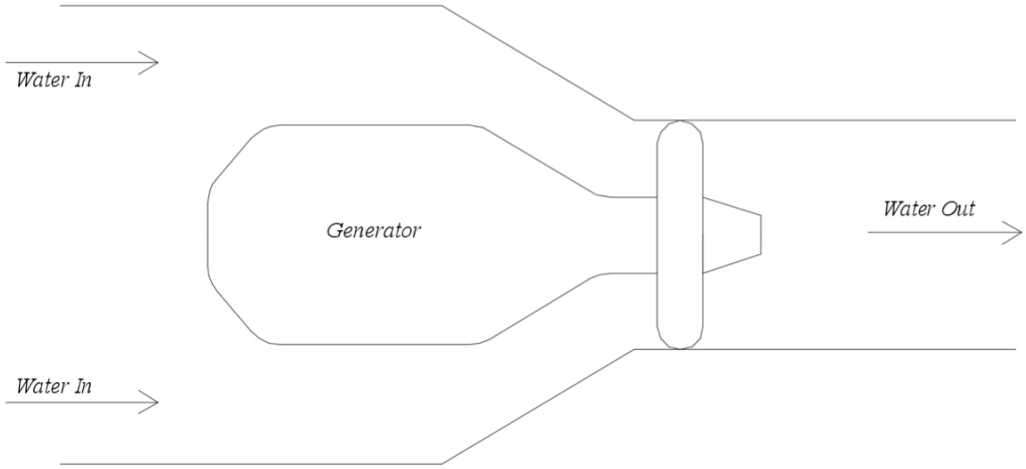

Figure 2-4: Bulb Turbine [23]

2.3.1.4 Straight-Flow Turbine

The straight flow turbine is similar to the bulb turbine with the exception of having a bulb that obstructs the waterway. This turbine sits in the flow of the water like a bulb turbine; however, the concept for this is that the turbine itself is used as both a turbine and as the rotor of a generator. This increases the amount of power that can be extracted from a given tidal resource. This design allows for easier speed regulation, as well as easy maintenance. Figure 2-5 below shows a typical straight-flow turbine configuration.

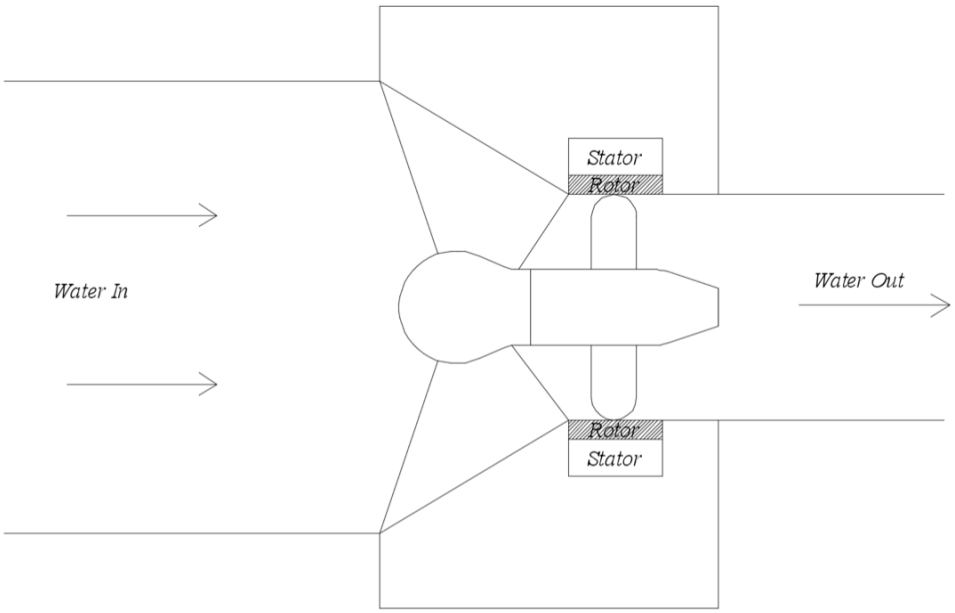

Figure 2-5: Straight-Flow Turbine [24]

2.3.2 Offshore Wind Turbines

There are two forms of wind turbines that are commonly used, a fixed blade design or a variable blade pitch design. The first design is used with constant speed rotors. The second is used for variable speed rotors. For offshore wind generation, typically horizontal axis wind turbines are used. The wind turbine design is what influences the energy harvesting efficiency in equation (2.10). Figure 2-6 below shows a typical horizontal wind turbine.

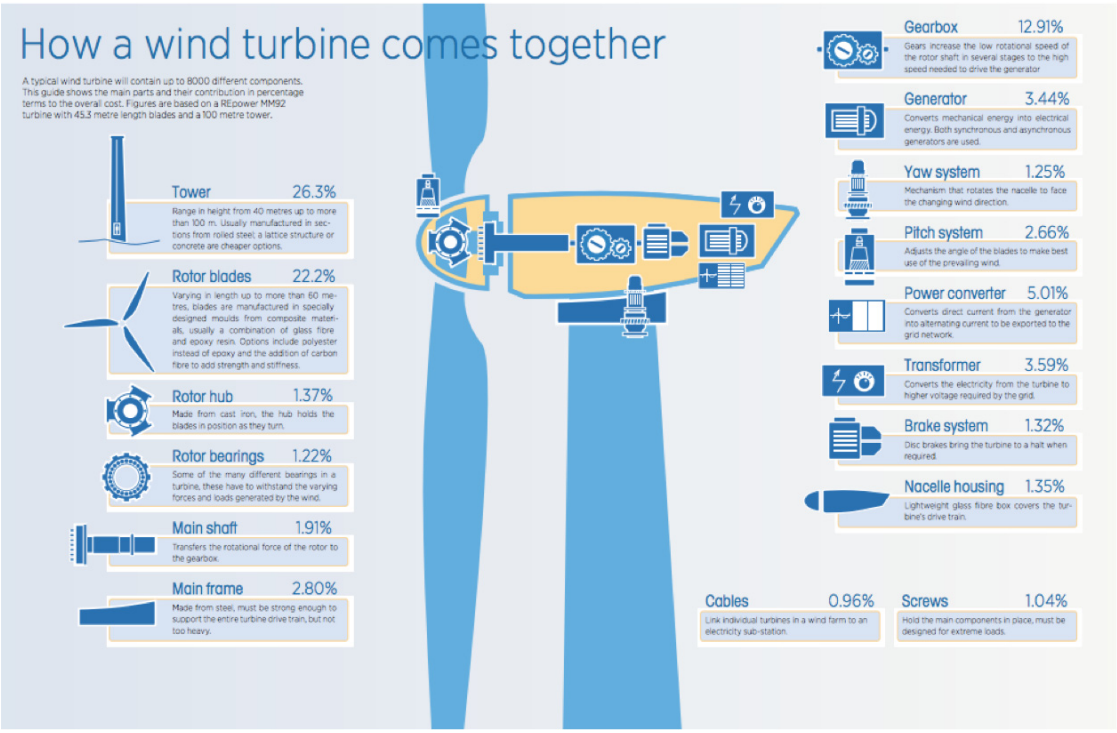

Figure 2-6: Horizontal Axis Wind Turbine [25]

Variable speed wind turbines have the drawback of being more expensive than fixed blade wind turbines. This is due to having the ability to control the pitch of the turbine blades, and having a control system to maintain the output frequency of the generator. Maintaining turbine speed is important when studying the electrical performance of a power grid.

2.4 Speed Regulation

In order to transfer power from a generation source to the load centers, the frequency and voltage of the power must match the power grid. In North America, the power grid operates at 60Hz. In order to have a fixed generating frequency, the rotors angular speed must be constant. The intermittent nature of wind and tidal energy sources result in difficulties

maintaining a constant angular speed. This results in frequency fluctuation os the voltage waveform that is produced by the generator.

2.4.1 Frequency Fluctuations

To demonstrate what occurs when the frequency of the power grid, 60Hz, and a generator connected to it are not matched, the network in Figure 2-7 below will be analyzed.

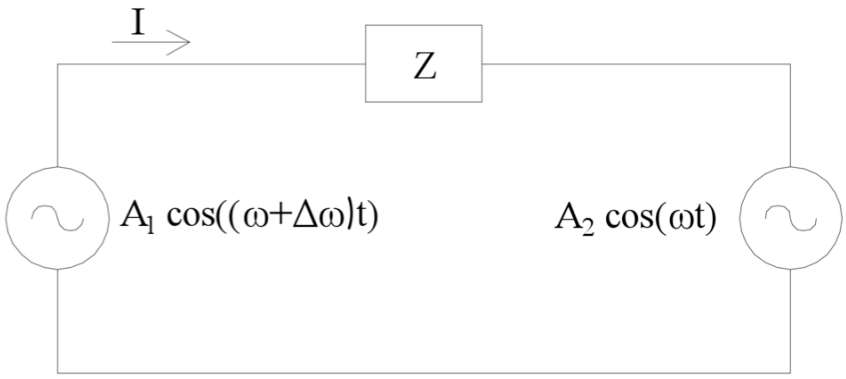

Figure 2-7: Network With Mismatched Frequency Sources

From this network, assuming that the impedance is equal to unity, the current, *I*, delivered to the grid can be found to be as follows:

$$I = \cos\omega t\,[A_1 \cos\Delta\omega t - A_2] - \frac{A_1}{2}[\cos(\omega t - \Delta\omega t) - \cos(\omega t + \Delta\omega t)] \quad (2.14)$$

If $\Delta\omega$ =0 and A_1=A_2,

$$I = 0 \quad (2.15)$$

Figure 3-8 below plots equation (2.14), the current injected to the power grid when the frequency deviation $\Delta\omega$ is 3 rad/s. When the frequency and amplitude of both sources are matched, there will be no current delivered to the grid. When the frequencies are

mismatched it can be seen that there will be a current flow to the grid even if conditions are designed to not have a current flow.

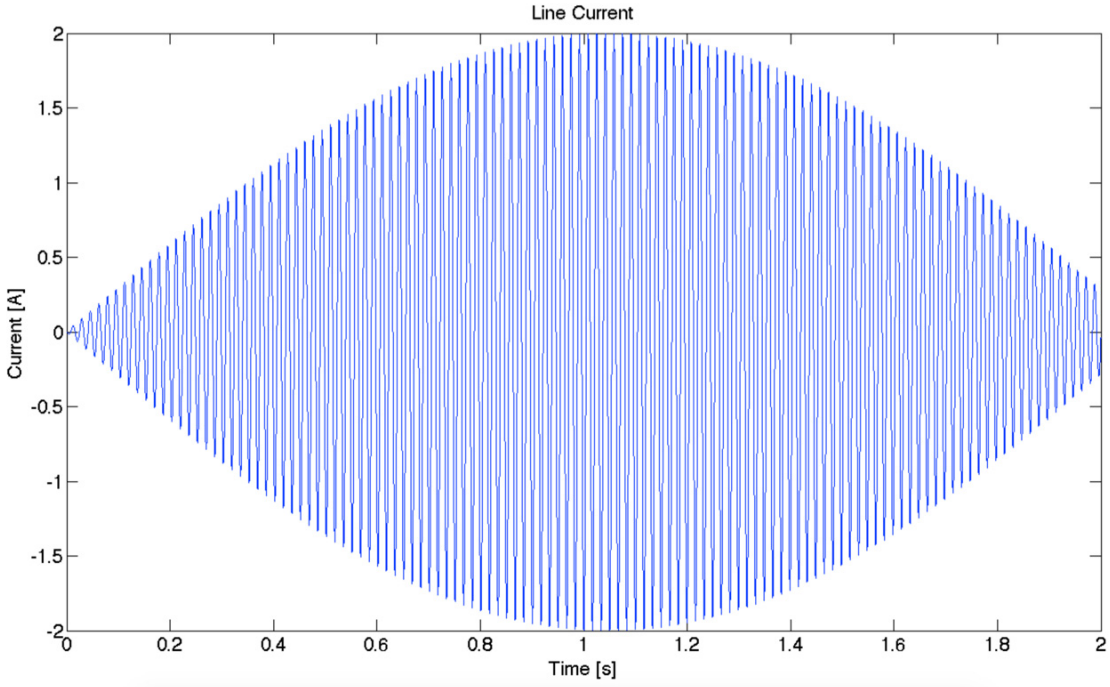

Figure 2-8: Current Delivered to The Grid

From this analysis it can be observed that caution must be taken in matching the frequency of a generator. This current could cause damage to both generation equipment and the consumer.

2.4.2 Methods to Maintain Constant Frequency

A constant rotor speed on a generator will ensure a constant output frequency. Ways to regulate the rotor speed could include the following:

1. Application of a governor system (varying the pitch of the wind turbine blades, wicket gates, etc.). The governor system takes a measurement of the speed of the rotor and adjusts the amount of kinetic energy allowed to the turbine such that speed is maintained.
2. Use of synchronous generators. These generators allow for a certain range of steady speed operation.
3. AC to DC power conversion followed by DC to AC power conversion. Converting the generated AC power to DC and then back to AC allows for the generation of whatever frequency is desired. This does not directly regulate the speed of the turbine, however it regulates the output frequency of the system.

Offshore power generators are typically small in size, in the order of megawatts. To compensate for the smaller generators, offshore generation is usually constructed in farms where many turbines are used to generate power. Having many generators producing power from an intermittent energy source would require the following:

- Each generator must have a means to regulate its output voltage frequency.
- Speed regulation methods 1 and 2 result in an AC output, which would require synchronization between each turbine if they are interconnected.
- Speed regulation method 3 results in a DC output, this allows for very simple interconnection of generators.

Each of these methods of speed regulation, and their consequences has various costs associated with them. They are factors that must be considered in the choice between AC and DC power transmission for an offshore power installation.

2.5 Generators

There are three main types of generator that are used for electric power generation. These are the synchronous machine, induction machine, and permanent magnet synchronous machine. Intermittent energy sources have implications regarding how to generate electric power. To connect a generator to the power grid, it is required that the output voltage frequency matches and remains matched to the power grid. The limitations of applicability of each type of generator will be discussed for offshore power systems.

2.5.1 Synchronous Generators

Synchronous generators have a rotor magnetic field that is produced by one of two sources, permanent magnets or electromagnets. Providing the rotor magnetic field allows a range of operation in which the generator will rotate at synchronous speed, and generate a fixed output voltage frequency. The synchronous rotational speed of a synchronous generator can be found to be as follows [26]:

$$N_s = \frac{120f}{P} \tag{2.16}$$

Where, N_s is the rotational speed in revolutions per minute, f is the generated output frequency of the generator, and P is the number of rotor poles. From equation (2.16) it can be observed that the output voltage frequency can remain fixed if the rotational speed of the rotor remains fixed. Having permanent magnets on the rotor provides the benefit of not

requiring a DC power supply for production of a magnetic field. Drawbacks to this include: a fixed magnetic field on the rotor and the high cost associated with manufacturing permanent magnets. Having an electromagnet on the rotor allows for control of the rotors magnetic field through the DC current supplied to the electromagnet. Synchronous generators have the capability to generate or absorb reactive power. This is a consequence of having the controllable field current for the generator. As a consequence of the generator requiring an external source providing a field current, there is no black start capability for a synchronous machine. It is the provided magnetic field on the rotor which allows for a range of constant output frequency with a synchronous generator. There are two main forms of rotor construction associated with these generators. These constructions are the cylindrical rotor, and the salient pole rotor.

2.5.1.1 Cylindrical Rotor

A cylindrical rotor generator is one where the rotor is cylindrical, resulting in a uniform air gap between the rotor and stator. The equivalent circuit model, per phase, for a cylindrical rotor synchronous machine can be observed in Figure 2-9 below.

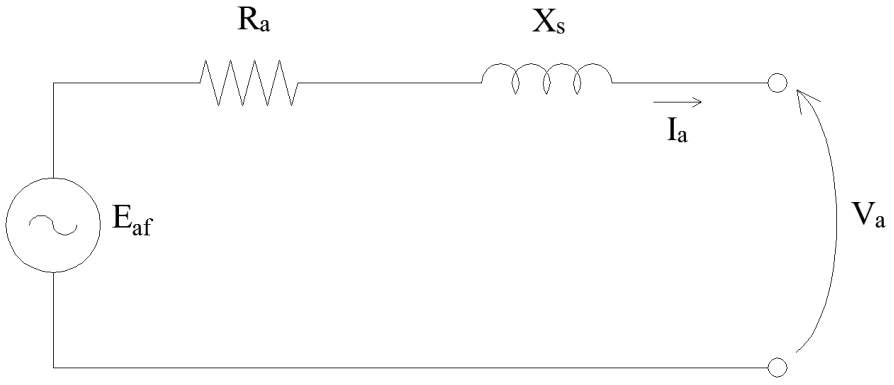

Figure 2-9: Cylindrical Rotor Synchronous Machine Equivalent Circuit

This equivalent circuit includes four terms, E_{af}, R_a, X_s, and V_a. These components will be discussed below:

- E_{af} represents the induced armature voltage by the field winding flux. This induced voltage is represented by the following equation [26]:

$$E_{af} = -2\pi f L_{af} I_f \sin(2\pi f t + \delta_{e0}) \tag{2.17}$$

Where L_{af} represents the armature to field mutual inductance, I_f represents the magnitude of the DC field current, and δ_{e0} represents the initial electrical angle of the rotor.

- R_a represents the resistance of the armature.

- X_s represents the synchronous reactance of the generator. Assuming that the generator is operating under balanced steady state conditions, the synchronous reactance can be evaluated to be as follows [26].

$$X_s = 2\pi f \left[L_{aa0} + L_{al} + \tfrac{1}{2} L_{aa0}\right] \tag{2.18}$$

The term L_{aa0} accounts for the air gap inductance due to phase a currents only, the term $\frac{1}{2} L_{aa0}$ accounts for the air gap inductances due to the other two phases, and L_{al} accounts for the phase a leakage flux.

- V_a represents the output voltage of the generator, the terminal voltage of the machine [26].

$$V_a = E_{af} - I_a[R_a + jX_s] \tag{2.19}$$

Where I_a is the generators armature current.

Cylindrical rotor synchronous machines are typically made with a fewer number of poles. This implies that to generate a 60Hz waveform, the generator must operate at higher speeds according to equation (2.14). As such they are typically used for thermal based power generation.

3.5.1.2 Salient Pole Rotor

Salient pole machines differ from the cylindrical rotor machines in that the salient pole machine has protruding poles, thus a non-uniform air gap. There are two air gaps that occur along the direct axis and quadrature axis. The direct axis air gap corresponds to the gap between the protruding pole and the stator. The quadrature air gap corresponds to the air gap of the region between poles and the stator [26]. From this, impedances for the direct axis and quadrature axis can be found, X_d and X_q respectively [26]. In Figure 2-10 below, the phasor diagram relating the direct and quadrature axis to the internal generated voltage, and the terminal voltage and current is shown.

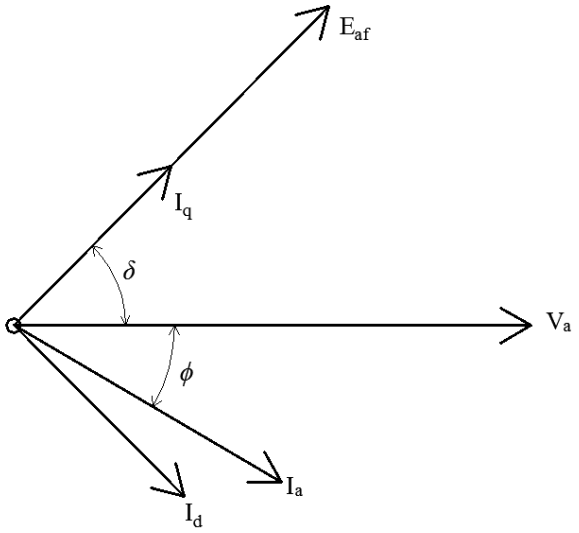

Figure 2-10: Salient Pole Machine Phasor Diagram

From this phasor diagram, the following relationships can be determined for a salient pole generator [26].

$$E_{af} = V_a + R_a I_a + jX_d I_d + jX_q I_q \tag{2.20}$$

$$I_a = I_d + I_q \tag{2.21}$$

$$\delta = \tan^{-1}\left(\frac{IM\{V_a + jX_q I_q\}}{RE\{V_a + jX_q I_q\}}\right) \tag{2.22}$$

In the phasor diagram in Figure 2-10, the terms I_a and V_a correspond to the terminal voltage and current of the generator. The term ϕ is the power factor angle at the terminal of the generator. The direct and quadrature currents are orthogonal to each other. Salient pole machines are generally constructed with a larger number of poles, which means they operate at slower rotational speeds. This makes them suitable for use in hydro, wind, or marine power generation.

2.5.1.3 Permanent Magnet

Permanent magnet synchronous generators are very similar to the previously discussed cases, the difference being that the rotor is constructed from permanent magnets and not an electromagnet. These generators are typically more energy efficient, however they suffer from only providing fixed excitation. The cost of making these generators is also relatively high. Due to this, these generators have limited application.

2.5.2 Induction Generators

Induction machines are different from synchronous machines in that a field current is not provided by an outside source. The relative motion between the stators magnetic field and rotation of the rotor develops the field current. This relative motion implies that no field current is produced if the rotation of the rotor is the same as that of the stators magnetic field. This implies that the induction generator can provide no torque if it is rotating at synchronous speed. Induction generators do not have a black start capability since an energy source is required to start the field current induction process. The equivalent circuit for an induction machine is similar to that of a transformer. Figure 2-11 below shows the equivalent circuit for an induction machine.

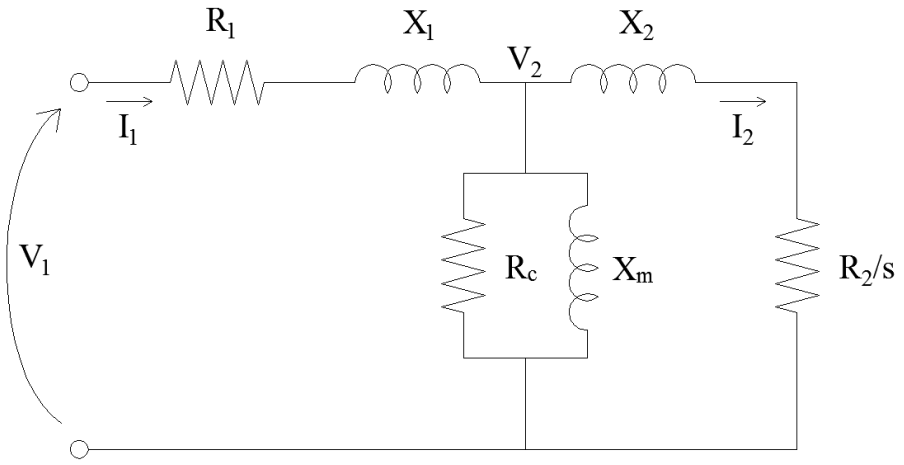

Figure 2-11: Induction Generator Equivalent Circuit

In this circuit, the rotor resistance is variable, since the induced field current is related to the relative motion between synchronous speed and the actual speed of the generator. This relative motion is called the slip and is defined as follows [26]:

$$s = \frac{N_s - N_r}{N_s} \tag{2.23}$$

From Figure 2-11, the terms in the equivalent circuit are defined as follows: V_1 is the stator line to neutral voltage, V_2 is the counter emf generated by the air gap flux, I_1 is the stator current, R_1 is the stator effective resistance, X_1 is the stator effective reactance, R_2 and X_2 are the rotor referred resistance and reactance, and R_c and X_m are the core losses and magnetizing reactance. The shaft power for the motor can be found to be as follows [26]:

$$P_{shaft} = \frac{3(1-s)\omega_s P}{4\pi f} {I_2}^2 \left(\frac{R_2}{s}\right) - P_{rot} \tag{2.24}$$

Where P_{rot} represents the frictional and winding losses of the machine. Induction machines are cheaper than synchronous machines to manufacture, however they have a variable

frequency output, which is undesirable. They are useful when the prime mover is a variable source, such as wind or tidal energy sources.

There is a second variety of induction machine that is used for offshore power generation. This is the doubly fed induction generator. The difference with this generator is that the grid supplies the rotor currents. The grid supply can be passed through a power converter, such that the frequency and current can be controlled for the rotor. This configuration is shown in Figure 2-12 below.

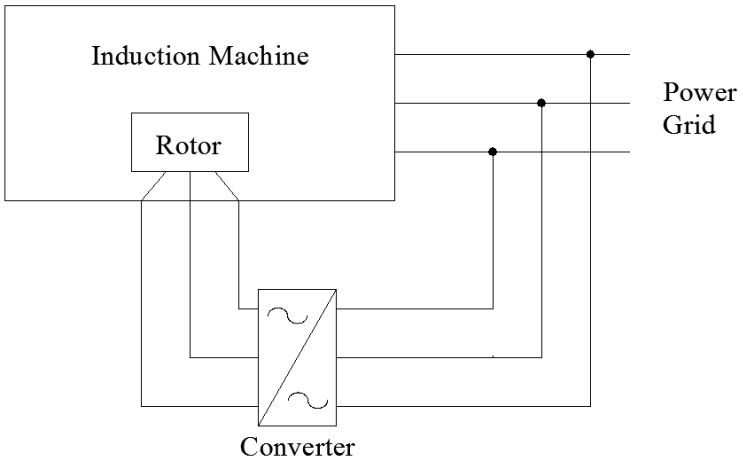

Figure 2-12: Doubly Fed Induction Generator

This generator configuration can allow for speed control by varying the rotor current and frequency. The benefit of this is that the input mechanical power can be allowed to deviate from synchronous speed, and a suitable output voltage and frequency can be produced.

2.5.3 DC Generators

Direct current generators produce an emf similar to how a two pole salient generators would. The DC machine uses brushes to switch the voltage polarity, which effectively rectifies the generated emf. The summation of these rectified coil voltages results in an approximately DC output voltage. The rotor field for these generators comes from five potential sources. These sources include: a series field, shunt field, hybrid of series and shunt fields, an independent field, and a field from a permanent magnet. The series/shunt hybrid DC motor model can be seen in Figure 2-13 below.

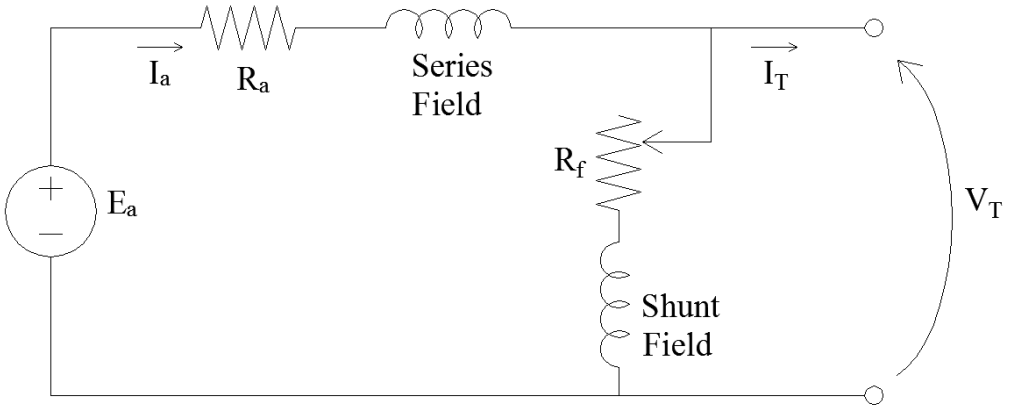

Figure 2-13: Hybrid Series/Shunt DC Motor

In this figure R_a represents the armature resistance and R_f the field resistance. A DC motors generated emf is proportional to the angular speed of the rotor as follows [26]:

$$E_a = k_a \Phi_D \omega_m \tag{2.25}$$

Where, k_a is the motor constant and ω_m is the angular speed of the rotor. The flux along the direct axis Φ_D can be defined as follows [22]:

$$\Phi_D = \sum I_f \tag{2.26}$$

The output electromechanical power is given by the following equation [26]:

$$P_{mech} = T_{mech}\omega_m = E_a I_a \tag{2.27}$$

Disadvantages of using DC motors include: the increased cost of production due to the complex armature windings and the increased amount of maintenance due to the brushes and commutator.

Chapter 3: Underwater Power Cables

This chapter provides an overview of underwater power cables. Generalizations regarding cable geometries, evaluation of the line parameters for various kinds of underwater cables, steady state performance, line approximations, transients, and harmonic propagation will be studied. The results will be contrasted with the results for overhead transmission lines.

3.1 Introduction

Underwater power cables have unique characteristics when contrasted to conventional overhead transmission lines. These characteristics will be studied in great detail such that the performance of underwater power cables can be determined. The models developed will be used to study how a current onshore power system will be affected by the inclusion of an offshore grid of generation. The performance of these cables is significant when determining whether AC or DC power transmission is to be chosen.

3.2 Cable Components

Underwater power cables differ from overhead power cables in a number of ways. Overhead power cables typically consist of just the core conductor or the core conductor in combination with steel reinforcement. These cables are surrounded by air, which is a natural insulation medium, thus additional insulation is not required around the conductor. Underwater power cables are submerged in impure water, which is a conductor of electricity. This necessitates that underwater cables have an electrical insulator that surrounds the core conductor [27,28]. If this insulation were not there, the electric current

would disperse within the body of water [27]. The insulations that are typically used for underwater cables are sensitive to water. The water, over time, will destroy the insulation thus destroying the cable [27]. To prevent this a sheath is added around the insulation. This prevents water or water vapor from attacking the insulation and forming water trees within it. Finally a protective PVC or semiconductor serving, armor, and final protective outer serving are added to the cable [27,28,29]. The purpose of this is to prevent water penetration and to protect the cable from external forces and external life destroying the cables integrity. Further reasoning and design considerations for these additional cable layers will be discussed in the proceeding sections.

3.2.1 Core conductor

The material chosen influences the ampacity of the cable, the diameter of the cable, the cables weight, and cost of the material. The cables ampacity and diameter are related to each other. Typically for a transmission line, the ampacity is determined and the conductor diameter is causal to this. Due to material costs and their inherent resistivity, there are only two common materials used for transmission line conductors, aluminum or copper [30]. The resistivity of aluminum is $2.82 \cdot 10^{-8}\,\Omega$m and copper is $1.68 \cdot 10^{-8}\,\Omega$m [27]. Assuming a specified cable ampacity it can be seen that the radius of the copper cable will be less than that of aluminum. In fact, $r_{CU} = 0.772 r_{AL}$. Copper is more expensive than aluminum, however it would allow for the underwater cable to have a smaller diameter. The density of copper is 8.96g/cm^3 and aluminum 2.7g/cm^3 at room temperature. This implies that given a specified ampacity, given the adjusted surface area requirement, that the copper conductor will weigh approximately twice that of the aluminum conductor. In

fact, $m_{CU} = 1.977 m_{AL}$. This additional weight is desirable for increased seafloor stability, preventing unwanted motion of the cable, however, it does make the laying of the cable more cumbersome and expensive [27].

The skin effect describes the tendency for the current density to concentrate in an annulus on the outer edge of a conductor as operating frequency increases. This uneven current distribution corresponds to an equivalent decrease in conductor surface area, thus increasing the resistance of the conductor. The skin depth for a conductor can be defined as follows [29, 30, 31]:

$$\delta = \frac{1}{\sqrt{\pi f \mu \sigma}} \tag{3.1}$$

Where *f* is the operating frequency, μ is the permeability and σ is the conductivity of the conductor's material. What this skin depth represents is the distance inward from the outer conductor edge to when the wave is diminished by e^{-1} (37%) of its original magnitude at the outer edge. For a copper conductor operating at 60Hz, the skin depth is approximately 8.4mm. This effective increase in the cables resistance diminishes the efficiency and ampacity of the cable [27, 29, 30].

The proximity effect is an attraction of an electrical current flow to one side or another in a conductor [27, 30]. This occurs due to the electromagnetic attraction between multiple conductors in close proximity to each other. Similar to the skin effect this causes the current flow to concentrate on one side of the cable. This decreases the effective useable surface area of the cable, thus increasing the cables resistance. To minimize this effect, the placement of cables must be taken into consideration.

The core conductor geometry typically takes one of the following forms: solid, stranded, profiled, or segmental. These Types of conductors can be seen in Figure 3-1 below.

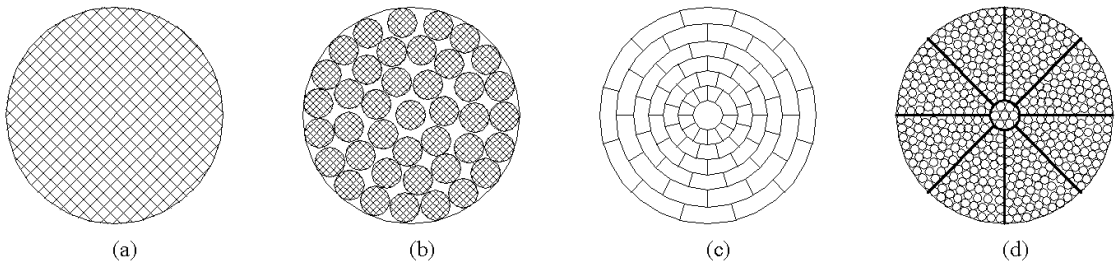

Figure 3-1 (a) Solid Core (b) Stranded (c) Profiled (d) Segmental

- Solid core conductors are typically used with a cross sectional area of 400mm^2 or less. This results in these conductor types being applied to lower voltage applications since the requirement for large cross sectional areas are more common in high voltage applications. These conductors are easy to manufacture, however, the insulation has a tendency to slip on the smooth conductor surface. This can cause issues when terminating or jointing the cables [27,31].

- Stranded conductors are most often used in underwater power cables. This form of conductor can achieve a 92% filling factor. It is also used when large cross sectional areas are required. This conductor topology allows for a weakening of the proximity effect if the strands are electrically isolated from one another. The skin effect cannot be reduced. A drawback is that the resistivity of the conductor

material is increased due to it being cold worked and the filling factor is lower than other conductors [27,31].

- Profiled conductors can achieve a 96% filling factor or larger. This type of conductor can take almost any form. It also has a lower resistivity due to the material not being cold worked. This type of conductor is used typically in large HVDC underwater power cables [27,31].

- Segmental conductors, also known as Milliken conductors, is a conductor topology that allows for a decrease in the skin effect. This conductor is similar to the stranded conductor except that it is sliced and each slice is insulated from each other. The way that the wires are twisted allows for a cancellation of the skin effect [27,31].

There are many advantages and disadvantages to be considered when choosing which conductor will be used for an underwater power cable. Determining the ampacity requirements, material, and topology are factors that are associated with choosing a core conductor.

3.2.2 Sea Water

The water surrounding the underwater power cables is typically salt water that is also used as the return path, or ground, for the cable. Single wire earth return is the grounding system of the cables inner layers, at several points along the length of the cable [29,31]. The single wire earth return is a viable option for grounding due to the relative immensity of the body

of water surrounding a cable. This makes the ground impedance of the water very small, even though water is not a good conductor in comparison to conductive metals. This will be discussed further in subsequent sections.

3.2.3 Insulation

The insulation is a layer that is used to separate the core conductor and the ground plane, which is embodied as the surrounding seawater. This insulation can be thought of as a means to maintain current flow through the core conductor and not the surrounding body of water. There are various types of insulation that have been used or are currently still being used for AC and/or DC power cables. These insulation mediums can be classified into the following categories: extruded insulation, paper insulated oil filled, and paper mass [27]. The various subclasses of these insulation mediums, their applications, and their limits of applicability will be discussed below.

3.2.3.1 Extruded Insulation

There are three subclasses of extruded insulation. These subclasses consist of polyethylene insulation, cross-linked polyethylene insulation, and ethylene propylene rubber insulation [27].

- Polyethylene (PE) insulation comes in three varieties; low, medium, or high density. These densities range from 0.9 to 0.97 g/cm^3. This medium of insulation performs better than paper insulation in that it has a lower dissipation factor and dielectric losses. The operating temperature of these cables is rather low, 70°C for nominal

operating temperature and 125°C for short circuit temperatures. Low-density PE insulation has been successfully used for up to 500kV cables [27].

- Cross-linked polyethylene (XLPE) insulation uses low-density polyethylene insulation that has had its long molecular strands linked together. This cross-linking provides the insulation with a higher operating temperature. This discovery of XLPE insulation made the ordinary PE insulation obsolete. The nominal operating temperature of XLPE cables is 90°C and a short circuit temperature of 250°C. These cables are available, in land usage, for voltages up to 550kV. For underwater applications, due to the flexible joints limits, voltage classes of 245-345kV can only be attained. If the cable can be manufactured in a single length where no joint is necessary then a higher voltage class can be used for the cable. Water trees are a concern for XLPE insulation. Water and water vapor can penetrate the insulation and degrade its dielectric strength. It is ideal to have the insulation protected from humidity through design of the layers outside the insulation. These cables can be produced in single and multi-core form. Up to 170kV for a three-core cable and 500kV for a single-core cable. Since flexible joints are not available for the 400/500kV range, it can be difficult to use these cables for long underwater paths. These cables are not suitable for use with high voltage DC applications. This is due to the insulations space charge phenomenon. These space charges would cause peaks in the electric field that exists in the insulation medium, which is undesirable and could cause insulation break down. There have however been special XLPE

formulations developed that allow for use with high voltage DC applications and can allow for up to a 320kV operating voltage [27].

- Ethylene propylene rubber (EPR) insulation is another form of extruded insulation. It has a larger dielectric loss and permittivity than XLPE cables. This limits EPR cables to be used in medium voltage underwater cables. EPR cables show better performance to moisture than XLPE insulation [27].

Factors that affect the life of extruded insulation are the operating temperature, operating voltage, and humidity. These effects can have significant impacts on the life of the underwater cable. The life time can be cut in half by a 8-10% increase in operating voltage or a 8-10°C temperature rise from nominal. The humidity causes degradation of the insulations dielectric strength. It is ideal to have a water and water vapor barrier present such that this water vapor does not intrude the cable [27].

3.2.3.2 Paper Insulated Oil Filled

Paper insulated oil filled insulation consists of a cable that is insulated with paper and then impregnated with low-viscosity oil or synthetic cable fluids such as linear alkylbenzene mixtures. The dielectric strength of this insulation depends on the pressure. Low pressure allows for gases in the oil to bubble, which can cause an electric break down of the insulation. The cables must be pressurized from an onshore unit. A return oil duct is required for these cables. In single-core cables this duct is placed in the center of the core conductor. In three-core cables this duct is placed in the middle of the cable. Typically

this insulation medium is not used for lengths greater than 30-60km. Oil filled cables can be used for voltages up to 800kV. These cables can allow a larger ampacity than XLPE cables due to them being able to operate with a higher core conductor temperature. These types of cables can be used for both AC and DC power transmission [27].

3.2.3.3 Paper Mass

Paper mass insulation is typically only used for high voltage DC or medium voltage AC applications. They are most often used for high voltage DC underwater power cables. This kind of insulation can be used up to 500kV DC. This kind of insulation can be used on very long underwater transmission line lengths since they do not require onshore pressurizing stations. Since these cables are used for DC power transmission, a higher density paper can be used since there are no dielectric losses [27].

3.2.4 Sheath

The dielectric strength of the insulation must be maintained by preventing water from attacking the insulation. Surrounding the insulation medium with a sheath can prevent water penetration of the insulation [27]. Typically sheaths are made of lead, aluminum, copper, or a polymer material [27]. For medium voltage cables, a water-absorbing layer would only be required to keep water from getting to the insulation. Higher voltage underwater cables typically have a sheath. The various materials used for the sheath will be discussed below.

- Lead sheaths can be virtually impermeable for water and humidity penetration. Lead is heavy and will make the cable heavier, thus increasing the stability of the cable on the sea floor. Since lead is a soft metal, it is important to protect it against external forces and fatigue. The softness of the metal also makes it hard to apply a uniform lead sheath without tearing the metal [27,32].

- Aluminum sheaths come in three forms, extruded, welded, or laminated. Welded aluminum sheaths require that the weld seam be inspected for gaps in the welding. In the event that there is a gap, water or water vapor can penetrate the sheath and deteriorate the insulation. Extruded sheaths are no longer used for underwater power cables due to corrosion problems. Laminated sheaths consist of a thin aluminum foil wrapped around the cable with a polymeric layer outside it. Again the seam created by this process can allow water or water vapor to penetrate the sheath [27].

- Copper sheaths are used because they are corrosion resistant and are capable of handling short circuit currents given the sheath is sized properly. Copper is resilient to fatigue and can be bent many times with no fatigue. Cables that are dynamically moving in the water will typically have a copper sheath for this reason [27].

- Polymeric sheaths can be used if no metallic sheath is present. These sheaths won't pass water through them, however water vapor can penetrate through them with time. These sheaths are also used, for example, in the case when the aluminum foil

sheath is used. These sheaths are also used as external cable layers or layers separating metallic cable components [27].

Multi-core underwater power cables typically have one of the following sheath configurations. A sheath surrounding each core, a sheath around the bundle, or a sheath around each core and the bundle. The same materials as described above would be used as the sheaths. Choice of the sheath depends on the voltage class, the dynamics of the cable, and the short circuit current carrying capacity.

3.2.5 Armor

The underwater power cables require protection from external forces such as the tensions in the cable while laying it, transporting it, external damage such as anchors or falling/dragging objects, wildlife, and electromechanical forces [27]. In additionally to this, the armor adds weight to the cable and increases the sea floor stability of the cable. The armor lay length and laying patter can be determined from how long the transmission link is and how much tension or torsion forces it is predicted to observe. Typically the armor is constructed from strands of round wire. Multiple layers of armor and/or weaving the layers in different directions can enhance the strength of the cable. Typically, either copper or steel is used for the armor. When transmitting AC power, an issue that arises with using steel armor is that it is a high permeability material, due to its iron content [29,31,33,34]. This means that there will be significant losses due to induction in this layer. Copper is a low permeability metal and would incur fewer losses. This is true for a single-core underwater cable, however for a three-core underwater cable it is not as significant. A

three-core underwater power cable has significant cancellation of the magnetic field, the summation of each of the phase currents equals zero [30]. This implies that fewer losses will be observed in a steel armor surrounding a three-core underwater power cable. This will be shown in a subsequent section where the magnetic fields of the various underwater power cables will be quantified. Strength requirements, cost, and efficiency of the transmission link are the deciding factors for which material is used as the armor.

3.2.6 Material Properties

The materials used in each of the cables various layers have unique electrical properties. These properties are the conductivity, permittivity, and permeability. Table 3-1 and 3-2 below show the electrical properties of the commonly used core conductors, sheaths, armor, insulation, and servings between metallic layers and outermost layer of the cable.

Table 3-1: Electrical Properties of Conductor Materials [27,34]

	Copper	**Aluminum**	**Lead**	**Sea Water**	**Steel**
$\boldsymbol{\sigma}$ **[S/m]**	5.96e7	3.5e7	4.55e6	4.8	1e7
$\boldsymbol{\varepsilon_R}$	1	1	1	70	1
$\boldsymbol{\mu_R}$	1	1	1	1	100

Table 3-2: Electrical Properties of Insulation Materials [27,34]

	XLPE	EPR	Rubber	Paper Mass	Oil Paper
$\boldsymbol{\sigma}$ **[S/m]**	1e-14	1e-14	1e-14	3.54e-13	1.22e-13
$\boldsymbol{\varepsilon_R}$	2.3-2.5	2.7-3	7	4	3.3-3.6
$\boldsymbol{\mu_R}$	1	1	1	1	1

The values of permittivity and permeability are the relative coefficient values with respect to the permittivity and permeability of free space, $\varepsilon_o = 8.8542 \cdot 10^{-12}\ F/m$ and $\mu_o = 4\pi \cdot 10^{-7}\ H/m$ respectively. The conductivity is measured in $(\Omega \cdot m)^{-1}$. The values presented in Tables 3-1 and 3-2 above are approximations for the electrical properties of the materials.

3.3 Grounding

How underwater power cables are grounded is of importance in defining what the line parameters of the cable will be and how the fault currents/imbalanced currents will flow. How the inner layers of the cables are grounded will define how the electric and magnetic field is constrained or negated and how much additional losses, brought on by additional return current flow, will be produced by the cable.

- The electric field produced by the core conductor of the cable is radial to the conductor and bounded by the location of the ground plane surrounding the core conductor. The capacitance of the cable depends on the electric field. How the electric field is bounded will thus affect the capacitance of the cable.

- The return currents flow through the neutral of a three-phase system. For an underwater three-phase transmission line these currents will flow through the ground path, which partially exists in the grounded cable layers, and partially in the seawater. Thus under balanced three-phase operation, there should be no neutral currents flowing. These neutral currents will only flow under the unbalanced conditions or when faults occur. These return currents can cause a cancellation in the magnetic field produced by the core conductor's current flow.

For underwater power cables it is ideal to have all of the inner metallic layers as equipotential surfaces. This implies that the metallic sheaths and armor, which surround the insulation, are to have the same potential as the seawater surrounding the cable. This can be done, practically, by using a single wire earth return system, where electrodes are used to bond the inner cable layers to the seawater [35,36,37,38,39]. To ensure that the inner layers are equipotential this bonding can occur at several points for a long underwater cable stretch. This eliminates the necessity of having an additional cable as a return path.

3.4 Configurations

There are two main configuration types for both AC and DC power transmission. These configurations are single-core and multi-core cables. These configurations are inherently similar, consisting of the main components discussed in the previous sections. From reviewing underwater power cable construction methods, a generic geometry can be developed for each of the cables. There are several other layers that are associated with underwater power cable construction that were not discussed in the previous sections.

These layers include the following: water absorbing barriers, cable jacket, separation layers, and string beddings [27]. For multi-core cables there are additional components, there is filler for all of the free space as well as fiber optic cables or pilot wires [27]. From knowledge of the electrical properties of these additional layers a generic geometric model can be constructed for underwater power cables. Figure 3-2a below shows the general geometric models for AC underwater power cables and Figure 3-2b shows the model for DC underwater power cables.

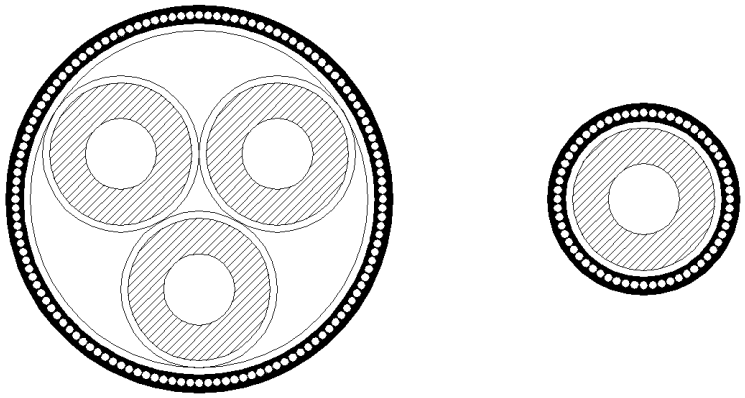

Figure 3-2a: AC Underwater Power Cables Geometric Model

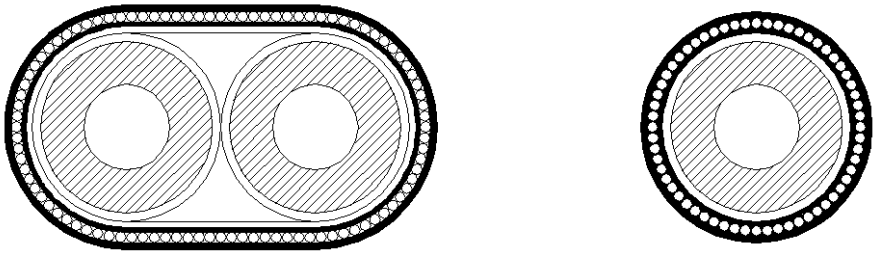

Figure 3-2b: DC Underwater Power Cables Geometric Model

There are several assumptions that have been made in developing this model. These assumptions are as follows:

- Pilot wires are neglected.
- The fiber optic cable in multi-core cables is assumed similar, electrically, as the filler.
- Multi-core cables have a metallic sheath around each core and potentially around the bundle.
- The additional cable layers are lumped into a serving between the sheath and armor.
- Materials are homogenous.
- Armor wires are touching along the length of the cable, it will be modeled as an annulus.

The geometric models for the cables include: core conductor(s), insulation, sheath around each core and possibly around the bundle, an insulation layer, armor, and an outer serving [29,31]. These geometric models will be used in analyzing the line parameters of these cables.

3.4.1 Single-Core or Multi-Core Cable

There is a choice to be made of whether to use single-core cables or a multi-core cable. There are many factors to be considered. The following are additional factors to be considered in choosing a single-core or multi-core cable.

- Trenches will be required for each of the underwater power cables. The trenches enhance the sea floor stability by confining where the cable can move. For single-core cables, multiple trenches will have to be made while multi-core cables will only require a single trench [27].

- Heat dissipation is better for single-core cables than for multi-core cables. This is due to the individual cores being separated [27].

- Typically, three single-core cables costs less than a multi-core cable [27].

- Single-core cables can be used in higher voltage ranges. Multi-core cables can become quite large as the insulation thickness increases. This makes the cable less flexible, heavy, and difficult to move [27].

- There are laying difficulties associated with both types of cables. Both kinds of cables can become heavy and inflexible, making them hard to handle. Multi-core cables are typically heavier and less flexible than single-core cables. Thus it is typically less strenuous to lay single-core cables [27].

- Redundancy is an important factor to consider when designing an underwater transmission link. The cables are expensive, however, should damage occur the system could be crippled. It is reasonable to presume that should damage occur to a multi-core cable that all the cables could be damaged or compromised. This

would require the replacement of the whole cable. Single-core cables are less likely to have more than one of the cables damaged at a time since they are spaced apart. Thus it could be reasonable to have a redundant cable [27].

- Cables experience electromechanical forces when there are electric currents flowing in the conductors. These forces are proportional to the current flowing in the cables. Under fault or transient conditions these forces can become of significance. Single-core cables could whip or multi-core cables could cause damage to insulation [27,34].

- Multi-core cables transmitting AC power experience the proximity effect. This is due to the close proximity of the core conductors. The magnetic fields produced by each of the cores pushes the electric charges in each of the cores. This causes an increase in the resistance of each phase [27,34].

- Steel armor can be used for multi-core cables. Special steels or copper armor must be used for single-core cables when transmitting AC power. Copper is more expensive than steel [27].

- The magnetic field outside the multi-core cable is much weaker than for single-core cables. This is due to the close proximity of the phases in the multi-core cable. This causes a significant cancellation of the magnetic field [27,29].

These are all important considerations to keep in mind when designing and analyzing which transmission link should be used for an offshore power application. There is another aspect which has not been discussed yet has been alluded to, the choice of AC or DC power transmission. This will be discussed in a subsequent section when the cables have been modeled and their performance evaluated.

3.5 Magnetic Field Effects

The magnetic field produced by the underwater power cables varies depending on if there is AC or DC power transmission, how many core conductors are in the cable, proximity of the cables to one another, and current flow through the conductors. This magnetic field affects the cables losses, electromechanical forces between cables, and wildlife.

3.5.1 Effects on Wildlife

The presence of artificial, man-made, magnetic fields present in the ocean is increasing. These artificial magnetic fields are superimposed onto the Earth's magnetic field. These added magnetic fields could influence spatial patterns in submarine life [40,41]. Some variants of underwater life use the Earth's magnetic field to navigate. These superimposed magnetic fields from underwater power cables could cause confusion of spatial orientation for underwater life [40,41]. The magnetic field from the Earth is static and has a flux of 60μT at the magnetic poles [40,41]. The flux at the equator is 30μT [40,41]. The worst-case magnetic flux per ampere of current would be $\frac{0.2}{r}$ μT/A for an underwater power cable. Where *r* is the distance from the core conductor. To minimize the impact of the underwater power cables for the underwater life it would be ideal to have the superimposed magnetic

fields to be small in comparison with the Earth's magnetic field. Ways to minimize the magnetic field outside the underwater power cable could be as follows [27]:

- High permeability metal for the cables armor
- Bundling of the conductors
- Smaller current loading
- Burying the cables
- Cable type

The static and time varying magnetic fields affect submarine life in different ways. Static magnetic fields affect submarine life more significantly than time varying magnetic fields [40,41]. A study of the wildlife at an offshore power installation site would have to be conducted in order to determine the sensitivity of the local wildlife to magnetic fields.

3.5.2 Electromechanical Forces

There are mechanical forces that exist between electric current carrying wires [34]. A current carrying conductor while in the presence of a magnetic field, which may be created by another conductor, will experience a mechanical force on it. This mechanical force is called the Lorentz force. For a current carrying conductor in the presence of a magnetic field, the force on the conductor can be described as follows [34]:

$$F = I\ell \times B \tag{3.2}$$

Where I is the electrical current flow in the conductor, ℓ is a vector whose magnitude is the length of the conductor and whose direction is the same as the current flow, and B is the

magnetic field in which the conductor is present. These mechanical forces can become quite significant if the conductors are placed close together, are long, or have a large current flow [34]. Larger current flows are observed during transient or fault conditions. This could cause the conductors to whip or cause damage to the insulation in the case of multi-core cables [31,34].

3.5.3 Magnetic Field Calculations

There are two methods of power transmission that are used, AC and DC. AC power transmission results in a time harmonic magnetic field. DC power transmission results in a static magnetic field. The magnetic fields for the various configurations of underwater power cables, Figures 3-2a and 3-2b, will be modeled and analyzed. It will be assumed that the system is operating in steady state and is balanced. The equation governing the magnetic field produced by current flowing through a wire is given as follows [34]:

$$B = \frac{\mu I}{2\pi\rho} \tag{3.3}$$

Where B is the magnetic field or flux density, I is the current flowing through the wire, μ is the permeability of the space surrounding the wire, and ρ is the radial distance outside the conductor.

3.5.3.1 Single-Core Magnetic Field for AC Transmission

For AC power transmission there are three conductors that are used to transmit the electrical power. Superposition can be applied to find the resultant magnetic field in the presence of these three conductors. For a balanced three-phase system, the following relation exists between the phase currents [30]:

$$I_A + I_B + I_C = 0 \tag{3.4}$$

The resultant magnetic field, using superposition can be determined to be as follows:

$$B_T = \frac{\mu_0 |I|}{2\pi}\left[\frac{\cos \omega t}{\sqrt{(x+D)^2+y^2}} + \frac{\cos\left(\omega t+\frac{2\pi}{3}\right)}{\sqrt{x^2+y^2}} + \frac{\cos\left(\omega t-\frac{2\pi}{3}\right)}{\sqrt{(x-D)^2+y^2}}\right] \tag{3.5}$$

Where an H configuration with spacing distance D has been assumed. The operating frequency of the transmission line has been assumed to be 60Hz. The magnetic field that is resultant at any point (x,y) is time varying. Figure 3-3a-f below show resultant simulations for the magnetic field with an assumed magnitude of current to be 1A and a H configuration spacing of 5m. The simulation was performed for six time points during one cycle of steady state operation of the transmission line.

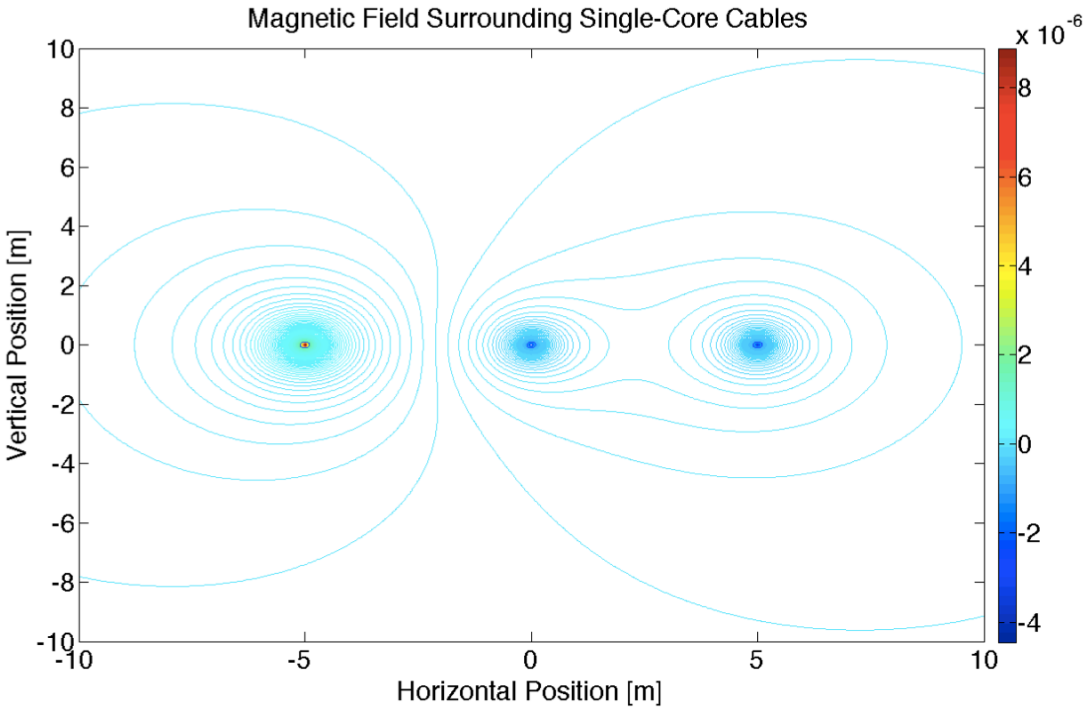

Figure 3-3a: Magnetic Field [T] at t=0s

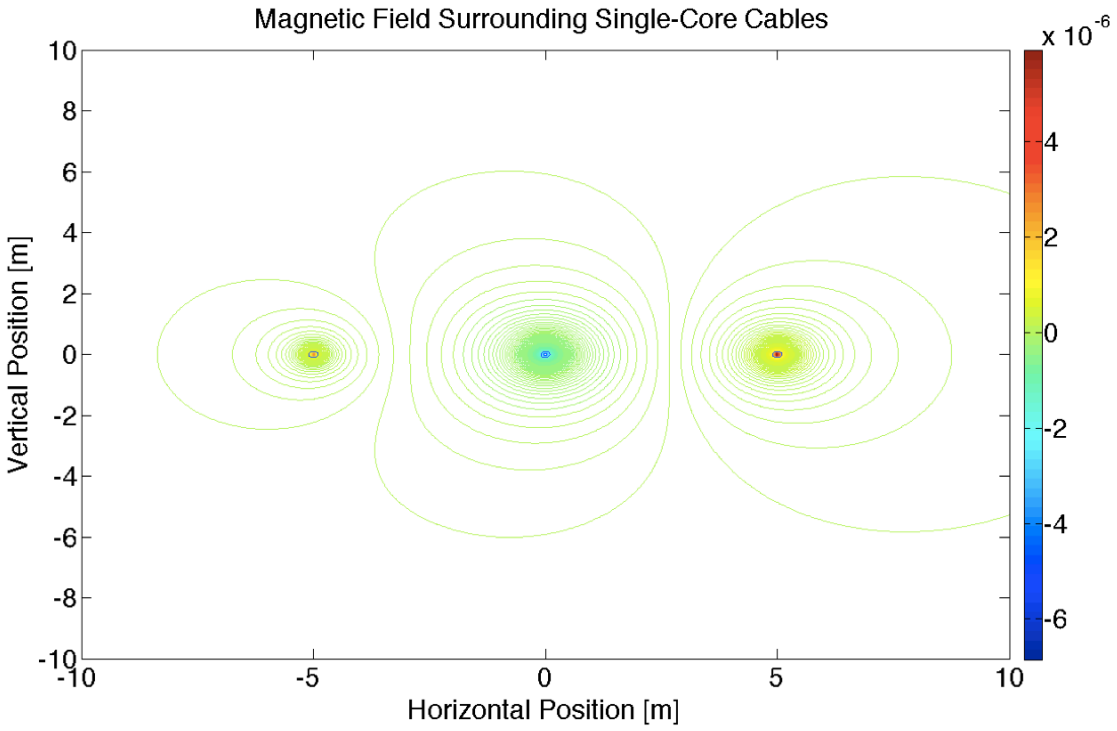

Figure 3-3b: Magnetic Field [T] at t=1/300s

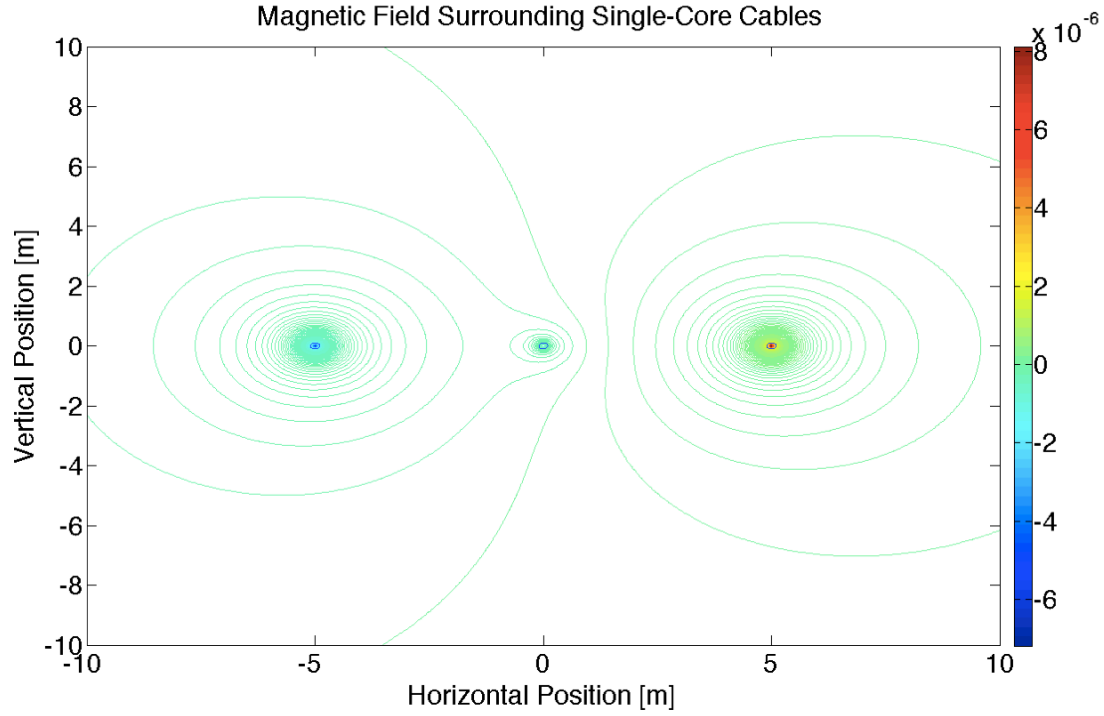

Figure 3-3c: Magnetic Field [T] at t=2/300s

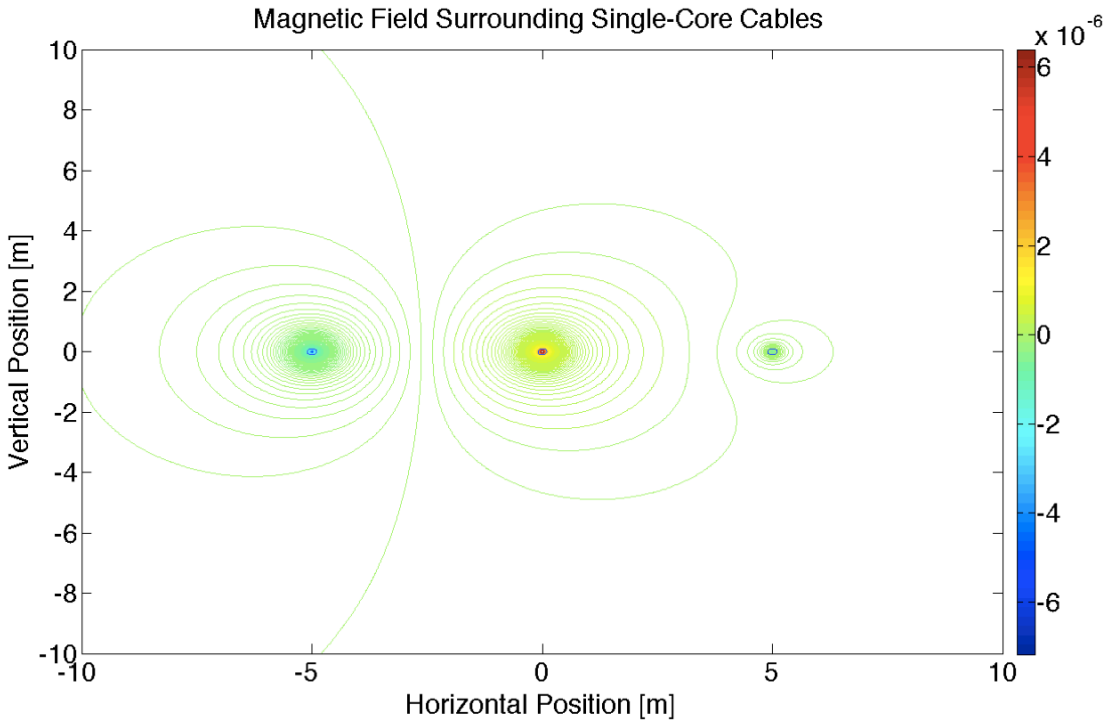

Figure 3-3d: Magnetic Field [T] at t=3/300s

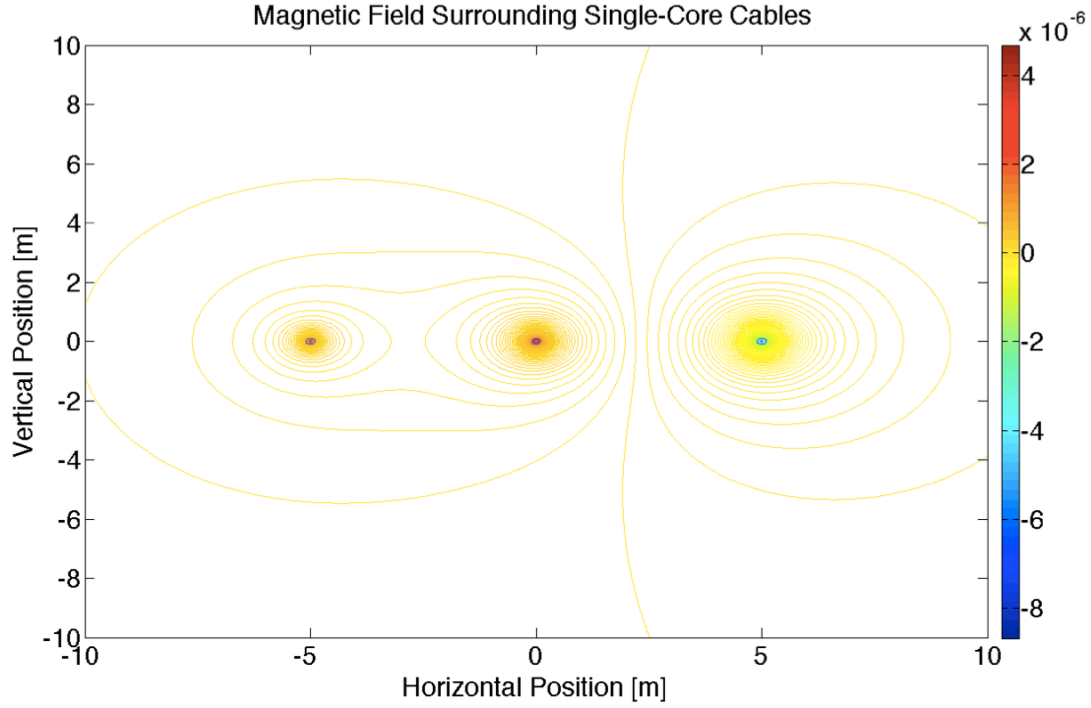

Figure 3-3e: Magnetic Field [T] at t=4/300s

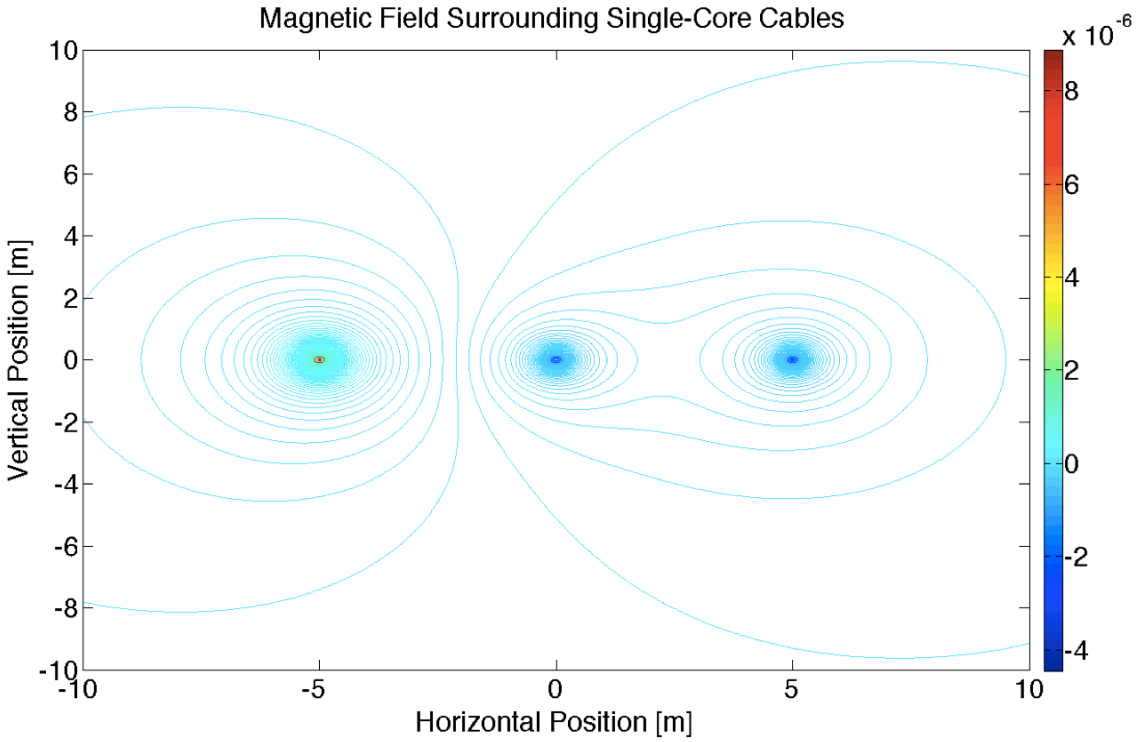

Figure 3-3f: Magnetic Field [T] at t=1/60s

These simulations show how the magnetic field will vary in space as time progresses. It can be observed that there is a region of magnetic field cancellation that fluctuates with time. Additionally, it can be seen that the magnetic field within less that one meters distance from the conductor has the strongest magnetic field. The magnetic field is approximately less than 1μT in this region. This will increase linearly as the magnitude of the balanced phase currents increases. There is no significant cancellation of the magnetic fields for this phase configuration.

3.5.3.2 Three-Core Magnetic Field for AC Transmission

This medium of AC power transmission utilizes a single three-core cable. If the radius of each core of the cable is defined as r, then the following equation can be developed to represent the magnetic field for a three-core cable:

$$B_T = \frac{\mu|I|}{2\pi}\left[\frac{\cos\omega t}{\sqrt{(x+r)^2+\left(y-\frac{r}{\sqrt{3}}\right)^2}} + \frac{\cos\left(\omega t+\frac{2\pi}{3}\right)}{\sqrt{(x-r)^2+\left(y-\frac{r}{\sqrt{3}}\right)^2}} + \frac{\cos\left(\omega t-\frac{2\pi}{3}\right)}{\sqrt{x^2+\left(y+\frac{2r}{\sqrt{3}}\right)^2}}\right] \quad (3.6)$$

The operating frequency of the transmission line has been assumed to be 60Hz. The magnetic field that is resultant at any point (*x,y*) is time varying. Figure 3-4a-f below show resultant simulations for the magnetic field with an assumed magnitude of current to be 1A. The simulation was performed for six time points during one cycle of steady state operation of the transmission line.

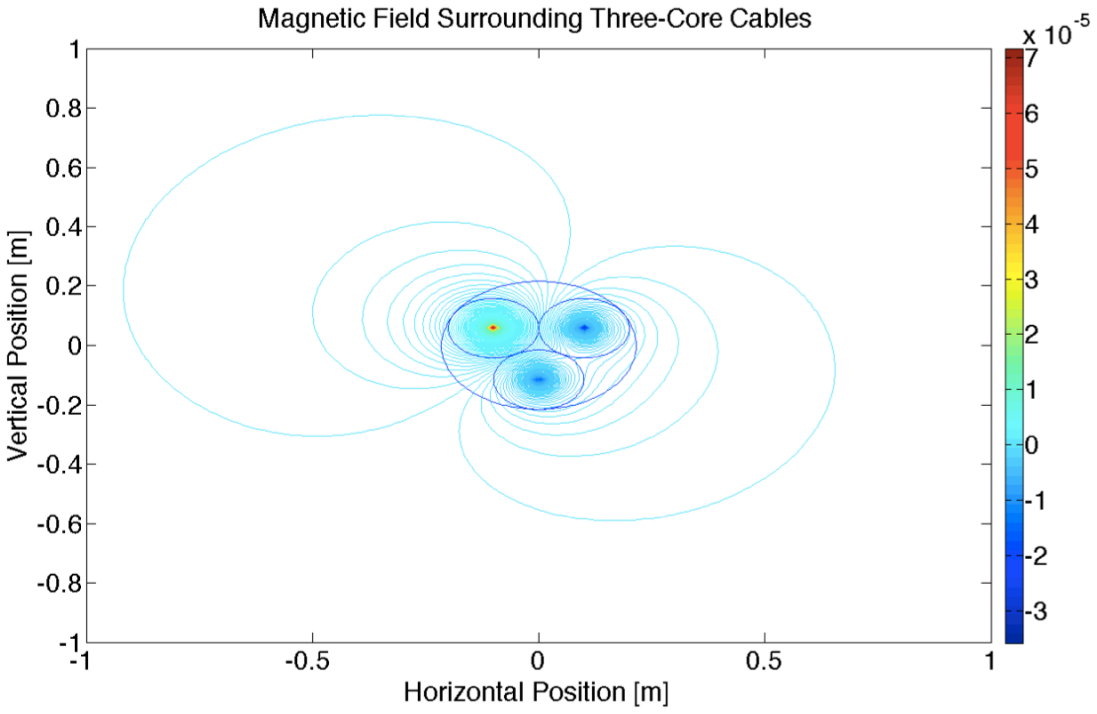

Figure 3-4a: Magnetic Field [T] at t=0s

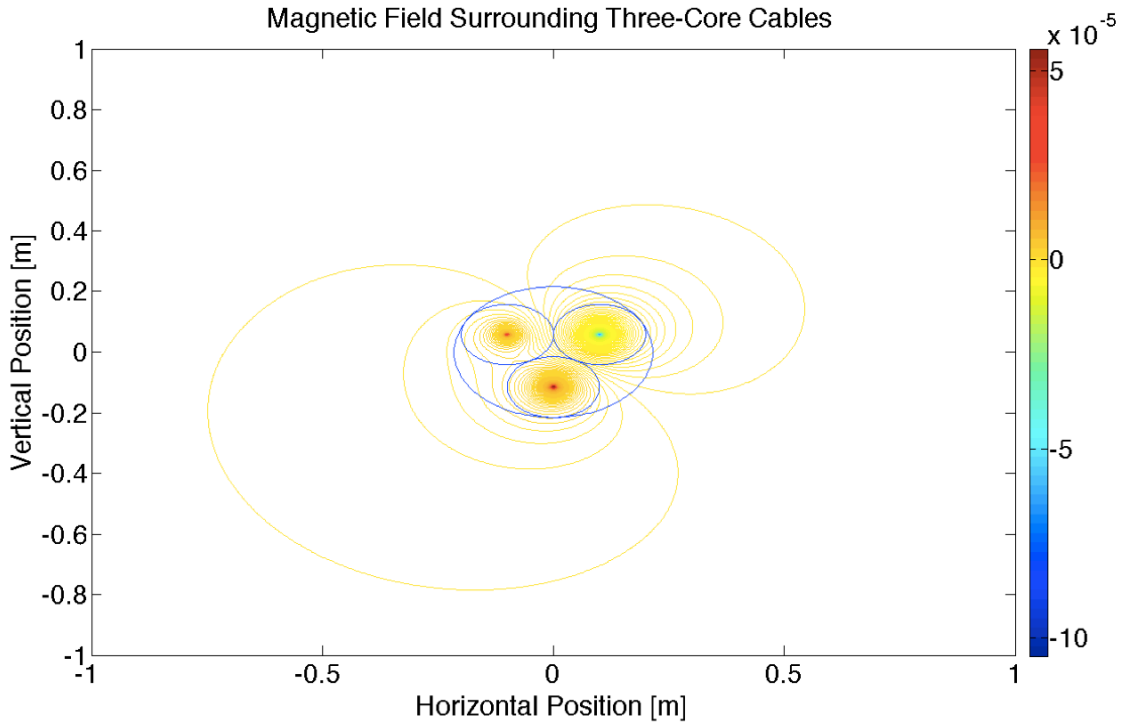

Figure 3-4b: Magnetic Field [T] at t=1/300s

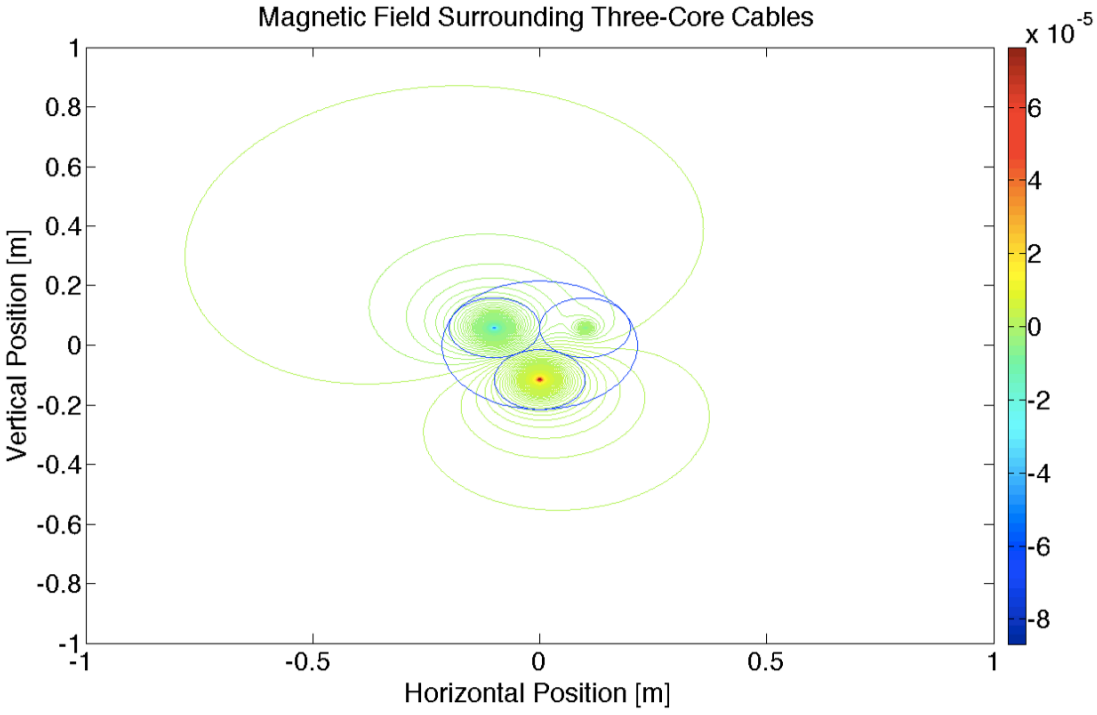

Figure 3-4c: Magnetic Field [T] at t=2/300s

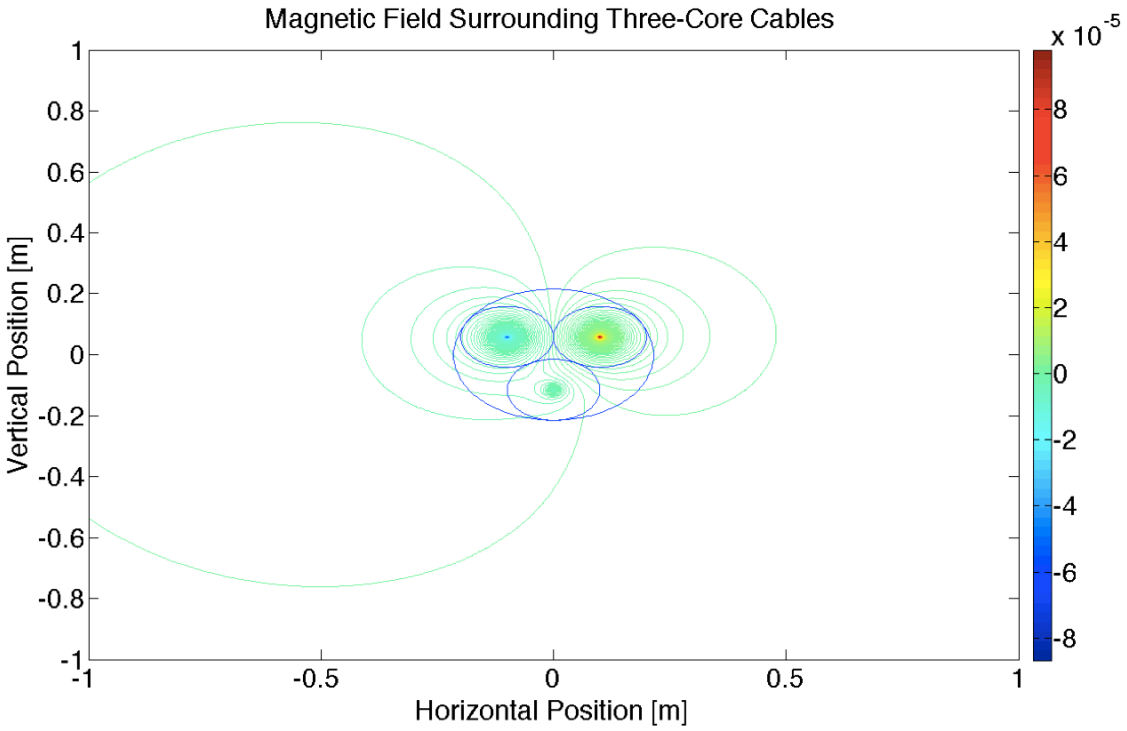

Figure 3-4d: Magnetic Field [T] at t=3/300s

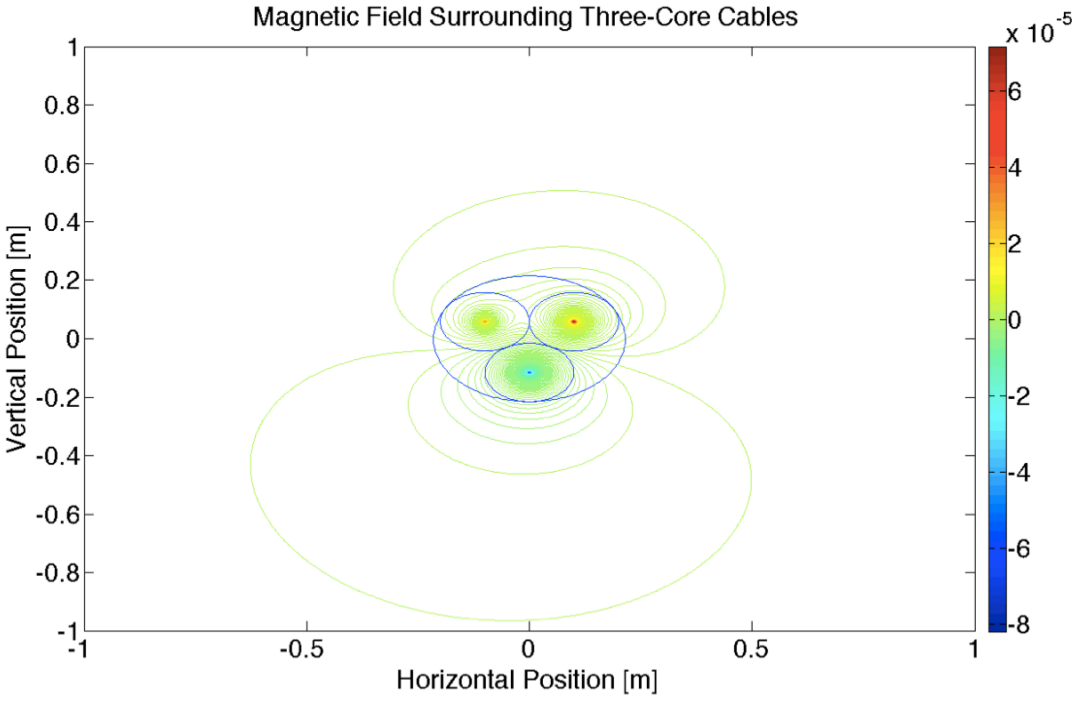

Figure 3-4e: Magnetic Field [T] at t=4/300s

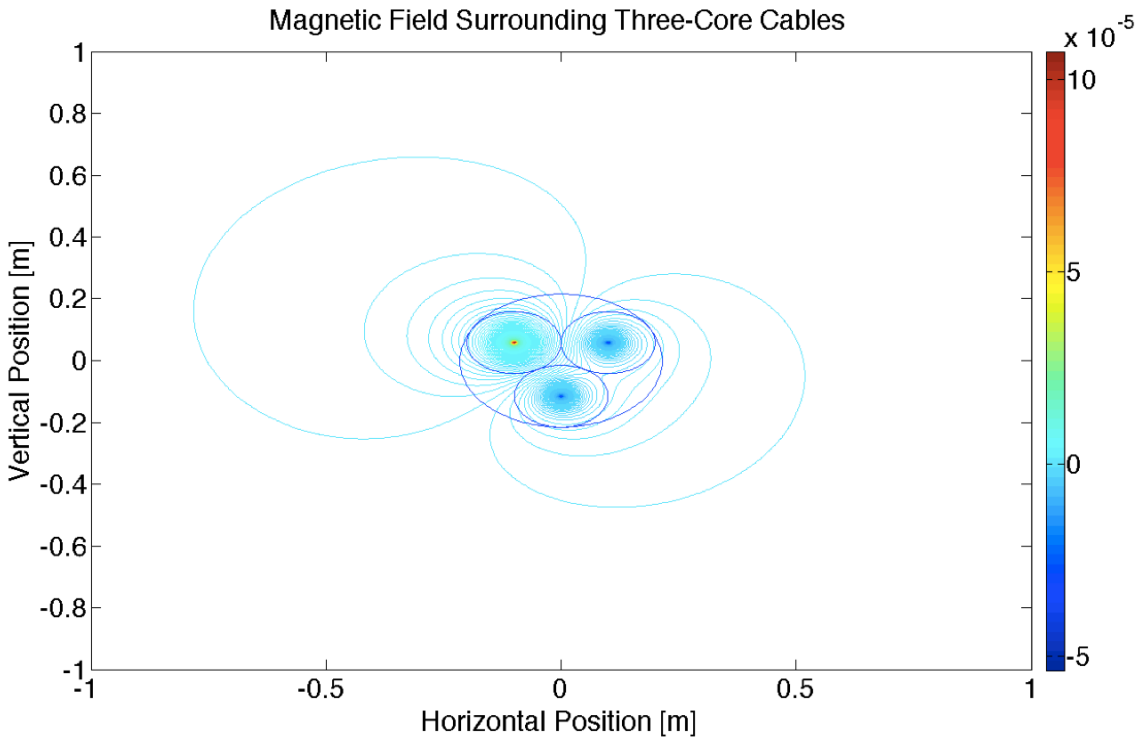

Figure 3-4f: Magnetic Field [T] at t=1/60s

These simulations show how the magnetic field will vary in space as time progresses. Further analysis of the equation describing the magnetic field shows that the magnitude of the magnetic field decays approximately proportional to $\frac{1}{\rho^2}$ outside of the cable. This can be justified by observing that the conductors are close together and the sum of the phase currents is zero. This causes a cancellation of the magnetic field. This result will be discussed further in a later section.

3.5.3.3 Single-Core Magnetic Field for DC Transmission

For DC power transmission there are two cables that are used to transmit the electric power. For a DC current flow, the magnetic field produced is static and not time varying. Again,

superposition of the magnetic fields can be applied to find the total field in the vicinity of the cables. For two single-core DC cables, the following relation exists for the currents in the cables [30]:

$$I_+ = -I_- = I \tag{3.7}$$

This relationship shows that the sending current is equal to the negative of the return current. The resultant magnetic field, assuming a cable separation, $2D$, can be found to be as follows:

$$B_T = \frac{\mu_0 |I|}{2\pi}\left[\frac{1}{\sqrt{(x+D)^2+y^2}} - \frac{1}{\sqrt{(x-D)^2+y^2}}\right] \tag{3.8}$$

The magnetic field that is resultant at any point (*x,y*) is time invariant. Figure 3-5 below shows the resultant simulation for the magnetic field with an assumed magnitude of current to be 1A, a cable spacing of 5m, and operating in steady state.

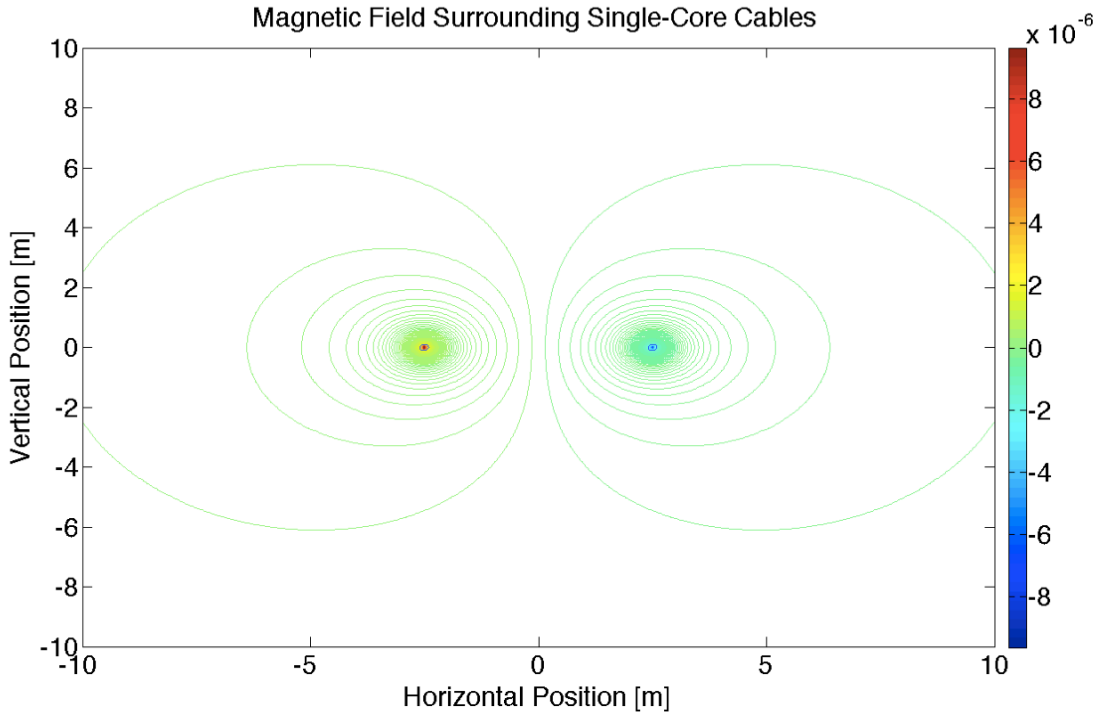

Figure 3-5: Magnetic Field [T] for DC Cables

These simulations show how the magnetic field will vary in space. It can be observed that there is a region of magnetic field cancellation at the midpoint between the conductors.

3.5.3.4 Two-Core Magnetic Field for DC Transmission

This medium of DC power transmission utilizes a single two-core cable. The equation for the magnetic field is a special case of the previous where two single-core cables were used. In this case the spacing between conductors is r, which is the radius of each core within the cable. The equation for the magnetic field will be as follows:

$$B_T = \frac{\mu_0 |I|}{2\pi}\left[\frac{1}{\sqrt{(x+r)^2+y^2}} - \frac{1}{\sqrt{(x-r)^2+y^2}}\right] \tag{3.9}$$

The magnetic field that is resultant at any point (x,y) is time invariant. Figure 3-6 below shows the resultant simulation for the magnetic field with an assumed magnitude of current to be 1A, a core spacing of 0.2m, and operating in steady state.

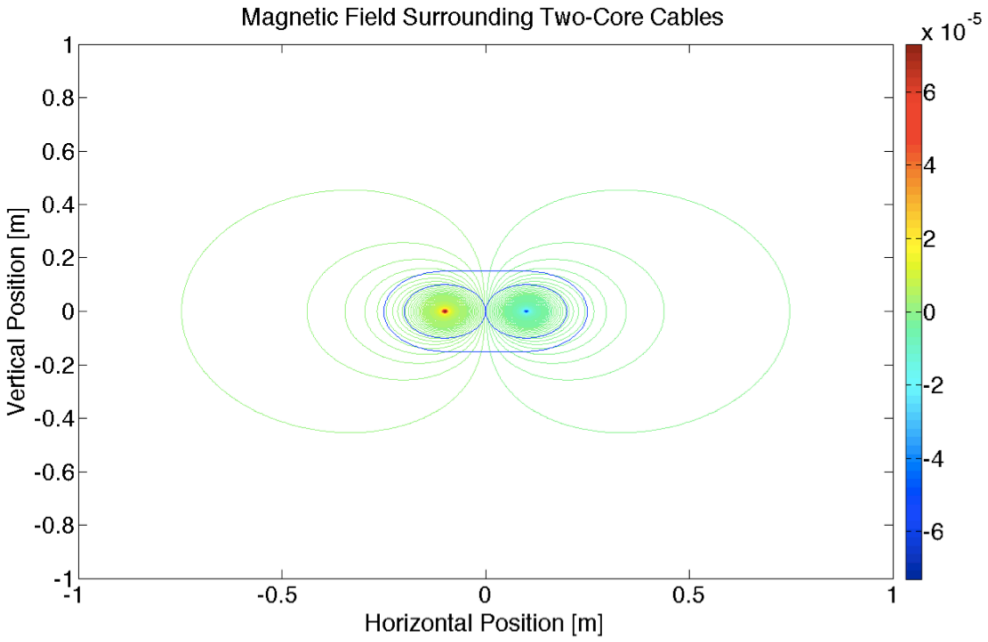

Figure 3-6: Magnetic Field [T] for DC Multi-Core Cable

These simulations show how the magnetic field will vary in space. These results are similar as for the previous case. In this case the conductors are much closer together. This allows for a more significant magnetic field cancellation far outside the cable.

3.6 The Wave Equation

Maxwell's equations for a linear, isotropic, homogenous, lossy dielectric, and charge free space are as follows [34]:

$$\nabla E_s = 0 \tag{3.10}$$

$$\nabla H_s = 0 \tag{3.11}$$

$$\nabla \times E_s = -j\omega\mu H_s \tag{3.12}$$

$$\nabla \times H_s = \sigma + j\omega\varepsilon \tag{3.13}$$

For a cylindrical coordinate system, the divergence and curl of a vector, $A = A_\rho \overrightarrow{a_\rho} + A_\phi \overrightarrow{a_\phi} + A_z \overrightarrow{a_z}$, can be described as follows [34]:

$$\nabla A = \frac{1}{\rho}\frac{\partial A_\rho}{\partial \rho}\left(\rho A_\rho\right) + \frac{1}{\rho}\frac{\partial A_\phi}{\partial \phi} + \frac{\partial A_z}{\partial z} \tag{3.14}$$

$$\nabla \mathrm{x} A = \left[\frac{1}{\rho}\frac{\partial A_z}{\partial \phi} - \frac{\partial A_\phi}{\partial z}\right]\overrightarrow{a_\rho} + \left[\frac{\partial A_\rho}{\partial z} - \frac{\partial A_z}{\partial \rho}\right]\overrightarrow{a_\phi} + \frac{1}{\rho}\left[\frac{1}{\rho}\frac{\partial(\rho A_\phi)}{\partial \rho} - \frac{\partial A_\rho}{\partial \phi}\right]\overrightarrow{a_z} \tag{3.15}$$

These are the definitions of the divergence and curl of a vector respectively. From these definitions, Maxwell's equations for a cylindrical coordinate system can be found to be as follows [34,42]:

$$\frac{\partial H_z}{\rho \partial \phi} - \frac{\partial H_\phi}{\partial z} = (\sigma + j\omega\varepsilon)E_\rho \tag{3.16}$$

$$\frac{\partial H_\rho}{\partial z} - \frac{\partial H_z}{\partial \rho} = (\sigma + j\omega\varepsilon)E_\phi \tag{3.17}$$

$$\frac{1}{\rho}\left[\frac{\partial(\rho H_\phi)}{\partial \rho} - \frac{\partial H_\rho}{\partial \phi}\right] = (\sigma + j\omega\varepsilon)E_z \tag{3.18}$$

$$\frac{\partial E_z}{\rho \partial \phi} - \frac{\partial E_\phi}{\partial z} = (-j\omega\mu)H_\rho \tag{3.19}$$

$$\frac{\partial E_\rho}{\partial z} - \frac{\partial E_z}{\partial \rho} = (-j\omega\mu)H_\phi \tag{3.20}$$

$$\frac{1}{\rho}\left[\frac{\partial(\rho E_\phi)}{\partial \rho} - \frac{\partial E_\rho}{\partial \phi}\right] = (-j\omega\varepsilon)H_z \tag{3.21}$$

For straight conductors, it is known that the magnetic field is circular and electric field is radial. This allows all partial derivatives with respect to ϕ be set to zero. This set of equations thus reduces to the following [42]:

$$-\frac{\partial H_\phi}{\partial z} = (\sigma + j\omega\varepsilon)E_\rho \tag{3.22}$$

$$\frac{\partial H_\rho}{\partial z} - \frac{\partial H_z}{\partial \rho} = (\sigma + j\omega\varepsilon)E_\phi \tag{3.23}$$

$$\frac{1}{\rho}\left[\frac{\partial(\rho H_\phi)}{\partial \rho}\right] = (\sigma + j\omega\varepsilon)E_z \tag{3.24}$$

$$-\frac{\partial E_\phi}{\partial z} = (-j\omega\mu)H_\rho \tag{3.25}$$

$$\frac{\partial E_\rho}{\partial z} - \frac{\partial E_z}{\partial \rho} = (-j\omega\mu)H_\phi \tag{3.26}$$

$$\frac{1}{\rho}\left[\frac{\partial(\rho E_\phi)}{\partial \rho}\right] = (-j\omega\varepsilon)H_z \tag{3.27}$$

These equations can be split into two special cases, when the magnetic field is circular, and when the electric field is circular. The equations for each case are summarized in Table 3-3 below.

Table 3-3: Maxwell's Equations

Circular Magnetic Field	Circular Electric Field
$-\frac{\partial H_\phi}{\partial z} = (\sigma + j\omega\varepsilon)E_\rho$	$\frac{\partial H_\rho}{\partial z} - \frac{\partial H_z}{\partial \rho} = (\sigma + j\omega\varepsilon)E_\phi$
$\frac{1}{\rho}\left[\frac{\partial(\rho H_\phi)}{\partial \rho}\right] = (\sigma + j\omega\varepsilon)E_z$	$-\frac{\partial E_\phi}{\partial z} = (-j\omega\mu)H_\rho$
$\frac{\partial E_\rho}{\partial z} - \frac{\partial E_z}{\partial \rho} = (-j\omega\mu)H_\phi$	$\frac{1}{\rho}\left[\frac{\partial(\rho E_\phi)}{\partial \rho}\right] = (-j\omega\varepsilon)H_z$

Taking the case when the magnetic field is circular, the equations can be substituted together to yield the following equation, which describes the magnetic field surrounding a conductor [42,43].

$$\frac{\partial}{\partial \rho}\left[\frac{1}{\rho}\frac{\partial(\rho H_\phi)}{\partial \rho}\right] + \frac{\partial^2 H_\phi}{\partial z^2} = \gamma^2 H_\phi \tag{3.28}$$

Where $\gamma^2 = (\sigma\omega\mu j - \omega^2\varepsilon\mu)$. The general solution to this can be obtained by using the separation of variables. Assuming that $H_\phi = R(\rho)\cdot Z(z)$ and substituting this into the above equation gives the following equation:

$$Z(z)\frac{\partial^2 R(\rho)}{\partial \rho^2} + \frac{1}{\rho}Z(z)\frac{R(\rho)}{\partial \rho} - \frac{1}{\rho^2}Z(z)R(\rho) + R(\rho)\frac{\partial Z(z)}{\partial z^2} - \gamma^2 R(\rho)Z(z) = 0 \tag{3.29}$$

Dividing this equation by $R(\rho)\cdot Z(z)$ gives the following equation:

$$\frac{1}{R(\rho)}\frac{\partial^2 R(\rho)}{\partial \rho^2} + \frac{1}{\rho}\frac{1}{R(\rho)}\frac{\partial R(\rho)}{\partial \rho} - \frac{1}{\rho^2} + \frac{1}{Z(z)}\frac{\partial^2 Z(z)}{\partial z^2} - \gamma^2 = 0 \tag{3.30}$$

This can then be separated into the following two equations:

$$\frac{1}{Z(z)}\frac{\partial^2 Z(z)}{\partial z^2} = \Gamma^2 \tag{3.31}$$

$$\frac{1}{R(\rho)}\frac{\partial^2 R(\rho)}{\partial \rho^2} + \frac{1}{\rho}\frac{1}{R(\rho)}\frac{\partial R(\rho)}{\partial \rho} - \frac{1}{\rho^2} = \gamma^2 - \Gamma^2 \tag{3.32}$$

Where the variable Γ^2 has been chosen such that a general solution can be formed. The solution to equation (3.31) is as follows:

$$Z(z) = Ae^{\Gamma z} + Be^{-\Gamma z} \tag{3.33}$$

This is the equation governing the wave propagation along the length of the transmission line. The coefficient Γ is known as the propagation constant along the length of the transmission line. The solution to equation (3.32) is in the form of Bessel functions [42]. The solution is as follows:

$$R(\rho) = C \cdot I_1\left(\rho\sqrt{\gamma^2 - \Gamma^2}\right) + D \cdot K_1\left(\rho\sqrt{\gamma^2 - \Gamma^2}\right) \tag{3.34}$$

For this equation it should be observed that γ is referring to the propagation constant radial to the transmission line. For a conductor operating at low frequency, the displacement current is negligible. The propagation constants thus become the following:

$$\Gamma = (1 + j)\sqrt{\pi f \mu \sigma} \tag{3.35}$$

$$\gamma = \sqrt{j\sigma\mu\omega} \tag{3.36}$$

Applying the boundary condition that H_ϕ goes to zero as the length of the transmission line approaches infinity, results in a simplified version of equation (3.33). This boundary condition necessitates that the coefficient A equal zero. This results in the following equation representing the wave propagation over the length of the transmission line:

$$Z = Be^{-\Gamma z} \tag{3.37}$$

The resultant equation representing H_ϕ is the product of equations (3.34) and (3.37) as follows:

$$H_\phi = e^{-\Gamma z}\left\{A \cdot I_1\left(\rho\sqrt{\gamma^2 - \Gamma^2}\right) + B \cdot K_1\left(\rho\sqrt{\gamma^2 - \Gamma^2}\right)\right\} \tag{3.38}$$

The coefficients *A* and *B* are combined constants. Applying Maxwell's equations (3.22) and (3.24) the following equations for the radial electric field and longitudinal electric field can be determined to be as follows:

$$E_\rho = \frac{\Gamma}{\sigma + j\omega\varepsilon} e^{-\Gamma z} \left\{ A \cdot I_1\left(\rho\sqrt{\gamma^2 - \Gamma^2}\right) + B \cdot K_1\left(\rho\sqrt{\gamma^2 - \Gamma^2}\right) \right\} \tag{3.39}$$

$$E_z = \frac{\Gamma}{\sigma + j\omega\varepsilon} e^{-\Gamma z} \left\{ A \cdot I_0\left(\rho\sqrt{\gamma^2 - \Gamma^2}\right) - B \cdot K_0\left(\rho\sqrt{\gamma^2 - \Gamma^2}\right) \right\} \tag{3.40}$$

Equations (3.39) and (3.40) were evaluated using two identities of Bessel functions. These identities are as follows [42,44]:

$$\frac{d}{dx}(x^n I_n) = x^n I_{n-1} \tag{3.41}$$

$$\frac{d}{dx}(x^n K_n) = -x^n K_{n-1} \tag{3.42}$$

Equations (3.38) through (3.40) represent the general solutions for the magnetic and electric fields that exist along a cylindrical conductor transmission line.

3.6.1 Surface Impedances

From the equations describing the magnetic and electric fields that exist for a cylindrical transmission line, surface impedances can be defined for various configurations of cylindrical conductor. There are three cases that will be examined; a solid conductor, an infinite conductor, and hollow cylindrical shells.

3.6.1.1 Solid Conductor

For a solid conductor with radius *b*, the impedance can be obtained from the longitudinal electric field. There are two boundary conditions to be observed for the solid core

transmission line. These boundary conditions are that if $\rho = 0$, the magnetic field is finite and if $\rho = b$ the magnetic field is defined as follows:

$$H_\phi = \frac{I}{2\pi b} \tag{3.43}$$

From equation (3.38), applying the first boundary condition results in the necessity of the constant *B* to be zero. Applying the second boundary condition results in the following equation defining the constant *A*.

$$A = \frac{I}{2\pi b} \frac{e^{\Gamma z}}{I_1\left(b\sqrt{\gamma^2-\Gamma^2}\right)} \tag{3.44}$$

Substituting this into equation (3.40) results in the following equation for the longitudinal electric field [42,45]:

$$E_z = I \frac{\Gamma}{2\pi b(\sigma+j\omega\varepsilon)} \frac{I_0\left(b\sqrt{\gamma^2-\Gamma^2}\right)}{I_1\left(b\sqrt{\gamma^2-\Gamma^2}\right)} \tag{3.45}$$

From this equation, the impedance of the solid core conductor can be found as the ratio of the longitudinal electric field to the current. Thus, the following equation represents the impedance of a solid core conductor per unit length.

$$Z_{solid\ core} = \frac{\Gamma}{2\pi b(\sigma+j\omega\varepsilon)} \frac{I_0\left(b\sqrt{\gamma^2-\Gamma^2}\right)}{I_1\left(b\sqrt{\gamma^2-\Gamma^2}\right)} \tag{3.46}$$

3.6.1.2 Infinite Conductor

For a hollow infinite conductor with inner radius, *a,* and infinite outer radius, the impedance can be found from the longitudinal electric field. There are two boundary conditions for the infinite conductor. These boundary conditions are that if $\rho = \infty$ the magnetic field is zero and at $\rho = a$ the magnetic field is defined as follows:

$$H_\phi = \frac{I}{2\pi a} \tag{3.47}$$

The first boundary condition implies that in equation (3.38) the constant coefficient *A* is zero. Applying the second boundary condition allows for the constant coefficient B to be determined as follows:

$$B = \frac{I}{2\pi a}\frac{e^{\Gamma z}}{K_1\left(a\sqrt{\gamma^2-\Gamma^2}\right)} \tag{3.48}$$

Substituting this into equation (3.40) results in the following equation for the longitudinal electric field [42,45]:

$$E_z = I\frac{\Gamma}{2\pi a(\sigma+j\omega\varepsilon)}\frac{K_0\left(a\sqrt{\gamma^2-\Gamma^2}\right)}{K_1\left(a\sqrt{\gamma^2-\Gamma^2}\right)} \tag{3.49}$$

From this equation, the impedance of the infinite hollow conductor can be found as the ratio of the longitudinal electric field to the current. Thus, the following equation represents the impedance of an infinite hollow conductor per unit length.

$$Z_{inf} = \frac{\Gamma}{2\pi a(\sigma+j\omega\varepsilon)}\frac{K_0\left(a\sqrt{\gamma^2-\Gamma^2}\right)}{K_1\left(a\sqrt{\gamma^2-\Gamma^2}\right)} \tag{3.50}$$

It can also be noted that the permeability of water is similar to that of air. If the cables are operating under balanced three phase conditions, there will be no neutral current flow. In the case of single-wire earth return, there will be no current flow in the water surrounding the cables. This implies that a similar approximation of the impedance as for the overhead conductors can be made. If the underwater cables are placed close to each other, the following can be used to approximate the impedance of the body of water surrounding the cables while including the mutual effects between the other cables [45].

$$Z_{inf} = j\omega\frac{\mu}{2\pi}ln\left(\frac{GMD}{a}\right) \tag{3.51}$$

Where *GMD* is the geometric mean distance between the cables [30], assuming the transmission line has been transposed.

3.6.1.3 Hollow Cylindrical Shells

This methodology for finding the impedance of conductors can be extended to the case of a hollow cylindrical shell. This hollow cylindrical shell will be defined as having an inner radius, *a*, and outer radius, *b*. It will be assumed for generality that the current enclosed by the inner surface is $-I_a$ and the current enclosed by the outer surface is I_b. This allows for the determination of the boundary conditions at the inner and outer conductor surface. Equation (3.38) can be written as the following equations, accounting for both of the boundary conditions [42,45].

$$\frac{-I_a}{2\pi a} = e^{-\Gamma z}\{A \cdot I_1(a\mathrm{T}) + B \cdot K_1(a\mathrm{T})\} \tag{3.52}$$

$$\frac{I_b}{2\pi b} = e^{-\Gamma z}\{A \cdot I_1(b\mathrm{T}) + B \cdot K_1(b\mathrm{T})\} \tag{3.53}$$

Where, $\mathrm{T} = \sqrt{\gamma^2 - \Gamma^2}$ for simplicity. From equations (3.52) and (3.53), the following can be used to evaluate constant coefficients *A* and *B*.

$$\begin{bmatrix} A \\ B \end{bmatrix} = \begin{bmatrix} I_1(a\mathrm{T}) & K_1(a\mathrm{T}) \\ I_1(b\mathrm{T}) & K_1(b\mathrm{T}) \end{bmatrix}^{-1} \begin{bmatrix} \frac{-I_a}{2\pi a} e^{\Gamma z} \\ \frac{I_b}{2\pi b} e^{\Gamma z} \end{bmatrix} \tag{3.54}$$

$$\begin{bmatrix} A \\ B \end{bmatrix} = \frac{1}{K_1(a\mathrm{T})I_1(b\mathrm{T}) - I_1(a\mathrm{T})K_1(b\mathrm{T})} \begin{bmatrix} \frac{I_a}{2\pi a} e^{\Gamma z} K_1(b\mathrm{T}) + \frac{I_b}{2\pi b} e^{\Gamma z} K_1(a\mathrm{T}) \\ -\frac{I_a}{2\pi a} e^{\Gamma z} I_1(b\mathrm{T}) - \frac{I_b}{2\pi b} e^{\Gamma z} I_1(a\mathrm{T}) \end{bmatrix} \tag{3.55}$$

Substituting these values for A and B into equation (3.40) for the longitudinal electric field, the following equations can be obtained for the inner and outer surface [42,45].

$$E_z(a) = \frac{\Gamma}{\sigma + j\omega\varepsilon}\left[\frac{I_0(\mathrm{T}a)K_1(\mathrm{T}b) + K_0(\mathrm{T}a)I_1(\mathrm{T}b)}{I_1(\mathrm{T}b)K_1(\mathrm{T}a) - I_1(\mathrm{T}a)K_1(\mathrm{T}b)} \frac{I_a}{2\pi a} + \frac{I_0(\mathrm{T}a)K_1(\mathrm{T}a) + K_0(\mathrm{T}a)I_1(\mathrm{T}a)}{I_1(\mathrm{T}b)K_1(\mathrm{T}a) - I_1(\mathrm{T}a)K_1(\mathrm{T}b)} \frac{I_b}{2\pi b}\right] \tag{3.56}$$

$$E_z(b) = \frac{\Gamma}{\sigma + j\omega\varepsilon}\left[\frac{I_0(\mathrm{T}b)K_1(\mathrm{T}b) + K_0(\mathrm{T}b)I_1(\mathrm{T}b)}{I_1(\mathrm{T}b)K_1(\mathrm{T}a) - I_1(\mathrm{T}a)K_1(\mathrm{T}b)} \frac{I_a}{2\pi a} + \frac{I_0(\mathrm{T}b)K_1(\mathrm{T}a) + K_0(\mathrm{T}b)I_1(\mathrm{T}a)}{I_1(\mathrm{T}b)K_1(\mathrm{T}a) - I_1(\mathrm{T}a)K_1(\mathrm{T}b)} \frac{I_b}{2\pi b}\right] \tag{3.57}$$

Applying the following Bessel function identity [44]:

$$I_0(x)K_1(x) + K_0(x)I_1(x) = \frac{1}{x} \tag{3.58}$$

Equations (3.55) and (3.56) then reduce to the following:

$$E_z(a) = \frac{\Gamma}{\sigma + j\omega\varepsilon}\left[\frac{I_0(\mathrm{T}a)K_1(\mathrm{T}b)+K_0(\mathrm{T}a)I_1(\mathrm{T}b)}{I_1(\mathrm{T}b)K_1(\mathrm{T}a)-I_1(\mathrm{T}a)K_1(\mathrm{T}b)}\frac{I_a}{2\pi a} + \frac{1}{I_1(\mathrm{T}b)K_1(\mathrm{T}a)-I_1(\mathrm{T}a)K_1(\mathrm{T}b)}\frac{I_b}{2\pi baT}\right] \tag{3.59}$$

$$E_z(b) = \frac{\Gamma}{\sigma + j\omega\varepsilon}\left[\frac{1}{I_1(\mathrm{T}b)K_1(\mathrm{T}a)-I_1(\mathrm{T}a)K_1(\mathrm{T}b)}\frac{I_a}{2\pi abT} + \frac{I_0(\gamma b)K_1(\gamma a)+K_0(\gamma b)I_1(\gamma a)}{I_1(\mathrm{T}b)K_1(\mathrm{T}a)-I_1(\mathrm{T}a)K_1(\mathrm{T}b)}\frac{I_b}{2\pi b}\right] \tag{3.60}$$

From these equations it can be seen that they take the following general form [45]:

$$E_z(a) = Z_i I_a + Z_m I_b \tag{3.61}$$

$$E_z(b) = Z_m I_a + Z_e I_b \tag{3.62}$$

Where the impedances are defined as follows [42,43,45,46]:

$$Z_i = \frac{\Gamma}{2\pi a(\sigma + j\omega\varepsilon)}\frac{I_0(\mathrm{T}a)K_1(\mathrm{T}b)+K_0(\mathrm{T}a)I_1(\mathrm{T}b)}{I_1(\mathrm{T}b)K_1(\mathrm{T}a)-I_1(\mathrm{T}a)K_1(\mathrm{T}b)} \tag{3.63}$$

$$Z_m = \frac{\Gamma}{2\pi abT(\sigma + j\omega\varepsilon)[I_1(\mathrm{T}b)K_1(\mathrm{T}a)-I_1(\mathrm{T}a)K_1(\mathrm{T}b)]} \tag{3.64}$$

$$Z_e = \frac{\Gamma}{2\pi b(\sigma + j\omega\varepsilon)}\frac{I_0(\mathrm{T}b)K_1(\mathrm{T}a)+K_0(\mathrm{T}b)I_1(\mathrm{T}a)}{I_1(\mathrm{T}b)K_1(\mathrm{T}a)-I_1(\mathrm{T}a)K_1(\mathrm{T}b)} \tag{3.65}$$

These equations define the internal, mutual, and external impedances of a hollow cylindrical shell respectively.

3.6.2 Coaxial Inductance

The external inductance is the inductance of an insulation medium between two coaxial pairs. If the inner conductor has radius, a, and outer coaxial return has radius b, where $b > a$, then the inductance of the insulation medium can be calculated as follows [34,42]:

$$L_e = \frac{\mu}{I}\int_a^b H_\phi d\rho \tag{3.66}$$

Where $H_\phi = \frac{I}{2\pi\rho}$ in the gap between the coaxial pairs. The inductance, knowing this magnetic field, can then be calculated to be as follows [34,42]:

$$L = \frac{\mu}{2\pi} ln\left(\frac{b}{a}\right) \tag{3.67}$$

This allows the determination of the inductance of the layer between coaxial pairs. The total impedance of a coaxial pair can be evaluated as the sum of the impedance of the solid core, insulation inductance, and internal impedance of the outer coaxial layer [42,45].

$$Z = Z_{solid\ core} + j\omega L_e + Z_{i,outer} \tag{3.68}$$

This property can be applied to multiple coaxial pairs if the term $Z_{i,outer}$ can be evaluated for the multiple cable layers.

3.7 Line Parameters of a Single-Core AC Cable

To find the total impedance of a single-core AC power cable, the cable can be separated into a series of coaxial layers. This approximate geometry of the single-core power cable can be observed in Figure 3-2. Applying the surface impedance techniques discussed previously an equivalent impedance can be obtained for the cable and its layers. Computing these layers as a equivalent impedance can be performed using the method of composition of impedances.

3.7.1 Composition of Impedances for Three Hollow Cylindrical Shells

To observe how the composition of impedances can be applied to form a equivalent impedance, a case study will be performed, where there are two conductors C_1 and C_2 separated by an insulator C_0. Figure 3-7 below shows the geometry that will be assumed for this study.

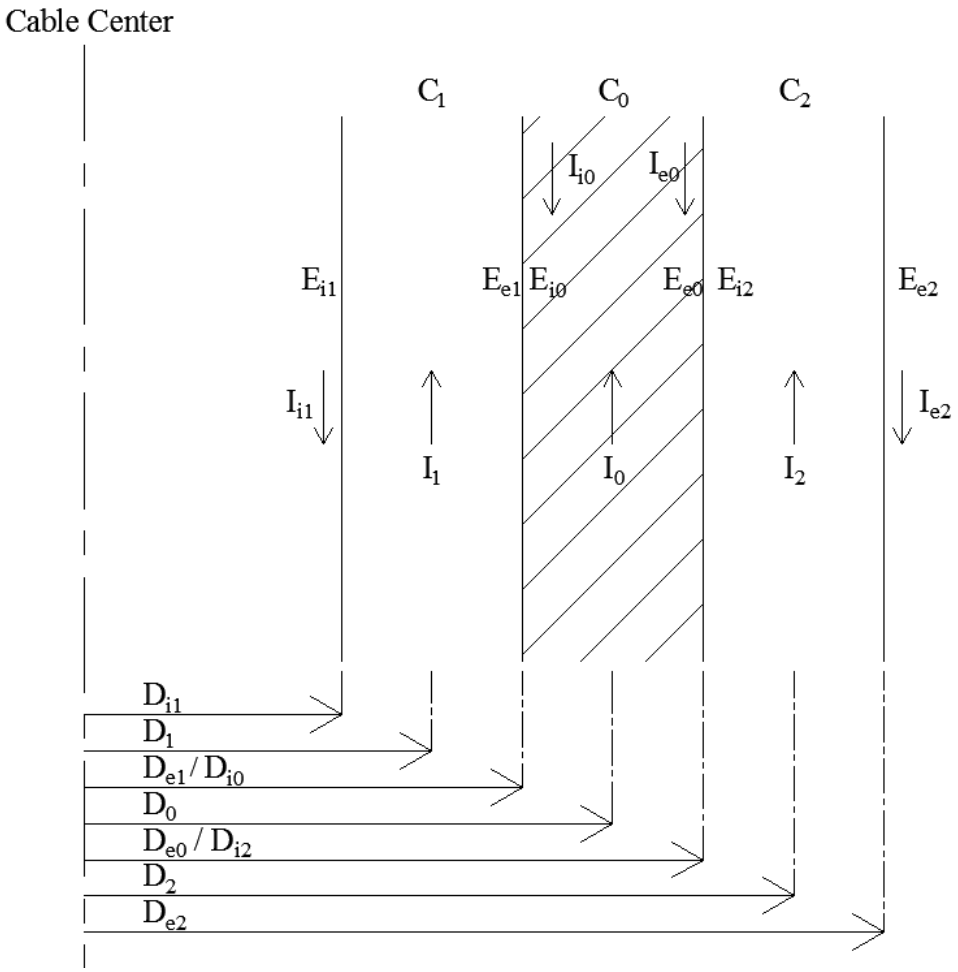

Figure 3-7: Cross Sectional View of the Three Layers

From Figure 3-7, the following statements concerning the electric currents and electric field intensities can be made at the various surfaces [45]:

$$E_i = E_{i1}$$

$$E_e = E_{e2}$$

$$E_{e1} = E_{i0}$$

$$E_{e0} = E_{i2}$$

$$E_{i0} - E_{e0} = j\frac{I_{i0}\omega\mu}{2\pi} ln\left(\frac{D_{e0}}{D_{i0}}\right) \tag{3.69}$$

$$I_i = I_{i1}$$

$$I_e = I_{e2}$$

$$I_{i0} = I_{i2} = -I_{e1} = -I_{e0}$$

These are the conditions that are applied at the boundaries between the cylindrical shells. Writing the set of equations (3.61) and (3.62) for each of the layers, the following equivalence can be created for the three hollow cylindrical shells [45]:

$$E_{i1} = I_{i1}\left[Z_{i1} - \frac{{Z_{m1}}^2}{j\omega L + Z_{e1} + Z_{i2}}\right] + I_{e2}\left[\frac{Z_{m1}Z_{m2}}{j\omega L + Z_{e1} + Z_{i2}}\right] \tag{3.70}$$

$$E_{e2} = I_{i1}\left[\frac{Z_{m2}Z_{m1}}{j\omega L + Z_{e1} + Z_{i2}}\right] + I_{e2}\left[Z_{e2} - \frac{{Z_{m2}}^2}{j\omega L + Z_{e1} + Z_{i2}}\right] \tag{3.71}$$

$$L = \frac{\mu}{2\pi} ln\left(\frac{D_{e0}}{D_{i0}}\right) \tag{3.72}$$

These equations show how the three layers have been formed into a single equivalent layer. The internal, external, and mutual surface impedances for this equivalent conductor is composed of the internal, external, and mutual surface impedances of the cylindrical shells and the inductance of the insulation medium.

3.7.2 Composition of Impedances for a Single-Core Cable

This can be extended to the case of a single-core underwater power cable. In the case of a single-core cable, using the geometry assumed in Figure 3-2, the cross sectional view of this cable can be observed to be as in Figure 3-8 below.

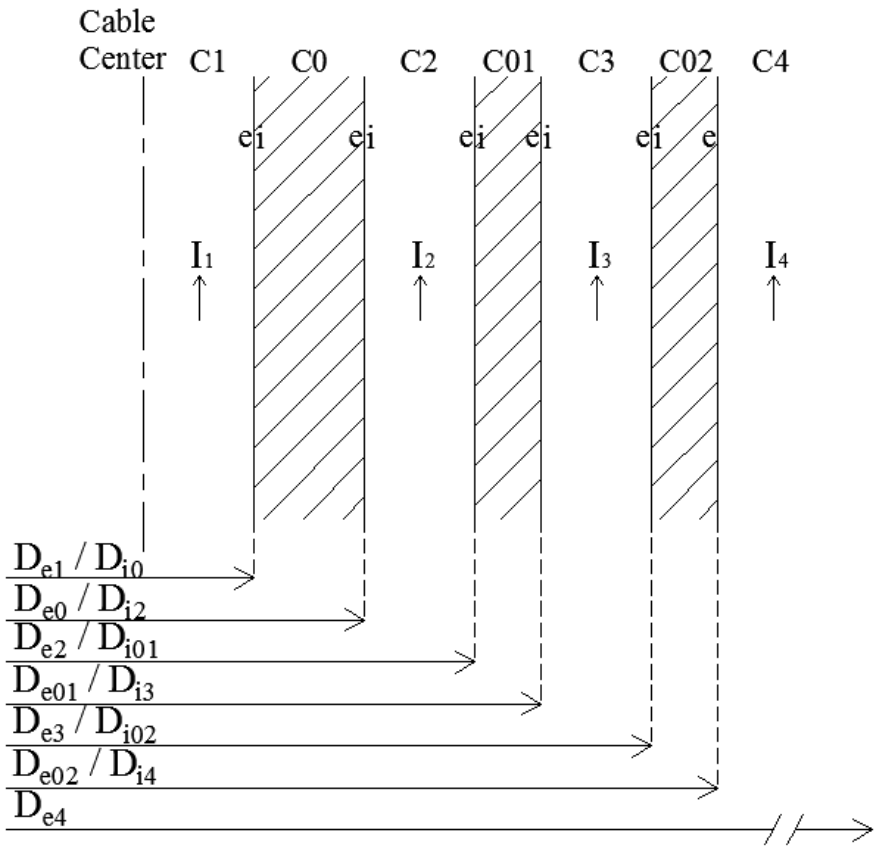

Figure 3-8: Cross Sectional View of a Single-Core Underwater Power Cable

The first layer C_1 is the core conductor, C_0 is the insulation medium, C_2 is the sheath, C_{01} is an insulation medium between the sheath and armor, C_3 is the armor, C_{02} is the outer serving of the cable, and C_4 is the sea water. Equation (3.68) can be applied to find the total impedance of the cable. In this case the internal impedance is the impedance of the core conductor C_1, the inductance term is the insulation layer C_0, and the external impedance is the internal impedance of the equivalent set of conductive layers. The boundary conditions, similar to those in equation set (3.69) can be determined for this case.

$$E_{i0} - E_{e0} = j\omega L_0$$

$$E_{i01} - E_{e01} = j\omega L_{01}$$

$$E_{i02} - E_{e02} = j\omega L_{02}$$

$$E_{e1} = E_{i0}$$

$$E_{e0} = E_{i2}$$

$$E_{e2} = E_{i01} \tag{3.73}$$

$$E_{e01} = E_{i3}$$

$$E_{e4} = E_{i02}$$

$$E_{e02} = E_{i4}$$

$$I_{i0} = I_{i2} = -I_{e0} = -I_{e1}$$

$$I_{i01} = I_{i3} = -I_{e01} = -I_{e2}$$

$$I_{i02} = I_{i4} = -I_{e02} = -I_{e3}$$

Applying all of these equations, the following relationship can be determined for the total impedance of the single-core cable [29,31]:

$$Z = Z_{e1} + j\omega L_0 + Z_{i2} - \left\{ \frac{{Z_{m2}}^2}{Z_{e2} + j\omega L_{01} + \frac{{Z_{m3}}^2}{(Z_{e3} + j\omega L_{02} + Z_{i4})}} \right\} \tag{3.74}$$

Where in this case Z_{el} and Z_{i4} are the special cases discussed previously for the solid core conductor, equation (3.46), and the infinite conductor, equation (3.50) or equation (3.51). Equation (3.74) can be used to find the inductance, and resistance of the underwater power cable per unit length.

3.7.3 Resistance and Inductance of Three Phase Single-Core AC Cables

The resistance per meter can be found from the real component of equation (3.74). The inductance per meter of the cable can be found from the imaginary part of equation (3.74) above. This resistance and inductance is for a single cable. There needs to be a term added which accounts for the mutual inductance between the cables. This term can be included into the internal impedance of the sea surrounding the cable. If each of the cables is separated by distance *d*, or on average are separated by distance *d*, the following equation can represent the equivalent internal impedance of the seawater [45].

$$Z_{i_4} = \frac{\Gamma}{2\pi a(\sigma + j\omega\varepsilon)} \frac{K_0\left(a\sqrt{\gamma^2-\Gamma^2}\right) - K_0\left(d\sqrt{\gamma^2-\Gamma^2}\right)}{K_1\left(a\sqrt{\gamma^2-\Gamma^2}\right)} \tag{3.75}$$

This is taking advantage of the knowledge that the cables are separated by 120 electrical degrees.

3.7.4 Capacitance and Conductance of Three Phase Single-Core AC Cables

The capacitance of an underwater power cable can be found from analysis of a coaxial cable. As mentioned previously, the inner layers of the cable are grounded. This causes the ground plane to exist just outside the insulation layer of the cable. For an imperfect coaxial cable, with conductor radius D_{e1} and radius to the outside of the insulation D_{e0} as per Figure 3-8, the admittance can be formulated from equations (3.38) and (3.39) as follows [42]:

$$\frac{I}{2\pi\rho} = e^{-\Gamma z}\left\{A \cdot I_1\left(\rho\sqrt{\gamma^2-\Gamma^2}\right) + B \cdot K_1\left(\rho\sqrt{\gamma^2-\Gamma^2}\right)\right\} \tag{3.76}$$

This represents the magnetic field between the core conductor and ground plane. Substituting the right hand side of this equation into equation (3.39) for the radial electric field results in the following equation for the radial electric field [42].

$$E_\rho = I\frac{\Gamma}{2\pi\rho(\sigma+j\omega\varepsilon)} \tag{3.77}$$

The potential between the inner conductor and the ground outside of the insulation can be found as follows:

$$V = \int_{D_{e1}}^{D_{e0}} I\frac{\Gamma}{2\pi\rho(\sigma+j\omega\varepsilon)}d\rho \tag{3.78}$$

The solution to equation (3.78) is as follows:

$$V = I\frac{ln\left(\frac{D_{e0}}{D_{e1}}\right)}{2\pi(\sigma+j\omega\varepsilon)} \tag{3.79}$$

From this the admittance can be found to be as follows [42]:

$$Y = \frac{2\pi(\sigma+j\omega\varepsilon)}{ln\left(\frac{D_{e0}}{D_{e1}}\right)} \tag{3.80}$$

This can be split into its real and imaginary components, where the real component is the conductance of the insulation medium and the imaginary component is the capacitance between the conductor and ground plane.

$$G = \frac{2\pi\sigma}{ln\left(\frac{D_{e0}}{D_{e1}}\right)} \tag{3.81}$$

$$C = \frac{2\pi\varepsilon}{ln\left(\frac{D_{e0}}{D_{e1}}\right)} \tag{3.82}$$

These equations (3.81) and (3.82) allow the determination of the conductance and capacitance per meter of the cable. These equations apply for all single-core underwater power cable since the internal cable layers are grounded.

3.8 Line Parameters of a Three-Core Cable

The impedance of a three-core cable can be found through numerical analysis. The expression representing the magnetic field surrounding a three-core cable is dependent on all three of the spatial dimensions. Approximations of the line parameters can be made based on observing the layer grounding and magnetic field cancellations.

3.8.1 Magnetic Field Analysis

The magnetic field produced by a three-core cable was shown previously in equation (3.6). Figure 3-9 below is a figure representing the geometry of the three-core cable that was used in the development of that equation.

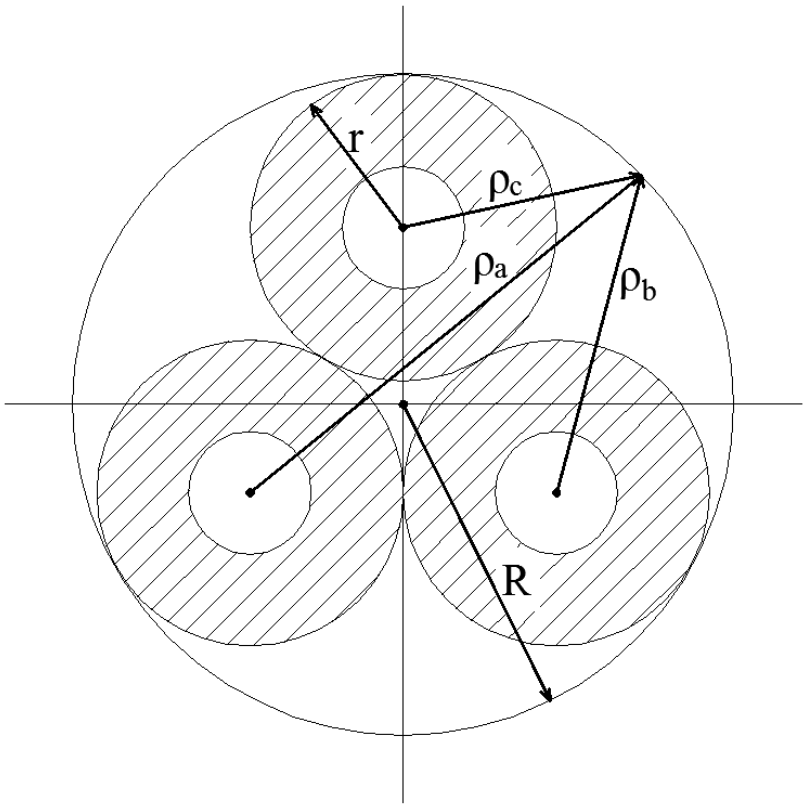

Figure 3-9: Three-Core Cable Geometry

Equation (3.6) for the magnetic field can be simplified further to the following form:

$$B = \frac{\mu}{2\pi}[K(R,\phi)\cos\omega t + I(R,\phi)\sin\omega t] \tag{3.83}$$

Where,

$$K(R,\phi) = \frac{1}{\rho_a} - \frac{1}{2\rho_b} - \frac{1}{2\rho_c} \tag{3.84}$$

$$I(R,\phi) = \frac{\sqrt{3}}{2}\left(\frac{1}{\rho_c} - \frac{1}{\rho_b}\right) \tag{3.85}$$

Where,

$$\rho_a = \sqrt{(R\cos\phi + r)^2 + \left(R\sin\phi - \frac{r}{\sqrt{3}}\right)^2} \tag{3.86}$$

$$\rho_b = \sqrt{(R\cos\phi - r)^2 + \left(R\sin\phi - \frac{r}{\sqrt{3}}\right)^2} \tag{3.87}$$

$$\rho_c = \sqrt{(R\cos\phi)^2 + \left(R\sin\phi + \frac{2r}{\sqrt{3}}\right)^2} \tag{3.88}$$

Where the parameter, *r,* is defined as the radius of each core in the cable as shown in Figure 3-9. It can be noted that at any fixed position, the magnetic field is time harmonic. The magnetic field at each angular position around the cable behaves like a standing wave. An example of this can be observed in Figure 3-10 below. Where the angle ϕ represents the angular position around the cable.

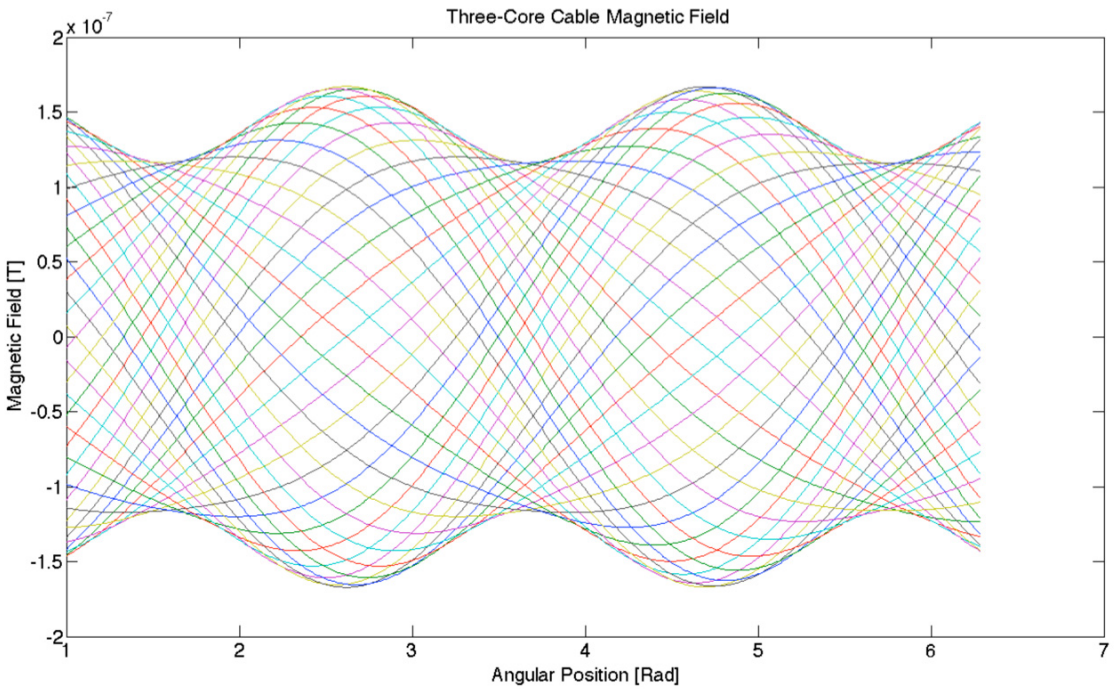

Figure 3-10: Magnetic Field Surrounding a Three-Core Cable

In Figure 3-10, it was assumed that the radius of the cable was 0.2155m and that the magnetic field was observed 0.5m from the cable center. The x-axis of this plot is the angular position surrounding the cable while the y-axis is the magnetic field. Each of the plots corresponds to a point in time between 0 and 1/60s, incremented by 1/2400s. The amplitude at each angular position is like a standing wave. The amplitude of the standing wave can be determined and averaged around the circumference of the cable. The decay of this average amplitude as distance away from the cable increases can be determined and the parameters of the regression found to be a function of the radius of each core in the cable. Figure 3-11 below shows how the decay of the average standing wave amplitude varies from that of a single-core cable.

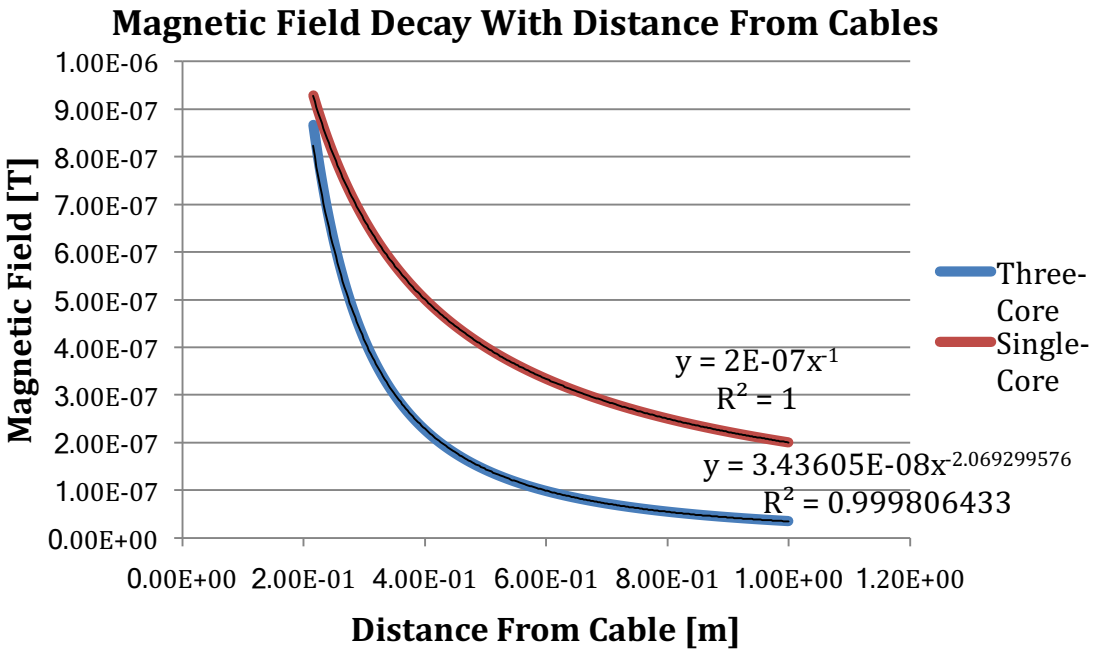

Figure 3-11: Three-Core Cable Magnetic Field Decay

The approximate equation that can subsequently be used to approximate the average magnetic field surrounding the cable:

$$B = \frac{\mu_0 |I|}{2\pi} \frac{\alpha}{R^{\gamma}} \sin(\omega t + \theta) \tag{3.89}$$

Where a regression can be performed to find the coefficients α and γ. This regression will involve the conductor/insulation core radius, r.

$$\alpha = 1.9535r - 0.0216 \tag{3.90}$$

$$\gamma = 0.3194r + 2.0059 \tag{3.91}$$

The regression models were developed for distances greater than $R = r\left(1 + \frac{2}{\sqrt{3}}\right)$ from the bundle. This corresponds to outside the outermost layer of the cable.

3.8.2 Impedance of a Three-Core Cable

The most significant impact on the impedance for a three-core cable would be due to the proximity effect. In multi-core cables, the conductors are inherently in close proximity to each other. This proximity will cause a distortion to the current density of each conductor. The three-core cable impedance can be modeled as a superposition of impedances, the skin effect, the proximity effect, and the mutual inductance added together [47,48,49]. The effects of the magnetic field on the current density are used to model the proximity effect. For a cable, the following equations can be used to determine the impedance of a cable [47,49]:

$$\nabla^2 A = \mu J \tag{3.92}$$

$$J = j\omega\sigma A \tag{3.93}$$

Substituting these equations together in the cylindrical coordinate system results in the following equation [47,49]:

$$\frac{\partial^2 A}{\partial \rho^2} + \frac{1}{\rho}\frac{\partial A}{\partial \rho} + \frac{1}{\rho^2}\frac{\partial^2 A}{\partial \theta^2} - j\omega\sigma\mu A = 0 \tag{3.94}$$

The solution to this equation is the following [47,49]:

$$A(\rho,\theta) = \sum_{n=0}^{\infty}\left[A_n I_n\left(\rho\sqrt{j\omega\sigma\mu}\right) + B_n K_n\left(\rho\sqrt{j\omega\sigma\mu}\right)\right]\cos n\theta \tag{3.95}$$

Where the coefficients A_n and B_n can be found from the boundary conditions of the given problem. When equation (3.95) is evaluated to find the current density in equation (3.93), the longitudinal electric field can be evaluated by the following equation [47,49]:

$$E_z = \rho J(\rho,\theta) \tag{3.96}$$

The impedance can then be found to have the following general form [47,48,49]:

$$Z = Z_{skin} + j\omega L_{mutual} + Z_{proximity} \tag{3.97}$$

The equations for Z_{skin} and L_{mutual} are given by equation (3.46) and (3.51) respectively. The additional coefficient for the proximity effect will be evaluated. For a three-core cable as depicted in Figure 3-9 above, with a conductor radius of r_c and conductor separation of s, where $s = 2r$ from Figure 3-9, the following approximation of the proximity effect can be evaluated [48]:

$$Z_{proximity} = \sum_{n=1}^{\infty} \frac{2\pi {r_c}^{2n}}{n} ||M_n||^2 \left\{ \left(1 - \left(\frac{J_{n+1}(jr_c\sqrt{j\omega\mu\sigma})}{J_{n-1}(jr_c\sqrt{j\omega\mu\sigma})}\right)^*\right)\left(1 + \frac{J_{n+1}(jr_c\sqrt{j\omega\mu\sigma})}{J_{n-1}(jr_c\sqrt{j\omega\mu\sigma})}\right) + \left(\frac{s}{2}\right)^n \cos\left(n\frac{\pi}{3}\right)\right\} \quad (3.98)$$

Where the following approximations can be made for the M_n terms [48],

$$M_1 = \frac{-1}{2\pi s}\left(1 + \left(\frac{r_c}{s}\right)^2 \frac{J_2(jr_c\sqrt{j\omega\mu\sigma})}{J_0(jr_c\sqrt{j\omega\mu\sigma})} + \left(\frac{r_c}{s}\right)^4 \frac{J_3(jr_c\sqrt{j\omega\mu\sigma})}{J_1(jr_c\sqrt{j\omega\mu\sigma})} + \left(\frac{r_c}{s}\right)^4 \left(\frac{J_2(jr_c\sqrt{j\omega\mu\sigma})}{J_0(jr_c\sqrt{j\omega\mu\sigma})}\right)^2\right) \quad (3.99)$$

$$M_2 = \frac{-1}{2\pi s}\left(1 + \left(\frac{r_c}{s}\right)^2 \frac{J_2(jr_c\sqrt{j\omega\mu\sigma})}{J_0(jr_c\sqrt{j\omega\mu\sigma})}\right) \quad (3.100)$$

$$M_3 = \frac{-1}{2\pi s} \quad (3.101)$$

These equations will allow for the approximation of the three-core cables impedance per unit length.

3.8.3 Admittance of a Three-Core Cable

The capacitance of a three-core underwater cable can be evaluated based on what layers of the cable are grounded. If each individual core in the cable has a grounded sheath or if the group of cores have a single grounded sheath. The former method of grounding has an equation for the capacitance that takes on a form similar to equation (3.82). Using the notation used in Figure 3-9, the capacitance can be found to be as follows [29,30,31,34]:

$$C = \frac{2\pi\varepsilon}{ln\left(\frac{r}{r_{cond}}\right)} \quad (3.102)$$

If the group of conductors has a grounded sheath, the capacitance can be evaluated using the method of images. Figure 3-12 below shows the method of images geometrical problem set up.

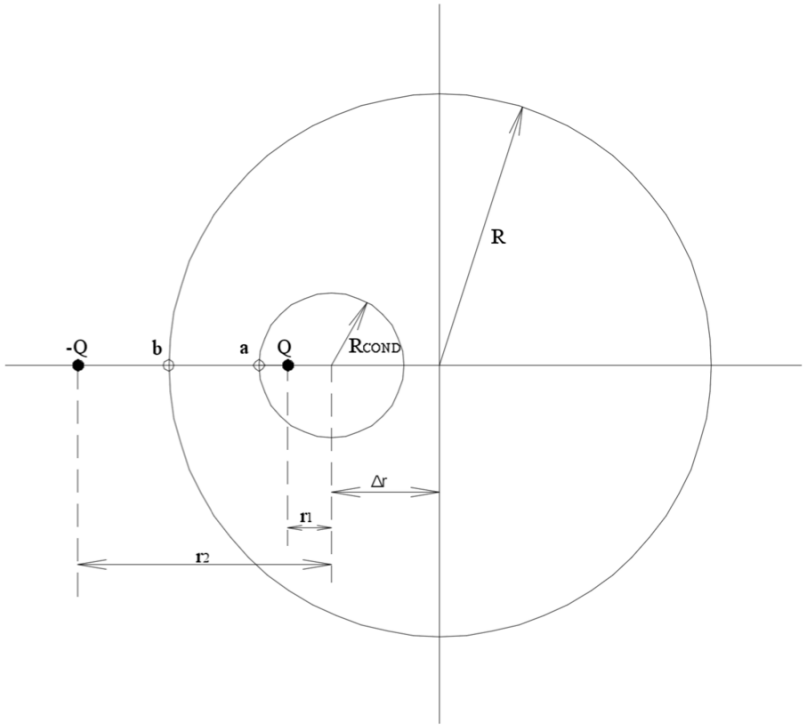

Figure 3-12: Method of Images For a Three-Core Cable

From this problem, superposition will be applied to evaluate the equivalent capacitance of each conductor to the grounded sheath. The following equations must be true to have an equipotential surface for the conductor and the outer sheath [34,51]:

$$r_1 r_2 = {r_{cond}}^2 \tag{3.103}$$

$$(r_1 + \Delta r)(r_2 + \Delta r) = R^2 \tag{3.104}$$

These equations originate from studying a line charge surrounded by a single cylindrical conductor. Since both of these equations must be true, they can be substituted together [51]:

$$r_1 = \frac{\left(R^2 - {r_{cond}}^2 - \Delta r^2\right) +/- \sqrt{\left(R^2 - {r_{cond}}^2 - \Delta r^2\right)^2 - 4{r_{cond}}^2 \Delta r^2}}{2\Delta r} \tag{3.105}$$

Where $R = r\left(1 + \frac{2}{\sqrt{3}}\right)$, $\Delta r = \frac{2r}{\sqrt{3}}$, and $r = r_{cond} + r_{insul}$. From this, the voltage difference between points *a* and *b* in Figure 3-10 can be evaluated. This potential difference is [51]:

$$\Delta V = V_a - V_b = 2\pi\varepsilon q \cdot ln\left(\frac{r_{cond}}{R}\left(1 + \frac{\Delta r}{r_1}\right)\right) \tag{3.106}$$

From this, the capacitance between the sheath and the conductor can be evaluated. The total capacitance is equal to the following:

$$C = 2\pi\varepsilon\left[\frac{1}{ln\left(\frac{2r}{r_{cond}}\right)} + \frac{1}{ln\left(\frac{r_{cond}}{r_1(2+\sqrt{3})}\right)}\right] \tag{3.107}$$

The first term to the right of the equal sign is due to the presence of other conductors while the second term is due to the capacitance from the conductor to sheath.

3.9 Line Parameters of a Single-Core DC Cable

Single-core DC power cables have much simpler expressions representing the line parameters. There is no alternating magnetic field thus there are no induced currents in the cables layers or any mutual coupling with other cables. This greatly simplifies the evaluation of the line parameters.

3.9.1 Impedance of Single-Core DC Cable

The resistance of a DC cable can be evaluated by the following equation [30,34]:

$$R = \frac{1}{\sigma}\frac{\ell}{A} \tag{3.108}$$

Here, σ is the conductivity of the conductor, ℓ is the length, and A is the cross sectional area. Table 3-1 above presents the room temperature values of conductivity of several conductor materials. The inductance does not play a roll in the steady state operation of a DC transmission line. The inductance comes into effect during the various transient states that the transmission line may endure. To model the transient states, the resistance and inductance of a DC transmission line can be evaluated identically as the methods for AC transmission lines.

3.9.2 Admittance of Single-Core DC Cable

The capacitance of a DC cable can be found in identically the same way as for single core AC cables. Similarly to inductance, the capacitance evaluated to perform transient analysis. The steady state analysis of a DC transmission line does not involve the capacitance.

3.10 Impedance and Admittance of a Two-Core Cable

The impedance and admittance of a two-core DC cable can be found the same way as for the single-core DC cable case in the steady state. The differences being that the conductors are closer together. To evaluate the impedance and admittance such that transient effects can be evaluated will require the AC analysis of the cable.

3.10.1 Impedance of a Two-Core Cable

In the steady state, the resistance is the same as for a single-core DC cable and the inductance has no role. For transient analysis the resistance and inductance can be evaluated in a similar manner as for three-core cables.

3.10.2 Admittance of a Two-Core Cable

In the steady state, the capacitance has no roll in the performance of the transmission line. To evaluate the capacitance to model transient effects, the models developed for a three-core cable could be applied to this cable.

3.11 Table of impedances

The following tables represent four underwater power cables and their associated line parameters for each of the four potential cable configurations. Additionally there will be a table representing an equivalent set of overhead conductors. Table 3-4 below represents the geometry of a select underwater power cable. Table's 3-5a-d represent the four different cable configurations and the equivalent overhead conductors line parameters.

Table 3-4: Geometry of Cable [28]

	Cable
Conductor	Copper, 23.2mm diameter
Insulation	XLPE, 13mm thickness
Sheath	Lead, 1.5mm thickness
Armor	Steel, 5mm thickness
Grounding	Single wire Earth return with bonded sheath

Table 3-5a: Single-Core AC Cables

	Cable
R [mΩ/km]	66.12
L [mH/km]	1.646
C [μF/km]	0.203

Table 3-5b: Three-Core AC Cables

	Cable
R [mΩ/km]	73.52
L [mH/km]	1.426
C [μF/km]	0.3085

Table 3-5c: Single-Core DC Cables

	Cable
R [mΩ/km]	66.12 (AC), 39.7 (DC)
L [mH/km]	1.646
C [μF/km]	0.203

Table 3-5d: Overhead Cables

	Cable
R [mΩ/km]	42.51
L [mH/km]	0.936
C [μF/km]	0.01256

3.12 Steady State Performance

The steady state analysis of the transmission line allows the determination of how the generated power is affected during transmission. Distributed component analysis is performed for a transmission line. Lumped component analysis proves inaccurate in the modeling of transmission lines [30,52]. This distributed component analysis results in the determination of two-port network theory for the transmission line.

3.12.1 Distributed Component Two-Port Network Theory

A distributed component model is used for the analysis of a transmission line; Figure 3-13 below can be used to represent an incremental length of a transmission line [30].

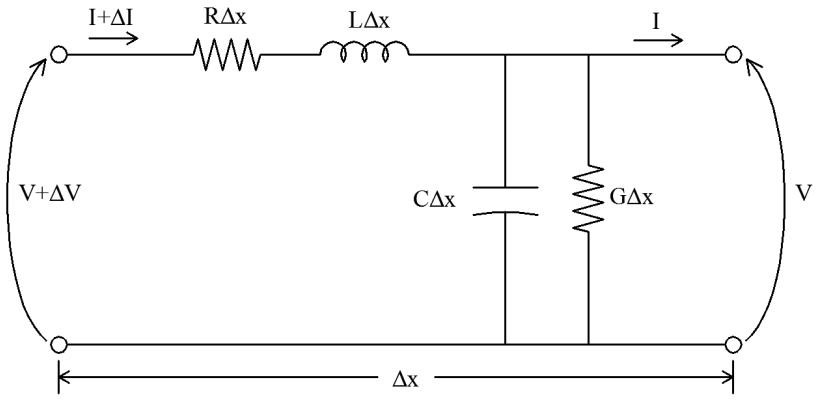

Figure 3-13: Incremental Length of Transmission Line

For this incremental length of transmission line, it is assumed that the receiving end voltage and current, V and I respectively, vary by ΔV and ΔI at the sending end. The line parameters, R, L, C, and G are in per unit length form. The term Δx refers to the incremental length of transmission line. From this incremental transmission line model, the following equations represent the voltage and current relationships [30]:

$$[V + \Delta V] - [I + \Delta I][R + j\omega L]\Delta x = V \tag{3.109}$$

$$[I + \Delta I] - V[G + j\omega C]\Delta x = I \tag{3.110}$$

These equations can alternatively be written as follows [30]:

$$\frac{\Delta V}{\Delta x} = [I + \Delta I][R + j\omega L] \tag{3.111}$$

$$\frac{\Delta I}{\Delta x} = V[G + j\omega C] \tag{3.112}$$

Taking the limit of this as Δx approaches zero results in the following equations [30]:

$$\frac{dV}{dx} = I[R + j\omega L] \tag{3.113}$$

$$\frac{dI}{dx} = V[G + j\omega C] \tag{3.114}$$

The term ΔI disappears since the limit was taken. These two equations represent mixed differential equations, solving for equations in terms of *V* and *I* alone result in the following [30]:

$$\frac{d^2V}{dx^2} = \Gamma^2 V \tag{3.115}$$

$$\frac{d^2I}{dx^2} = \Gamma^2 I \tag{3.116}$$

Where,

$$\Gamma^2 = [R + j\omega L][G + j\omega C] \tag{3.117}$$

The solution to these differential equations has the following form [30]:

$$V(x) = C_1 e^{\Gamma x} + C_2 e^{-\Gamma x} \tag{3.118}$$

$$I(x) = \frac{1}{Z_0}[C_1 e^{\Gamma x} - C_2 e^{-\Gamma x}] \tag{3.119}$$

Where,

$$Z_0 = \sqrt{\frac{R+j\omega L}{G+j\omega C}} \tag{3.120}$$

The constants C_1 and C_2 in the above equations can be found from knowing the voltage and current at the sending end of the transmission line. These constants can be determined to be as follows [30]:

$$C_1 = \frac{V(0)+Z_0 I(0)}{2} \tag{3.121}$$

$$C_2 = \frac{V(0)-Z_0 I(0)}{2} \tag{3.122}$$

Substituting these constants into the voltage and current equations results in the following equations describing the output voltage and current of the transmission line in terms of the inputs [30].

$$V(x) = V(0)\frac{e^{\Gamma z}+e^{-\Gamma z}}{2} + I(0)\frac{e^{\Gamma z}-e^{-\Gamma z}}{2}Z_0 \tag{3.123}$$

$$I(x) = V(0)\frac{e^{\Gamma z}-e^{-\Gamma z}}{2}\frac{1}{Z_0} + I(0)\frac{e^{\Gamma z}+e^{-\Gamma z}}{2} \tag{3.124}$$

It is apparent that this equation can be simplified by use of hyperbolic functions. Applying the definitions for hyperbolic cosine and sine results in the following equations [30]:

$$V(x) = V(0)\cosh(\Gamma x) + I(0)Z_0\sinh(\Gamma x) \tag{3.125}$$

$$I(x) = V(0)\frac{1}{Z_0}\sinh(\Gamma x) + I(0)\cosh(\Gamma x) \tag{3.126}$$

This can be further simplified to be a set of two-port network equations. This set of equations can be written as follows [30]:

$$\begin{bmatrix} V_s \\ I_s \end{bmatrix} = \begin{bmatrix} A & B \\ C & D \end{bmatrix}\begin{bmatrix} V_R \\ I_R \end{bmatrix} \tag{3.127}$$

Where the ABCD parameters are defined as follows [30]:

$$A = D = \cosh\Gamma x \tag{3.128}$$

$$B = Z_0\sinh\Gamma x \tag{3.129}$$

$$C = \frac{1}{Z_0}\sinh\Gamma x \tag{3.130}$$

These equations allow the analysis of a distributed component transmission line as a set of two-port network equations. From these equations it can be seen that definition of one set of parameters allows the determination of the other set of parameters. These equations also allow for determination of a transmission lines steady state performance.

3.12.2 Steady State Performance

The steady state performance for a transmission line can be characterized by the following parameters: the receiving end power, reactive power, power factor, efficiency, and voltage regulation. For the transmission line it will be assumed that the sending end voltage, V_S, magnitude of apparent power, S, and power factor, δ, are known. The apparent power and power factor can be converted to the real and reactive power components as follows [30]:

$$S_s = P_s + jQ_s = |S|[\delta \pm j\sin(\cos^{-1}\delta)] \tag{3.131}$$

Where the imaginary component is positive if the power factor is lagging, and negative if the power factor is leading. From this definition of the apparent power and the sending end voltage, the sending end current can be determined. The current is defined as follows:

$$I_s = \left(\frac{S_s}{V_s}\right)^* \tag{3.132}$$

From this, the following equations can be used to describe the receiving end voltage and current:

$$I_R = A\left(\frac{S_s}{V_s}\right)^* - CV_S \tag{3.133}$$

$$V_R = DV_s - B\left(\frac{S_s}{V_s}\right)^* \tag{3.134}$$

The receiving end apparent power, real power, reactive power, and power factor can then be defined as follows:

$$S_R = \left[DV_s - B\left(\frac{S_s}{V_s}\right)^*\right]\left[A\left(\frac{S_s}{V_s}\right)^* - CV_S\right]^* \tag{3.135}$$

$$P_R = RE\{S_R\} \tag{3.136}$$

$$Q_R = IM\{S_R\} \tag{3.137}$$

$$\delta_R = \cos\left(\tan^{-1}\frac{Q_R}{P_R}\right) \tag{3.138}$$

The transmission line efficiency will be defined as the ratio of received real power to sent real power. The equation is as follows [30]:

$$\eta = 100\% \cdot \frac{P_R}{P_S} \tag{3.139}$$

The voltage regulation is defined as the difference between no load voltage and full load voltage normalized by the full load voltage. The equation describing this is as follows [30]:

$$VR = 100\% \cdot \frac{|V_{nl}| - |V_{fl}|}{|V_{fl}|} \tag{3.140}$$

The no load voltage can be found from the transmission line two-port network equations by setting I_R equal to zero. This results in the following simplification:

$$VR = 100\% \cdot \frac{\left|\frac{V_S}{A}\right| - |V_R|}{|V_R|} \tag{3.141}$$

The voltage regulation allows for a measure of how the voltage will vary as the transmission line is loaded.

3.13 Model Approximation

The two-port network model using distributed component analysis only allows for determination of steady state values [30]. For transient performance, the transmission line must be transformed into an approximation using lumped circuit components [52]. This allows for a determination of the transmission lines initial conditions. Underwater power cables have a significant capacitance, and it is expected that modified networks must be developed to model them accurately [52]. Three lumped component topologies will be studied, and the limitations of the transmission line length will be determined. This will be determined by finding the error between the lumped component model and the distributed component model [52]. The receiving end voltage and apparent power errors will be used

as the performance criteria. The following equations can be used to evaluate the relative error [52]:

$$e_{V_R} = 100\% \cdot \left| \frac{DV_S - BI_S - D_1 V_S + B_1 I_S}{DV_S - BI_S} \right| \tag{3.142}$$

$$e_{S_R} = 100\% \cdot \left| \frac{(DV_S - BI_S)(AI_S - CV_S)^* - (D_1 V_S + B_1 I_S)(A_1 I_S - C_1 V_S)^*}{(DV_S - BI_S)(AI_S - CV_S)^*} \right| \tag{3.143}$$

It is assumed that the acceptable error is less than 1%. It should be noted that there is a relationship between voltage and insulation thickness as well as a relationship between current flow and conductor radius [52]. These relationships have been incorporated into the analysis. This results in only three parameters that vary, the sending end voltage, the sending end apparent power, and the line length. Sweeping these parameters and finding the regions of similarity between the two error plots, generalizations regarding the line length limitations can be made. The region of error less than 1% will be found by varying the sending end voltage and line length, and finding plots for various values of apparent power. The error plots for an apparent power of 2MVA with power factor of 0.95 lagging will be shown in the subsequent sections. The generalizations regarding the line lengths are made from comparisons of multiple values of apparent power.

3.13.1 Short Line Approximation

The nominal-pi network can approximate a short length of underwater power cable [52]. The admittance component for underwater power cables is significant and must be accounted for. Figure 3-14 below shows the equivalent network for the nominal-pi model.

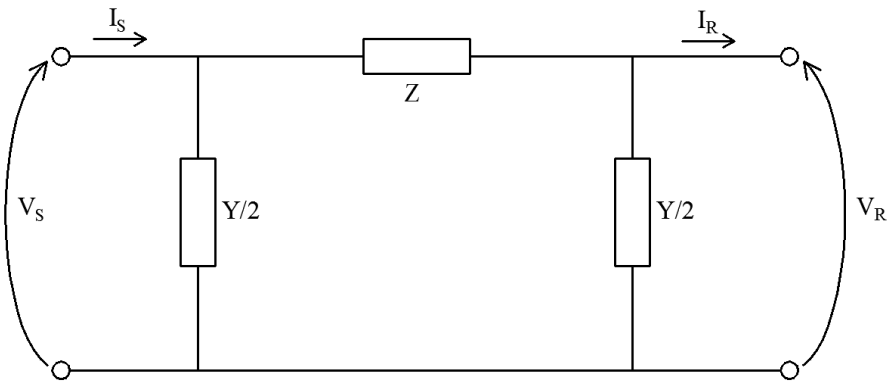

Figure 3-14: Nominal-Pi Network

The two-port network parameters for this transmission line model can be found to be as follows:

$$A = D = 1 + \frac{ZY}{2} \tag{3.144}$$

$$B = Z \tag{3.145}$$

$$C = Y + \frac{ZY^2}{4} \tag{3.146}$$

Where, $Z = (R + j\omega L)\ell$ and $Y = (G + j\omega C)\ell$. Taking this model and comparing it with the exact model for the transmission line, the region of acceptable error can be seen in Figures 3-15a through 3-15c below:

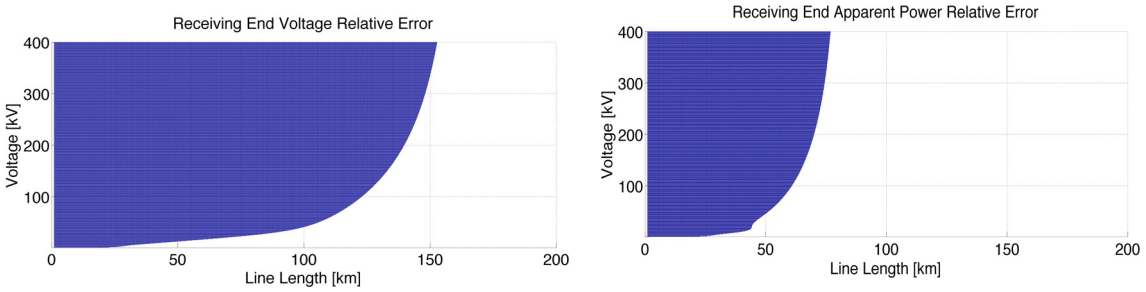

Figure 3-15a: Single-Core Copper Armor Voltage and Apparent Power Error

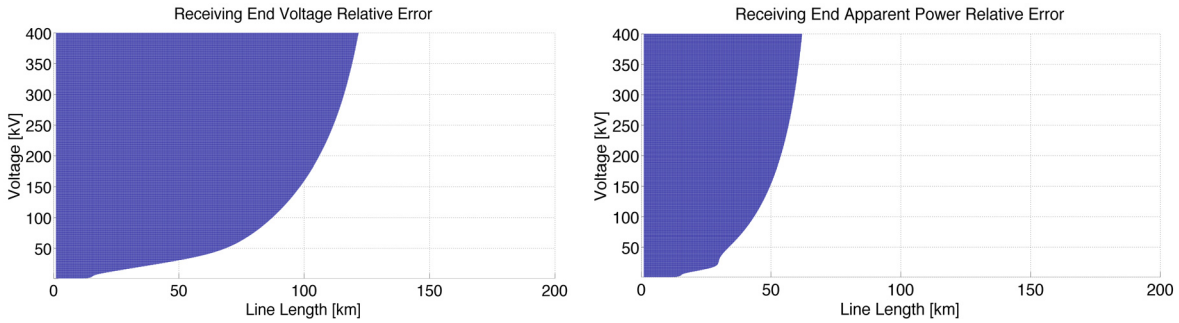

Figure 3-15b: Single-Core Steel Armor Voltage and Apparent Power Error

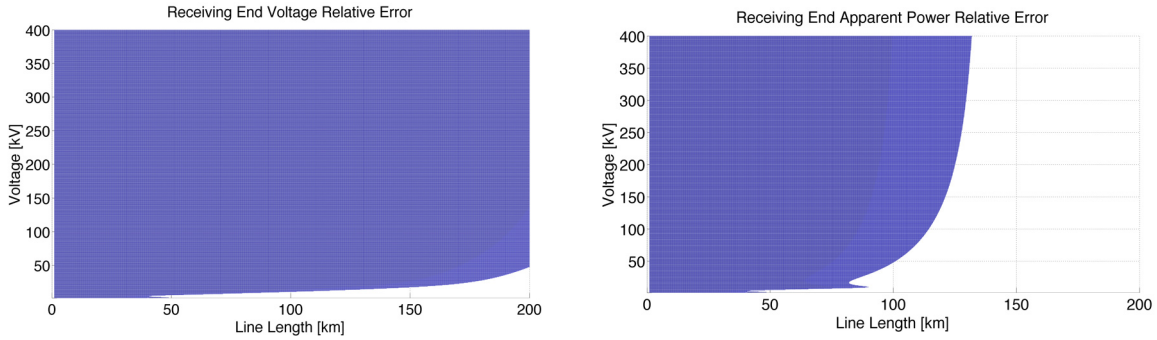

Figure 3-15c: Three-Core Voltage and Apparent Power Error

The regions in blue represent a relative error less than 1%. It can be generalized that this model is accurate for line lengths up to 25km for single-core copper armor cables, 10km for single-core steel armor cables, and 40km for three-core cables [52].

3.13.2 Medium Line Approximation

To study the medium line approximations, a modification must be made to the short line approximation [52]. It is desired to modify the topology as slightly as possible and study the validity of the model. Two topologies will be studied as a medium line approximation. These two topologies will be similar in that they are two short line models in cascade. Model 1 will consist of two cascaded pi networks. This is effectively the same as saying a

longer transmission line is two shorter transmission lines [52]. Model 2 will have the same topology, however, the admittances will be abstracted. A non-uniform admittance distribution will be assumed, and a distribution that provides the best approximation of the transmission line may be used [52]. These two models will be discussed in the proceeding sections.

3.13.2.1 Model 1

This transmission line approximation is composed of two cascaded short line models. The topology for this model can be seen in Figure 3-16 below.

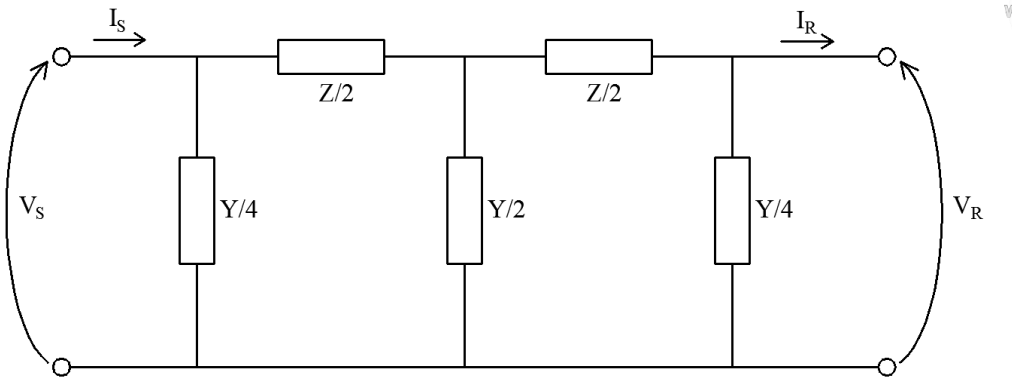

Figure 3-16: Medium Line Approximation Model 1

The two-port network parameters for this model are as follows [52]:

$$A = D = 1 + \frac{ZY}{2} + \frac{Z^2Y^2}{32} \tag{3.147}$$

$$B = Z + \frac{Z^2Y}{8} \tag{3.148}$$

$$D = Y + \frac{3ZY^2}{16} + \frac{Z^2Y^3}{128} \tag{3.149}$$

Where, $Z = (R + j\omega L)\ell$ and $Y = (G + j\omega C)\ell$. Taking this model and comparing it with the exact model for the transmission line, the region of acceptable error can be seen in Figures 3-17a through 3-17c below:

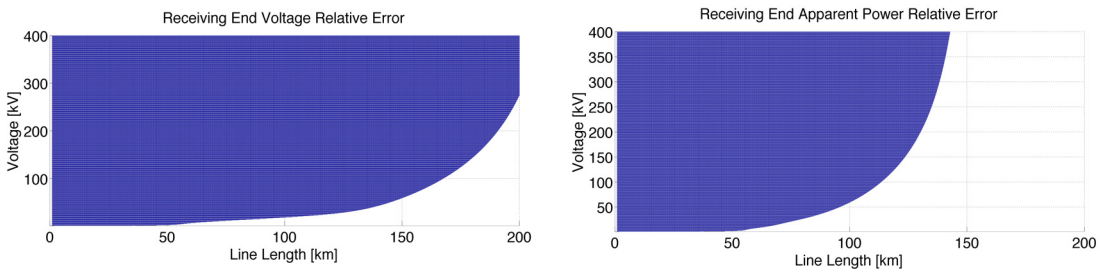

Figure 3-17a: Single-Core Copper Armor Voltage and Apparent Power Error

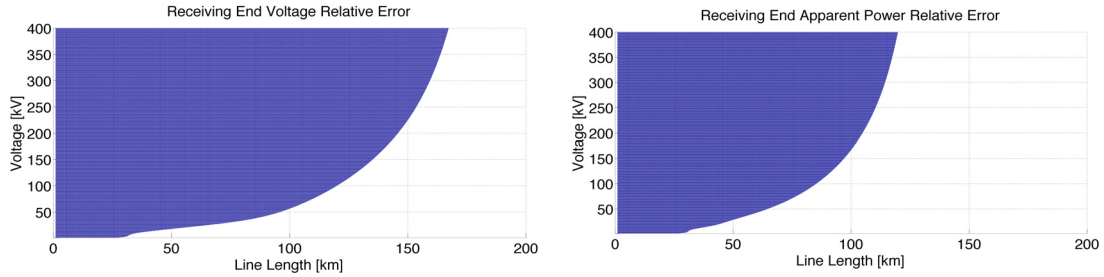

Figure 3-17b: Single-Core Steel Armor Voltage and Apparent Power Error

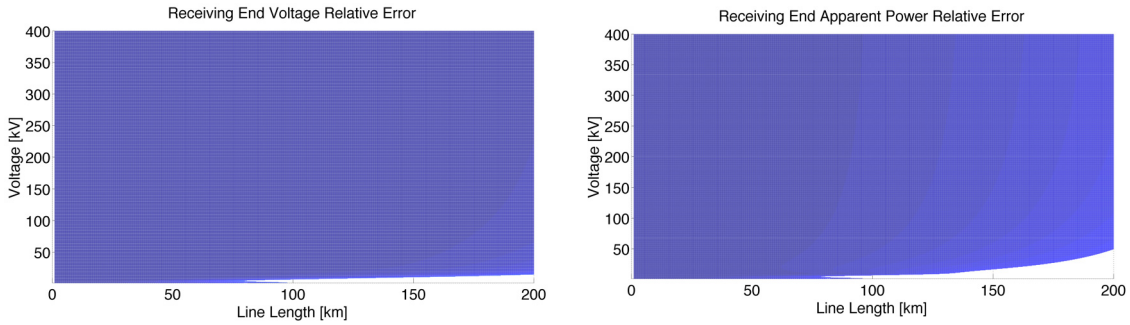

Figure 3-17c: Three-Core Voltage and Apparent Power Error

It can be generalized that this model is accurate for line lengths up to 50km for single-core copper armor cables, 30km for single-core steel armor cables, and 75km for three-core cables [52].

3.13.2.2 Model 2

This model has a similar topology as model 1; however, the admittance components have variability associated with them. Figure 3-18 is the modified nominal pi topology. The term *k* is a variable used to distribute the admittance amongst the three admittance components [52]. Note that if *k*=4 this model results in being model 1.

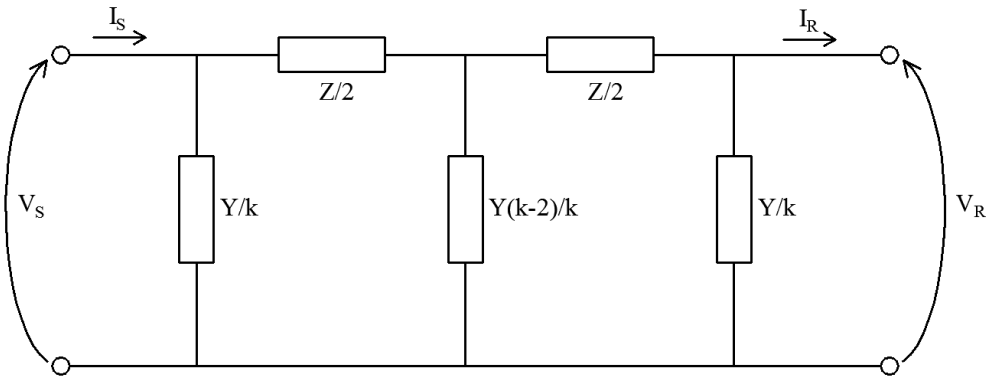

Figure 3-18: Medium Line Approximation Model 2

The two-port network parameters for this model are shown below [52]:

$$A = D = 1 + \frac{ZY}{2} + \left(\frac{1}{4k} - \frac{1}{2k^2}\right) Z^2Y^2 \tag{3.150}$$

$$B = Z + \left(\frac{1}{4} - \frac{1}{2k}\right) Z^2Y \tag{3.151}$$

$$C = Y + \left(\frac{1}{k} - \frac{1}{k^2}\right) ZY^2 + \left(\frac{1}{4k^2} - \frac{1}{2k^3}\right) Z^2Y^3 \tag{3.152}$$

Where, $Z = (R + j\omega L)\ell$ and $Y = (G + j\omega C)\ell$. Taking this model and comparing it with the exact model for the transmission line, the region of acceptable error can be seen in Figures 3-19a through 3-19c below for a value of k=5:

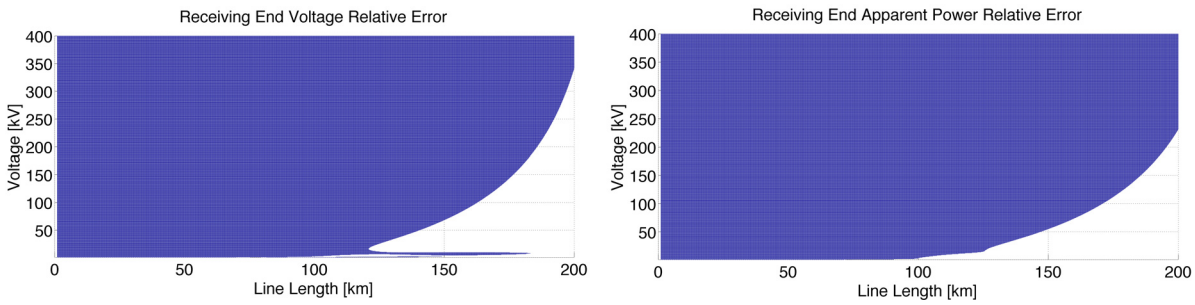

Figure 3-19a: Single-Core Copper Armor Voltage and Apparent Power Error

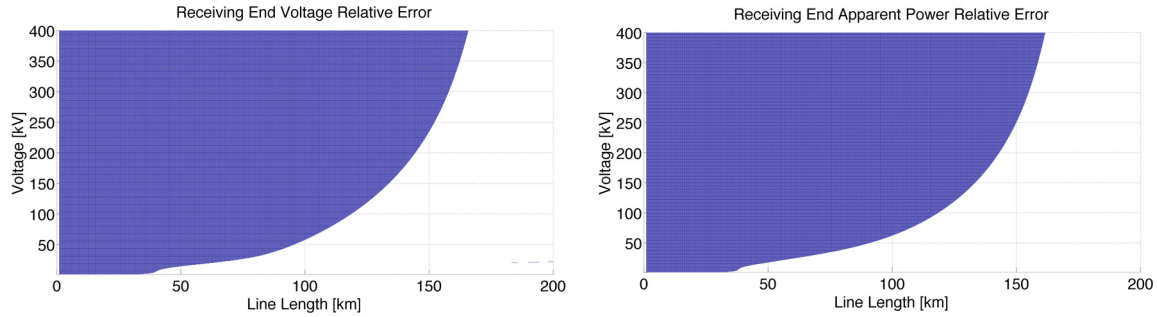

Figure 3-19b: Single-Core Steel Armor Voltage and Apparent Power Error

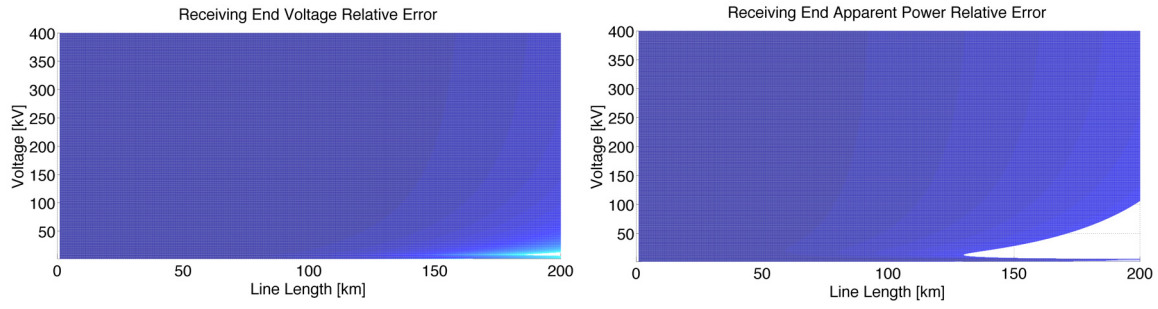

Figure 3-19c: Three-Core Voltage and Apparent Power Error

It can be generalized that this model is accurate for line lengths up to 100km for single-core copper armor cables, 40km for single-core steel armor cables, and 125km for three-core cables with the optimal *k* value chosen [52].

3.14 Transient Analysis

The transient performance will be analyzed when a thevenin equivalent of the power grid is connected to the receiving end of the transmission line. This thevenin equivalent represents the impedance of the assumed infinite bus that is the grid, and the voltage of the infinite bus [30]. For this analysis it will be assumed that the grid voltage is adjusted to allow the desired power flow from an offshore generator to the grid. The initial conditions for the network can be determined from the steady state analysis of the lumped component network. Figure 3-20 below shows an *N* segment representation of a transmission line. As *N* approaches infinity, the model resembles the one used for the two-port network theory.

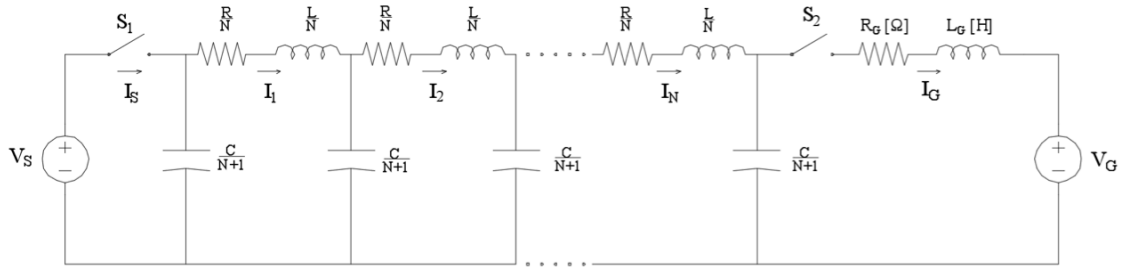

Figure 3-20: N-segment Transmission Line

This general network will be used as the basis for the development of generalized equations to solve for the transient performance of AC and DC power cables. The approximation

models are but a subset of these general equations. In Figure 3-20, the following can be defined.

- R_G and L_G represent the grid thevenin equivalent impedance
- V_G is the grid thevenin equivalent voltage
- δ_G is the phase difference between the grid equivalent voltage and the generator voltage
- $V_{c_i}(0)\,, i = 0,1, \dots, N$, is the initial voltage across each capacitor in the network
- $I_j(0), j = 1,2, \dots, N$, is the initial current through each inductor in the network

3.14.1 AC Cable Transient Analysis

Using the circuit model in Figure 3-18 as the transmission line model allows for the transient performance to be quantified. To analyze the transient conditions, the initial conditions for voltages and currents through capacitors and inductors respectively must be found [53,54,55]. These can be found from the steady state analysis of this model. From Figure 3-18, the following system of equations can be developed for when switch S_1 is closed and S_2 is open.

$$\begin{bmatrix} Y & -Y & 0 & 0 & 0 & 0 \\ -Y & Z & -Y & 0 & 0 & 0 \\ 0 & -Y & Z & -Y & 0 & 0 \\ 0 & 0 & -Y & \ddots & \ddots & 0 \\ 0 & 0 & 0 & \ddots & Z & -Y \\ 0 & 0 & 0 & 0 & -Y & Z \end{bmatrix} \begin{bmatrix} I_S \\ I_1 \\ I_2 \\ \vdots \\ I_{N-1} \\ I_N \end{bmatrix} = \begin{bmatrix} \frac{|V_S|s}{s^2+\omega^2} \\ 0 \\ 0 \\ \vdots \\ 0 \\ 0 \end{bmatrix} \tag{3.153}$$

Where s is the Laplace variable. The following system of equations can be developed for when switch S_1 has been closed, and then S_2 is closed:

$$\begin{bmatrix} Y & -Y & 0 & 0 & 0 & 0 \\ -Y & Z & -Y & 0 & 0 & 0 \\ 0 & -Y & Z & -Y & 0 & 0 \\ 0 & 0 & -Y & \ddots & \ddots & 0 \\ 0 & 0 & 0 & \ddots & Z & -Y \\ 0 & 0 & 0 & 0 & -Y & Z_G \end{bmatrix} \begin{bmatrix} I_S \\ I_1 \\ I_2 \\ \vdots \\ I_N \\ I_G \end{bmatrix} = \begin{bmatrix} \frac{|V_S|s}{s^2+\omega^2} - \frac{V_{C_0}}{s} \\ \frac{1}{s}\left(V_{C_1} - V_{C_2}\right) + \frac{L}{N} I_1(0) \\ \frac{1}{s}\left(V_{C_2} - V_{C_3}\right) + \frac{L}{N} I_2(0) \\ \vdots \\ \frac{1}{s}\left(V_{C_{N-1}} - V_{C_N}\right) + \frac{L}{N} I_N(0) \\ \frac{V_{C_N}}{s} - |V_G| \frac{s\cos\delta_G + \omega \sin\delta_G}{s^2+\omega^2} \end{bmatrix} \tag{3.154}$$

Where, $Y = \frac{N+1}{sC}$, $Z = 2\frac{N+1}{sC} + \frac{R}{N} + \frac{sL}{N}$, and $Z_G = \frac{N+1}{sC} + R_G + sL_G$.

3.14.1.1 Short Line Transient Analysis

The short line model can be represented by Figure 3-18 when *N=2*. The transient performance for this transmission line model when switch S_1 is closed and S_2 is open can be represented by the following set of equations:

$$\begin{bmatrix} \frac{2}{sC} & -\frac{2}{sC} \\ -\frac{2}{sC} & \frac{4}{sC} + R + sL \end{bmatrix} \begin{bmatrix} I_S \\ I_L \end{bmatrix} = \begin{bmatrix} \frac{|V_S|s}{s^2+\omega^2} \\ 0 \end{bmatrix} \tag{3.155}$$

The following series of equations represents the transient performance when switch S_1 and S_2 are both closed:

$$\begin{bmatrix} \frac{2}{sC} & -\frac{2}{sC} & 0 \\ -\frac{2}{sC} & \frac{4}{sC} + R + sL & -\frac{2}{sC} \\ 0 & -\frac{2}{sC} & \frac{2}{sC} + R_G + sL_G \end{bmatrix} \begin{bmatrix} I_S \\ I_L \\ I_R \end{bmatrix} = \begin{bmatrix} \frac{|V_S|s}{s^2+\omega^2} - \frac{V_{C1_0}}{s} \\ \frac{V_{C1_0}}{s} - \frac{V_{C2_0}}{s} + Li_{L_0} \\ \frac{V_{C2_0}}{s} - \frac{|V_G|(s\cos\delta_G + \omega\sin\delta_G)}{s^2+\omega^2} \end{bmatrix} \tag{3.156}$$

3.14.1.2 Medium Line Transient Analysis

Since both medium length transmission line models are similar, model 2 will be analyzed since model 1 is a specific case of it, when *k=4*. This model can be evaluated from Figure

3-18 when *N=3*. The following equations describe the performance of this model when switch S_1 is closed and S_2 is open:

$$\begin{bmatrix} \frac{k}{sC} & -\frac{k}{sC} & 0 \\ -\frac{k}{sC} & \frac{R}{2}+s\frac{L}{2}+\frac{k}{sC}\frac{k-1}{k-2} & -\frac{k}{sC} \\ 0 & -\frac{k}{sC} & \frac{R}{2}+s\frac{L}{2}+\frac{k}{sC}\frac{k-1}{k-2} \end{bmatrix}\begin{bmatrix} I_s \\ I_1 \\ I_2 \end{bmatrix} = \begin{bmatrix} \frac{|V_s|s}{s^2+\omega^2} \\ 0 \\ 0 \end{bmatrix} \tag{3.157}$$

The following equations describe the performance of this model when switch S_1 is closed and S_2 is closed:

$$\begin{bmatrix} \frac{k}{sC} & -\frac{k}{sC} & 0 & 0 \\ -\frac{k}{sC} & \frac{R}{2}+s\frac{L}{2}+\frac{k}{sC}\frac{k-1}{k-2} & \frac{-k}{sC(k-2)} & 0 \\ 0 & \frac{-k}{sC(k-2)} & \frac{R}{2}+s\frac{L}{2}+\frac{k}{sC}\frac{k-1}{k-2} & -\frac{k}{sC} \\ 0 & 0 & -\frac{k}{sC} & R_G+sL_G+\frac{k}{sC} \end{bmatrix}\begin{bmatrix} I_s \\ I_1 \\ I_2 \\ I_R \end{bmatrix} = \begin{bmatrix} \frac{|V_s|s}{s^2+\omega^2}-\frac{V_{C1_0}}{s} \\ \frac{V_{C1_0}}{s}-\frac{V_{C2_0}}{s}+Li_{L1_0} \\ \frac{V_{C2_0}}{s}-\frac{V_{C3_0}}{s}+Li_{L2_0} \\ \frac{V_{C3_0}}{s}-\frac{|V_G|(s\cos\delta_G+\omega\sin\delta_G)}{s^2+\omega^2} \end{bmatrix} \tag{3.158}$$

3.14.2 DC Cable Transient Analysis

In the steady state a DC power cable is modeled by a resistance component. For the transient analysis a more complete model must be used [53]. The models described in the previous sections would be required to be used. In the previous case, an AC source was being connected to an AC power grid. In the case of a DC transmission line, a step response for a generator being connected to a transmission line, then a step response for the connection to the grid can be performed. The following equation represents the step response for a generator being connected to a transmission line with switch S_1 closed and S_2 open.

$$\begin{bmatrix} sY & -sY & 0 & 0 & \dots & 0 \\ -Y & Z & -Y & 0 & \dots & 0 \\ 0 & -Y & Z & -Y & 0 & \vdots \\ 0 & 0 & -Y & Z & \ddots & 0 \\ \vdots & \vdots & \ddots & \ddots & \ddots & -Y \\ 0 & 0 & \dots & 0 & -Y & Z \end{bmatrix}\begin{bmatrix} I_1 \\ I_2 \\ I_3 \\ \vdots \\ I_{N-1} \\ I_N \end{bmatrix} = \begin{bmatrix} V_s \\ 0 \\ 0 \\ \vdots \\ 0 \\ 0 \end{bmatrix} \tag{3.159}$$

To model the step response when this generator and transmission line is connected to the grid, switch S_1 is closed and S_2 is closed

$$\begin{bmatrix} sY & -sY & 0 & 0 & \dots & 0 \\ -Y & Z & -Y & 0 & \dots & 0 \\ 0 & -Y & Z & -Y & 0 & \vdots \\ 0 & 0 & -Y & Z & \ddots & 0 \\ \vdots & \vdots & \ddots & \ddots & \ddots & -Y \\ 0 & 0 & \dots & 0 & -Y & Z_G \end{bmatrix} \begin{bmatrix} I_1 \\ I_2 \\ I_3 \\ \vdots \\ I_N \\ I_G \end{bmatrix} = \begin{bmatrix} V_s - V_{C_0} \\ \left\{\frac{1}{s}\left(V_{C_1} - V_{C_2}\right) - \frac{L}{N} I_1\right\} \\ \left\{\frac{1}{s}\left(V_{C_2} - V_{C_3}\right) - \frac{L}{N} I_2\right\} \\ \vdots \\ \left\{\frac{1}{s}\left(V_{C_{N-1}} - V_{C_N}\right) - \frac{L}{N} I_N\right\} \\ \frac{V_{C_N}}{s} - V_G \end{bmatrix} \tag{3.160}$$

It should be noted that if the transmission line were left long enough to charge, then the initial conditions take the following form:

$$V_{C_i} = V_s \, , for \; i = 0,1, \dots, N$$

$$I_i = 0 \, , for \; i = 1,2, \dots, N$$

This results in the following system of equations:

$$\begin{bmatrix} -sY & sY & 0 & 0 & \dots & 0 \\ Y & -Z & Y & 0 & \dots & 0 \\ 0 & Y & -Z & Y & 0 & \vdots \\ 0 & 0 & Y & -Z & \ddots & 0 \\ \vdots & \vdots & \ddots & \ddots & \ddots & Y \\ 0 & 0 & \dots & 0 & Y & -Z_G \end{bmatrix} \begin{bmatrix} I_1 \\ I_2 \\ I_3 \\ \vdots \\ I_N \\ I_{N+1} \end{bmatrix} = \begin{bmatrix} 0 \\ 0 \\ 0 \\ \vdots \\ 0 \\ -\frac{V_s}{s} + V_G \end{bmatrix} \tag{3.161}$$

3.14.3 Transient Performance Sample Analysis

The transient analysis will be performed for a 10km span of underwater transmission line. Figures 3-21 through 3-23 below represent the transient generator current, receiving end voltage, and generator input apparent power when switch S1 is closed while S2 is open.

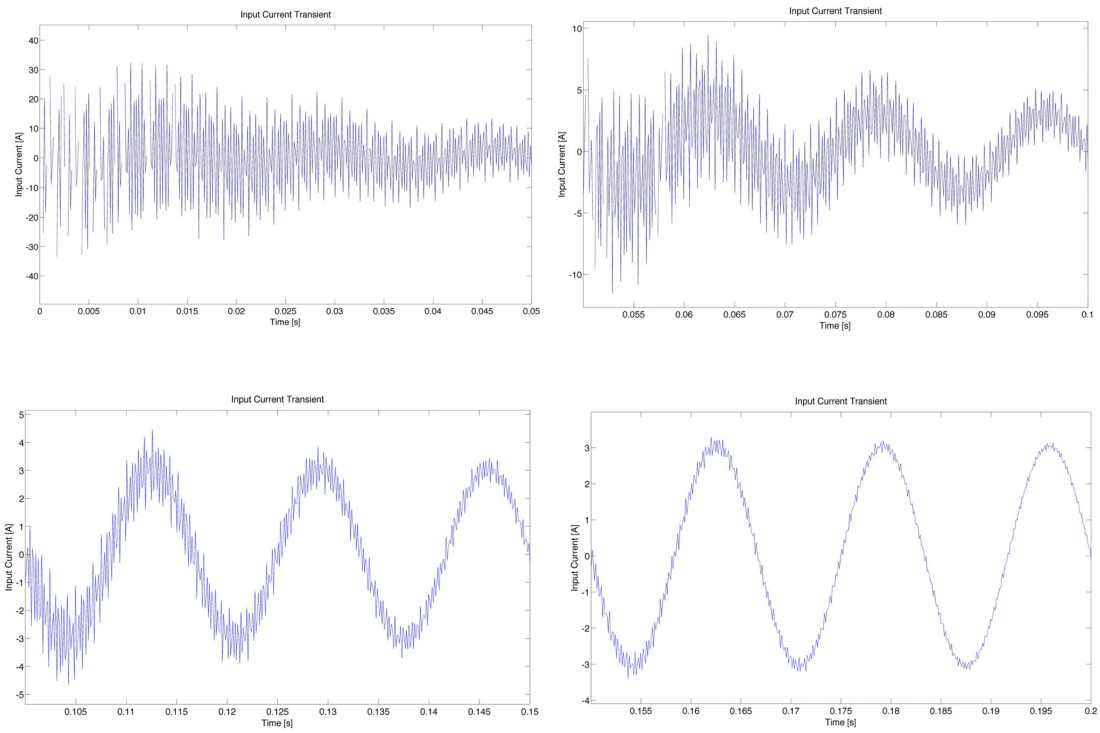

Figure 3-21: Input Current Transient for 12 Cycles

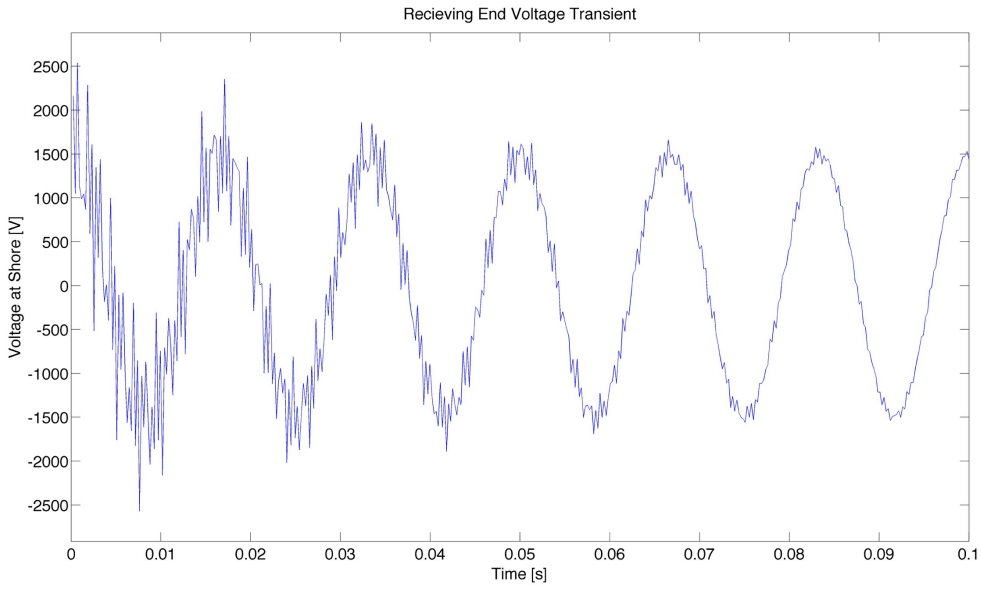

Figure 3-22: Receiving End Voltage Transient For 6 Cycles

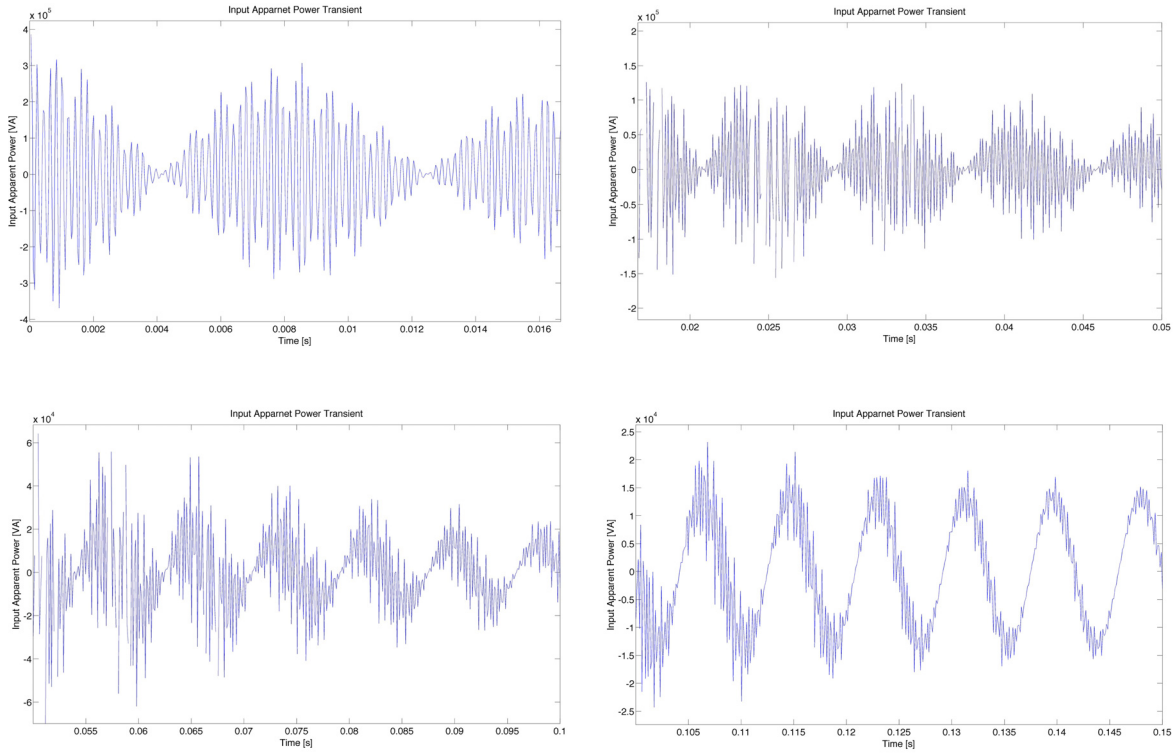

Figure 3-23: Input Apparent Power Transient For 9 Cycles

At a time t_s, the transmission line is switched onto the power grid. Figures 3-24 through 3-27 below show the transient performance when a load is connected. Additionally, the analysis is performed for multiple varieties of cable.

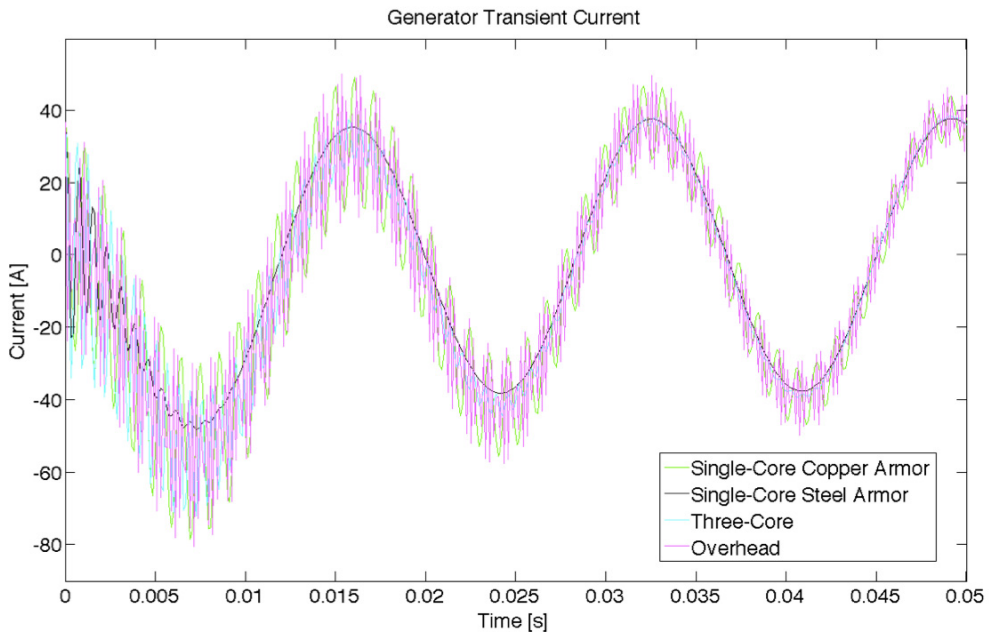

Figure 3-24: Transient Sending End Current

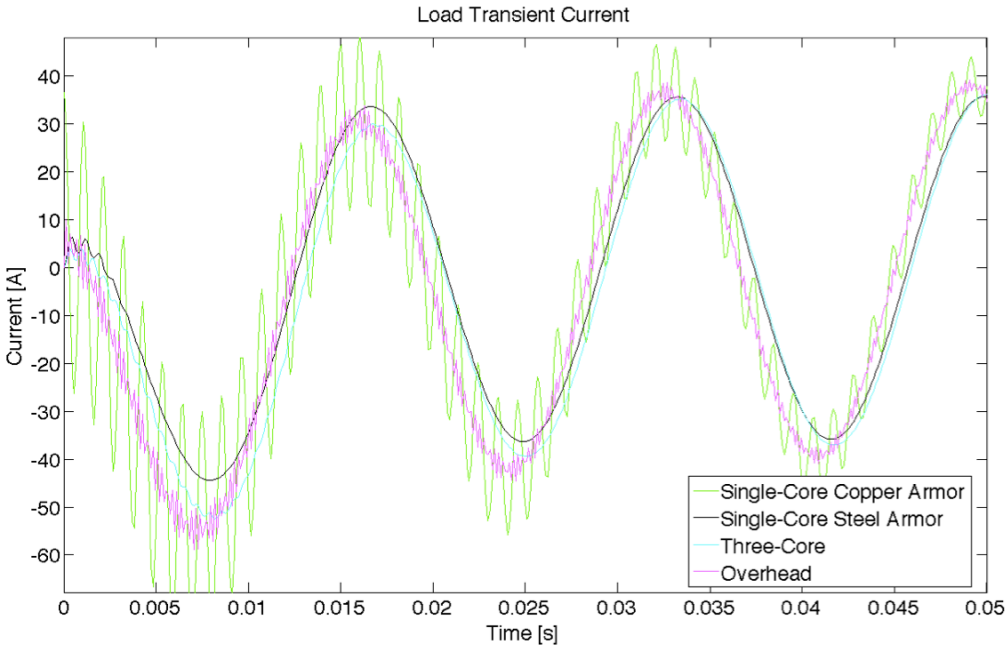

Figure 3-25: Transient Receiving End Current

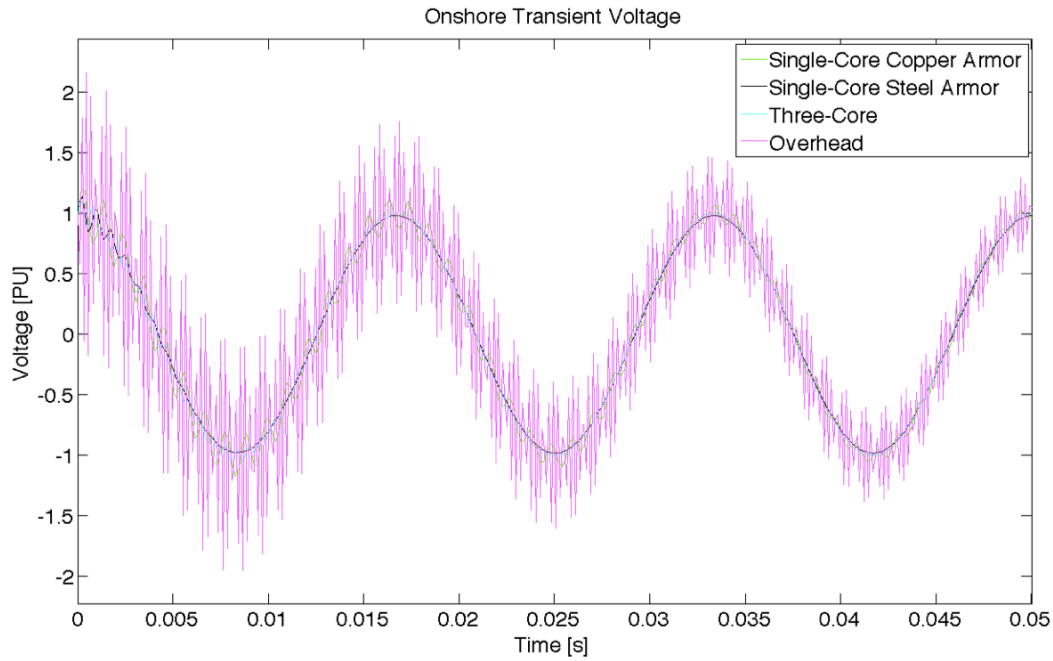

Figure 3-26: Transient Receiving End Voltage

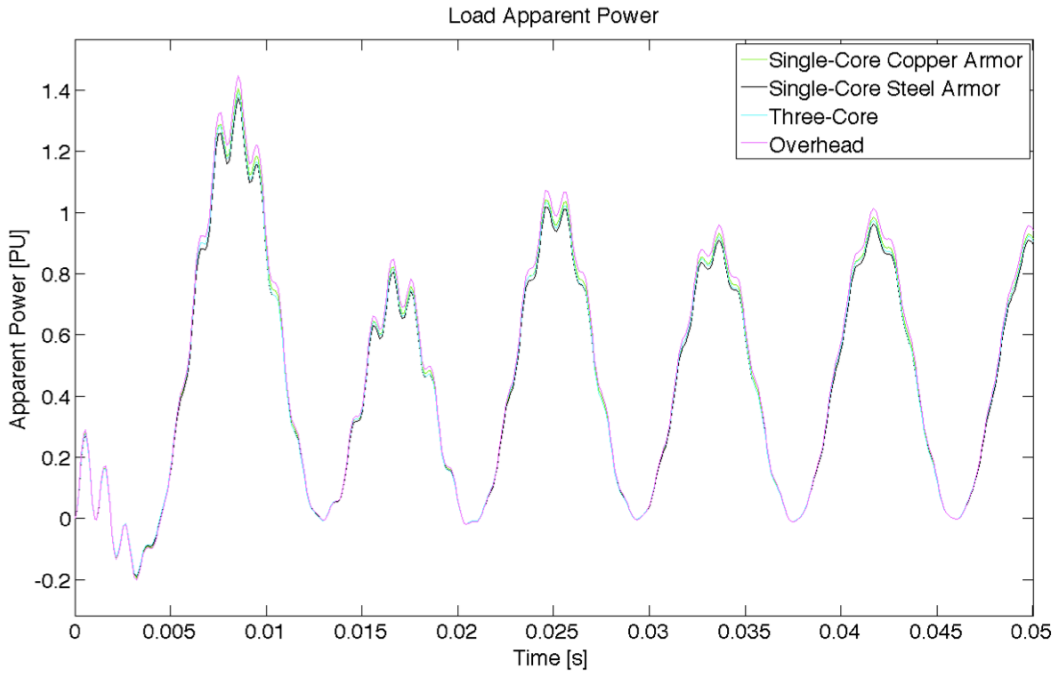

Figure 3-27: Transient Load Apparent Power

Offshore power cables, generally have a better transient performance, in terms of the settling time, peak overhsoot. This is due to the larger resistance and capacitance associated with the cables [31]. It can be observed from the input apparent power that there is significant reactive power that the cable absorbs. This can be observed when the cable is disconnected from the power grid.

3.15 Harmonic Analysis

Underwater power cables have unique characteristics only seen by very long overhead transmission lines. The harmonic analysis of these cables will show how harmonic components will be amplified or attenuated [56,57,58]. If any harmonics are to be transmitted on the cable, it is important to know if they occur at resonance points of the cable. If they do, damage could potentially be done to the cable due to electrical stress on the insulation. For the harmonic analysis, there are two cases to study, when the cable is loaded and when it is unloaded. When the cable is loaded, the two port network equations provide the following relationship:

$$\frac{V_R}{V_S} = D - B\frac{S_S^*}{|V_S|^2} \tag{3.162}$$

When the cable is unloaded, the following relationship holds:

$$\frac{V_R}{V_S} = \frac{1}{A} \tag{3.163}$$

To analyze the frequency response, it should be noted that the resistance and inductance of the cables is a function of frequency. This frequency variability will be accounted for when performing the analysis.

3.14.1 Unloaded Cable

The unloaded transmission analysis will be conducted with the same cable that will be used for the loaded case. This cable is chosen suitably such that it can transmit 3MVA at 0.95 leading power factor at 32.5kV at the sending end of the transmission line. A harmonic response will also be produced for an equivalent overhead transmission line. Figures 3-28a-d below show the harmonic responses for the various cables.

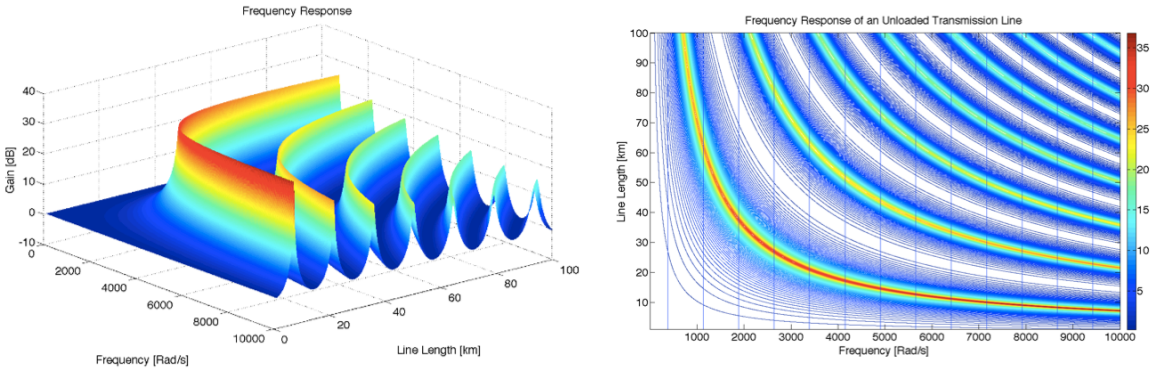

Figure 3-28a: Single-Core Copper Armor Cable Harmonic Response

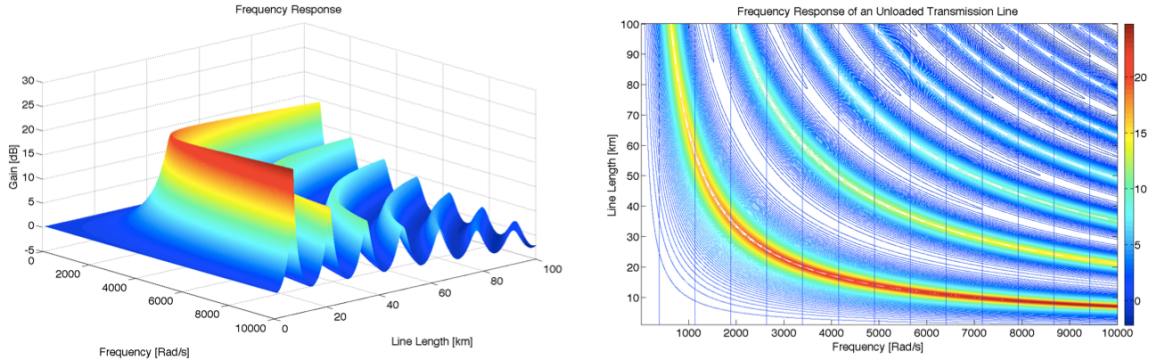

Figure 3-28b: Single-Core Steel Armor Cable Harmonic Response

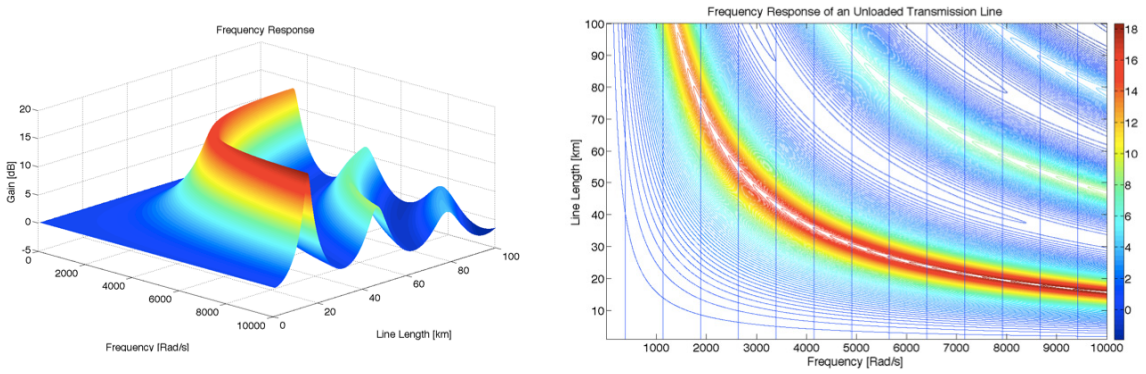

Figure 3-28c: Three-Core Cable Harmonic Response

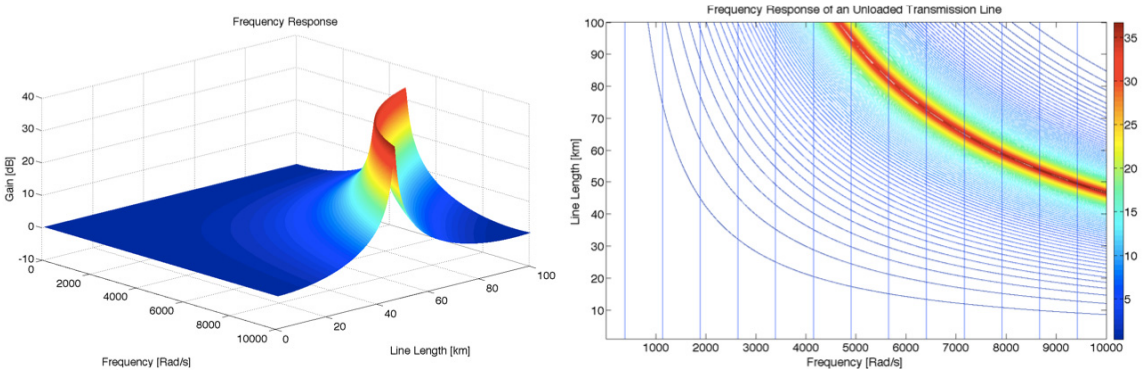

Figure 3-28d: Overhead Cable Harmonic Response

From Figure 3-28, the following observations can be made regarding the harmonic response for unloaded underwater power cables:

- The length of an underwater transmission lines should be considered when there is no load; a resonance will occur at the fundamental frequency sooner than overhead cables.

- If the harmonic components are large enough, there could potentially be high voltages at various spots along the underwater power cable. This is due to the resonances.
- Single core cables with iron armor and three core cables have reduced resonance peaks.
- Three core cables have fewer resonances in the range of study while overhead cables have the least.

3.14.2 Loaded Cable

The loaded transmission analysis as stated previously will employ a cable chosen suitably such that it can transmit 3MVA at 0.95 leading power factor at 32.5kV at the sending end of the transmission line. Again, a harmonic response will also be produced for an equivalent overhead transmission line. Figures 3-29a-d below show the harmonic responses for the various cables.

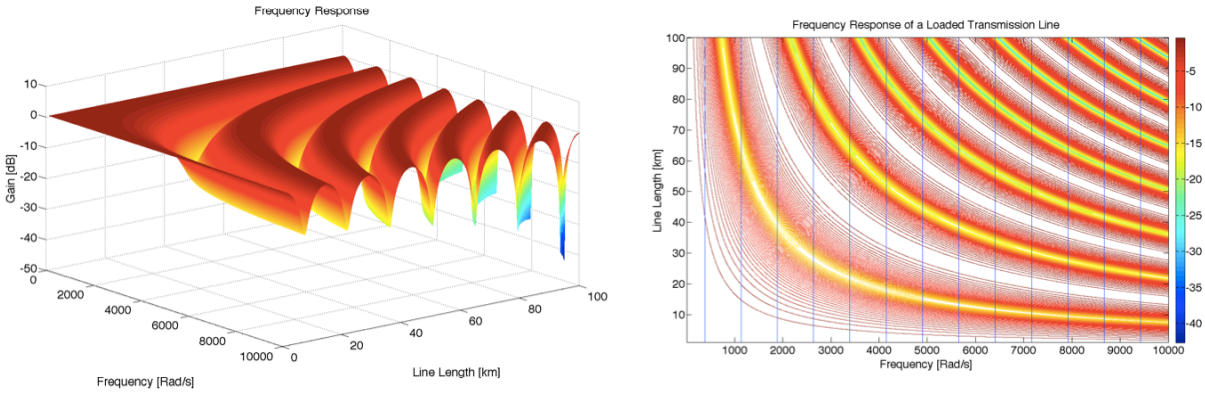

Figure 3-29a: Single-Core Copper Armor Cable Harmonic Response

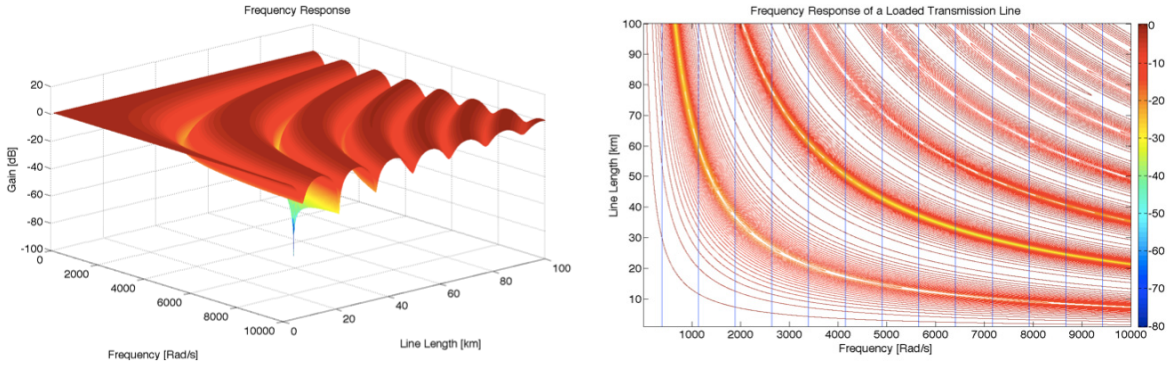

Figure 3-29b: Single-Core Steel Armor Cable Harmonic Response

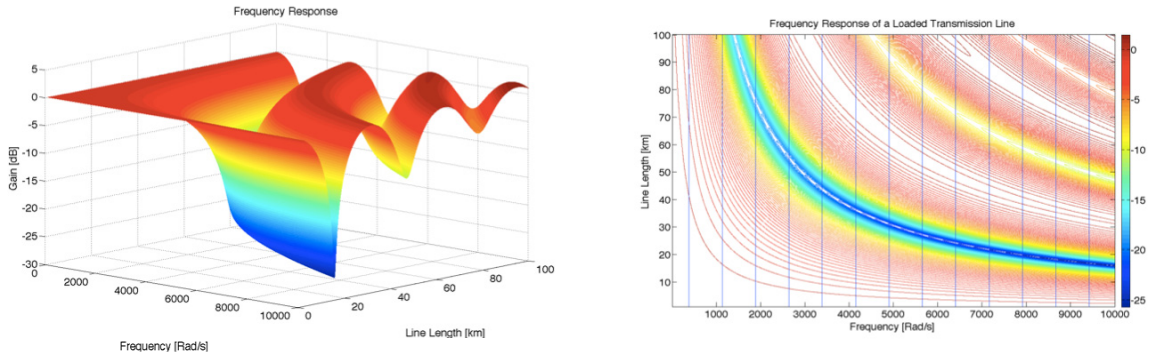

Figure 3-29c: Three-Core Cable Harmonic Response

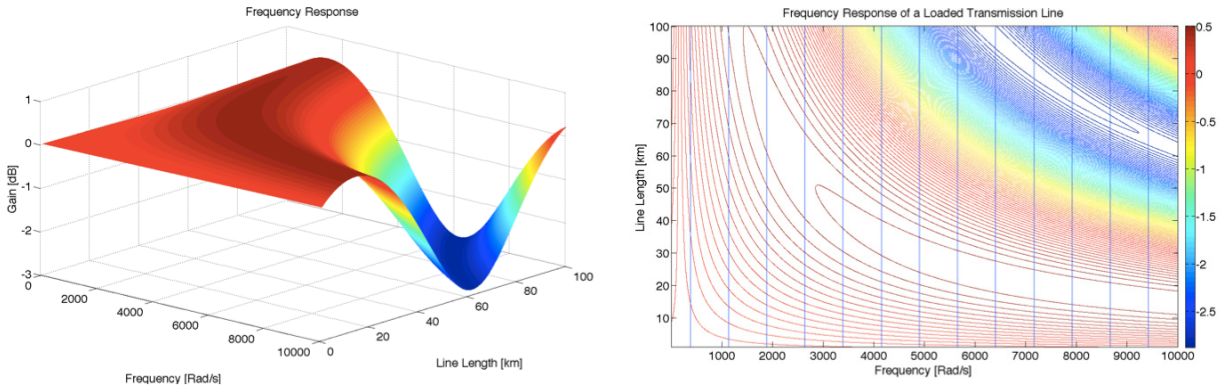

Figure 3-29d: Overhead Cable Harmonic Response

From Figure 3-29, the following observations can be made regarding the harmonic response for loaded underwater power cables:

- Underwater power cables have voltage decay sooner than overhead cables.
- When implementing underwater power lines greater than 100km it is possible for the receiving end voltage to be zero.
- Underwater power cables have more voltage trough regions.
- Single-core cables with copper armor have significant dampening as length and frequency are increased.
- Three-core cables have slightly more voltage troughs than overhead cables.
- Single-core cables with steel armor have a point in this range where the reflection coefficient is -1, a voltage zero.
- Minimal voltage gain for the cables in this range of study.

Chapter 4: Power Conversion

This chapter will summarize power converters that are commonly used with renewable energy applications. Power converters are used in offshore applications for a variety of reasons. Converting an AC waveform to DC would allow for the use variable frequency generators. Transmitting DC as opposed to AC may also be necessary depending on the underwater transmission line length. The various power converters that are used in offshore power applications will be discussed, models developed for them, and observations will be made about how the generated harmonics will affect an underwater power cable.

4.1 Introduction

There are several reasons to use power converters in offshore power applications. These reasons include frequency regulation, and AC to DC conversion for power transmission. Underwater power cables have a large capacitance associated with them. This makes AC power transmission difficult for long transmission line lengths. Transmitting DC power makes this added capacitance inconsequential for steady state operation. There are four categories of power converters. These are converters are as follows [59]:

- AC input – DC output, also known as a rectifier
- DC input – AC output, also known as an inverter
- DC input – DC output
- AC input – AC output

This chapter will focus only on the first two converter types. There are several topologies in which the power converters can be used. The first is to convert the generated AC voltage waveform to DC and then back to AC for power transmission. What this effectively does

is it can allow for regulation of the output frequency of the converter. The second is to convert the generated power to DC and transmit it to shore. Once on shore the DC power will be converted back to AC for integration with the power grid.

4.2 Switches

Power converters are centered on the concept of having controllable switches that convert a current or voltage waveform to a desirable form. An ideal switch has the following characteristics [59]:

- An infinite voltage blocking capability
- No current flows when the switch is off
- An infinite current capability when the switch is on
- Zero voltage drop across the switch when its on
- No switching or conducting losses
- An ability to operate at any frequency

There are several kinds of switch technologies used in power converters. These include diodes, thyristors, and transistors [59]. The selection of which kind of switch to use in a power converter depends on the voltage operating point, the required current capacity, controllability requirement of the switch, speed of switching, and the switching losses [30,59]. Each of these switches has a different performance and for a given application, a suitable set of switches must be used.

4.2.1 Diode

A diode is a simple electronic switch that is uncontrollable. This switch turns on and off based on the voltage and current characteristics of the circuit that it is in. The equation relating the diodes current and voltage drop is given as follows [59]:

$$I_D = I_S\left(e^{\frac{V_D}{nV_T}} - 1\right) \tag{4.1}$$

This equation represents the 'on' characteristic of the diode. There are several caveats that must be discussed with diodes. When a sufficient negative voltage is applied across a diode, there will be a current flow in the opposite way than expected. Also, in the transition between 'on' and 'off' the diode will allow a reverse recovery current to flow. A negative current will flow as the diode transitions to the 'off' state. The amount of time that this negative current flows is called the reverse recovery time. This can become quite significant in high frequency applications [59].

4.2.2 Thyristor

A thyristor is an electronic switch, which has a control that allows conduction [30,59]. An alternative name for thyristors are silicon controlled rectifiers. These devices are capable of passing large currents and blocking high voltages. This makes them ideal for use in high power applications [30,59]. These devices suffer from lower switching speeds [59]. For a thyristor to conduct, the control terminal must have a current applied while there is a positive voltage across the device. The device will continue to conduct while the current flowing through the switch is positive and above a certain value called the holding current level. There are also gate turnoff thyristors, which operate similarly to the previously discussed thyristor, with the exception that they can be turned off with a negative gate

current [59]. Thyristors were in the past used frequently in power conversion technologies. They are still used however; power transistor ratings have increased significantly, making them desirable for use in power conversion along with thyristors [59].

4.2.3 Transistors

Transistors are constructed similarly to diodes with the exception that these devices are controllable switches. There are several kinds of transistors typically used, which include MOSFETs, BJTs, and IGBTs [59]. Transistors have a small resistance between the drain and source terminals when operating in the 'on' state. This resistance is typically in the order of milliohms. Transistors typically have faster switching speeds than the other switching elements [59]. These devices allow for complete control of the on/off state, unlike thyristors, which must become reverse biased to turn off after it has been turned on [59].

4.3 DC Transmission Links

There are three conventional ways to implement a DC transmission system. These methods utilize a monopolar, bipolar, or homopolar link [30]. These various transmission links each have limitations in applicability. It is assumed that a three phase AC source is being converted. The preceding figures represent the single line diagrams. These DC transmission links and their limits of applicability will be discussed in the proceeding sections.

4.3.1 Monopolar Link

A monopolar DC transmission link is one in which there is a single conductor and earth return is used as a ground [30,60,61]. In the case of offshore power systems, the seawater could be used as the return. This transmission link requires one underwater transmission line, as well as one set of power converters. Figure 4-1 below shows the topology for a monopolar DC transmission link.

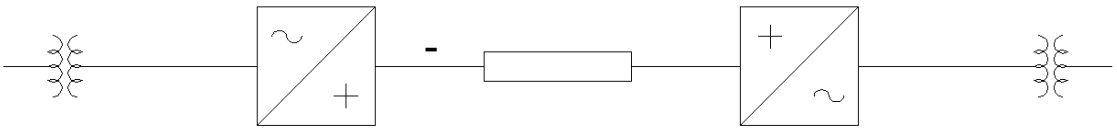

Figure 4-1: Monopolar Transmission Link

Drawbacks to this topology include power transfer limitations as well as no forms of redundancy should a fault occur [30].

4.3.2 Bipolar Link

A bipolar transmission link uses two underwater cables, one with a positive polarity and the other with a negative polarity [30,60,61]. This makes an earth return system unnecessary in the balanced case. In addition to this, two sets of power converters are required. Figure 4-2 below shows the topology for a bipolar DC transmission link.

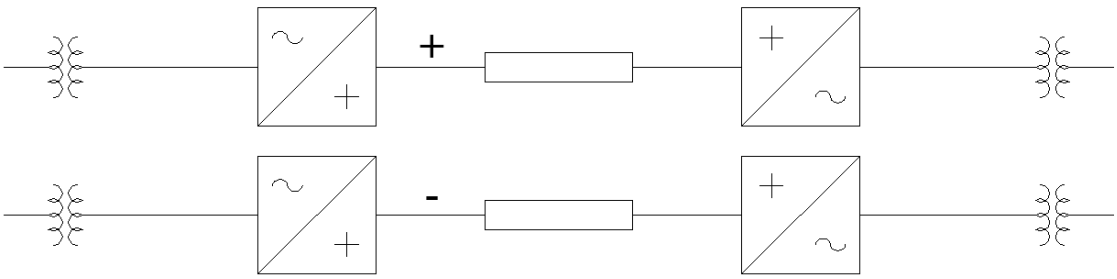

Figure 4-2: Bipolar Transmission Link

There are several advantages to this method of transmission. There is introduced redundancy to the system. Each cable could be transformed into a monopole transmission link with an earth return. This means that under fault conditions, half the load could still be provided. Since there are two cables, half the power is delivered by each, which means that each conductor carries half the current. This results in having two cables with a smaller core conductor.

4.3.3 Homopolar Link

A homopolar link consists of two or more DC transmission lines, each with the same polarity [30]. These transmission links typically operate with a ground return [30,61]. Figure 4-3 below shows a typical homopolar transmission link.

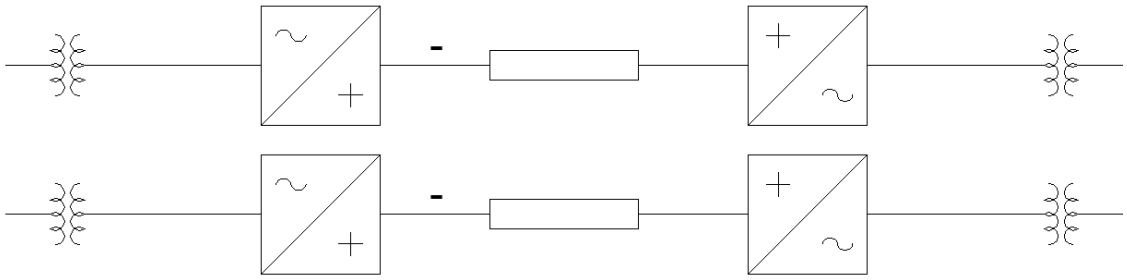

Figure 4-3: Homopolar Transmission Link

Advantages of this topology are that any of these cables/converter systems can be interchanged. So under fault conditions, there is redundancy [30].

4.4 AC to DC Conversion

The conversion from AC to DC involves use of rectifiers. This is the process of using diodes or thyristors to take a three-phase AC source and create a DC source. This is beneficial for underwater power transmission. This is because the capacitance associated with underwater power cables is significant and provides problems for long transmission lengths. Conversion to DC also minimizes the complexity of synchronizing all the AC generators. A drawback to the power conversion process is the generation of harmonics in the process of converting the AC waveform to DC. The most practical/common rectifier used in power systems is the Graetz circuit [30,59,61]. This circuit provides a full wave rectification of a three-phase voltage source. This is the rectifier that will be analyzed in subsequent sections.

4.4.1 Graetz Circuit

The Graetz circuit is commonly used in AC to DC power conversion. The reasoning is for its simplicity and quality of the output waveform. The circuit for this rectifier is shown in Figure 4-4 below.

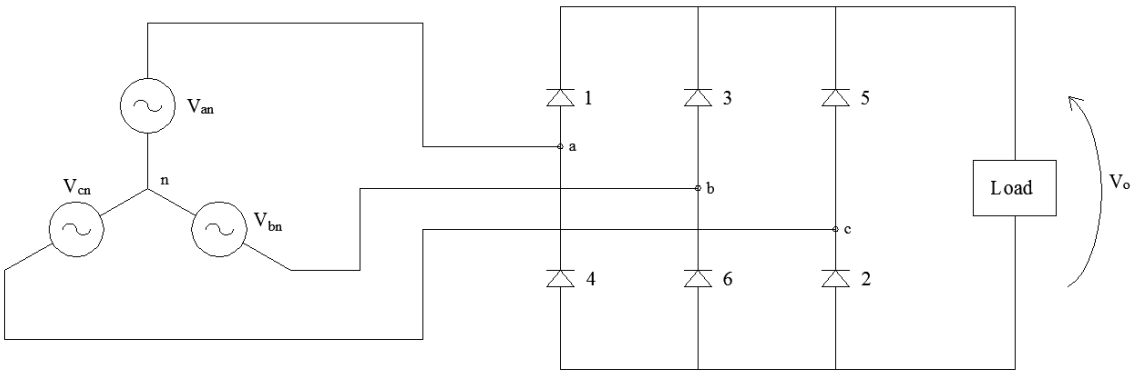

Figure 4-4: Graetz Circuit

This circuit utilizes six diodes or thyristors in the rectification process [30,59,60,61]. This circuit will be modeled using both diodes and thyristors in the proceeding sections.

4.4.2 Graetz Circuit Using Diodes

There are several observations that can be made about this circuit that will allow for an understanding of its operation. It is assumed that we are operating in the steady state and that it is a three-phase system. In this case, the phase voltages will be as shown in Figure 4-5 below.

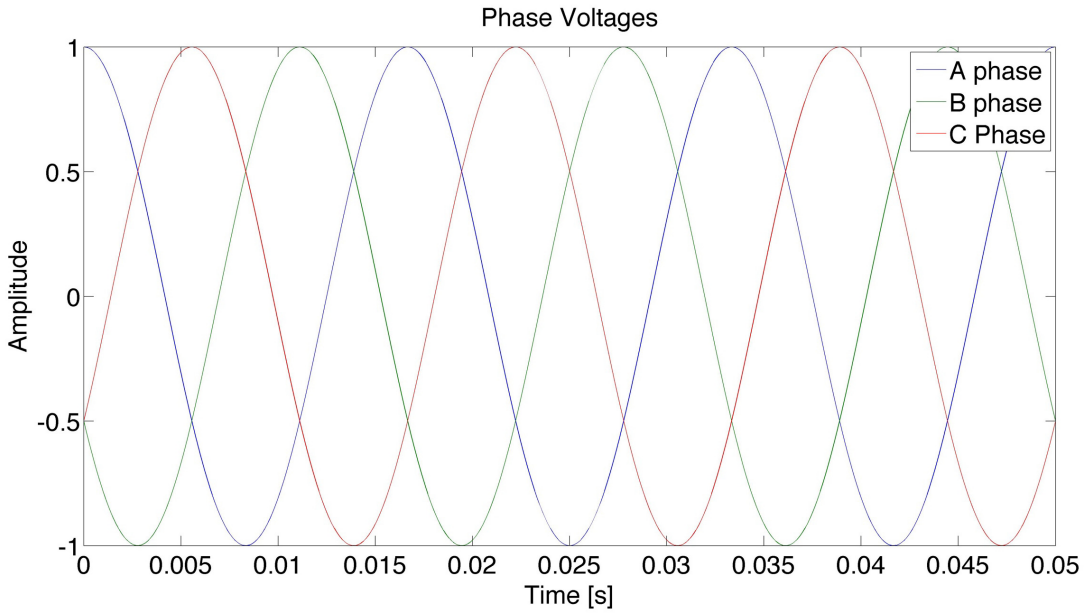

Figure 4-5: Three Phase Voltages

Applying this to the Graetz circuit, it can be observed that:

- The largest phase voltage will turn on a single diode in the top half, diodes 1, 3, or 5. The diode that turns on is the one associated with the largest voltage. The phase voltages oppose each other, and if one is larger than the rest, then the diode associated with that phase voltage would turn on and suppress the others from turning on.

- The smallest phase voltage will turn on a single diode in the bottom half, diodes 2, 4, or 6. The diode that turns on is the one associated with the smallest voltage. The rationale for this is similar to the top half. The most negative voltage will oppose the other bottom diodes from turning on.

- The output voltage is the maximum line-to-line voltage that is possible at any given time.

- Both diodes in a branch cannot be on at the same time. Diodes 1 and 4 can't be on simultaneously for example. This is due to that fact that if diode 1 is on, it is impossible for diode 4 to turn on.

- Provided the assumed phase voltages in Figure 4-5, the following sequence of maximum and minimum can be found: (A, B) (C, B) (C, A) (B, A) (B, C) (A, C). This sequence is recursive and repeats itself every cycle. It corresponds to the following diodes being on: (1, 6) (5, 6) (5, 4) (3, 4) (3, 2) (1, 2). The output voltage will be as follows (V_{AB}) (V_{CB}) (V_{CA}) (V_{BA}) (V_{BC}) (V_{AC}). Each sequence occurs for $\frac{1}{360}$ seconds.

4.4.2.1 Graetz Circuit Steady State Output Voltage

The output from this rectifier is periodic with a period of $\frac{1}{360}$ seconds. This window or periodicity can be modeled by the following equation [59]:

$$V_o(t) = V_{m_{L-L}} \sin(\omega t), \quad \frac{\pi}{3} \leq \omega t \leq \frac{2\pi}{3} \tag{4.2}$$

The window of this sin wave represents the periodic section of the rectifier output. Since this is periodic, the Fourier series can then be written for this.

$$V_o(t) = A_0 + \sum_{n=1}^{\infty} \left[A_N \cos\left(\frac{2\pi n\omega t}{T}\right) + B_N \sin\left(\frac{2\pi n\omega t}{T}\right) \right] \tag{4.3}$$

The coefficients for the Fourier series can be found to be as follows:

$$A_0 = \frac{1}{T}\int_{\frac{\pi}{3}}^{\frac{2\pi}{3}} V_{m_{L-L}} \sin(\omega t)\, d(\omega t) \tag{4.4}$$

This is the DC component of the rectifiers output. Solving for this yields the following DC component.

$$A_0 = \frac{3V_{m_{L-L}}}{\pi} \tag{4.5}$$

The coefficient representing the even component of the signal, A_N, can be found from the following equation:

$$A_N = \frac{2}{T}\int_{\frac{\pi}{3}}^{\frac{2\pi}{3}} V_{m_{L-L}} \sin(\omega t)\cos\left(\frac{2\pi n\omega t}{T}\right) d(\omega t) \tag{4.6}$$

This can be expanded to the following form:

$$A_N = \frac{3V_{m_{L-L}}}{\pi}\int_{\frac{\pi}{3}}^{\frac{2\pi}{3}} \sin(k_1\omega t) + \sin(k_2\omega t)\, d(\omega t) \tag{4.7}$$

Where, $k_1 = 1 + 6n$ and $k_2 = 1 - 6n$.

$$A_N = \frac{-3V_{m_{L-L}}}{\pi k_1 k_2}\left[k_2\left\{\cos\left(k_1\frac{2\pi}{3}\right) - \cos\left(k_1\frac{\pi}{3}\right)\right\} + k_1\left\{\cos\left(k_2\frac{2\pi}{3}\right) - \cos\left(k_2\frac{\pi}{3}\right)\right\}\right] \tag{4.8}$$

Applying trigonometric identities it can be seen that the term on the right is equal to -2. This results in the following expression for A_N.

$$A_N = \frac{-6V_{m_{L-L}}}{\pi(36n^2-1)} \tag{4.9}$$

The coefficient for the odd component, B_N, can be found in a similar way as above.

$$B_N = \frac{2}{T}\int_{\frac{\pi}{3}}^{\frac{2\pi}{3}} V_{m_{L-L}} \sin(\omega t)\sin\left(\frac{2\pi n\omega t}{T}\right) d(\omega t) \tag{4.10}$$

$$B_N = \frac{3V_{m_{L-L}}}{\pi}\int_{\frac{\pi}{3}}^{\frac{2\pi}{3}} \cos(k_1\omega t) - \cos(k_2\omega t)\, d(\omega t) \tag{4.11}$$

$$B_N = \frac{-3V_{m_{L-L}}}{\pi k_1 k_2}\left[k_1\left\{\sin\left(k_2\frac{2\pi}{3}\right) - \sin\left(k_2\frac{\pi}{3}\right)\right\} + k_2\left\{\sin\left(k_1\frac{2\pi}{3}\right) - \sin\left(k_1\frac{\pi}{3}\right)\right\}\right] \tag{4.12}$$

When this is evaluated further using trigonometric identities it can be seen that this term is equal to zero.

$$B_N = 0 \tag{4.13}$$

The Fourier series representing the output of the rectifier can then be modeled by the following equation [59]:

$$V_o(t) = \frac{3V_{m_{L-L}}}{\pi} + \sum_{n=1}^{\infty}\left[\frac{-6V_{m_{L-L}}}{\pi(36n^2-1)}\cos(6n\omega t)\right] \tag{4.14}$$

The harmonics that are resultant at the output of the rectifier can be found by observing the Fourier series. The output when using twenty of the Fourier series terms can be observed in Figure 4-6 below. The term $V_{m_{L-L}}$ was chosen to be unity.

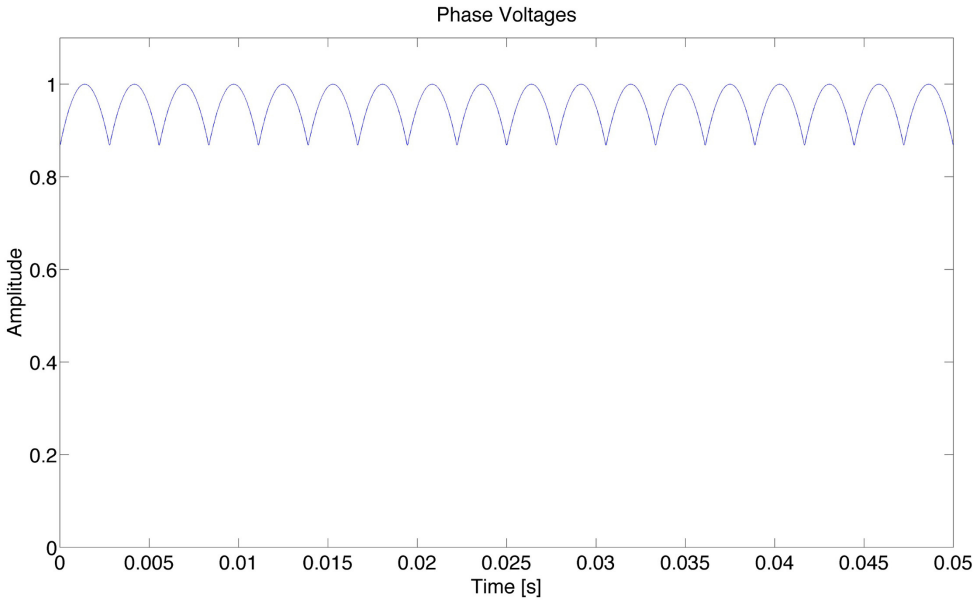

Figure 4-6: Graetz Rectifier Using Diodes Output Voltage Waveform

4.4.2.2 Graetz Circuit Output Voltage Harmonics

The output voltage of this power converter has a significant DC component but also has harmonics associated with it. Ideally speaking, the output of the rectifier should only be a DC waveform. These additional harmonics must be removed from the waveform by use of either the underwater transmission line it is connected to, or additional filtering. The normalized amplitudes of the harmonics for this rectifier output can be found to be as follows:

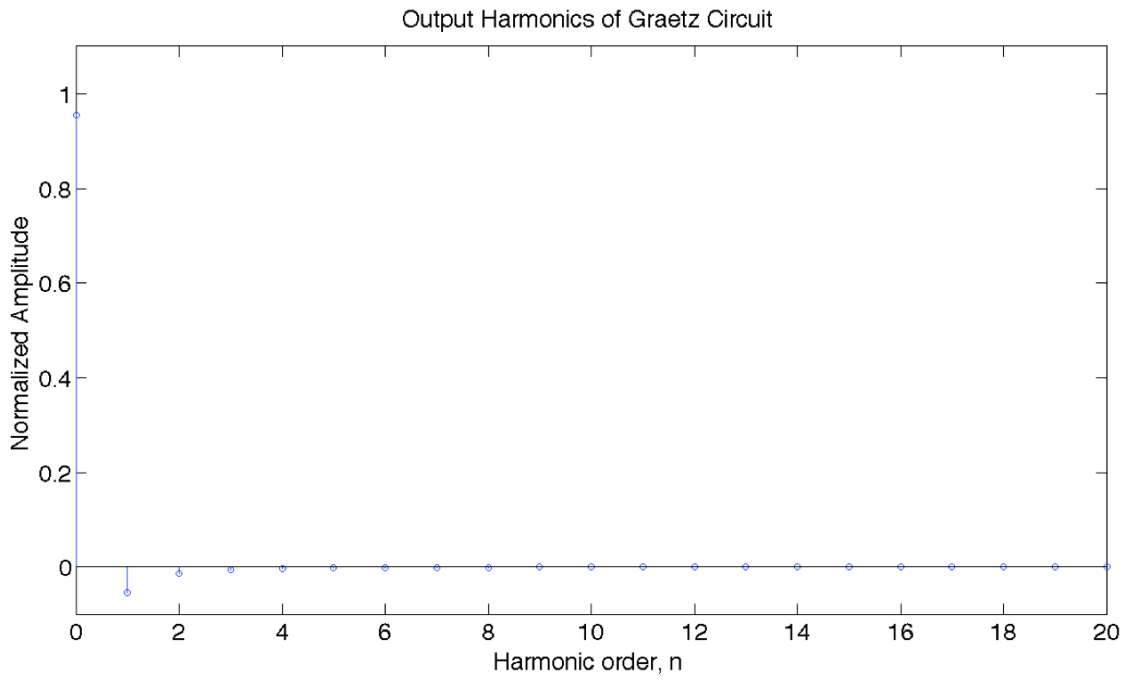

Figure 4-7: Harmonics Output of the Graetz Circuit

The harmonics shown in Figure 4-7 are normalized with respect to the input $V_{m_{L-L}}$. Figure 4-7 shows which harmonic components are most significant in modeling the output of the rectifier. It is worth noting that the frequency of each of the harmonics is given by the following equation:

$$f_n = 360n \tag{4.15}$$

These frequencies are relatively large and can be easily removed with use of filters. The harmonic distortion associated with the output of this rectifier can be defined as follows [30,59]:

$$THD = \frac{\sqrt{\sum_{n=1}^{\infty}\left[\frac{-6V_{m_{L-L}}}{\pi(36n^2-1)}\right]^2}}{\frac{3V_{m_{L-L}}}{\pi}} \tag{4.16}$$

Where *THD* is the total harmonic distortion. When this is evaluated, the following result is obtained:

$$THD = 0.0593 \tag{4.17}$$

This figure of merit for the power converter gives an idea of how much the harmonics are distorting the DC component.

4.4.3 Graetz Circuit With Thyristor Control

The Graetz circuit previously discussed assumed the use of ideal diodes as the switching devices. Now to be discussed is the Graetz circuit with thyristor control. The thyristors allow for control over conduction [59]. This allows for the control of the average output voltage from the converter. The ideal case discussed previously will be used as a starting point in this analysis. It will be assumed that the period of conduction is the same, however, the time in which conduction happens is delayed by a phase angle α. From this definition, the following can be used to describe what the output of the converter will be. The periodic component at the output of the converter will then be defined as follows [59]:

$$V_o(t) = V_{m_{L-L}} \sin(\omega t), \quad \frac{\pi}{3} + \alpha \leq \omega t \leq \frac{2\pi}{3} + \alpha \tag{4.18}$$

The average voltage for this can then be defined to be as follows:

$$V_{o_{avg}} = \frac{3V_{m_{L-L}}}{\pi} \int_{\frac{\pi}{3}+\alpha}^{\frac{2\pi}{3}+\alpha} \sin(\omega t)\, d(\omega t) \tag{4.19}$$

The result of this integration results in the following average output voltage for each period.

$$V_{o_{avg}} = \frac{3V_{m_{L-L}}}{\pi} \cos\alpha \tag{4.20}$$

The closed form expression representing the harmonic amplitudes for the output voltage is difficult to display and is best shown graphically. It can be noted that the frequency of the harmonics will be the same as for the ideal Graetz circuit. The harmonic amplitudes would be found in a similar method to equations (4.3), (4.6), and (4.10) with exception that in this case the bounds of integration are different. The bounds of integration are shifted by the time delay, α. The harmonic magnitudes also have a phase associated with them. The Fourier series can alternatively be expressed in the following form:

$$V_o(t) = A_0 + \sum_{n=1}^{\infty} \left[C_N \cos\left(\frac{2\pi n\omega t}{T} + \phi_n\right)\right] \tag{4.21}$$

Where,

$$C_N = \sqrt{{A_N}^2 + {B_N}^2} \tag{4.22}$$

$$\phi_n = -\tan^{-1}\frac{A_N}{B_N} \tag{4.23}$$

Figure 4-8 below shows the first five harmonic amplitudes, as well as the DC component, as a function of the delay angle α. These harmonic amplitudes will be normalized with respect to the line-to-line voltage $V_{m_{L-L}}$.

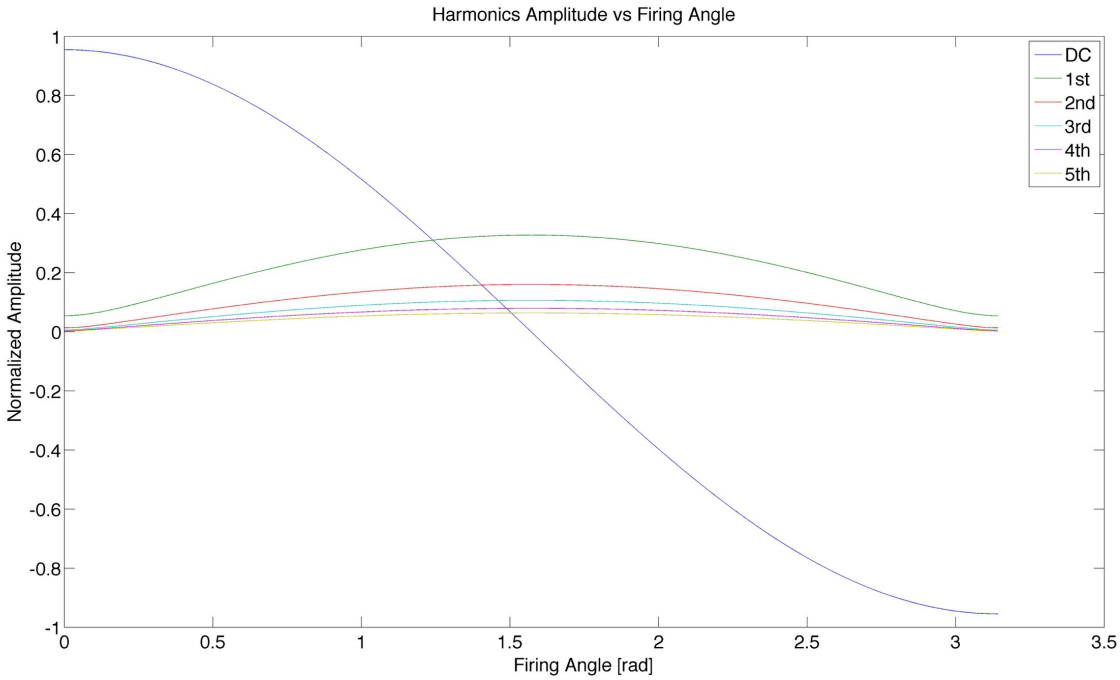

Figure 4-8: Controlled Graetz Circuit Harmonic Amplitudes.

The harmonic amplitudes increase and the DC component decreases as the firing angle increases. A firing angle of zero or pi radians result in maximization of the DC component and minimization of the generated harmonic amplitudes.

For each of the harmonic magnitudes there exists a phase plot. These phase plots complete the Fourier series analysis of the controlled Graetz circuit. Figure 4-9 below gives an example of the phase plot for the first harmonic of this circuit.

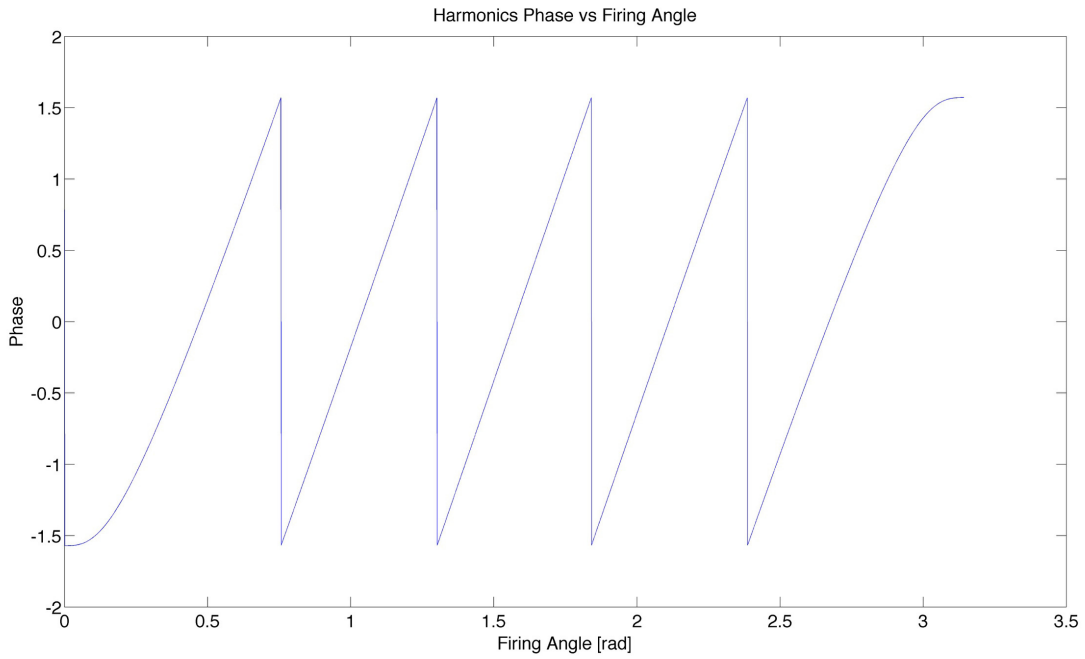

Figure 4-9: First Harmonic Phase

The phase plots are periodic and the frequency varies with the harmonic order. The trend is similar for each of the harmonics. Comparing the results obtained for the controlled Graetz circuit to the non-controlled Graetz circuit, the following observations can be made:

- The harmonics at the output of the controlled Graetz circuit can be an order of magnitude larger.
- The DC component can be varied through control of the delay angle.
- More significant filtering may be required for the controlled Graetz circuit.

To maintain the real power transfer from the AC power source to the DC transmission line, the following observations can be made [30]:

$$P_{AC} = P_{DC} \tag{4.24}$$

$$P_{AC_{RMS}} = \frac{\sqrt{3}}{2} V_{L-L} I_L \cos\phi \tag{4.25}$$

$$P_{DC} = V_D I_D \tag{4.26}$$

$$V_D = \frac{3V_{L-L}}{\pi} \cos\alpha \tag{4.27}$$

$$I_L = \frac{2\sqrt{3}}{\pi} I_D \tag{4.28}$$

In equations (4.27) and (4.28), V_D and I_D correspond to the RMS output voltage and current of the Graetz circuit. Substituting equations (4.24) to (4.28) together yields the following result [30]:

$$cos\phi = \cos\alpha \tag{4.29}$$

This implies that the power factor angle must match the delay angle for optimal power transfer [30].

4.4.4 Graetz Circuit and Underwater Transmission Lines

From equation (4.14) it can be observed that the output of the Graetz circuit consists of a DC voltage and the summation of various frequency sinusoids. To study how the harmonics from this will be amplified or attenuated during transmission, the superposition of signals can be applied. The two-port network theory discussed in Chapter 3 can be applied for each of these components of the waveform. As was demonstrated in Chapter 3, the worst case occurs when the transmission line is open circuited on the load side; this is the case that will be studied. Applying the results in Chapter 3, the gain at the receiving end of an underwater power cable can be found to be as follows:

$$\frac{V_R}{V_{m_{L-L}}} = \frac{3}{\pi} + \frac{\sum_{n=1}^{\infty}\left[\frac{-6}{\pi(36n^2-1)}\right]}{\cosh\Gamma\ell} \tag{4.30}$$

Where $\cosh \Gamma \ell$ is the term A from the two-port network parameters as defined in Chapter 3. It should be noted that A is a function of frequency since the resistance and inductance are frequency dependent parameters. If the first four harmonic values are taken for an underwater power cable, the gain and phase at the receiving end of the transmission line can be accurately modeled. Figures 4-10 and 4-11 below show the gain and phase for an assumed underwater power cable.

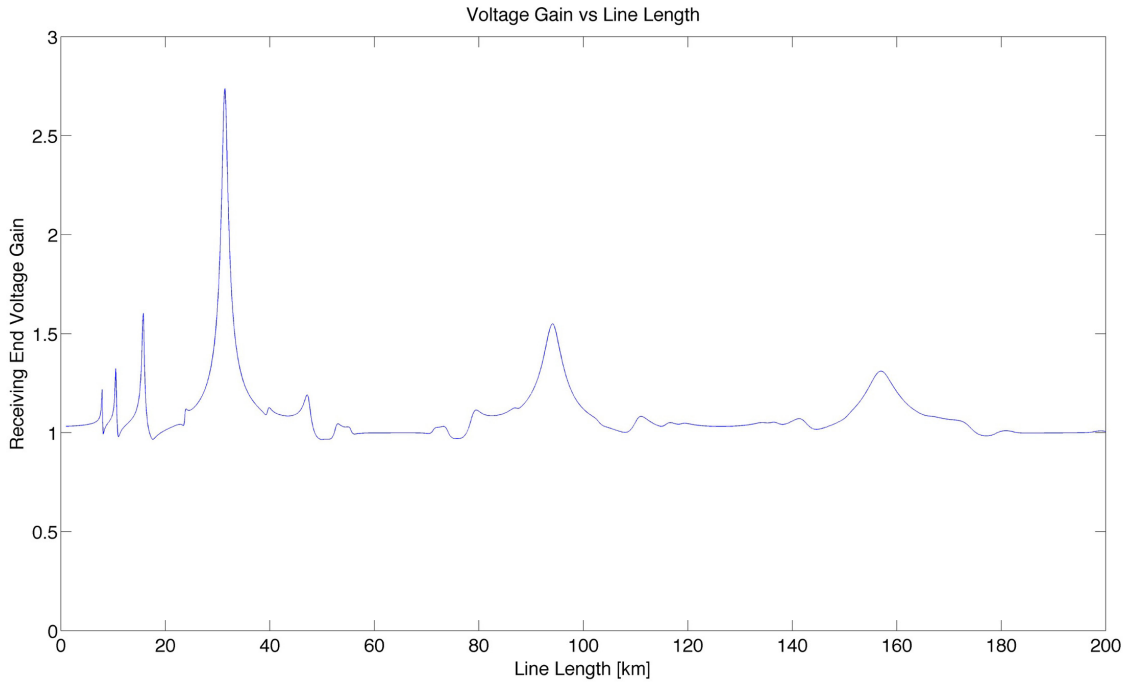

Figure 4-10: Receiving End Voltage Gain

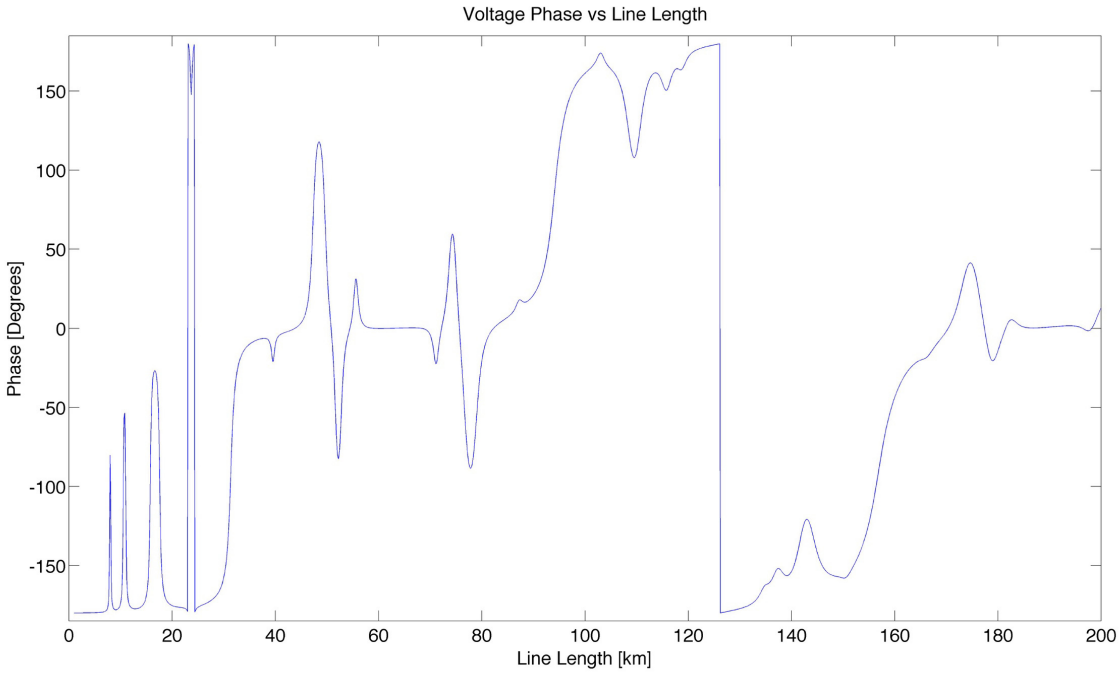

Figure 4-11: Receiving End Voltage Phase

This same result can be shown in three dimensions where the output of the transmission line is plotted as a function of time and line length. Figure 4-12 below shows the three-dimensional plot.

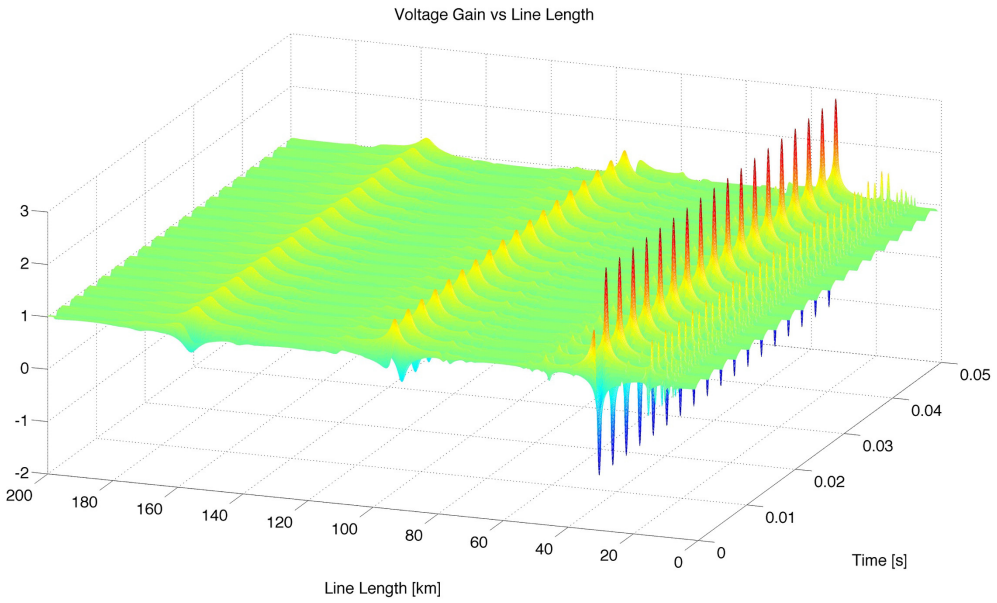

Figure 4-12: Receiving End Voltage vs Line Length and Time

From Figures 4-10 through 4-12, the following observations can be made regarding the output of the transmission line when a Graetz circuit is used for power conversion. The results of this are concluded based on these results and those obtained in Chapter 3 regarding harmonic propagation along a transmission line.

- The first harmonic (360Hz) represents the spikes at 31km, 94.2km, and 157km. These have gains of 2.8, 1.5, and 1.3 respectively.
- The second harmonic (720Hz) represents the spike at 15.8km with a gain of 1.6.
- The third harmonic (1080Hz) represents the spike at 11km with a gain of 1.3.
- The fourth harmonic (1440Hz) represents the spike at 7.9km with a gain of 1.2.
- The harmonic contribution for harmonics above the second are negligible beyond a line length of 20km.

- These voltage spikes, if not removed, could cause insulation damage if they are not accounted for through use of filtering or insulation thickness choice.

This analysis presumed a situation where the load at the receiving end of the transmission line is lost. This results in the most severe voltage gains along the length of the transmission line. As demonstrated in chapter 4, when the transmission line is loaded, the inverse response occurs.

4.4.5 Filtering Options

Due to the generated harmonics from the Graetz circuit and the resonances that can occur on a transmission line, filtering may be a necessity. There are several different ways to remove these harmonics using static passive components. These methods involve the use of a series inductor or use of a two-stage LLC low pass filter. These are the simplest form of passive filtering that can be used in a power system application.

4.4.5.1 Series Inductance

The simplest way to mitigate the harmonics is to place an inductor in series with the line. This blocks the higher frequency harmonics from transmitting through the transmission line. Figure 4-13 below shows the diagram of the network that will be analyzed with a series inductor added to filter the harmonics.

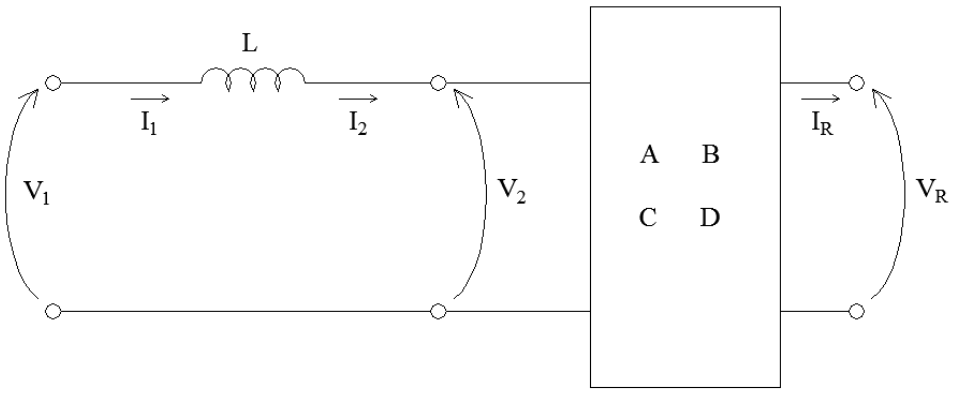

Figure 4-13: Filter Network

The equation describing the voltage loss across this element is as follows:

$$V_2 = V_1 - j\omega L I_1 \tag{4.31}$$

So it can be seen from equation (4.19) that if the frequency is zero, V_2=V_1, but if the frequency is large and inductance is large, then V_2 approaches zero. To observe how the harmonics propagate along the transmission line, the following relationship can be found between the input to the series inductor and the receiving end of the transmission line:

$$\begin{bmatrix} V_1 \\ I_1 \end{bmatrix} = \begin{bmatrix} A + CZ & B + DZ \\ C & D \end{bmatrix} \begin{bmatrix} V_R \\ I_R \end{bmatrix} \tag{4.32}$$

Where $Z = j\omega L$. If the receiving end of the transmission line is again assumed to be open circuited, then the following relationship holds for the gain provided by the transmission line:

$$\frac{V_R}{V_1} = \frac{1}{A+CZ} \tag{4.33}$$

If a 1H series inductor is placed in line with the transmission line, the resultant open circuit harmonic voltage gain can be observed in Figure 4-14 below.

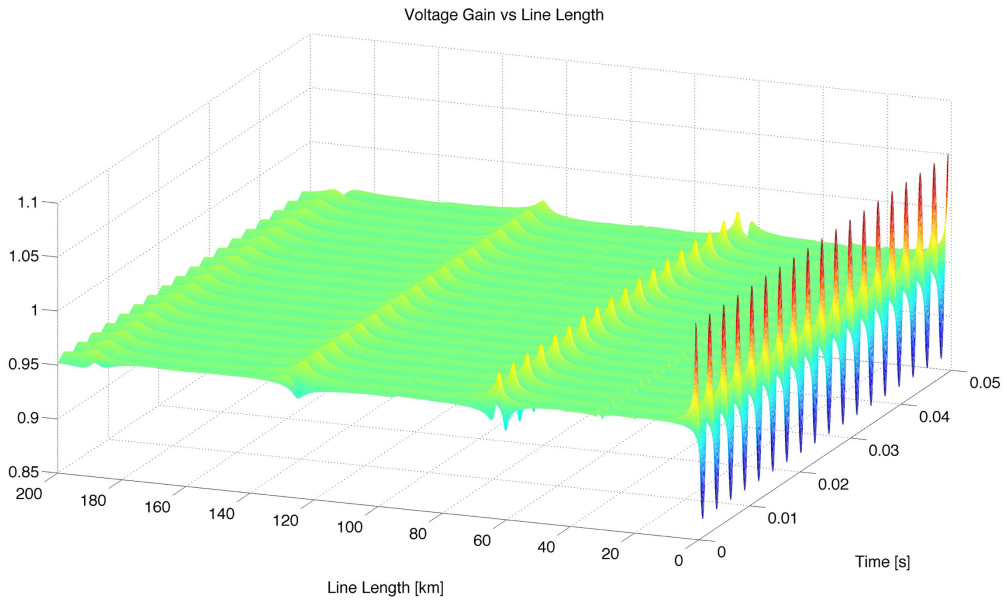

Figure 4-14: Harmonics Gain vs. Line Length and Time with a Series Inductor

The gain provided by the harmonics is at its worst approximately 1.05 times larger than the applied voltage. This demonstrates the attenuation characteristics that a series inductor has on the harmonics. From Figure 4-14 the following observations can be made:

- The output is generally flatter than previously with no series inductor.
- The peak output gain is 1.05 when the transmission line length is less than one kilometer in length.
- Additional resonance has been created by the inclusion of the inductor, however it is minimal in comparison to what it was without a series inductor.
- As the series inductance approaches infinity, the output voltage gain solely becomes the contribution due to the DC component of the input.

4.4.5.2 Two Stage Low Pass Filter

There are several kinds of low pass filters used in power systems. The simplest of these is the two-stage filter. This low pass filter consists of three reactive components, two inductors and one capacitor. Figure 4-15 below shows the topology for this filter.

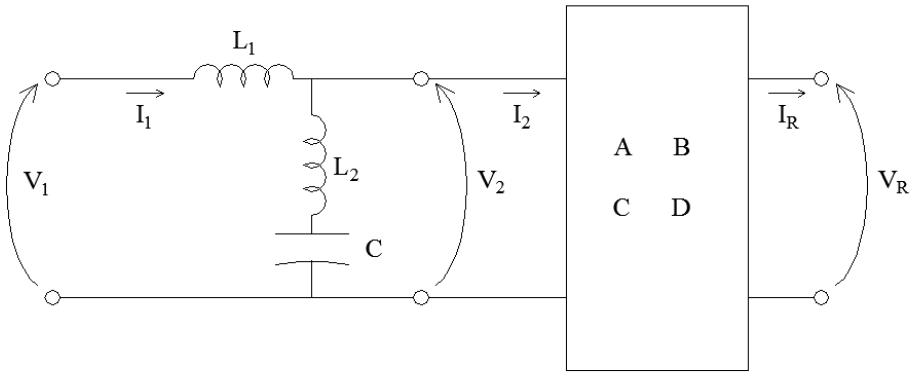

Figure 4-15: Two-Stage Low Pass Filter

This filter is both simple and should provide sufficient attenuation to the harmonics. This is provided that the series inductor, which could be used to reduce the harmonics, is either insufficient or too large for practical purposes. This filter introduces a resonance, however it can be designed to be far away from any of the harmonic components. The attenuation that this filter provides saturates to the following value:

$$A_{max} = 20log_{10}\left(\frac{L_2}{L_1+L_2}\right) \tag{4.34}$$

The resonant and notch peaks occur at the following frequencies:

$$\omega_R = \frac{1}{\sqrt{L_1 C}}, \omega_N = \frac{1}{\sqrt{L_2 C}} \tag{4.35}$$

These three definitions can assist in the design of this filter. The two-port network model of this filter is as follows:

$$\begin{bmatrix} V_2 \\ I_2 \end{bmatrix} = \begin{bmatrix} 1 & -Z_1 \\ -Z_2 & 1 + Z_1 Z_2 \end{bmatrix} \begin{bmatrix} V_1 \\ I_1 \end{bmatrix} \tag{4.36}$$

Where $Z_1 = j\omega L_1$ and $Z_2 = j\omega L_2 + \frac{1}{j\omega C}$. This two-port network model can be used in cascade with a transmission line to observe how the cable naturally filters the harmonics from the Graetz circuit. This filter, when designed properly will allow for even greater attenuation of the harmonics.

4.5 DC to AC Conversion

For a DC transmission link, the generated AC voltage is converted to DC, but it must be converted back to AC such that it can be integrated with the power grid. There is a second possible application of the DC to AC converter, which is as a means to regulate the generated frequency. This interim stage would involve underwater transmission of the inverted waveform. There are two general approaches to inverting a DC signal. The first concept is to reproduce a sinusoidal waveform with use of square pulses [59]. The more square pulses that are used, the closer the signal is to representing a sinusoid. The second concept is to use pulse width modulation and filter out the produced harmonics [59]. The various methods of inversion and their consequences for offshore power systems will be discussed in the subsequent sections.

4.5.1 Voltage Source Converters

The three-phase inverters objective is to take the DC transmission and convert it into an AC voltage waveform such that the system can be interconnected with the power grid. Generally speaking, the inversion process uses square pulses to generally take the form of

a sinusoid [60]. The number of different voltage level pulses that can be used, the more the resultant waveform looks like a sinusoid. Issues with this are the resultant harmonics. The harmonics produced are very close to the 60Hz fundamental frequency and are large in amplitude. Using multiple stage inverters helps reduce the amplitude of these harmonics. Use of pulse width modulation allows for the harmonics to be shifted in frequency, which allows for easier filtering of them. Reduction of the harmonics is a necessity when interconnecting a DC transmission link to the power grid. The harmonics that are generated from power inversion can result in damage to power consumer devices. There are strict regulations regarding what the total harmonic distortion is allowed to be for an interconnected DC link. The various inverter topologies will be discussed in the proceeding sections. The Maritime Link project that is presently under construction is a bipolar +/- 200kV, 500MW transmission line. The power conversion in this project, from DC to AC, is using modern VSC technology [62,63]. VSC technology is usually not implemented in high power or high voltage DC applications [60] but the technological advancements in this area is allowing for larger amounts of power and higher voltages to be converted [64]. This makes VSC power converters a very important power conversion technique to analyze and model for offshore power applications.

4.5.1.1 Single Stage Inverter

The single stage inverter uses three voltage levels to represent a sinusoid. The waveform that is created is similar to a sinusoid. Figure 4-16 below shows generally what the output waveform can be from a single stage inverter [59,60].

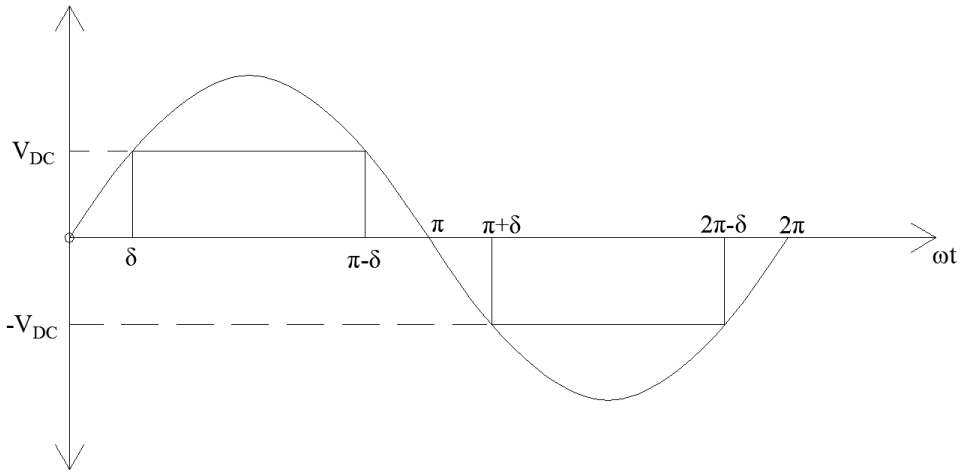

Figure 4-16: General Output Waveform

A single period of this waveform can be modeled by the following:

$$V_o(t) = \begin{cases} V_{DC} & \delta \le \omega t \le \pi - \delta \\ -V_{DC} & \pi + \delta \le \omega t \le 2\pi - \delta \\ 0 & Otherwise \end{cases} \quad (4.37)$$

This output voltage waveform can also be represented by use of the Heaviside functions. If this notation were used to represent equation (4.37) then the following equation can be developed:

$$V_o(\omega t) = V_{DC}\{u(\omega t - \delta) - u(\omega t - \pi + \delta) - u(\omega t - \pi - \delta) - u(\omega t - 2\pi + \delta)\} \quad (4.38)$$

From the symmetry of the problem since the waveform begins at a zero it can be observed that only B_n terms from the Fourier transform are required to model the waveform. It can also be observed that the integration over one full period will be zero, thus the A_0 component is also zero. This results in the following statements:

$$A_n = 0 \quad (4.39)$$

$$A_0 = 0 \quad (4.40)$$

$$B_n = \frac{V_{DC}}{\pi} \int_0^{2\pi} V_o(\omega t) \sin(n\omega t) d(\omega t) \quad (4.41)$$

Solving for this, the following expression can be obtained for the B_n coefficients [59]:

$$B_n = \frac{2V_{DC}\cos(n\delta)}{n\pi}(1-(-1)^n) \tag{4.42}$$

This can further be simplified to the following form [59]:

$$B_n = \frac{4V_{DC}\cos(n\delta)}{n\pi} \tag{4.43}$$

Equation (4.43) only applies for odd values of n. B_n is zero for any value of n that is even. The output voltage waveform Fourier series representation can be observed in Figure 4-17 below.

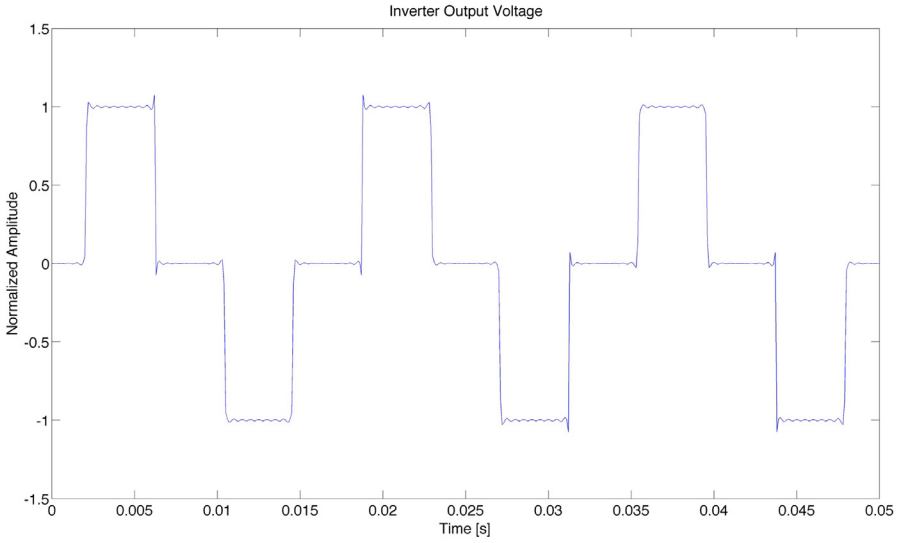

Figure 4-17: Output Voltage, Delay Angle $\pi/4$

The harmonics that are introduced by this vary as a function of the delay angle, however, most importantly is the fact that these harmonics are close in frequency to the fundamental and have a relatively significant amplitude. Figure 4-18 below shows these harmonic amplitudes as a function of the delay angle.

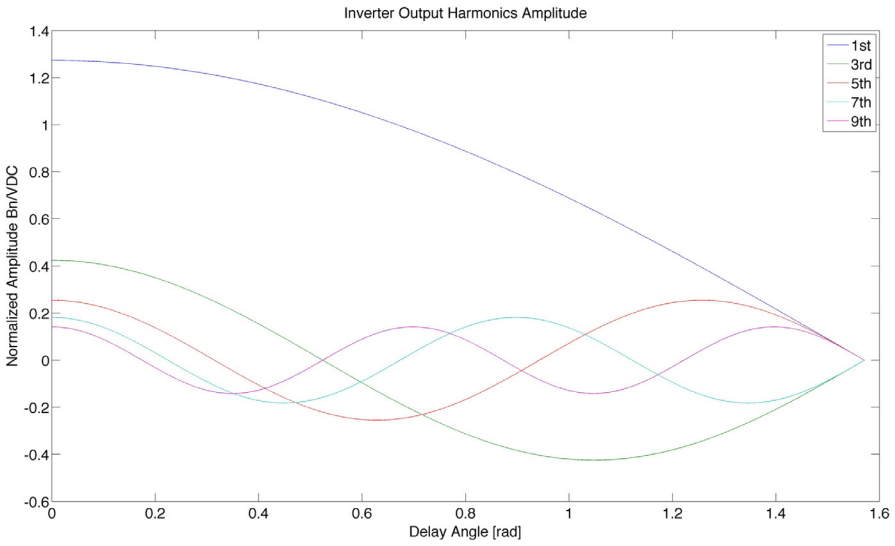

Figure 4-18: Single Stage Inverter Output Harmonics

In this figure the first harmonics is representing the fundamental 60Hz harmonic amplitude. From Figure 4-18, the following observations can be made:

- $f_n = 60(2n-1)\ Hz.$
- The harmonics are close in frequency.
- The 180Hz harmonic amplitude is approximately 1/3 of the fundamental at its maximum value.
- Varying the delay angle can allow there to be a 180Hz harmonic zero.
- The total harmonic distortion can be modeled by the following expression [59]:

$$THD = \frac{\sqrt{\sum_{n=2}^{\infty}\left(\frac{\cos(\delta(2n-1))}{2n-1}\right)^2}}{\cos\delta} \tag{4.44}$$

From this, the total harmonic distortion can be analyzed as a function of the delay angle. Figure 4-19 below shows the total harmonic distortion for a simple single stage power inverter.

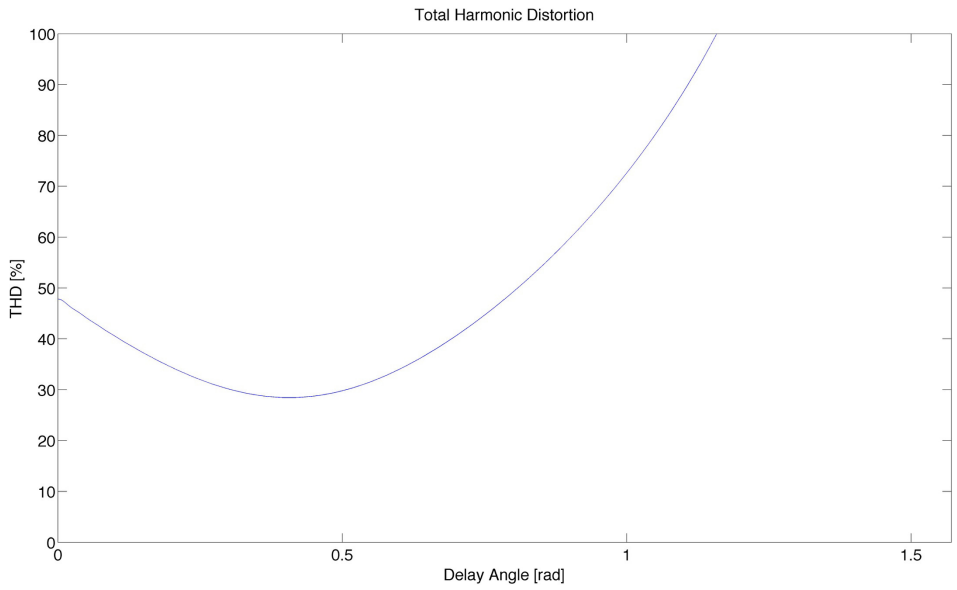

Figure 4-19: Single Stage Inverter Total Harmonic Distortion

It can be observed that the total harmonic distortion reaches a minimum of 28.3% at a delay angle of 0.4 radians. This results is a large total harmonic distorition, however it is approximately two times smaller than a conventional square wave. To improve this further, more stages can be added to the inverter.

4.5.1.2 Multi-Level Inverter

To begin the analysis of the output harmonics from a multi-stage inverter, a two-stage inverter will first be analyzed. The two-stage inverter uses five voltage levels to represent a sinusoid. Figure 4-20 below shows generally what the output waveform can be from a two-stage inverter.

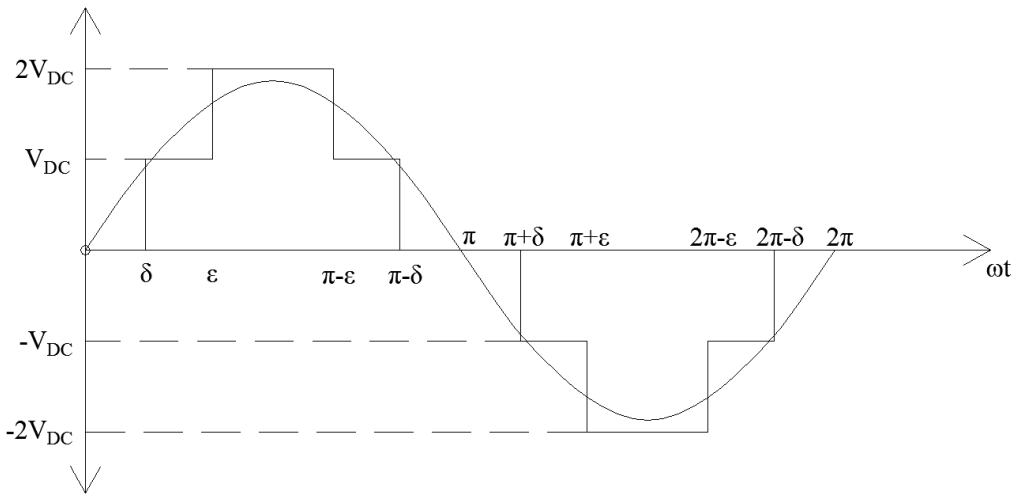

Figure 4-20: General Output Waveform

A single period of this waveform can be modeled by the following:

$$V_o(t) = \begin{cases} V_{DC} & \delta \le \omega t \le \varepsilon \\ -V_{DC} & \pi + \delta \le \omega t \le \pi + \varepsilon \\ 2V_{DC} & \varepsilon \le \omega t \le \pi - \varepsilon \\ -2V_{DC} & \pi + \varepsilon \le \omega t \le 2\pi - \varepsilon \\ 0 & otherwise \end{cases} \tag{4.45}$$

This output voltage waveform can also be represented by use of the Heaviside functions. If this notation were used to represent equation (4.45) then the following equation can be developed:

$$V_o(\omega t) = V_{DC}\begin{Bmatrix} u(\omega t - \delta) + u(\omega t - \varepsilon) - u(\omega t - \pi + \varepsilon) - u(\omega t - \pi + \delta) \\ -u(\omega t - \pi - \delta) - u(\omega t - \pi - \varepsilon) + u(\omega t - 2\pi + \varepsilon) + u(\omega t - 2\pi + \delta) \end{Bmatrix} \tag{4.46}$$

From the symmetry of the problem since the waveform begins at a zero it can be observed that only B_n terms from the Fourier transform are required to model the waveform [59]. This results in the following statements:

$$A_n = 0 \tag{4.47}$$

$$A_0 = 0 \tag{4.48}$$

$$B_n = \frac{V_{DC}}{\pi}\int_0^{2\pi} V_o(\omega t)\sin(n\omega t)d(\omega t) \tag{4.49}$$

Solving for this, the following expression can be obtained for the B_n coefficients:

$$B_n = \frac{2V_{DC}}{n\pi}(1-(-1)^n)\{\cos(n\delta)+\cos(n\varepsilon)\} \tag{4.50}$$

This can also be explained by the observation that this two-stage square wave is the same as the superposition of two single stage square waves studied in the previous section with different delay angles. Equation (4.50) can further be simplified to the following form:

$$B_n = \frac{4V_{DC}\{\cos(n\delta)+\cos(n\varepsilon)\}}{n\pi} \tag{4.51}$$

Equation (4.51) only applies for odd values of n. B_n is zero for any value of n that is even. The equation that represents the output of the inverter will be as follows:

$$V_o(t) = \sum_{n\ odd}^{\infty}\left[\frac{4V_{DC}\{\cos(n\delta)+\cos(n\varepsilon)\}}{n\pi}\sin(n\omega t)\right] \tag{4.52}$$

The output voltage waveform Fourier series representation can be observed in Figure 4-21 below.

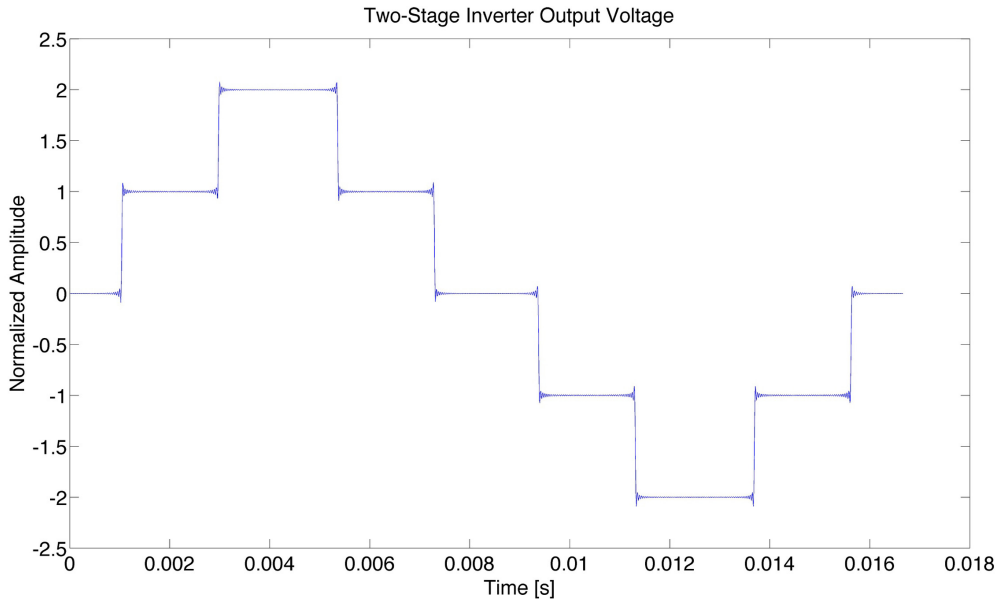

Figure 4-21: Two-Stage Inverter Output

In Figure 4-21 it was assumed that the delay angles were δ=0.393 radians and ε =1.122 radians. This result can be further generalized for any number of stages added. The generalized equation for the harmonic amplitudes of an *m* stage inverter is as follows:

$$B_n = \frac{4V_{DC}}{n\pi}\sum_{i=1}^{m}\cos n\delta_i \tag{4.53}$$

These delay angles can be used to cancel harmonics as was demonstrated in Figure 4-18 above. This harmonic cancellation will now be explored.

4.5.1.3 Multi Stage Inverter Harmonic Cancellation

As discussed previously, it is possible to design the firing angles of a multi stage inverter such that harmonics are cancelled. Given equation (4.53), the output voltage waveform from the inverter will be as follows:

$$V_o(t) = \sum_{n\,odd}^{\infty}\left[\left\{\frac{4V_{DC}}{n\pi}\sum_{i=1}^{m}\cos n\delta_i\right\}\sin(n\omega t)\right] \tag{4.54}$$

Expanding equation (4.54) will result in the following system of equations [59]:

$$\begin{gathered}\cos(\delta_1)+\cos(\delta_2)+\cos(\delta_3)+\cdots+\cos(\delta_m)=mM_i\\ \cos(3\delta_1)+\cos(3\delta_2)+\cos(3\delta_3)+\cdots+\cos(3\delta_m)=0\\ \cos(n\delta_1)+\cos(n\delta_2)+\cos(n\delta_3)+\cdots+\cos(n\delta_m)=0\end{gathered} \tag{4.55}$$

For all values of *n* that are odd these equations can be written. From this expansion it can be observed that there is a possibility for cancelling specific harmonics. There are *m* variables, and thus only *m* equations can be solved. This implies that the fundamental harmonic amplitude can be chosen and that *m-1* harmonics can have zero amplitude. Solutions to these equations can be found from iterative techniques. There are several caveats that must be addressed regarding the iteration techniques. The solutions are not unique, but some solutions are better than others. It will be presumed that a solution that

yields the largest possible value of M_i is desired. The numbers being iterated tend to large values and must be kept within the region of $0 \leq \delta_i \leq 2\pi$. Table 4-1 below lists the largest values of M_i that are possible to achieve for various numbers of firing angles.

Table 4-1: Largest M_i Coefficients for Various Levels of Inverter

Number of Firing Angles	M_i
2	0.87
3	0.81
4	0.67
5	0.8
6	0.69
7	0.61
8	0.63
9	0.61

Calculating these firing angles allows for harmonic cancellations, which allows for easier filtering of the higher frequency components. To study this, an inverter with nine firing angles will be analyzed. The results from this will be contrasted to another inverter with nine firing angles. The two sets of firing angles will be defined as follows:

1. Firing angles chosen to cancel out the eight harmonics after the fundamental
2. Uniformly spaced firing angles

From these two methods, the output waveform in time, harmonic amplitude, and total harmonic distortion will be provided for comparison purposes. Figures 4-22 and 4-23 below represent the nine-stage inverter with designed firing angles. Figure 4-22 is the

waveform as it would appear in time and Figure 4-23 is the waveform, as it would appear in frequency.

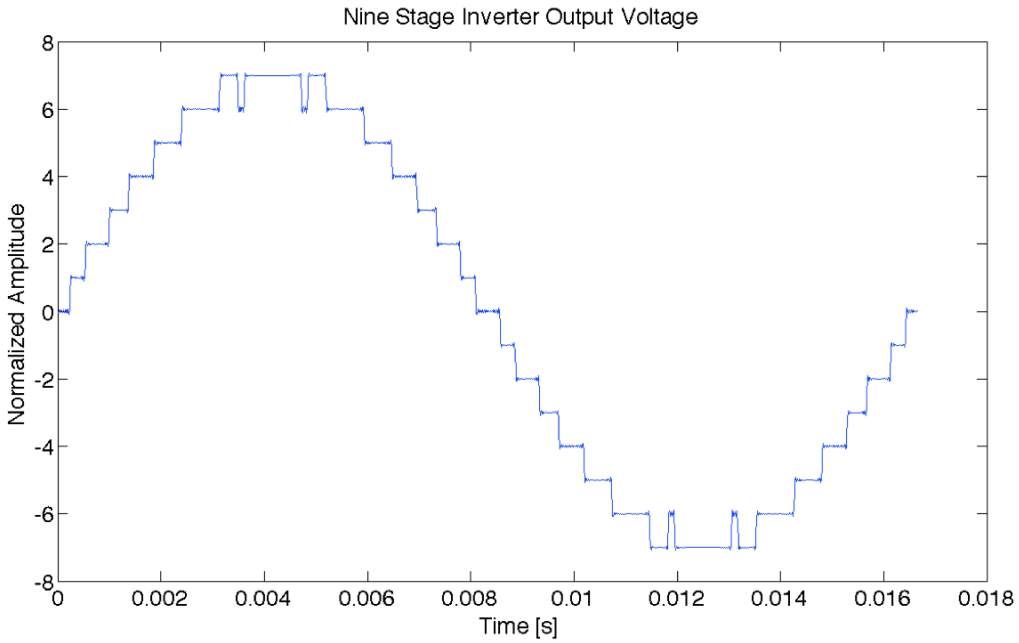

Figure 4-22: Nine-Stage Inverter Output With Designed Firing Angles

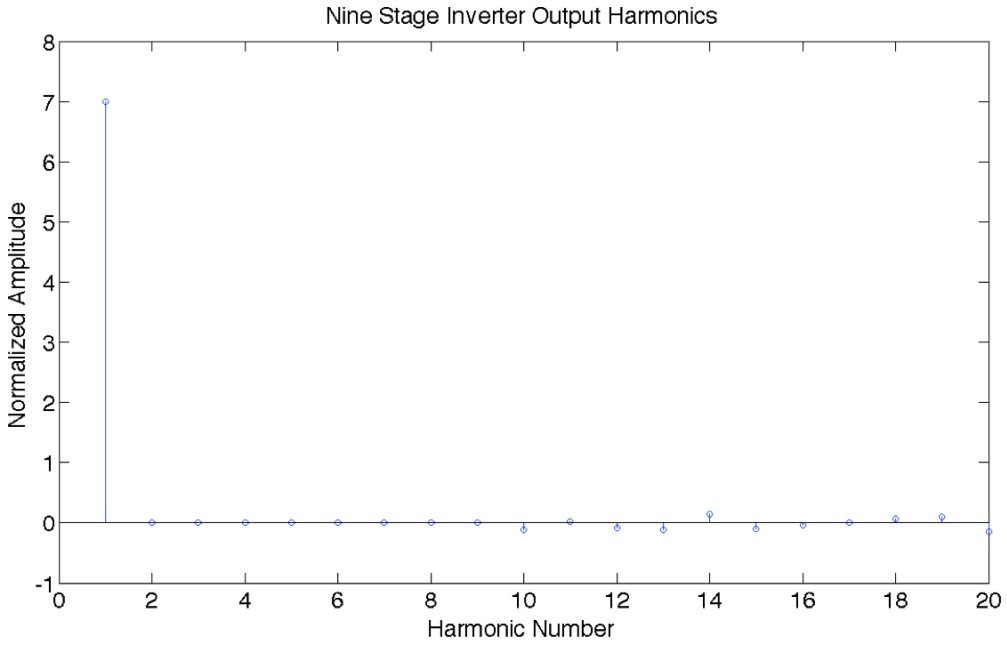

Figure 4-23: Nine-Stage Inverter Harmonics With Designed Firing Angles

The resultant total harmonic distortion for this nine level inverter, with designed firing angles, is 0.0618. This is the harmonic distortion before any filtering is applied at the output of the inverter.

Figures 4-24 and 4-25 below represent the nine-stage inverter with uniform firing angles. Figure 4-24 is the waveform as it would appear in time and Figure 4-25 is the waveform, as it would appear in frequency.

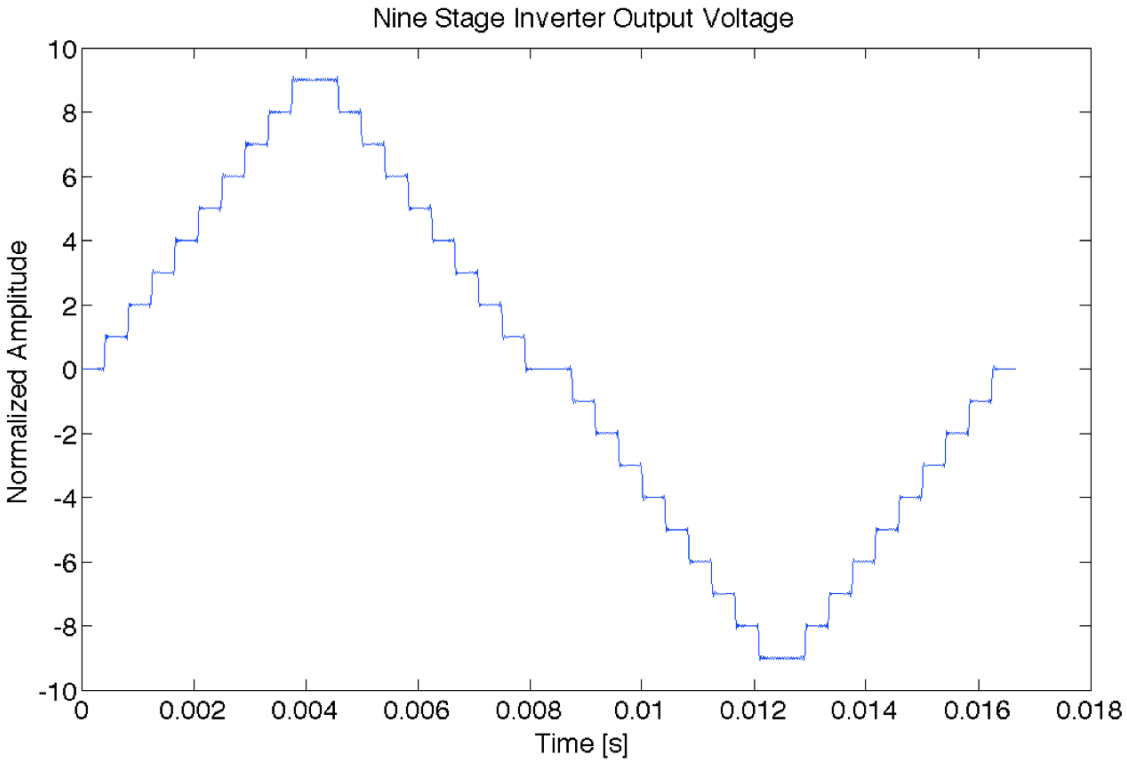

Figure 4-24: Nine-Stage Inverter Output With Uniform Firing Angles

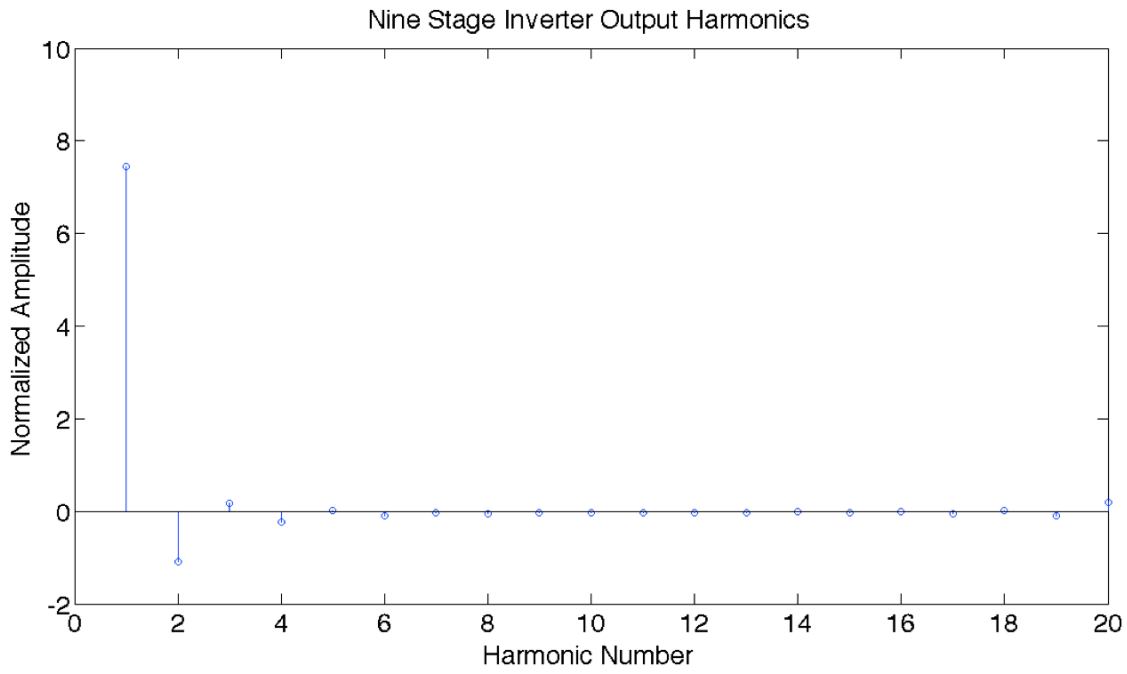

Figure 4-25: Nine-Stage Inverter Harmonics With Uniform Firing Angles

The resultant total harmonic distortion for this nine-level inverter, with designed firing angles, is 0.1617. This is the harmonic distortion before any filtering is applied at the output of the inverter. It can also be noted in Figure 4-25 that the second harmonic has significant amplitude. To reduce the total harmonic distortion, this harmonic would have to be removed. To remove that harmonic, a high order filter would be required.

This result shows that selection of the firing angles allows for a significant decrease in the total harmonic distortion. Use of a simple lower pass filter will result in a very small total harmonic distortion. The consequence for the improvement of the total harmonic distortion is a reduction in amplitude of the fundamental frequency component.

4.5.1.4 Pulse Width Modulation Inverter

The pulse width modulation (PWM) inverter is designed such that the harmonics produced by the inverter are at a much higher frequency then the fundamental. The tradeoff is that the control circuitry is quite complex and there will be a larger amount of switching power loss [59,60]. The PWM inverter generates an output from the comparison of a reference signal to a carrier signal. For power inverters, the reference signal is a sinusoidal waveform and the carrier signal is a triangular waveform.

For bipolar switching, a subtraction is performed between the sin wave and the triangle wave. If the sin wave is larger, the output will be $+V_{DC}$. If the sin wave is smaller, the output will be $-V_{DC}$. Figure 4-26 below shows what the output waveform will be for this switching technique.

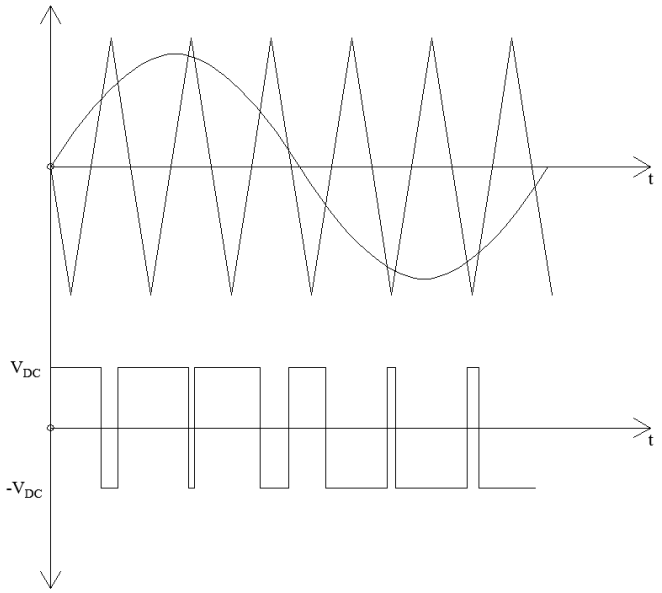

Figure 4-26: Bipolar PWM

For unipolar switching, two waveforms are generated and their difference will represent the output of the inverter. The first waveform outputs $+V_{DC}$ if the sin wave is larger than the triangle wave and zero if the smaller. The second waveform compares a sin wave that is the negative of the one used for the first waveform. The output will be $+V_{DC}$ if this negative sin wave is larger than the triangle wave and zero if smaller. Figure 4-27 below shows the output waveform generated from this switching technique.

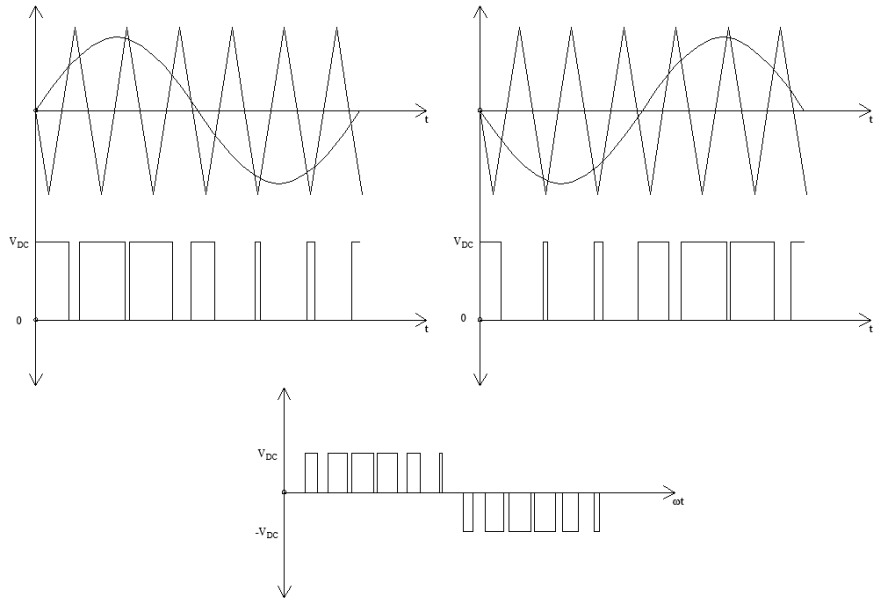

Figure 4-27: Unipolar PWM

Application of PWM does not necessarily make the output waveform better than the previous inversion methods. The harmonics at the output can be quite substantial in comparison to the fundamental frequency, however they occur at much higher frequencies than with the other inverters [59]. The output harmonics from the inverter can be modeled by the analysis of each pulse produced from the inverter and taking the summation of these

for all pulses in a complete cycle. What can be noted from Figure 4-26 and 4-27 is that the period of the pulses that are produced are small in comparison to that of the fundamental frequency. This implies that the frequency components will exist at higher frequencies. This allows for simpler, lower order filters be used to eliminate the harmonics produced from the PWM. To find the Fourier series of bipolar PWM, a generalized square wave with a variable duty cycle can be assumed. The generalized square wave can be observed in Figure 4-28 below.

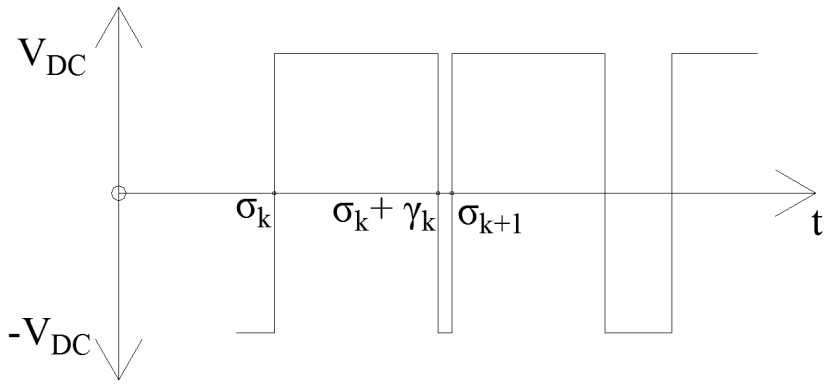

Figure 4-28: Generalized PWM Waveform

If the frequency of the triangular waveform is an odd multiple of the sinusoidal waveform, then the PWM output will be odd, thus containing only the odd Fourier series components. The PWM output voltage can thus be represented as follows [59]:

$$V_o(t) = \sum_{n=1}^{\infty} B_n \sin(n\omega t) \tag{4.56}$$

Where the coefficients can be evaluated for each of the pulses in the PWM signal as follows, with use of Figure 4-28:

$$B_{n_k} = \frac{2}{T}\int_{\sigma_k}^{\sigma_{k+1}} [2V_{DC}u(t-\sigma_k) - 2V_{DC}u(t-\sigma_k-\gamma_k)] \sin\left(\frac{2\pi n\omega t}{T}\right) d\omega t \tag{4.57}$$

When equation (4.57) is simplified, the following results for the Fourier series coefficients [59]:

$$B_{n_k} = \frac{2V_{DC}}{n\pi}\left[\cos(n\sigma_k) + \cos(n\sigma_{k+1}) - 2\cos\left(n(\sigma_k + \gamma_k)\right)\right] \tag{4.58}$$

This can be simulated by use of a 60Hz sin wave that is modulated by a 2460Hz triangular waveform as can be seen in Figure 4-29 below.

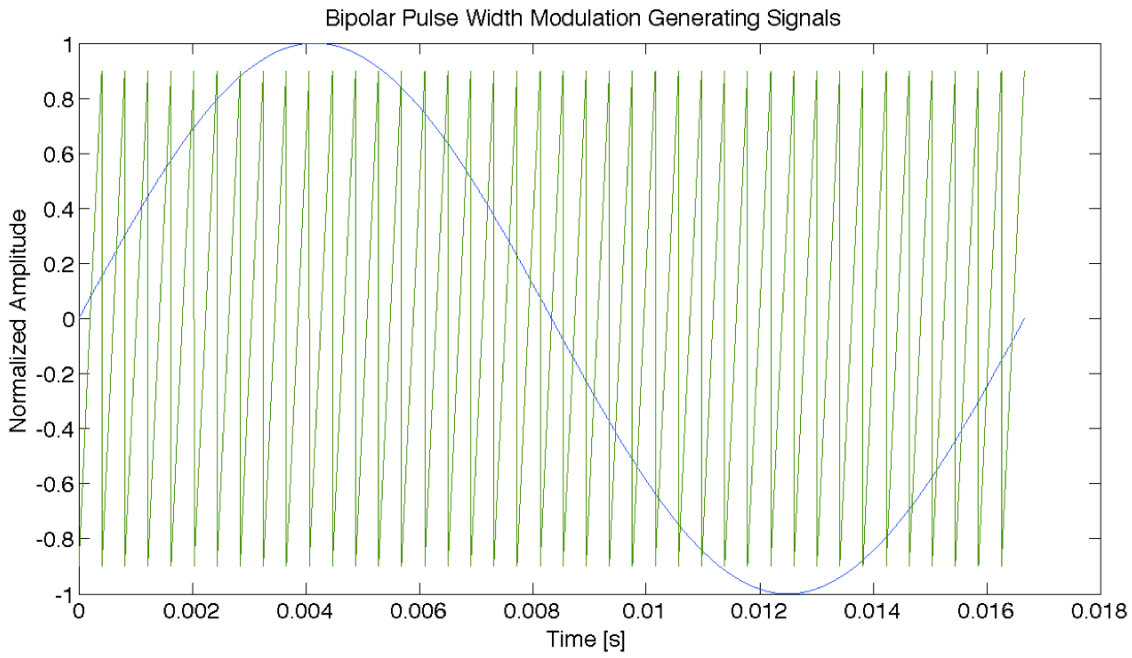

Figure 4-29: PWM Generating Signals

It was further assumed that the triangular waveform had amplitude of 0.9. From this, the bipolar PWM output waveform can be generated as discussed previously. Figure 4-30 below shows what the PWM output waveform will be.

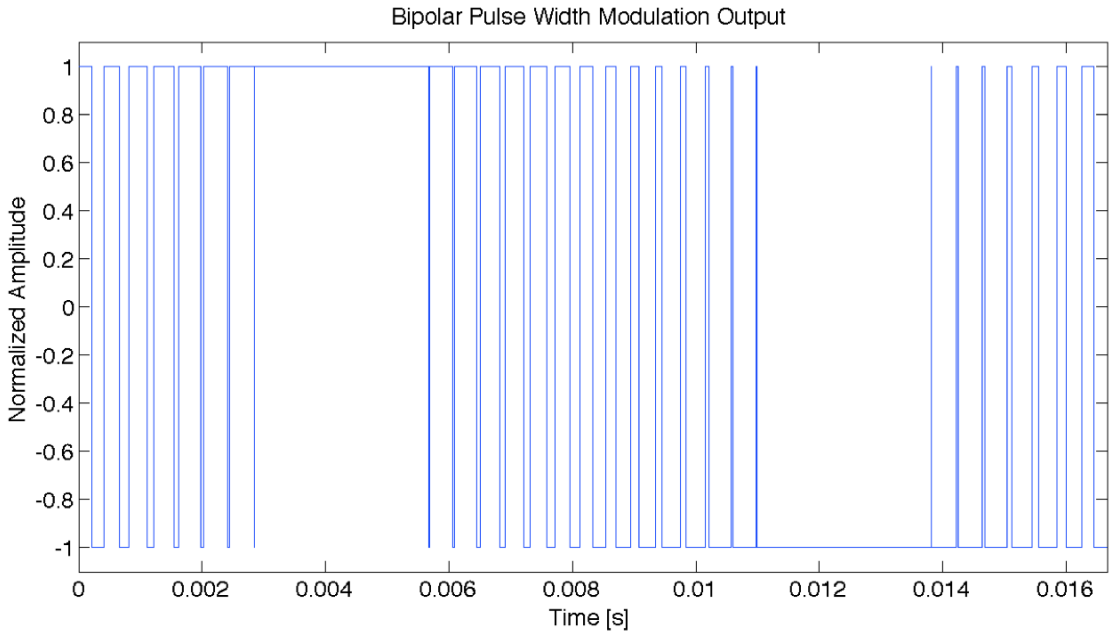

Figure 4-30: PWM Output Waveform

Representing this waveform as a series of Fourier Coefficients will yield the result shown in Figure 4-31 below.

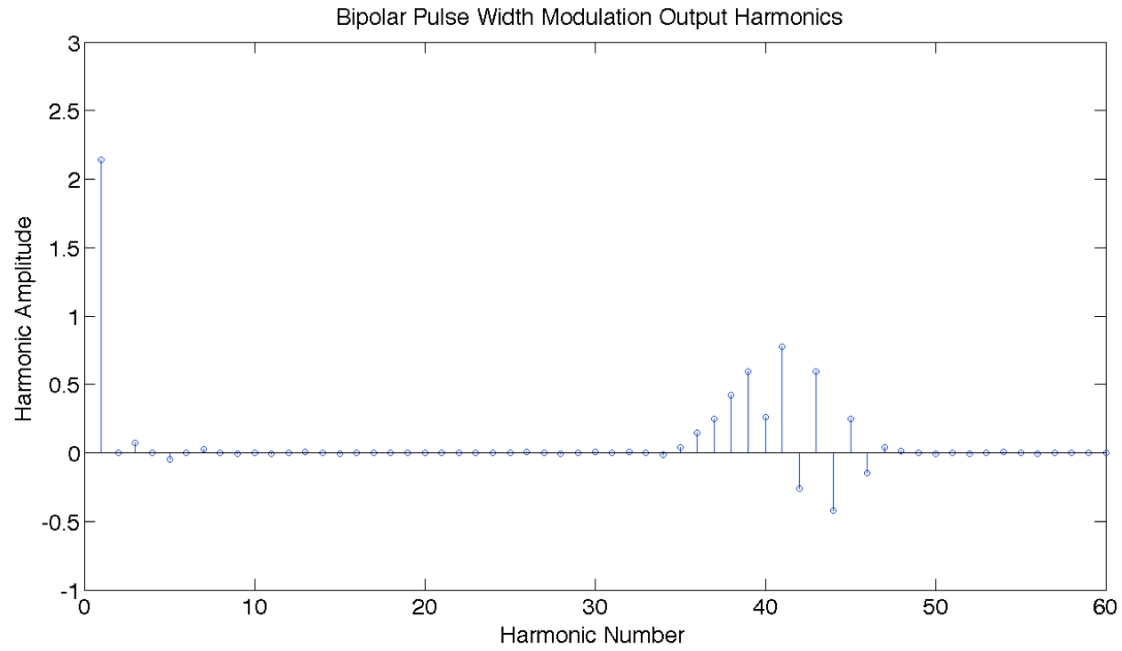

Figure 4-31: Fourier Series of PWM Output

From Figure 4-31 the following can be observed, regarding the harmonics:

- The THD incorporating all harmonics is 0.8641, which is very large
- The THD for the first 30 harmonics is 0.0424, which is significantly less than the prior THD
- Filtering will yield a minimally distorted fundamental frequency
- The filtering of higher order harmonics is quite simple to do, the carrier frequency can be increased, pushing the harmonics further away from the fundamental.
- The Fourier series has clusters of harmonics centered at multiples of the triangular waveform frequency

4.5.2 Filtering Options

The applied filtering for power inverters are low-pass filters, similar to those discussed previously for AC to DC power conversion. The objective is that the fundamental 60Hz wave is passed and all others filtered out. For PWM inverters this allows the use of a low order filter, such as the single-stage low pass filter discussed previously. As shown previously, if the firing angles of the inverter are chosen, the low frequency harmonics can be eliminated, causing a decrease in the total harmonic distortion as well as reducing the filtering requirements. A summary of the THD for various inverter technologies before and after filtering is as follows:

- Single stage inverter >28.3%
- Nine stage inverter 6.18%
- Nine stage inverter after LCL filter 0.0904%
- PWM with no filter 86.41%, 4.24% with a first order filter

For other converter types, there will be required a higher order filter, many stages of low pass filter, since the harmonics are very close in frequency to the fundamental. These filtering systems can become quite complex and could potentially be designed to provide dynamic filtering under certain conditions.

4.5.3 DC to AC Conversion and Underwater Transmission Lines

In certain circumstances, inverters may be used in an application to regulate the frequency of the of underwater AC transmission. The effect that the underwater cable will have on this is that some harmonics will be filtered when the cable is loaded, while resonances are produced when the cable is not loaded. In this case, filtering before transmission is required such that the harmonic resonances can be eliminated. The analysis of the cables influence on the harmonics would be similar to the analysis described in the AC to DC power conversion process.

4.6 Power Grid Harmonic Constraints

The modern power grid has constraints on how polluted the 60Hz voltage waveform can be with harmonics. The purpose for these constraints is for safety of user devices that are using power from the grid as well as the power providers' equipment [30,65]. Harmonics can cause additional heating losses, as well as potential premature dielectric breakdown of insulation materials [27,30,65]. The IEEE Standard 519-1992 as well as its 2014 revisions provides an idea of limitations regarding the total harmonic distortion. This standard gives an idea of what the worst-case total harmonic distortion should be for a given power system. The results from this standard are summarized in Table 4-2, 4-3, 4-4, and 4-5 below.

Table 4-2: Voltage Distortion Limitations [65]

Bus Voltage	Individual Harmonic Distortion [%]	Total Voltage Distortion THD [%]
Below 1kV	5.0	8.0
Below 69kV, above 1kV	3.0	5.0
Below 161kV, above 69kV	1.5	2.5
Above 161kV	1.0	1.5

Table 4-3: Current Distortion Limitations, 120V through 69kV [65]

I_{SC}/I_L	3≤h≤10	11≤h≤16	17≤h≤22	23≤h≤34	35≤h≤50	TDD
Below 20	4	2	1.5	0.6	0.3	5
Below 50, above 20	7	3.5	2.5	1	0.5	8
Below 100, above 50	10	4.5	4	1.5	0.7	12
Below 1000, above 100	12	5.5	5	2	1	15
Above 1000	15	7	6	2.5	1.4	20

Table 4-4: Current Distortion Limitations, 69kV through 161kV [65]

I_{SC}/I_L	3≤h≤10	11≤h≤16	17≤h≤22	23≤h≤34	35≤h≤50	TDD
Below 20	2	1	0.75	0.3	0.15	2.5
Below 50, above 20	3.5	1.75	1.25	0.5	0.25	4
Below 100, above 50	5	2.25	2	0.75	0.35	6
Below 1000, above 100	6	2.75	2.5	1	0.5	7.5
Above 1000	7.5	3.5	3	1.25	0.7	10

Table 4-5: Current Distortion Limitations, above 161kV [65]

I_{SC}/I_L	3≤h≤10	11≤h≤16	17≤h≤22	23≤h≤34	35≤h≤50	TDD
Below 25	1	0.5	0.38	0.15	5.0	1.5
Below 50, above 25	2	1	0.75	0.3	3.0	2.5
Above 50	3	1.5	1.15	0.45	1.5	3.75

Where I_{SC} is the maximum short circuit current at the point of common connection, I_L is the maximum demand load current, from the fundamental component, under normal operating conditions, and h is the harmonic order.

The limits that are listed in Table 4-2 through 4-5 represent the absolute worst-case steady state harmonic distortion that is allowed at a point of common connection in the power grid. It is common practice to check the harmonic distortion periodically at points in the system where it is predicted to be the worst [65]. It is important to make sure that the transmission lines, transformers, and filters are not being overstressed. Also it is important to make sure that no resonances in the system are being caused by the harmonics.

4.7 Modern HVDC Applications

Presently, as of 2016 there are a number of HVDC projects under construction. These projects represent what the common power converter technology and bounds of the power converter technology are. A few of these projects are:

1. The Maritime Link Project, Canada, Bipolar +/- 200kV, 500MW, 170km, IGBT [62,63]

2. NORD.LINK Project, Germany to Norway, 525kV, 1400MW, 623km, Thyristor [66]
3. DolWin3 Project, UK, Bipolar +/- 320kV, 900MW, 160km, IGBT [67]
4. DolWin2 Project, Germany, Bipolar +/- 320kV, 900MW, 135km, IGBT [68]
5. Western HVDC Link Project, UK, 600kV, 2200MW, 422km, Thyristor [69]
6. SydVäslänken Project, Sweden, Bipolar +/- 300kV, 1440MW, IGBT [70]

There are just a handful of projects presently under construction in North America and Europe at present. The power carrying capability, voltage class, and transmission length of these projects are increasing rapidly.

Chapter 5: AC vs. DC Offshore Systems

This chapter provides an analysis detailing how a selection between an AC or DC offshore system can be performed. There are many factors to evaluate when considering if the offshore transmission should be AC or DC. These factors will be summarized in the subsequent sections.

5.1 Introduction

Deciding on whether AC or DC power should be transmitted is not a trivial matter for offshore systems. There are many economic considerations for both AC and DC transmission. Generalizing a transmission line length for which underwater AC power transmission is no longer practical is difficult to quantify. Several methods for generalizing this can be used, equivalent losses and cable, or equivalent losses and power transfer. These two methods will result in different cost crossover points. Observations from the steady state performance can be used to sectionalize transmission line length regions. These two regions will have different costs associated with them. In addition to creating methods to analyze the cost of an AC or DC system, the cost functions for all the differential equipment must be determined. The results of the economic analysis will help to determine which kind of system, AC or DC, should be used for a given offshore power application.

5.2 Decision Factors

There are many similarities between an AC and DC offshore system. There are also, however, many differences. Listed below are some of the considerations that must be taken

into account when deciding whether an AC or DC offshore system is suitable for a given application.

- Thermal limitations in ampacity of the cable
- Forces applied to lay the cable in the water/tidal currents, electromechanical forces between the conductors under transient conditions, and external sources of damage. These are mechanical forces seen by underwater power cables.
  - The armour material choice and thickness affects the efficiency of the cable
- The choice of using AC or DC transmission
  - DC transmission will require power converters
    - Introduction of harmonics
  - AC will potentially require reactive power support
    - Design of a cable's insulation thickness could potentially provide the reactive power support for an induction machine
    - Harmonic resonances are produced
  - DC allows for higher cable ampacity
  - AC transmission has a significant Ferranti effect
    - Voltage swells at the receiving end of the transmission line
  - DC systems only require two cables for bipolar transmission, AC requires three
  - DC would allow easier interconnection of multiple offshore power installations
- The choice of cable configuration
  - Single-core cables can sustain higher voltages than multi-core cables

- Single-core cables allow for better heat dissipation
- More underwater trenches required for single-core cable applications
- Three-core cables do not allow for cheap redundancy if a single core fails. Also increases the probability of more than one core failing due to external damage.
- Steel armour causes diminished cable efficiency in single-core cables
- Magnetic field in the environment surrounding a three-core cable diminishes faster than for a single-core cable

Figures 5-1 and 5-2 below show what a typical offshore DC or AC system would be composed of respectively.

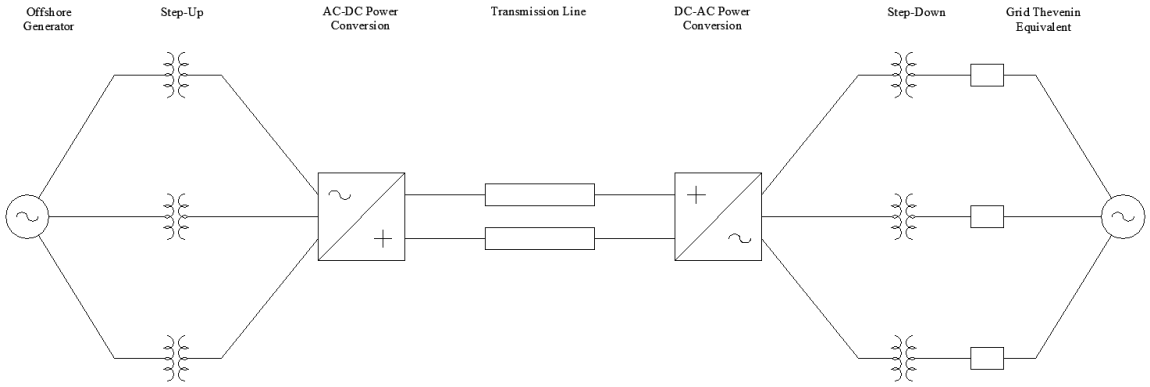

Figure 5-1: DC Bipolar Transmission Link

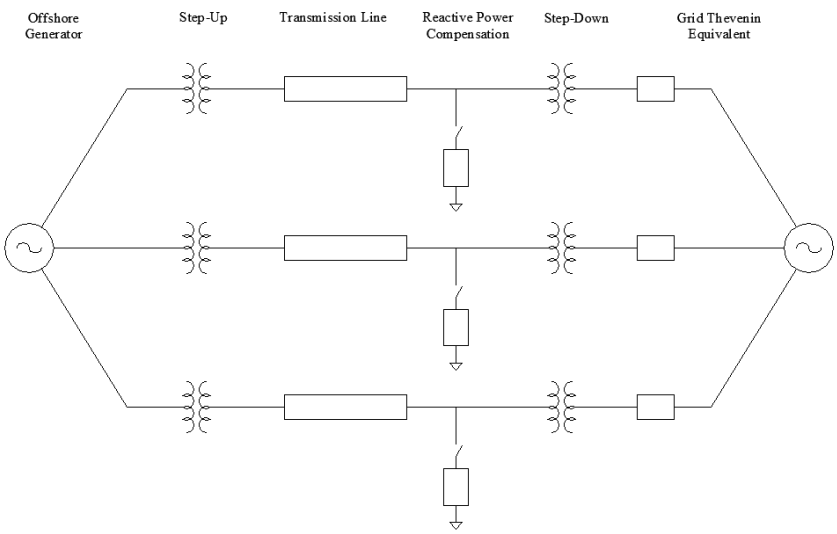

Figure 5-2: AC Transmission Link

Comparing and contrasting these systems, the following observations/assumptions can be made regarding the two systems:

- Both systems are assumed to use induction generators, due to the fact these are the cheaper of the AC generators
- Both systems are connected to an AC power grid on the shore
- Both systems have step-up and step-down transformers
- The DC system has two power conversion stations
- The AC system has a potential need for reactive power compensation
- The DC system has two transmission lines
- The AC system has three transmission lines
- Multi-core cable systems will be neglected

From this, the cost for each system can be generally defined as follows:

$$C_{DC} = C_{GEN} + C_{XFMR_1} + C_{RECTIFIER} + nC_{DC_{CABLE}} + C_{XFMR_2} + C_{INVERTER} \quad (5.1)$$

$$C_{AC} = C_{GEN} + C_{XFMR_1} + 3C_{AC_{CABLE}} + C_{XFMR_2} + C_{PF\_CORRECTION} \quad (5.2)$$

The difference in cost can also be found:

$$C_{AC} - C_{DC} = 3C_{AC_{CABLE}} + C_{PF_{CORRECTION}} - nC_{DC_{CABLE}} - C_{CONVERSION} \quad (5.3)$$

If this total cost differential, $C_{AC} - C_{DC}$, is greater than zero then AC is desirable over DC. If the total is less than zero then DC is desirable over AC. Each of the costs above can be defined as follows:

- $C_{AC_{CABLE}}$ is related to the length of the transmission line, ampacity, and the insulation thickness.

$$C_{AC_{CABLE}} = f(l, r_{cond}, th_{insul}) \quad (5.4)$$

- $C_{DC_{CABLE}}$ is related to the length of the transmission line, ampacity, and the insulation thickness

$$C_{DC_{CABLE}} = f(l, r_{cond}, th_{insul}) \quad (5.5)$$

- It is worth observing that the core conductor radius is related to the ampacity of the cable and the insulation thickness is related to the voltage class.
- $C_{CONVERSION}$ is the cost of the rectification process to convert AC to DC and an inverter system to convert DC to AC. All DC transmission links would require these converter stations. To properly model this cost, there is the cost of the converter station, plus a penalty factor for the harmonics that are introduced into the system due to the extra power losses in the power system, the k-factor rating of transformers, and the potential cost of a filtering network. Converter station costs

depend on the required voltage level and the output current capabilities. In the case of offshore power conversion, the power converters are constructed on platforms above sea level. This introduces another base cost associated with the power conversion process.

$$C_{CONVERSION} = f(V, I) + f(harmonics) + C_{platform} \quad (5.6)$$

- $C_{PF_{CORRECTION}}$ is the cost of having shunt capacitor or inductor banks. In the case of offshore power, inductor banks would be required. If an induction generator is used for an offshore power installation, the reactive power draw of the machine will offset some of the reactive power supplied by the transmission line. If an onshore power factor is specified, then a cut-off transmission line length could be evaluated where, at this point, reactive power support would begin to be required. This cost would thus be a function of transmission line length, cable selection, and generator selection.

$$C_{PF_{CORRECTION}} = f(l, cable, generator) \quad (5.7)$$

5.3 Cost Crossover for Power Transmission

There are several approaches to analyze the cost crossover point between AC and DC power transmission. These approaches are as follows:

- Equivalent cable and line losses assumption
- Equivalent power transfer and line losses assumption

Both of these models will neglect the additional costs associated with AC or DC power transmission, such as the power conversion process and reactive power support. These two approaches are different in their assumptions regarding how to compare whether AC or DC

transmission should be used. The equivalent cable approach assumes that a cable has been selected for an offshore power installation. This implies that the core conductor radius and insulation thickness are equivalent for both AC and DC power transmission. The second approach is to assume that the line losses and power transfer are equivalent. This approach puts constraints on the insulation thickness and core conductor radius. For both approaches, the same approximation for the DC and AC resistance will be used. Accounting for the skin effect defined in (3.1), the DC and AC resistances can be approximated as follows:

$$R_{DC} = \frac{\ell}{\pi\sigma {r_{DC}}^2} \tag{5.8}$$

$$R_{AC} = \frac{\ell}{\pi\sigma\delta(2r_{AC}-\delta)} \tag{5.9}$$

These equations for resistance are used for evaluating the line losses for the cables. These are simplified approximations of the cables resistance. The exact formulations for the resistance can be found in Chapter 3.

5.3.1 Equivalent Losses and Cable Geometry

If it is assumed that a cable has been pre-selected for a given offshore power installation and it is required to determine whether AC or DC power should be transmitted, the following constraints can be applied for analysis: the core conductor radius is equivalent, the insulation thickness is equivalent, meaning that the peak AC voltage can be equivalent to the DC voltage, the line losses are equivalent, and a bipolar DC transmission link is to be used. As a result, the difference between AC and DC losses can be approximated to be as follows:

$$\Delta P_L = P_{L_{AC}} - P_{L_{DC}} = \frac{\ell}{\pi\sigma}\left(\frac{3{I_{L_p}}^2}{2\delta(2r-\delta)} - \frac{2{I_D}^2}{r^2}\right) \tag{5.10}$$

If the losses are equivalent, then the following relationship can be determined:

$$\frac{I_{L_p}}{I_D} = \sqrt{\frac{4}{3}\frac{\delta(2r-\delta)}{r^2}} \tag{5.12}$$

Since it has been assumed that the peak AC voltage is equivalent to the DC voltage [30], the ratio of power transfer can be defined as follows:

$$\frac{P_{AC}}{P_{DC}} = \frac{3}{4}\frac{I_{L_p}}{I_D} \tag{5.11}$$

Substituting this into equation (5.11) results in the following relationship:

$$\frac{P_{AC}}{P_{DC}} = \sqrt{\frac{3}{4}\frac{\delta(2r-\delta)}{r^2}} \tag{5.13}$$

It can be observed that for a specified cable, equation (5.13) is a constant. Since the losses are equivalent, equation (5.13) defines the ratio of profit capability of one transmission medium over the other. The cable electrical losses, being assumed equivalent for the AC and DC power transmission, is an equivalent statement to saying that the wear of the cables is equivalent. This is because the electrical losses translate to heat, which affects the life of the insulation. Figure 5-3 below shows a plot of the power ratio as the radius of the core conductor varies.

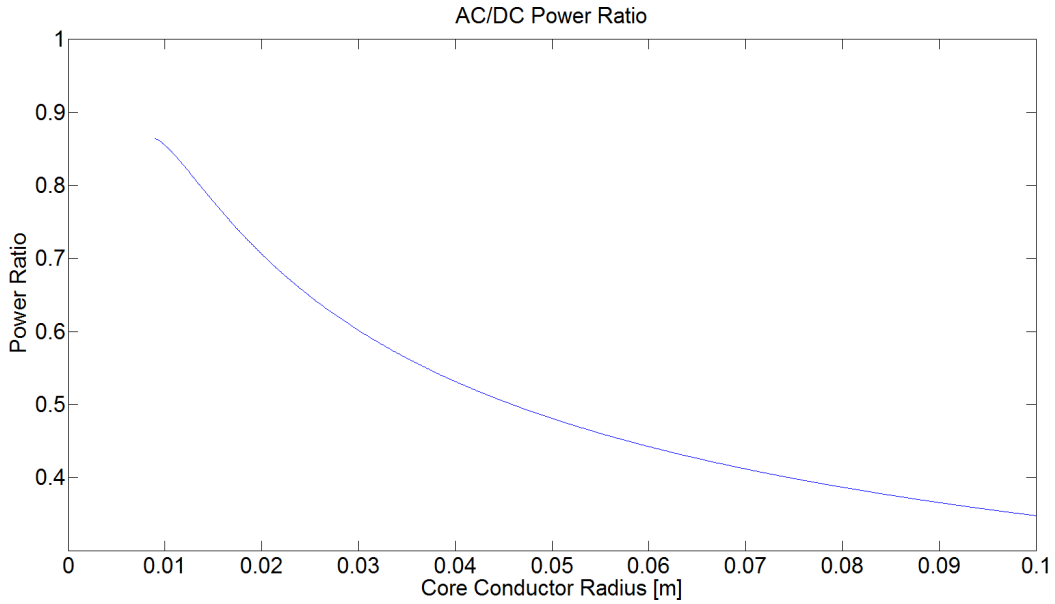

Figure 5-3: Power Ratio vs. Conductor Radius

It can be observed from this plot that the ratio is never greater than unity. This implies that given the constraints listed above, a DC cable will be able to transmit more power than an AC cable.

Assuming that this is a short transmission line, less than 15km, where an AC system can be assumed to require no power factor correction, the difference in cost between the two systems can be simplified to be as follows:

$$\Delta C = -C_{CONVERSION} + (3-n)C_{cable} + P_{AC_{nom}}\beta\tau(1-\gamma^{-1}) \tag{5.14}$$

Where β is the price per megawatt-hour that can be obtained for the power, n is the number of DC cables which in this case is two since a bipolar DC link was assumed, γ is the power ratio defined by equation (5.13), τ is the average operating time at nominal capacity of the

generator, and $P_{AC_{nom}}$ is the nominal generating capacity of the generator. From this equation it can be found how long it would take to pay for the added converter stations.

5.3.2 Equivalent Losses and Power Transfer

An alternative way to compare the transmission lines is to assume that the line losses and power transfer are equal for both cables [30]. This implies that electrically speaking both cables operate equivalently. The line losses and power transfer for AC and DC cables can be defined as follows [30]:

$$P_{L_{AC}} = \frac{3}{2} {I_{L_p}}^2 R_{AC} \tag{5.15}$$

$$P_{L_{DC}} = 2{I_D}^2 R_{DC} \tag{5.16}$$

$$P_{AC} = \frac{3}{2} V_{LN_p} I_{L_p} \tag{5.17}$$

$$P_{DC} = 2V_D I_D \tag{5.18}$$

Where I_{L_p} is the amplitude of the current waveform and V_{LN_p} is the amplitude of the voltage waveform. To accurately compare the two cables, the average AC power must be compared to the DC power. It has been assumed that the peak values of voltage and current are used. The relation between the peak values and the RMS values is given as follows:

$$V_{LN_p} = \sqrt{2} V_{RMS} \tag{5.19}$$

$$I_{L_p} = \sqrt{2} I_{RMS} \tag{5.20}$$

Using this definition, equating the line losses provides the following relationship:

$$\frac{I_D}{I_{L_p}} = \sqrt{\frac{3}{4} \frac{{r_{DC}}^2}{\delta(2r_{AC} - \delta)}} \tag{5.21}$$

Where r_{DC} and r_{AC} are the radii of the core conductors for the DC and AC transmission line respectively.

If the current carrying capacity of the cables were desired to be equivalent, then the following relationship will exist for the radii of the core conductors of the cables:

$$r_{DC} = \sqrt{\frac{4\delta}{3}(2r_{AC} - \delta)} \tag{5.22}$$

Applying the result in equation (5.21), and assuming that the input powers are equivalent, which in this case is synonymous with equivalence of received power, the following can be observed:

$$\frac{V_{LN_p}}{V_D} = \sqrt{\frac{4}{3}\frac{{r_{DC}}^2}{\delta(2r_{AC}-\delta)}} \tag{5.23}$$

This represents the relationship between AC and DC voltage required to have equivalent line losses and equivalent power delivery. Equation (5.21) represents the ratio of current carrying capacity required such that the cables have equivalent line losses. Equation (5.23) represents the ratio of required voltage.

For underwater power cables, the current requirement defines the radius of the core conductor and the voltage class defines the thickness of the insulation. Equations (5.21) and (5.23) provide these ratios. The core conductor radius and insulation thickness define the cost of the cable. In this case, since losses are equivalent and power transfer is also equivalent, then the only factor that offsets the DC converter station is the differential cost of the cables. This is assuming that the transmission length is less than 15km, where power factor correction is not required for an AC transmission line. With this assumption in mind, the following equation can be developed to represent the differential cost of an AC and DC system:

$$\Delta C = -C_{CONVERSION} + 3C_{AC_{cable}} - 2C_{DC_{Cable}} \tag{5.24}$$

This again is assuming the application of a bipolar DC transmission link. It is worth noting that under these constraints, AC power transmission would be most economic.

5.4 Power Factor Compensation

Underwater power cables are a source of significant reactive power [29,31]. As such, they may require reactive power compensation for longer transmission line length [29]. Since the cables are dominated by their capacitance, inductive reactive power would be required to balance this. If it is assumed that an induction generator is connected to a transmission line, then it is expected that the onshore power factor will have the following trend: the power factor would begin at the power factor of the induction machine, increase to unity, and then decrease as the line length increases. Figure 5-4 below shows an example of the onshore power factor as line length is varied.

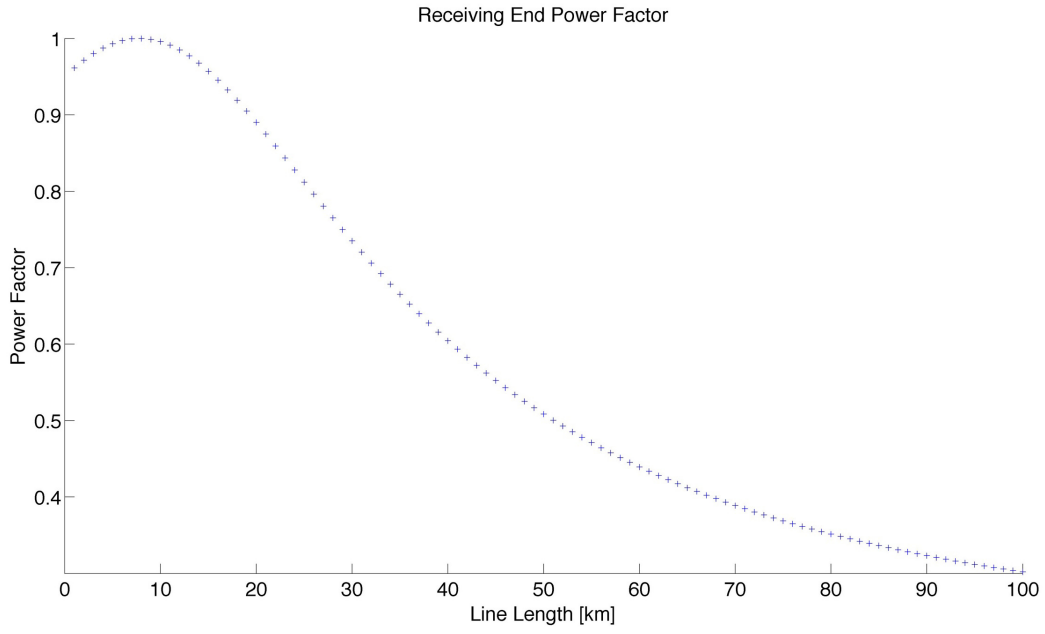

Figure 5-4: Onshore Power Factor

From Figure 5-4 it can be observed that for an offshore power cable, there is a region in which the power factor is greater than that of the induction machine. Within this region it can be said that no power factor correction would be required for the transmission line. If line lengths begin to exceed this region, power factor correction will begin becoming a necessity. The reactive power provided by the transmission line on shore for various underwater transmission lines can be found to have the trend shown in Figure 5-5 below.

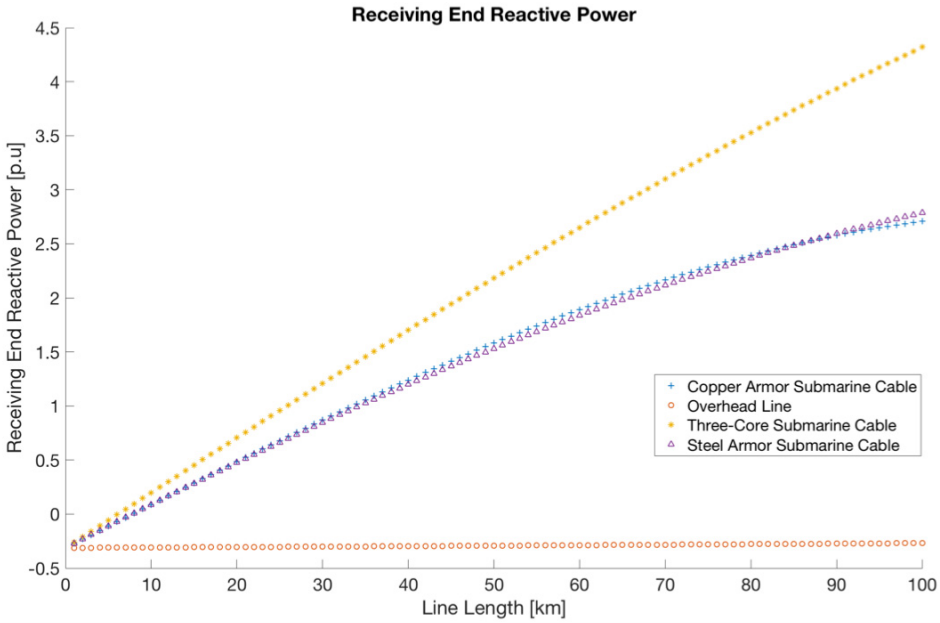

Figure 5-5: Onshore Reactive Power

Observations that can be made regarding the reactive power supplied by an underwater transmission line are the following:

- The reactive power can be approximated as being linear or quadratic functions of transmission line length.
- The intercept of the approximations would correspond to the power factor of the generator.

So for a given transmission line, a regression can be performed to approximate the reactive power requirement for the cable in terms of the transmission line length. Observing that for a specified offshore power system, a fixed amount of reactive power would be required. This implies that fixed reactor banks could be connected onshore to supplement the reactive power provided by the transmission line. Assuming the transmission line length is longer than the region where the power factor is greater than the induction generator, the cost of power factor correction can be defined as follows:

$$C_{PF_{CORRECTION}} = \alpha f(\ell) \tag{5.25}$$

Where, α is the cost per megavar of reactive power compensation and $f(\ell)$ is the regression model representing how many megavars are supplied by the transmission line. The full equation for the cost of power factor correction can be defined as follows:

$$C_{PF_{CORRECTION}} = \begin{cases} 0, & \ell \leq \ell_0 \\ \alpha f(\ell), & \ell > \ell_0 \end{cases} \tag{5.26}$$

Where ℓ_0 represents the cut-off transmission line length where the power factor remains above that of the induction generator.

5.5 Cost Functions

To evaluate the cost crossover points described previously, the cost functions for the various power system equipment must be known. This equipment includes, the cost of AC cables, DC cables, the installation cost of the cables, the cost of power conversion, the cost of required offshore platforms, the cost of reactive power compensation if it is required, and the price of energy. The cost functions that will be described are best-fit functions from manufacturer data.

5.5.1 Cable Costs

The cost of power cables can be generalized as being a function of voltage class and ampacity. In general, the only cable layers that vary are the conductor diameter and insulation thickness. The additional protective layers are typically invariant unless it has been specifically requested that they be different. In addition to the cost of the physical cable itself, there is a cost associated with laying the cable underwater.

5.5.1.1 AC Cable Cost

The per kilometer cost associated with AC cables, in millions of Euros, is defined to be as follows [71,72,73]:

$$C_{AC_{Cable}} = \alpha_{AC} + \beta_{AC} e^{\frac{\gamma_{AC} I}{100000}} \; M€/km \tag{5.27}$$

Where I is the ampacity of the cable and the coefficients α, β, and γ are coefficients that depend on the voltage class of the cable. Table 5-1 below shows various values of these parameters as the cable voltage is varied.

Table 5-1: AC Cable Cost Coefficients [71,72]

Voltage [kV]	α_{AC} [M€/km]	β_{AC} [M€/km]	γ_{AC} [1/A]
30-36	0.05208	0.07551	234.34
132	0.24972	0.02648	379.5
230	0.4032	0.01394	462.1

5.5.1.2 DC Cable Cost

The cost of DC cables is different from AC cables in that the cost doesn't vary exponentially with the ampacity. A justification for this would be the lowering of the ampacity of an AC cable due to the skin effect. The cost of a DC cable can be defined to be as follows [71,72,73]:

$$C_{DC_{Cable}} = \psi_{DC} + \frac{\sigma_{DC}}{1000} VI \; M€/km \tag{5.28}$$

Where V and I are the cables voltage rating in kV and ampacity in A. The coefficients ψ and σ depend on the voltage class of the cable. Table 5-2 below shows various values of these parameters as the cable voltage is varied.

Table 5-2: DC Cable Cost Coefficients [72]

Voltage [kV]	ψ_{DC} [M€/km]	σ_{DC} [€/kmVA]
5	-0.03806	0.04488
40	-0.03454	0.006789
160	-0.011	0.001804
230	0.00836	0.00132
300	0.03146	0.00010659

5.5.1.3 Offshore Cable Installation Cost

The cost of laying the cables depends significantly on the application. It depends entirely on the depth of water between a ship and the seabed and the composition of the seabed. The cost per kilometer to install the cable offshore is approximately three times more expensive than on land, costing on average between *0.264* to *0.365M€/km* to install offshore [71,73].

5.5.2 Power converter Cost

The cost of power conversion comes in three variants, the cost of DC/AC conversion, DC/DC conversion, and DC/AC conversion. In this section, only the process of rectification (AC/DC) and inversion (DC/AC) will be analyzed. The cost of these converters will be related to the amount of power it is desired for them to convert. In addition to the cost of the power conversion equipment is the cost of the offshore platform.

5.5.2.1 Rectifier Cost

The cost function used to represent the cost of AC to DC power conversion is all-inclusive. The cost is *0.072 M€/MW* for this converter and all associated components [73]. This is an average value for a power converter that is in the 150MVA range. Smaller power converters will cost slightly more, bigger converters will cost slightly less than this cost figure [73].

5.5.2.2 Inverter Cost

The inverter cost function can be quite complicated to model. The reasoning for this is that the cost will be a function of the required power conversion and also of how complicated the inverter system is. The cost of a single stage inverter or a pulse width modulation inverter would be equivalent to that of a rectifier, since it will use the same quantity and kind of components. This cost will be *0.072 M€/MW* [72,73]. For a multistage inverter, more switches are required in order to produce a waveform. It can be proposed that the cost of an n-level inverter can have a cost function of *0.072n M€/MW*.

5.5.3 Offshore Platform Cost

In the event that an offshore platform is required for a power converter, the cost associated with that will be *2.534 M€* [71,73].

5.5.4 Reactive Power Compensation Cost

The cost of reactive power compensation in the form of an inductive reactor is approximately 2/3 the cost of a power transformer of an equivalent power rating [71]. A linear model representing this cost is given as follows [71,72]:

$$C_{reactor} = 0.1264 + 0.003542 \cdot Q \; M€ \tag{5.29}$$

Where Q is the reactive power required by the system in MVAr. The average cost of a static VAR compensator is 0.077 *M€/MVAr*. An offshore platform would also be required for the reactive power support. It is assumed that the cost of the power converter platforms is similar to what is required for the reactive power compensation. Choice of which method of power factor correction depends entirely upon how much reactive power is required. In the case of AC cables being used to transmit power to shore, if the transmission length is less than 20km, no power factor compensation may be required.

5.5.5 Energy Prices

Energy prices vary quite significantly from region to region. In Canada the cost per kilowatt-hour can vary from 0.072 to 0.165 CAD as of May 2015 [74,75]. The average cost of energy in the United States is 0.1293 USD cents per kilowatt-hour as of June 2015 [76]. In the United Kingdom, prices of energy averaged 0.201 EU as of 2014 [77]. In Europe, the average cost of energy is 0.208 EU per kilowatt-hour [77].

5.6 Analysis of Cost Crossover Threshold

To analyze the cost crossover point between an AC and DC transmission link, the differential cost given by equation (5.24) will be applied along with the cost functions defined in the previous section. The specifications for this transmission link are the following:

- The choice is to use 230kV AC transmission or +/-230kV DC transmission to transmit 500MW of power.
- Reactive power support will be included in the model
- A VSC power inverter will be assumed to be used to convert the DC waveform to an AC waveform

The results of this analysis can be observed in Figure 5-6 below.

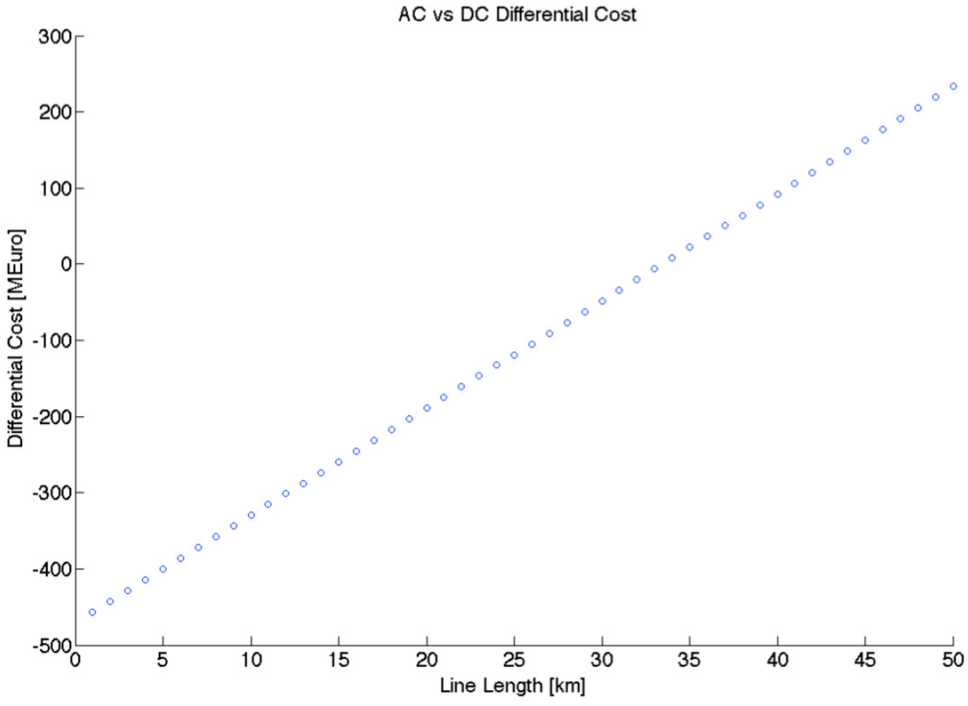

Figure 5-6: AC vs DC Differential Cost, Analysis 1

From Figure 5-6 it can be observed that a transmission length between 33km and 34km results in the cost crossover point. This means that: for transmission lines up to 33km AC transmission is economically viable and for transmission length above 34km, DC transmission is economically viable. It should be noted that this analysis was for a large offshore generation installation. For a smaller power installation, the following specifications can be provided for analysis:

- The choice is to use 36kV AC transmission or +/-36kV DC transmission to transmit 10MW of power.
- Reactive power support will be included in the model
- A VSC power inverter will be assumed to be used to convert the DC waveform to an AC waveform

The results of this analysis can be observed in Figure 5-7 below.

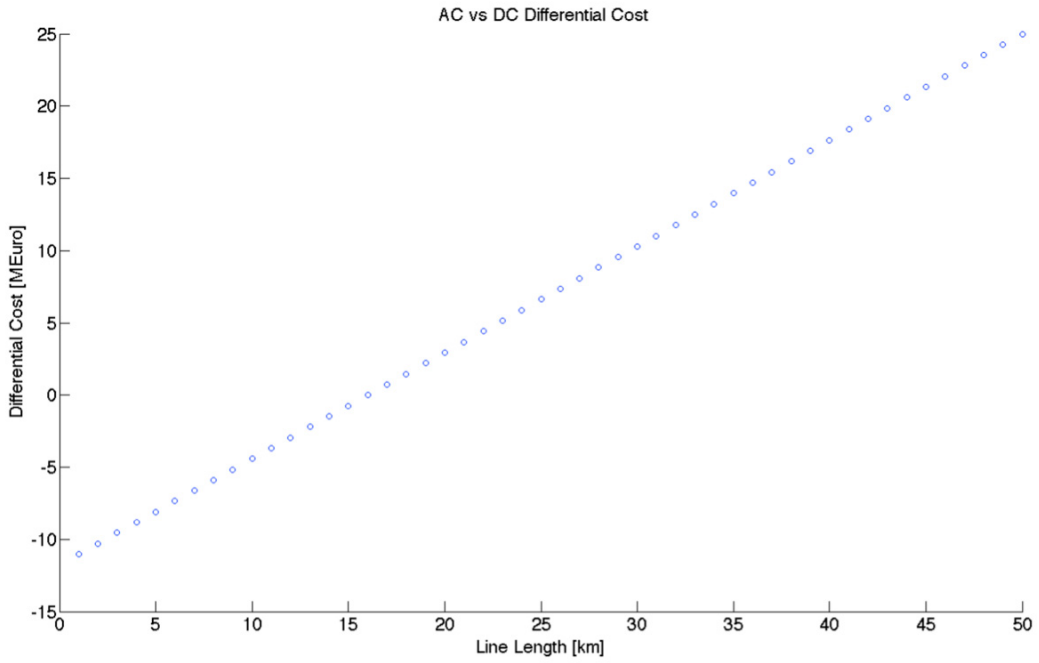

Figure 5-7: AC vs DC Differential Cost, Analysis 2

From this result it can be observed that the cost cross over point occurs at approximately 15km. This means that for transmission lengths less than 15km, AC transmission is the most economic, and for transmission lengths over 15km, DC transmission most economical.

5.7 Selection of a Transmission Line

For a given offshore power installation, it is required to be able to choose the transmission line geometry. This can be done evaluating the most cost effective voltage and current for the application. The cost of an AC power cable is given by expression (5.27). This cost function has various values of the parameters α_{AC}, β_{AC}, and γ_{AC}. These parameters depend on the voltage class of the cable. A regression can be performed on these parameters to find them as a function of voltage. The regression on this data set results in the following equations [71,72]:

$$\alpha_{AC} = 0.0019V - 0.0166 \tag{5.30}$$

$$\beta_{AC} = 0.1091e^{-0.009V} \tag{5.31}$$

$$\gamma_{AC} = 1.1842V + 190.83 \tag{5.32}$$

Where V is the line-to-line voltage measured in kV. These were the equations that resulted in minimum regression error for the data points collected. Applying these parameter regressions can allow for a general cost plot to be created as a function of both voltage and current. Plotting this results in the contour plot shown in Figure 5-8a and Figure 5-8b below.

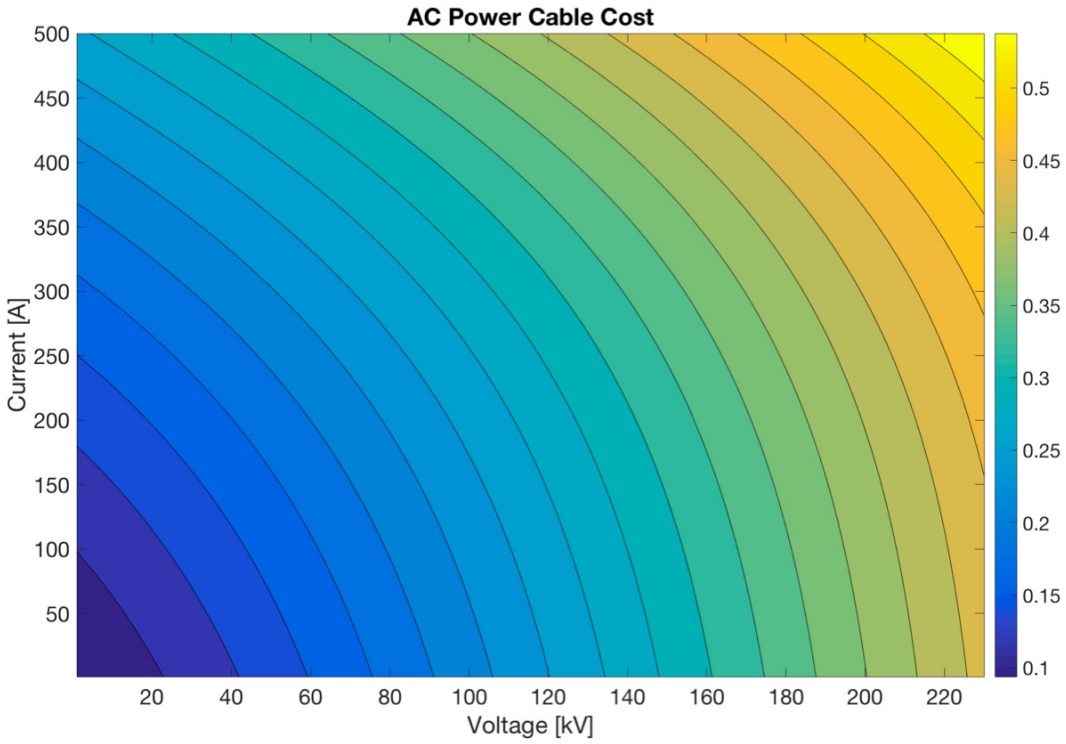

Figure 5-8a: AC Power Cable Cost

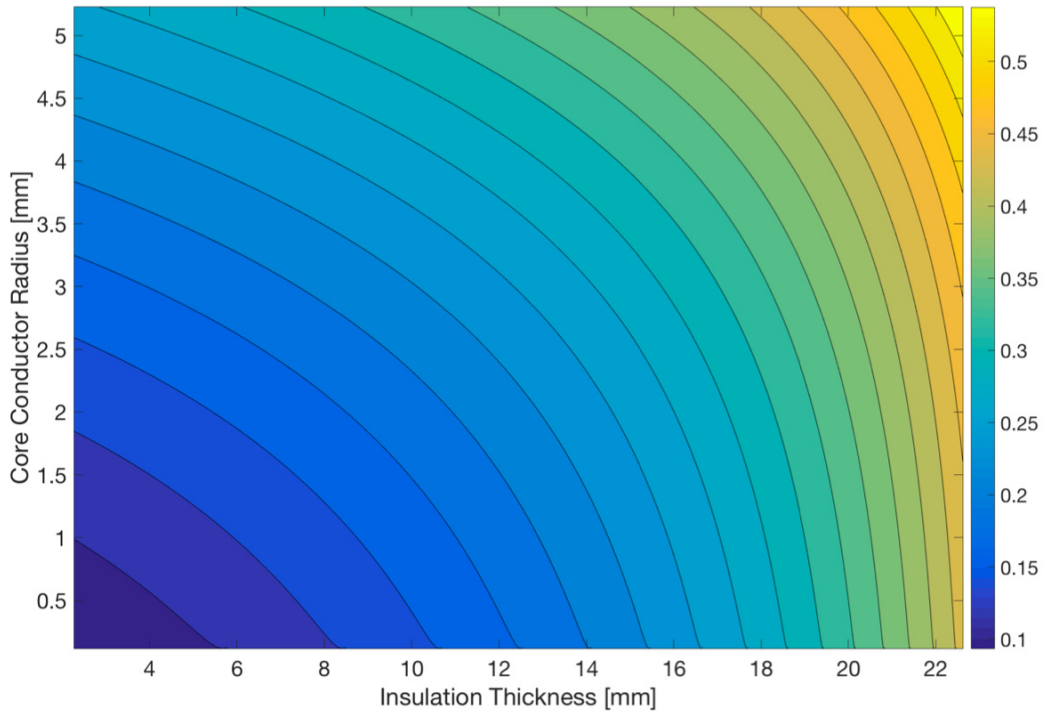

Figure 5-8b: AC Power Cable Cost

From Figure 5-8a and 5-8b, it can be observed that as the voltage and current rating of the cable increase, so does the cost. The voltage rating of the cable can be translated to a specific insulation thickness and the current rating can be translated to a specific conductor radius. The voltage/insulation thickness and current/conductor radius relationship has been used previously when modelling the underwater power cables. Again, a regression was performed on present cable manufacturer data found in [28]. Applying this results in the Figure shown in 5-8b. From these plots, it is desired to select the most cost economic cable. It should be worth noting that this analysis applies for underwater power cables of length less than 15km. For longer underwater cables, a penalty factor would have to be introduced to account for reactive power compensation or application of power electronics. The result in Figure 5-8a and 5-8b can be used to select a specific cable for an application by applying the power constraint equation for the application. The power constraint is given by the following equation:

$$\frac{|S|}{1000\sqrt{3}\cdot|I|} - \frac{3R_{AC}}{1000\sqrt{3}}|I| = |V| \tag{5.33}$$

Where $|V|$ is the magnitude of voltage in kV, $|I|$ is the magnitude of the current, $|S|$ is the magnitude of apparent power in VA, and R_{AC} is the AC resistance of the cable. The AC resistance of the cable depends on the core conductor material and cross sectional area. From [28] a regression equation can be determined for the resistance of typical underwater power cables. This equation is as follows:

$$R = \frac{\ell}{\sigma(0.0011I^2 - 0.0113I + 0.1677)} \tag{5.34}$$

Regression equations can also be determined for the insulation thickness, th, and core conductor radius, r, for typical underwater power cables from [28]. These equations are as follows:

$$th = 2.0937 + 0.1725V - 0.0005V^2 + 6 \cdot 10^{-7}V^3 \tag{5.35}$$

$$r = \frac{1}{\pi}\sqrt{0.0011I^2 - 0.0113I + 0.1677} \tag{5.36}$$

Applying equation (5.33) and plotting this on top of the cost contour plot results in Figure 5-9 below.

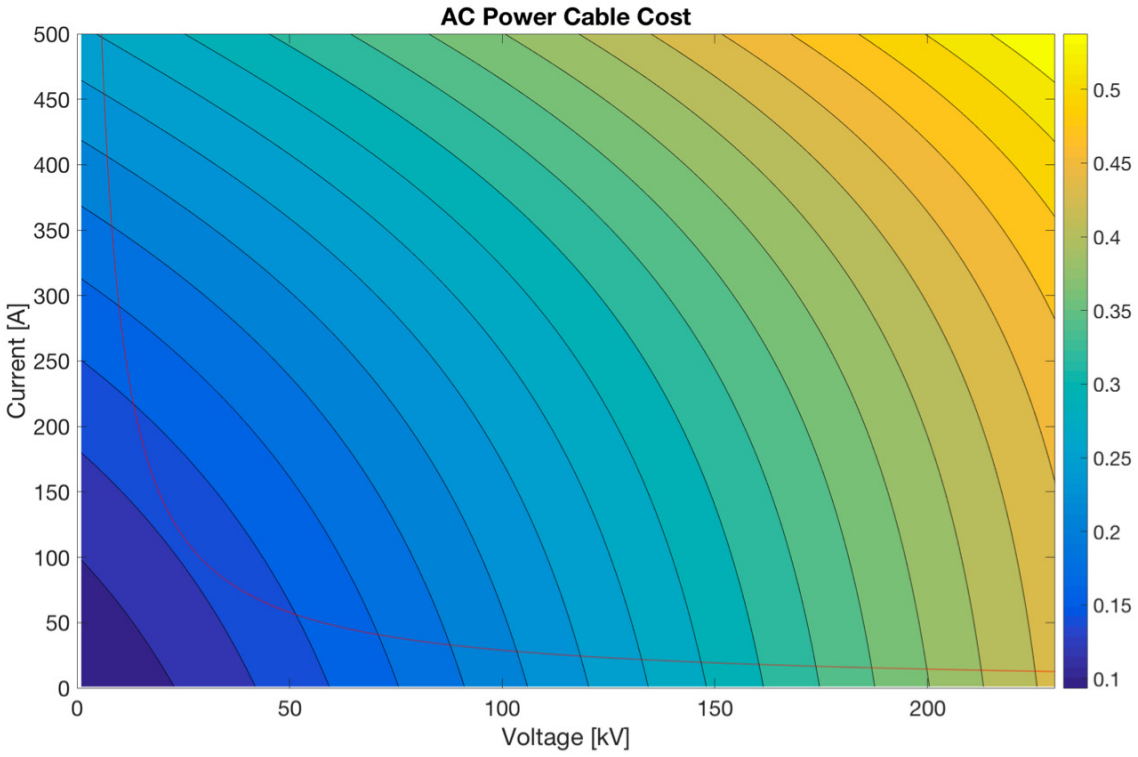

Figure 5-9: Cost of Cable With Power Balance Equation

In Figure 5-9, the single red curve represents equation (5.33). This equation represents all of the possible combinations of voltage and current that will result in the magnitude of apparent power of 5MVA. It is also assumed that the cable length was 1km. It can be observed that the corner in the red curve corresponds to the most economic cable selection. Figure 5-9 will result in the selection of the most economic voltage class and cable cross section for the given power installation. This can then be translated to the physical

geometry of the cable from equations (5.35) and (5.36). In the event that the required transmission line length were to be longer than 15km, the same analysis would be true for the cost of the transmission line. There would be an additional cost associated with the necessary power electronics and/or the power factor correction. This analysis methodology is also applicable to the case where a DC cable may be required. The difference being that the cost function for DC power cables is different.

Chapter 6: Offshore Micro-Grids

This chapter provides an overview of offshore power system topologies. These various topologies apply for when there are multiple offshore generation sites. The selection of topology has implications on the offshore cluster generation performance as well as cost. The model for an offshore micro-grid will be developed from the study of these various topologies. The implications and consequences of interconnecting the offshore micro-grid with the onshore power system will be analyzed.

6.1 Introduction

Offshore micro-grid generation is applied for the large offshore wind farms described in Chapter 1. These wind farms can be comprised of over 100 wind turbines. The same application could be used for tidal based power generation as well. The power generated from the cluster of generators is typically centralized and transmitted to shore using a single transmission line. This is typically necessary so as to minimize the project cost. There are four main offshore topologies that are used to interconnect generators and transmit the power to shore: star, radial, ring, and point-to-point. The first three topologies, star, radial, and ring are necessary when a large number of turbines are used. Point-to-point would typically be used if few offshore generators were used. In the previous chapters, the analysis performed was for the situation where there was a single generator connected to a single transmission line. The various offshore micro-grid topologies will be analyzed and the effects they have on the offshore micro-grid and the micro-grids effect to the onshore grid will be discussed for both AC and DC applications. The study of this will be generalized such that the analysis will apply for an offshore cluster of generators, either

wind or tidal based, groups of these generator clusters, singular distributed generation, and offshore loads. Figure 6-1 below provides a general diagram for what the micro-grid will consist of.

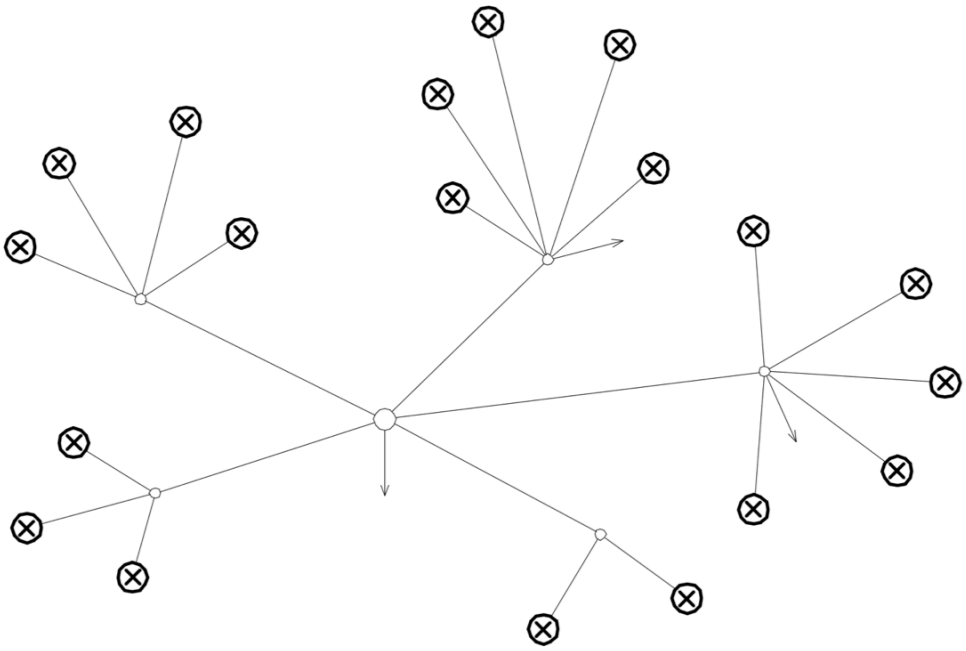

Figure 6-1: Micro-Grid Model

From this model, each generator could be represented by an equivalent of a cluster of generators or singular generators. Loads local to these clusters will be incorporated into the modelling of the different topologies. The model of the micro-grid in Figure 6-1 can be generalized to allow for multiple onshore connection points from the various generation clusters.

6.2 Offshore Micro-Grid Generator Cluster Topologies

Often when constructing offshore power generation sites, multiple generators are installed in close proximity to each other. When there are multiple generators, there are various ways in which the power can be transmitted to shore. The features that will be used to define an offshore micro-grid are the following:

- A cluster or several clusters of offshore wind and/or tidal generators will form the backbone of the micro-grid
- Inclusion of singular generators in close proximity to this aforementioned array of generators
- Inclusion of offshore loads
- Inclusion of energy storage

These features will allow for a starting point in the analysis of offshore micro-grids.

6.2.1 Offshore Generation Cluster Interconnections

Offshore generator cluster interconnection topologies involve the various ways in which this power can be transmitted to shore. The various topologies that can be applied for an offshore power installation are the following [82,83]:

1. Star connection
2. Radial Connection
3. Ring Connection
4. Point-to-Point Connection

The first three topologies can be observed in Figure 6-2 below in order from left to right. The point-to-point connection was not represented in Figure 6-2. This connection topology involves each generator having its own transmission line to shore.

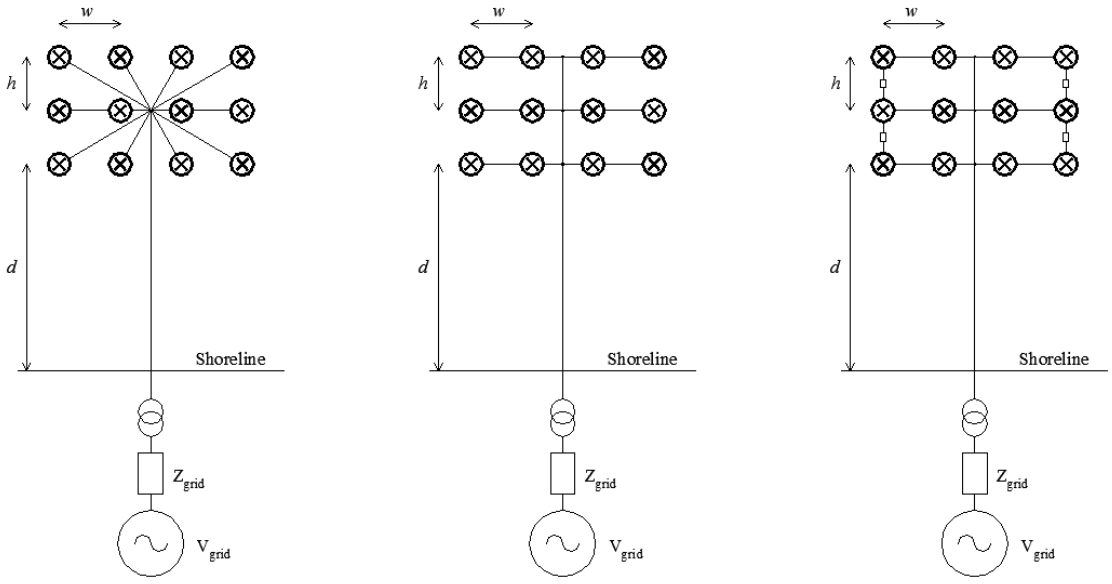

Figure 6-2: Offshore Grid Interconnections, Star, Radial, and Ring

For these topologies it has been assumed that the array contains *n* turbines in each row and there are *m* rows. The distance between each turbine in the row was assumed to be, *w*, and the distance between rows, *h*. These various topologies each have their own benefits and disadvantages, which will be discussed in the subsequent sections.

6.2.1.1 Star Connection

This topology creates an underwater power hub in which all the generators are connected. The generators are connected to the hub by a lower capacity power cable. A higher capacity cable is then used to transmit the power to shore. The number of cable segments required for this topology is as follows:

$$Cable\ Segments = nm \tag{6.1}$$

If it is assumed that the underwater power hub is constructed in the middle of the array, the minimum total length, per phase or pole, of transmission line required is given as follows:

$$\ell_{cable} = d + h\frac{m-1}{2} + \sum_{j=1}^{m}\sum_{i=1}^{n}\sqrt{w^2\left(i - \frac{n+1}{2}\right)^2 + h^2\left(j - \frac{m+1}{2}\right)^2} \tag{6.2}$$

6.2.1.2 Radial Connection

This topology daisy chains several generators together. These groups of generators will require larger capacity cables as well as the creation of hubs when these groups of generators are connected together. Again, a larger capacity cable is used to transmit the power to shore. The total number of cable segments required is as follows:

$$Cable\ Segments = nm - 1 \tag{6.3}$$

The minimum total length of cable required, per phase or pole, will be as follows:

$$\ell_{cable} = d + m(n-1)w + h(m-1) \tag{6.4}$$

6.2.1.3 Ring Connection

This topology is similar to the radial connection. With exception that there are loops created between the generators. This increases the reliability of the system, however it is more expensive due to the extra cable lengths required, as well as the offshore switchgear. The total number of cable segments for this topology is as follows:

$$Cable\ Segments = m(n+2) - 3 \tag{6.5}$$

The minimum total length of cable required, per phase or pole, is as follows:

$$\ell_{cable} = d + m(n-1)w + 3h(m-1) \tag{6.6}$$

6.2.1.4 Point-to-Point Connection

This topology has the best reliability, since each generator has its own transmission line to shore. Due to this, lower capacity cables can be used for the power transmission. This can become expensive if the number of generators gets large. Typically point-to-point connections are only used for smaller scale applications because of this. The total number of cable segments for this topology is as follows:

$$Cable\ Segments = nm \tag{6.7}$$

The minimum total length of cable, per phase or pole, would be as follows:

$$\ell_{cable} = mn(d + h\frac{m-1}{2}) \tag{6.8}$$

6.2.1.5 Interconnection Choice

The choice of which topology is used for transmitting the offshore power to the shore depends on many factors [82,83].

- The size of the installation both in terms of quantity of turbines and amount of generation power. Larger numbers of turbines render point-to-point unfeasible due to the cost of all the cable. Due to this, one of the other three topologies must be applied. The amount of power from each generator is also significant because it will affect the size of the cable required to interconnect the generators [82,83].

- The length of cable required is significant both in cost, and in terms reactive power capabilities if AC power transmission is used. Generally speaking, from equations (6.2), (6.4), (6.6), and (6.8) above, the following can be generalized regarding the

length of cable required: radial, ring, star, and point-to-point is the ordering from shortest to longest cable requirements [82,83].

- The number of subsea components, such as breakers, transformers, and hubs is another cost associated with the four topologies. The ring topology requires more breakers due to the additional connections between generators. The star topology requires one hub, point-to-point requires no hub, and the radial/ring topology requires multiple hubs [82,83].

- The number of joints created with the underwater power cable is another factor to consider when analyzing the cost. The number of required joints is proportional to the number of cable segments [82,83].

- Minimized power losses are another ideal characteristic of the offshore interconnection. The losses are related to the geometry choice and composition for the cables as well as the length of the cable. The geometry and composition account for the effects due to the selection of voltage class and ampacity requirements of the cable. Selecting appropriate materials for the cables outer layers as well as minimizing the length of cable used can mitigate additional losses [82,83].

- Power quality can be thought of in two different respects depending on whether AC or DC power is being transmitted. For AC power, the length of cable corresponds to a certain amount of reactive power being injected into the network. This injected

reactive power could balance with the reactive power demand from the induction generators. For DC power, the harmonic attenuation is what determines the quality of the power. The attenuation of harmonics is related to the line parameters of the cable and the cables length. It is ideal to maximize the quality of the power that is received onshore; this corresponds to unity power factor onshore, or zero total harmonic distortion [82,83].

- Reliability is an important aspect to consider when choosing a topology. It is ideal, that when a failure happens, that each or all generators can be disconnected from the power grid. It is also ideal to be able to reroute the power such that if a transmission line were to fail, power can still be generated and delivered to shore. The trade-off with reliability is the cost. A system must be chosen that provides reasonable reliability for a reasonable additional cost [82,83].

- Synchronization requirements for offshore power installations using induction machines can be quite difficult or expensive to achieve. The requirements of synchronization are quite different for the various topologies [82,83].

6.2.2 Inclusion of Remote Generation and Offshore Loads

For the topologies described above, models will be developed to incorporate the possible addition of other offshore generators, which are not part of the main cluster, as well as loads. An example of an additional offshore turbine would be the inclusion of several offshore tidal generators to the common hub of an offshore wind farm. An example of a

load would be an offshore oil platform. The inclusion of all these components results in a general model for an offshore micro-grid.

6.3 Offshore AC Generation Micro-Grid

If it was required to have an AC offshore micro-grid, there are several requirements that must be specified. The offshore generators must be synchronized, frequency regulated if an induction machine is used, voltage regulated, and the transmission lengths must be less than approximately 35km. Synchronization requires that at the point of common connection there is a fixed voltage and phase. The star and radial topologies will be analyzed to determine the synchronization requirements for the generators as well as determining the equivalent model of the micro-grid.

6.3.1 Micro-Grid Model

To begin the analysis, a generalized topology for the problem must be created. This will include the main generator cluster, remote generation that is interconnected to the cluster, and loads. The generalized topology can be observed in Figure 6-3 below.

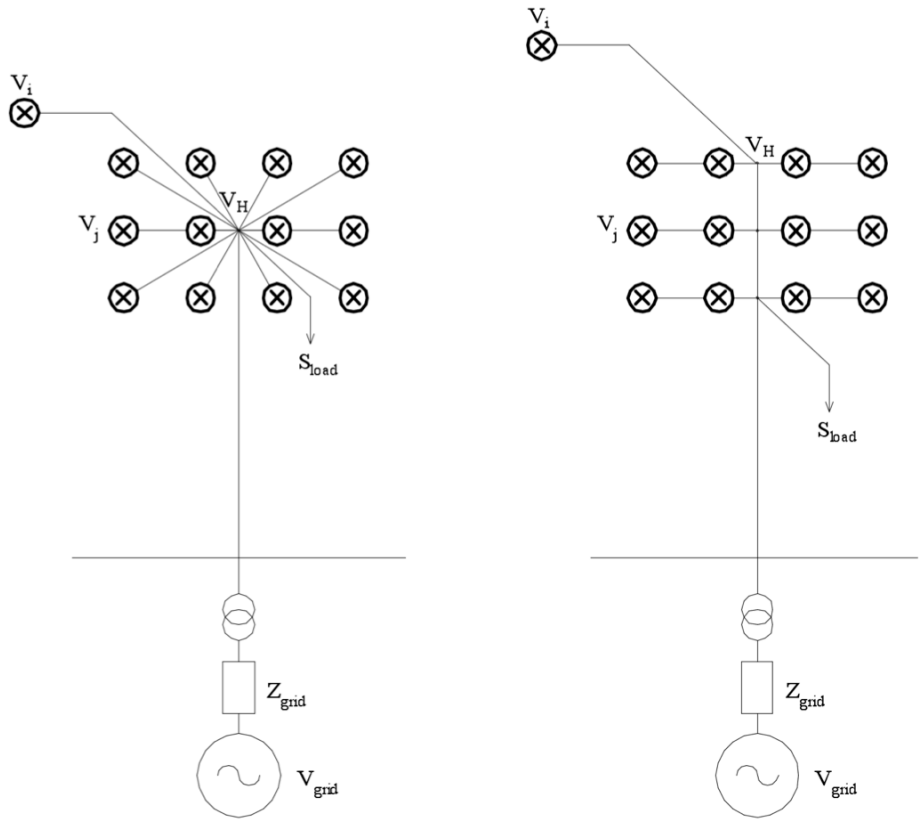

Figure 6-3: Generalized Offshore Micro-Grid Star and Radial Topologies

In Figure 6-3, V_H is the voltage and phase at the common hub, V_j is the voltage and phase for each generator in the main cluster, V_i is the voltage and phase for each of the other interconnected turbines, and S_{load} represents various loads that may be connected to the hub. It should be noted that the non-cluster generator(s) could represent an equivalent circuit for another offshore generator cluster. For the analysis, the following assumptions about the system will be made:

- The magnitude of generator voltage is known
- The apparent power and power factor for each generator is known

- The hub voltage phase angle is assumed to be the reference
- The equivalent of the micro-grid will be represented as an equivalent sending end voltage and current such that two-port network analysis can be performed for the transmission line to shore. The sending end voltage is V_H and the sending end current is the summation of current from each generator branch.

Finding the equivalent model for a single cluster of generators in Figure 6-3 will allow for the analysis of larger systems.

6.3.2 Star Topology

To formulate an equivalent of this topology, it should be noted that the hub voltage is unknown but common among all the generators. Since an underwater power cable connects each generator to the hub, two-port network analysis can be applied as follows:

$$|V_j|\angle\delta_j = A|V_H| + \frac{B}{A}\left(\frac{|S_j|}{|V_j|}\angle(\delta_j - \phi_j) - C|V_H|\right) \tag{6.9}$$

Where δ_j is the phase angle of the generator and ϕ_j is the power factor of the generator. Separating this into its real and imaginary components results in the following equations:

$$|A||V_j|\cos(\alpha + \delta_j) - |B|\frac{|S_j|}{|V_j|}\cos(\beta + \delta_j - \phi_j) = |V_H| \tag{6.10}$$

$$|A||V_j|\sin(\alpha + \delta_j) - |B|\frac{|S_j|}{|V_j|}\sin(\beta + \delta_j - \phi_j) = 0 \tag{6.11}$$

Where α is the phase angle of A and β is the phase angle of B. Equation (6.11) has only the unknown parameter δ_j in it. This equation can be evaluated to find the phase angle of the generator. The following relationship can be created:

$$\frac{|A||V_j|^2}{|B||S_j|} = \frac{\sin(\beta+\delta_j-\phi_j)}{\sin(\alpha+\delta_j)} \tag{6.12}$$

This equation is non linear and can be iterated to find a solution. Once the solution of δ_j has been evaluated, equation (6.10) can be evaluated to find what the hub voltage will be. Once these have been evaluated, the current injected to the hub from each generator can be evaluated. The total current transmitted to shore is the summation of each current injected into the hub from each generator. The following observations can be made regarding this topology:

- Each generator has its own transmission line to the hub. Each transmission line will have its own ABCD parameters due to the different transmission line lengths and potentially different cable geometry.
- If each generator and transmission line are equivalent, the phase angle of each generator will also be equivalent.
- If the generator and transmission line are not equivalent, then equation (6.12) would result in a different solution for each generator. This means that the hub voltage must be determined and remain constant.
- Equation (6.12) will be used to evaluate the hub voltage for each generator. The absolute error between each generator voltage and hub voltage will be used to evaluate what the hub voltage must be. The generator with the numerically largest error and its associated hub voltage will be selected to define the hub voltage. For the remaining generators, the phase angles will be determined from equation (6.10) given the hub voltage previously evaluated.

- The load will be modeled by evaluating the current draw at the sending end of the loads transmission line. This current will be subtracted from the hub current.
- For additional generators, the i^{th} generator, a similar analysis as described above will occur.
- Once the hub voltage and current are evaluated, an equivalent for the micro-grid will have been determined. Two-port network analysis can then be performed for the transmission line to shore as discussed in Chapter 3.

6.3.3 Radial Topology

To formulate an equivalent for this topology, a circuit representing each branch of the radial network will be constructed. This circuit can be observed in Figure 6-4 below.

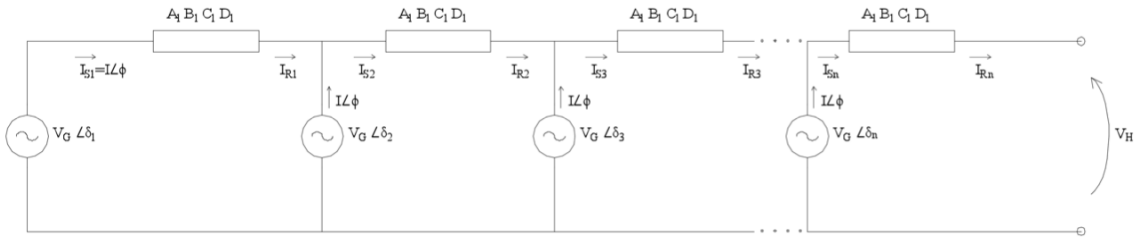

Figure 6-4: Equivalent Circuit of Each Branch in a Radial Network

From Figure 6-4, the following equations can be written for the first stage:

$$|A_1|\cos(\alpha_1 + \delta_1) - \cos(\delta_2) = \frac{|B_1||I|}{|V_G|}\cos(\beta_1 + \phi) \tag{6.13}$$

$$|A_1|\sin(\alpha_1 + \delta_1) - \sin(\delta_2) = \frac{|B_1||I|}{|V_G|}\sin(\beta_1 + \phi) \tag{6.14}$$

$$I_{R_1} = \frac{|I|\angle\phi - C_1|V_G|\angle\delta_2}{A_1} \tag{6.15}$$

$$I_{S_2} = I_{R_1} + |I|\angle\phi \tag{6.16}$$

Equations (6.13) and (6.14) can be iterated to find a solution for the generator phase angles. When the phase angles are evaluated, the receiving end current for the first transmission line can be evaluated. Once this is complete, cascaded two-port network analysis can be performed to find the hub voltage and injected current. This forward analysis is applicable for a single radial branch or for multiple identical radial branches. Evaluation of the phase angles of each generator when the hub voltage is known will be evaluated in a different form of analysis. An equivalent model, as discussed in Appendix A, of the transmission lines will be used. Figure 6-5 below is the simplified radial topology.

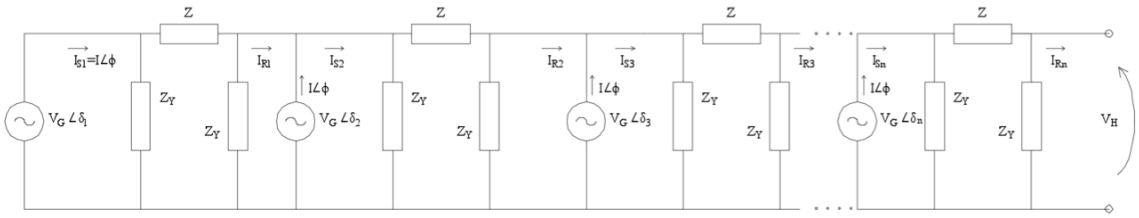

Figure 6-5: Equivalent Radial Topology

This transmission line model is appropriate since the generators in a radial branch will be close in proximity. From Figure 6-5, where the hub voltage and phase angle is defined, the following system of equations can be written to enable evaluation of each generators phase angle:

$$|I|\angle\phi - \left(\frac{|V_n|\angle\delta_n - |V_{n-1}|\angle\delta_{n-1}}{Z}\right) - 2\left(\frac{|V_n|\angle\delta_n}{Z_Y}\right) - \left(\frac{|V_n|\angle\delta_n - |V_H|\angle\delta_H}{Z}\right) = 0$$

$$\vdots$$

$$|I|\angle\phi - \left(\frac{|V_G|\angle\delta_2 - |V_G|\angle\delta_1}{Z}\right) - 2\left(\frac{|V_G|\angle\delta_2}{Z_Y}\right) - \left(\frac{|V_G|\angle\delta_2 - |V_G|\angle\delta_3}{Z}\right) = 0 \tag{6.17}$$

$$|I|\angle\phi - \left(\frac{|V_G|\angle\delta_1}{Z_Y}\right) - \left(\frac{|V_G|\angle\delta_1 - |V_G|\angle\delta_2}{Z}\right) = 0$$

From this system of equations, the phase angles of each generator can be designed such that the hub voltage is matched. The following observations can be made about this topology:

- Groups of generators are daisy-chained together to form a branch of the radial network
- If each branch is different, synchronization becomes relatively difficult to achieve.
- The same hub voltage selection criteria will be applied as with the star topology.
- The load will be modeled by evaluating the current draw at the sending end of the loads transmission line. This current will be subtracted from the hub current.
- For additional generators, the i^{th} generator, the star analysis will be applied to determine how to synchronize that generator.
- Once the hub voltage and current are evaluated, an equivalent for the radial topology micro-grid will have been determined.

6.4 Offshore DC Generation Micro-Grid

The offshore DC generation micro-grid will consist of clusters of AC generators which have had the power converted to DC. The topologies utilized for the DC generation micro-grid will be equivalent to Figure 6-3. In the matter of interconnection requirements, it can be observed that for a DC micro-grid, matching of voltage magnitude at the output of the rectification stage is all that is required. As discussed in Chapter 4, this is a matter of controlling firing angles.

6.4.1 Star Topology

To begin analyzing this topology, the DC component of the rectifier output will be analyzed. All of the power generated should be contained in the DC component. In reality there are energy losses associated with the power conversion process as well as contained within the resultant harmonics. The model shown in Figure 6-3 for the star topology can be simplified for this analysis. Each of the transmission lines that connect the generators to the hub can be modelled by a single resistive element. If the voltage at the hub is required to be a constant, then the DC voltage at the output of the rectifier for each generator must be evaluated. For the i^{th} generator, the following equation can be used to evaluate what this voltage should be, assuming that bipolar DC transmission is applied.

$$V_i = \frac{V_H}{2} + \sqrt{\left(\frac{V_H}{2}\right)^2 + \frac{R_i P_i}{2}} \tag{6.18}$$

From this equation, the DC voltage required from the generator can be determined for each of the generators in the network. This voltage can be controlled from the firing angle of the rectifier. This interconnection requirement is much simpler to achieve than for an AC cluster of generation where there is both concern for the voltage magnitude as well as the phase angles. The current delivered to the hub is equal to the summation of currents from each generator. To determine what the hub voltage must be for a generator cluster, the following equation can be applied for each generator:

$$V_H = V_i - \frac{P_G R_i}{2V_i} \tag{6.19}$$

Where the V_i term for each generator is obtained from the magnitude of the DC component of the controlled Graetz circuit from Chapter 4. This results in the following equation:

$$V_H = \frac{3}{\pi} V_{LL} \cos(\alpha) - \frac{P_G R_i \pi}{6 V_{LL} \cos(\alpha)} \tag{6.20}$$

From this equation the maximum hub voltage can be evaluated for each generator. The equation describing the maximum hub voltage is the following:

$$\frac{dV_H}{d\alpha} = 0 = -\frac{3}{\pi}V_{LL}\sin(\alpha) + \frac{P_G R_i \pi \cos(\alpha)}{6V_{LL}\sin^2(\alpha)} \tag{6.21}$$

Which results in the following equation:

$$0 = \cos\alpha - \frac{18{V_{LL}}^2}{\pi^2 P_G R_i}\sin^3\alpha \tag{6.22}$$

This equation can be solved using an iterative method. This will evaluate the firing angle resulting in the maximum hub voltage for each of the generators. When these maximum values are determined, the hub voltage will be set at the minima of these values. Once this has been evaluated, equation (6.18) can be used to evaluate the generator voltage for each of the remaining generators. The methodology is similar to the AC micro-grid. It has been assumed that sufficient filtering is employed with each rectifier that there are negligible effects due to harmonics.

6.4.2 Radial Topology

This topology will be analyzed with similar constraints as the star topology. The difference is in the interconnection, which is similar to Figure 6-4. For this application there is a resistive component connecting each of the generators together. It is assumed that the hub voltage is known and is constant. From this topology, the following equation can be created to determine what the DC voltage for each generator in a radial branch must be. Again, it is assumed that bipolar DC transmission is being applied.

$$V_n = V_{n+1} + R_n \sum_{i=1}^{n} \frac{P_i}{2V_i} \tag{6.23}$$

This equation allows for the backwards evaluation of the generators DC voltages, starting at the hub. The current delivered to the hub is equal to the summation of currents from each generator.

6.5 Power Flow Solution with IEEE 14 Bus System

The previous sections have discussed a means to form an equivalent model for an offshore micro-grid. The next step is to evaluate the performance of an onshore power grid when there is an interconnection with an offshore micro-grid. To perform this analysis, a sample offshore micro-grid will be defined. This micro-grid will replace a generator in the IEEE 14 bus system as shown in Figure 6-6 below. The object of studying the small IEEE 14 bus system is to simulate the effects that offshore micro-grid generation would have for a small community. This model could also apply for onshore wind micro-grid generation.

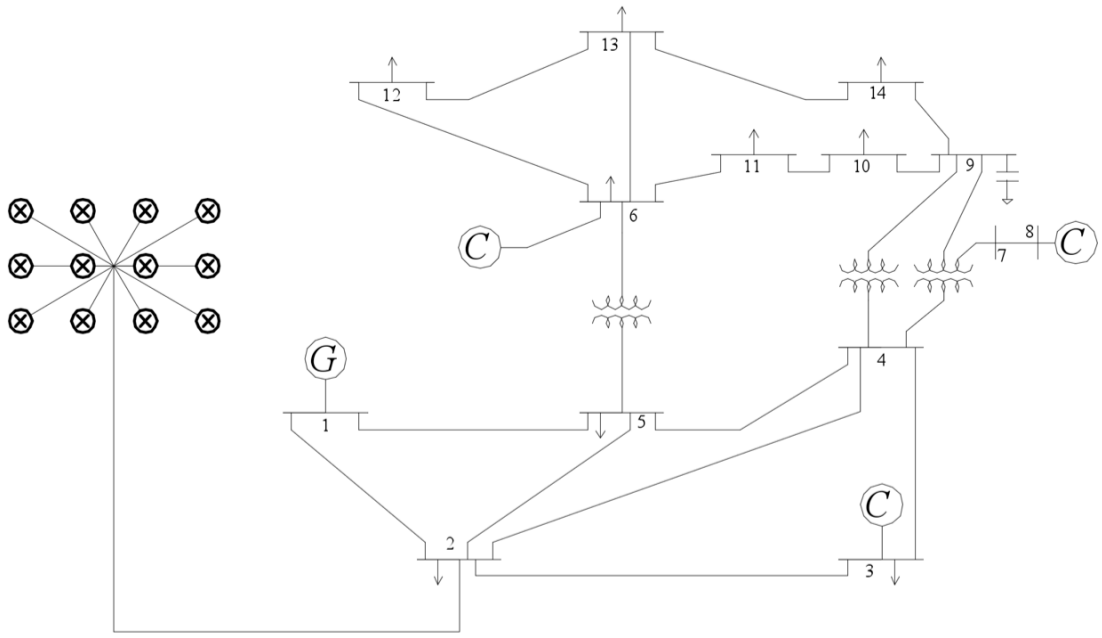

Figure 6-6: IEEE 14 bus System With Offshore Micro-Grid Inclusion

In Figure 6-6, the generator on second bus has been replaced with an offshore micro-grid, which has been denoted by a cluster of generators. The equivalent model of this micro-grid must first be defined; an equivalent circuit evaluated, and finally is included into the load flow formulation for the 14-bus system as was evaluated in Appendix A.

6.5.1 Offshore Micro-Grid Specifications

The micro-grid that will be analyzed will be composed of the following elements:

- 40 offshore wind turbines in a star configuration with *w* and *h* spacing of 0.5km. The grid will have 8 columns and 5 rows. The hub will be at the center of this grid. The hub is 15km from shore. Each generator is rated for 10MVA at a 0.95 leading power factor. The voltage rating for each generator is 32.5kV.

- 2 offshore tidal turbines that are 10km and 5km from the hub. Each generator is rated for 10MVA at a 0.95 leading power factor. The voltage rating for each generator is 32.5kV.
- 1 offshore load that is 15km from the hub. This load draws 10MW and 10MVAR.

6.5.2 Equivalent Model of Offshore Micro-Grid

To begin the analysis, the distances of each generator to the collection hub must be evaluated. The equation that will describe the distance of each generator the hub is given as follows:

$$\ell_{i,j} = 0.5\sqrt{(i-4.5)^2 + (j-3)^2} \tag{6.24}$$

The distances can then be evaluated to be the following:

$$\ell_{i,j} = \begin{pmatrix} 2.0156 & 1.6008 & 1.25 & 1.0308 & 1.0308 & 1.25 & 1.6008 & 2.0156 \\ 1.82 & 1.3463 & 0.9014 & 0.559 & 0.559 & 0.9014 & 1.3463 & 1.82 \\ 1.75 & 1.25 & 0.75 & 0.25 & 0.25 & 0.75 & 1.25 & 1.75 \\ 1.82 & 1.3463 & 0.9014 & 0.559 & 0.559 & 0.9014 & 1.3463 & 1.82 \\ 2.0156 & 1.6008 & 1.25 & 1.0308 & 1.0308 & 1.25 & 1.6008 & 2.0156 \end{pmatrix} \tag{6.25}$$

Based on the generator specified previously, a transmission line can be specified. A copper core conductor with a cross sectional area of approximately 150mm^2 or a diameter of 14mm. The XLPE insulation thickness should be 8mm. The lead sheath should have a thickness of 1.4mm. There will be one layer of steel armor that is 5mm in thickness. This specified cable would be sufficient for use with each specified generator. It will be assumed that single core cables will be used for the generator interconnection. The line parameters per kilometer can be evaluated to be the following:

$$\begin{pmatrix} R \\ L \\ G \\ C \end{pmatrix} = \begin{pmatrix} 0.138 & \Omega/km \\ 0.0017 & H/km \\ 8.33 \cdot 10^{-11} & S/km \\ 1.837 \cdot 10^{-7} & F/km \end{pmatrix} \tag{6.26}$$

From these line parameters, the two-port network parameters can be evaluated for each of the transmission lines. From these two-port network parameters the following equations can be used to evaluate the phase angles of each generator in the micro-grid.

$$\delta^{k+1} = \delta^{k} - \left(\frac{\frac{|A||V_G|^2}{|B||S_G|}\sin(\alpha+\delta^k) - \sin(\beta+\delta^k-\phi_G)}{\frac{|A||V_G|^2}{|B||S_G|}\cos(\alpha+\delta^k) - \cos(\beta+\delta^k-\phi_G)} \right) \tag{6.27}$$

$$\delta^{k+1} = \delta^{k} + \left(\frac{|V_H| - |A||V_G|\cos(\alpha+\delta^k) + \frac{|B||S_G|}{|V_G|}\cos(\beta+\delta^k-\phi_G)}{-|A||V_G|\sin(\alpha+\delta^k) + \frac{|B||S_G|}{|V_G|}\sin(\beta+\delta^k-\phi_G)} \right) \tag{6.28}$$

The solution method for equations (6.27) and (6.28) is as follows:

1. Solve equation (6.27) for each generator.
2. Evaluate the hub voltage using equation (6.10) and absolute error between generator and hub voltage.
3. Select the hub voltage associated with the numerically largest error as the hub voltage.
4. Evaluate equation (6.28) for all of the other generators in this micro-grid.

This solution method will yield the phase angles for each generator, the hub voltage, and the current injected into the hub. The sum of the currents injected to the hub from each generator minus the sum of the current drawn from the offshore loads will yield the total current that must be transmitted to shore. The phase angles, in degrees, for each of the generators in the main grid are as follows:

$$\delta_{i,j} = \begin{pmatrix} 0.7331 & 0.5826 & 0.4552 & 0.3754 & 0.3754 & 0.4552 & 0.5826 & 0.7331 \\ 0.6622 & 0.4902 & 0.3284 & 0.2038 & 0.2038 & 0.3284 & 0.4902 & 0.6622 \\ 0.6368 & 0.4552 & 0.2733 & 0.0912 & 0.0912 & 0.2733 & 0.4552 & 0.6368 \\ 0.6622 & 0.4902 & 0.3284 & 0.2038 & 0.2038 & 0.3284 & 0.4902 & 0.6622 \\ 0.7331 & 0.5826 & 0.4552 & 0.3754 & 0.3754 & 0.4552 & 0.5826 & 0.7331 \end{pmatrix} \tag{6.29}$$

The phase angles, in degrees, for the two tidal generators are as follows:

$$\delta = \begin{pmatrix} 0.6357 \\ 0.7274 \end{pmatrix} \tag{6.30}$$

Where the first angle corresponds to the tidal generator that is 10km from the hub and the second to the tidal generator that is 5km from the hub. Having determined these phase angles, two-port network analysis can be performed to evaluate the receiving end current and thus the current injected into the hub. The absolute difference between the generator voltage and the hub voltage it would produce according to equation (6.10) is defined as follows:

$$e = V_{Gen} - V_{Hub} \tag{6.31}$$

The difference associated with each of the generators in the main generator cluster is as follows measured in [V]:

$$e_{i,j} = \begin{pmatrix} -24.95 & -19.84 & -15.51 & -12.8 & -12.8 & -15.51 & -19.84 & -24.95 \\ -22.54 & -16.7 & -11.2 & -6.95 & -6.95 & -11.2 & -16.7 & -22.54 \\ -21.68 & -15.51 & -9.32 & -3.11 & -3.11 & -9.32 & -15.51 & -21.68 \\ -22.54 & -16.7 & -11.2 & -6.95 & -6.95 & -11.2 & -16.7 & -22.54 \\ -24.95 & -19.84 & -15.51 & -12.8 & -12.8 & -15.51 & -19.84 & -24.95 \end{pmatrix} \tag{6.32}$$

The difference for the two tidal generators is as follows:

$$e = \begin{pmatrix} -95.4304 \\ -57.9668 \end{pmatrix} \tag{6.33}$$

Where the first difference corresponds to the tidal generator that is 10km from the hub and the second to the tidal generator that is 5km from the hub. From these voltage difference computations it can be seen that the hub voltage will be chosen to be the resultant voltage due to the generators closest to the hub. This results in the single-phase hub voltage being 18478.32V. The phase angle for these two generators is 0.0912 degrees. The phase angles of all the other generators will now be evaluated using equation (6.28) now that the hub voltage has been established.

$$\delta_{i,j} = \begin{pmatrix} 3.5172 & 3.02 & 2.553 & 2.23 & 2.23 & 2.553 & 3.02 & 3.5172 \\ 3.2885 & 2.687 & 2.023 & 1.372 & 1.372 & 2.023 & 2.687 & 3.2885 \\ 3.204 & 2.553 & 1.758 & 0.0783 & 0.0783 & 1.758 & 2.553 & 3.204 \\ 3.2885 & 2.687 & 2.023 & 1.372 & 1.372 & 2.023 & 2.687 & 3.2885 \\ 3.5172 & 3.02 & 2.553 & 2.23 & 2.23 & 2.553 & 3.02 & 3.5172 \end{pmatrix} \quad (6.34)$$

$$\delta = \begin{pmatrix} 10.03 \\ 6.35 \end{pmatrix} \quad (6.35)$$

Equations (6.34) and (6.35) are in degrees and represent the phase angles of each generator such that a single phase hub voltage of 18478.32V is achieved. The total apparent power delivered to the hub can now be evaluated. The current injected into the hub can be evaluated from the following equation:

$$I_{H_{i,j}} = \frac{I_S - V_S\frac{C}{A}}{D - \frac{BC}{A}} \quad (6.36)$$

From equation (6.36), the current from each generator that is injected into the hub can be evaluated. From this and the known hub voltage, the power injected into the hub can be evaluated. The total power injected into the hub from all generators is equal to the following:

$$S_{HUB_{GEN}} = 392.54MW - j145.31MVAR$$

The total power generated from all generators is equal to the following:

$$S_{GEN} = 399MW - j131.14MVAR$$

This result has the following implications:

- The efficiency is 98.4%
- The power factor went from 0.95 leading to 0.9378 leading
- The hub voltage is 18.478kV line to neutral

The next step in the evaluation of the offshore micro-grid is the inclusion of the offshore load. This will be analyzed by observing that the apparent power delivered to the load is known as well as the hub voltage is known. Using the power relationship at the output of the transmission line delivering power to the load as well as the two-port network theory, the following equations can be created to define what the voltage and voltage phase angle at the load will be.

$$|V_{Hub}|^2|V_{Load}|^2 = (|B||S_{load}|\cos(\beta+\phi) + |A|\cos(\alpha)\,|V_{Load}|^2)^2 + (|B||S_{load}|\sin(\beta+\phi) + |A|\sin(\alpha)\,|V_{Loadd}|^2)^2 \quad (6.37)$$

$$\tan(-\delta) = \frac{|B||S_{load}|\sin(\beta+\phi)+|A|\sin(\alpha)|V_R|^2}{|B||S_{load}|\cos(\beta+\phi)+|A|\cos(\alpha)|V_R|^2} \quad (6.38)$$

Equation (6.37) can be solved to find the magnitude of the voltage at the load. Equation (6.38) can then be used to evaluate what the phase angle of voltage across the load will be. For this particular load the voltage across the load was evaluated to be 16.072kV at an angle of -4.9045 degrees. Two-port network parameters can then be used to evaluate what the power draw from the hub will be to power this load. This set of two-port parameters is defined as follows:

$$\begin{bmatrix} V_{Hub} \\ V_{Load} \end{bmatrix} = \begin{bmatrix} \frac{A}{C} & B - \frac{AD}{C} \\ \frac{1}{C} & \frac{-D}{C} \end{bmatrix} \begin{bmatrix} I_{Hub} \\ I_{Load} \end{bmatrix} \quad (6.39)$$

From this the apparent power drawn from the hub can be evaluated to be the following:

$$S_{LOAD} = 10.512MW + j11.444MVAR$$

Combining all of these results, the following can be defined regarding the hub:

- The hub line to neutral voltage is 18.478kV
- The hub apparent power is $S_{HUB} = 388.488MW - j142.584MVAR$
- This includes all 40 turbines in the cluster, 2 tidal turbines, and 1 offshore load.

The next step in the analysis is to model this micro-grid with the transmission line connecting the hub to shore. This transmission line will be analyzed using the two-port network theory developed in Chapter 3. The transmission line that will be used to transmit the power to shore will have the following parameters:

$$\begin{pmatrix} R \\ L \\ G \\ C \end{pmatrix} = \begin{pmatrix} 39.7916 & m\Omega/km \\ 1.642 & mH/km \\ 6.569 \cdot 10^{-11} & S/km \\ 1.5365 \cdot 10^{-7} & F/km \end{pmatrix}$$

It has been assumed that the voltage is transformed to a reasonable value, 320kV, to transmit the power to shore. At the output of the transmission line, the power delivered to shore has the following specifications:

$$V_R = 322.32 \ \angle -2.034° \ [kV]$$

$$I_R = 704.6216 \ \angle 7.838° \ [A]$$

$$P_R = 387.55 \ [MW]$$

$$Q_R = -67.44 \ [MVAR]$$

$$PF = 0.9852 \ Leading$$

$$\eta = 99.76\%$$

The global efficiency between generation and reception of the power on shore is 97.13%. The power factor has also improved from 0.95 leading to 0.9852 leading. This increase in power factor is due to the capacitance of the underwater transmission line. In discussing the power factor it should be observed that as more generators are added to the micro-grid, the further the micro-grid could be from shore.

6.5.3 Incorporation With the IEEE 14 Bus System Power Flow Solution

Incorporating this offshore micro-grid with the IEEE 14-bus system will require a modification of the power flow formulation developed in Appendix A. This power flow model assumed that the voltage and real power output from a generator were controllable. In the case of an offshore micro-grid that uses induction generators, there is limited control of the reactive power that is generated. To incorporate this micro-grid into the power flow formulation, the following method can be applied:

- The voltage, real power, and reactive power at the shore are known.
- The reactive power draw of the micro-grid can be modeled by a shunt inductance at the on-shore bus. Where the equivalent inductance can be found from the following equation:

$$L = \frac{1}{2\pi f}\frac{|V_{shore}|^2}{Q_{Shore}} \tag{6.40}$$

- It will be assumed at this point that the micro-grid acts as if it were a classic generator bus. In the power flow solution, the voltage and real power are known while the phase angle and reactive power are unknown.
- The phase angle will be evaluated. This will require a re-evaluation of the hub voltage phase angle as well as the phase angle of each generator using the reverse process described previously.
- The reactive power that is evaluated from the power flow will determine what additional reactive power support is required at the on-shore bus. This reactive power support can be provided from a switched capacitor bank, synchronous condenser, or a static VAR compensator.

The new 14-bus system will have the topology shown in Figure 6-7 below.

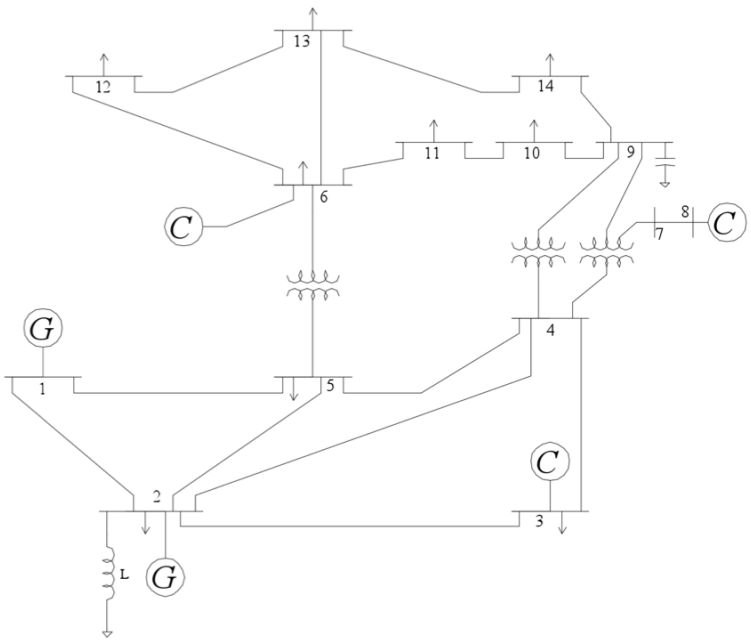

Figure 6-7: Modified IEEE 14-bus System With Micro-Grid

For the current case study, the inductance can be found to be L=4.0863H.

6.5.4 Power Flow Solution

Given the modified system in Figure 6-7, the power flow formulation can be modified by changing the real power at bus 2 to be 0.38755 per unit and including the shunt inductance on bus 2. It is expected that the resulting power flow solution will be virtually identical to what was previously analyzed. The sole difference being that the reactive power on bus 2 is increased by the value Q_R evaluated previously.

$$x = \begin{bmatrix} V_4 \\ V_5 \\ V_7 \\ V_9 \\ V_{10} \\ V_{11} \\ V_{12} \\ V_{13} \\ V_{14} \\ \delta_2 \\ \delta_3 \\ \delta_4 \\ \delta_5 \\ \delta_6 \\ \delta_7 \\ \delta_8 \\ \delta_9 \\ \delta_{10} \\ \delta_{11} \\ \delta_{12} \\ \delta_{13} \\ \delta_{14} \end{bmatrix} = \begin{bmatrix} 0.9936 \\ 1.0027 \\ 0.992 \\ 0.8671 \\ 0.9933 \\ 0.9939 \\ 0.9855 \\ 1.034 \\ 0.9752 \\ -0.1325 \\ -0.2968 \\ -0.2575 \\ -0.2170 \\ -0.3088 \\ -0.3782 \\ -0.3782 \\ -0.4402 \\ -0.4230 \\ -0.3701 \\ -0.2824 \\ -0.2424 \\ -0.3738 \end{bmatrix}$$

This result has only a slight deviation from what was evaluated in Appendix A. The phase angles at each bus have changed slightly. This is due to the generated power reducing to be 0.3877 per unit as opposed to 0.4 per unit. There are some observations that must be made regarding this result. From this result, it can be demonstrated that an underwater transmission lines effects, of length less than 20km, are negligible for an offshore cluster of generation using AC generators. For longer transmission line lengths, HVDC would be the best means of power transmission. The issue to overcome with offshore renewable energy sources can be simplified to the fact that they are intermittent by nature.

6.6 Energy Storage in the Offshore Power Micro-Grid

The previous analysis was a special case scenario. It was analyzing how to model the micro-grid when generation was fully available. In reality, these sources are intermittent whereas the load profile of a community is relatively rigid. Tidal based power is predictable while offshore wind is not. This raises the issue of unit commitment as well as the necessity for some form of energy storage. The IEEE 14-bus system that was modelled previously can be looked at in a few ways:

1. Bus 1, which is the slack bus, is the power grid, which supports the load that the community draws.
2. Bus 1, is a local generator and the 14-bus system is an island.
3. Bus 1 is potentially grid connected and connected to a local generator, a hybrid of the previous two.

For the sake of this discussion it will be assumed that the community in question wishes to minimize power purchased from the grid and/or minimize the usage of the local generator. The local generator is assumed to use fossil fuels to generate electricity. Assuming offshore tidal and offshore wind were the only source of renewable energy, prediction models for the wind and tides would have to be developed such that daily generation profiles can be predicted. With the load profile and the predicted renewables generation profile, the difference is what would be required to be supplied by the grid or local generator. To maximize the usage of renewable energy, all the renewable energy would have to be extracted when it is available. This may lead to the following situations:

1. Renewable generation is greater than the load, this allows for energy to be stored or energy sold to the grid [84].
2. Renewable generation is less than the load; this requires energy to be drawn from the storage or energy purchased from the grid [84].

By evaluating these profiles, evaluation of what energy storage would be required for a community can be performed. The energy storage device, to be of best use, should start each day at a specified energy state. This way, the energy storage device can absorb power when there is excess or provide power when it is needed. The factors associated in design of an energy storage system are the following:

1. Allowable depth of discharge and maximum charge
2. Maximum rate of charge and discharge
3. Starting day and end of day state of charge
4. Number of charge/discharge cycles (for some energy storage mediums)
5. Fossil fuel generator minimum loading requirements and optimal operation

For a system in which there exist only a fossil fuel generator and an energy storage device, with knowledge of the historical hourly load profile, a storage system can be specified. Running a fossil fuel generator at a constant power set point with minimal step changes in generation per day would be ideal. However, the longer the generator power set point is held constant, the greater the depth of charge/discharge will be. This would require a large energy storage device. Figure 6-8 below provides a sample daily generation profile for a community.

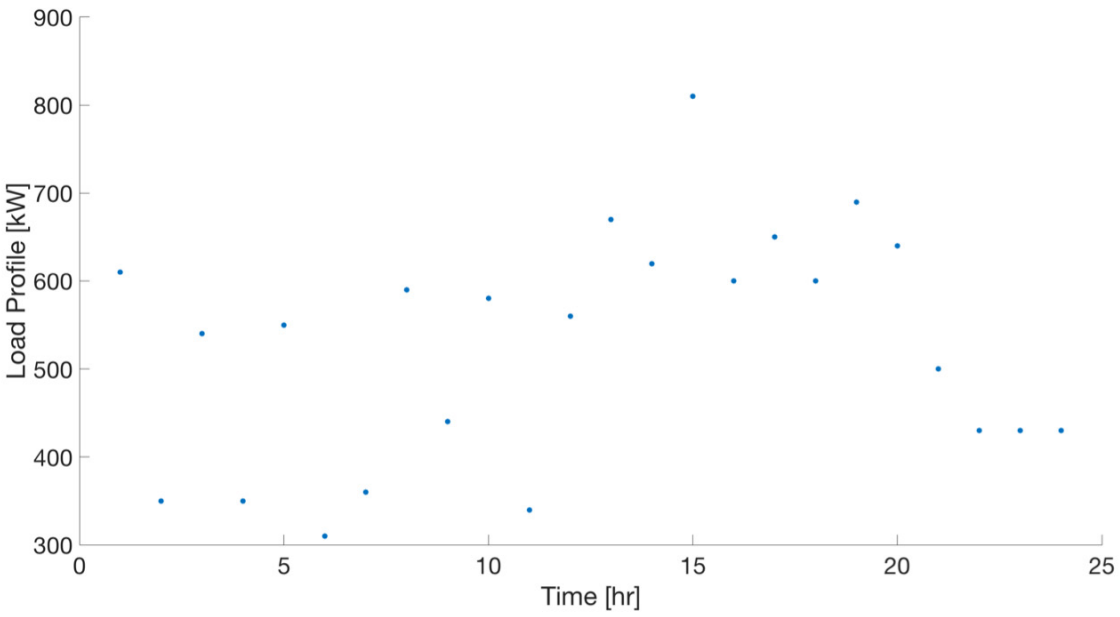

Figure 6-8: Example Load Profile

From Figure 6-8, the average load is 527.08kW for the whole 24-hour time scale. Figure 6-9a and 6-9b below represent the plots for the cumulative depth of discharge that an energy storage system would have to provide for a 24h and 6h power set-point averaging time window.

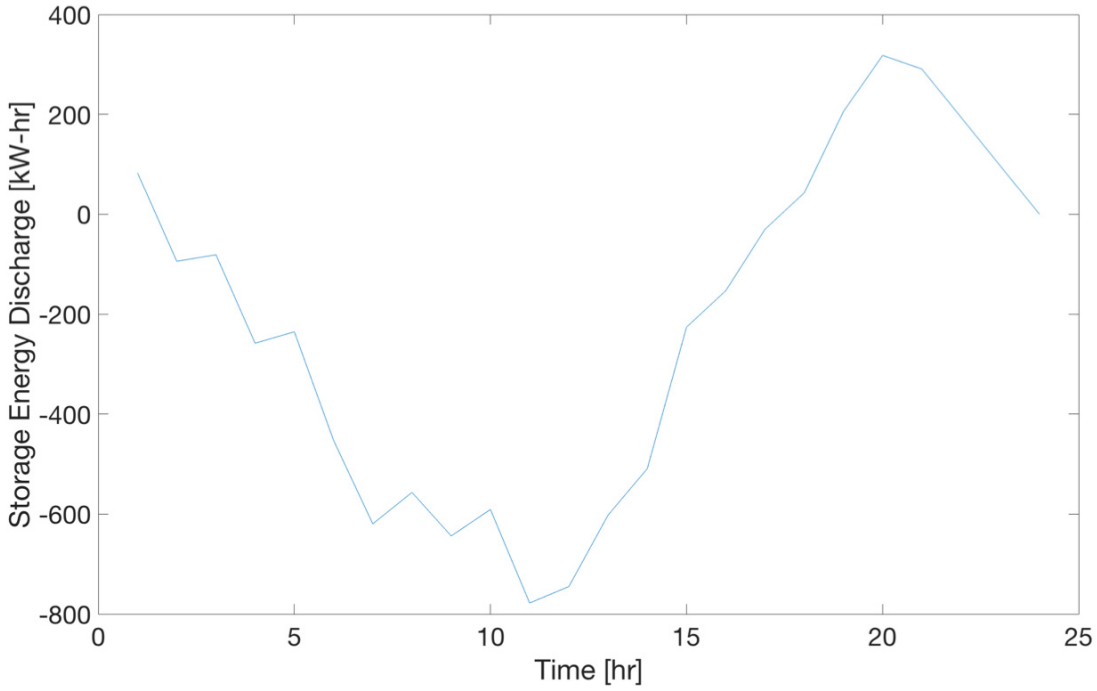

Figure 6-9a: 24h Power Set Point Averaging

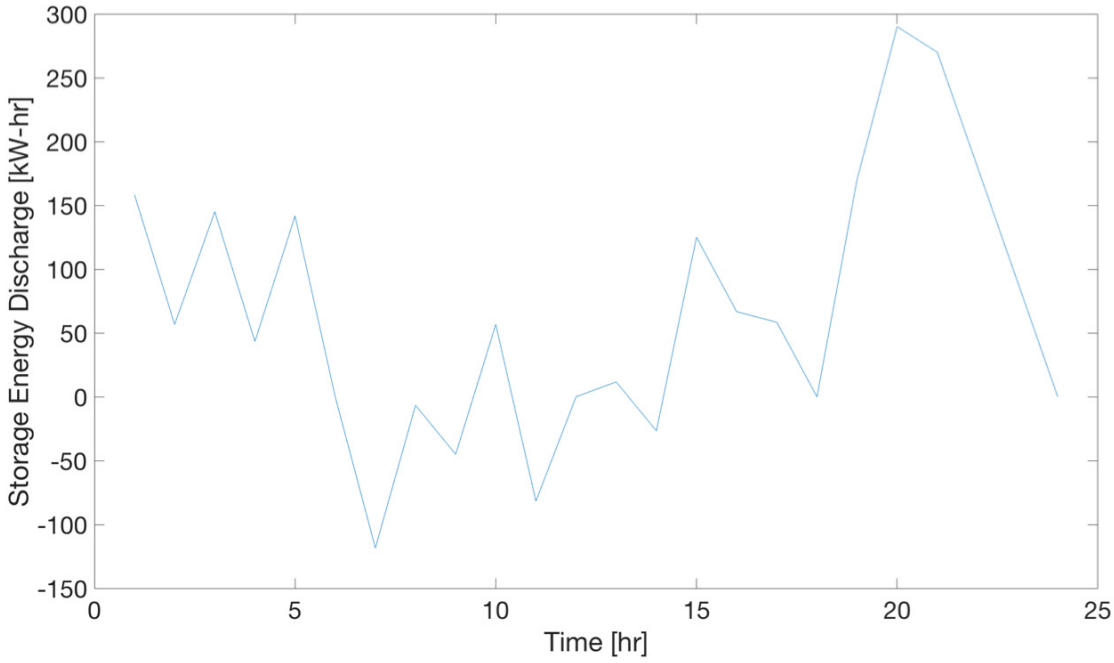

Figure 6-9b: 6h Power Set Point Averaging

As can be observed from these plots, the cumulative depth of discharge is greatly reduced by having a change in the generator power set point every six hours. From Figure 6-9a it can be observed that the energy storage device must be able to cumulatively store 800kWh of energy and cumulatively be able to discharge 300kWh from a nominal state of charge at the beginning of that day. In Figure 6-9b it can be observed that there is approximately a 125kW-hr charge and 300kW-hr discharge that the energy storage device must be able to achieve. These two results would lead to very different energy storage systems. Incorporation of the practical constraints of the generator operation and historical load data would allow for long term historical analysis to determine what the global maximum depth of charge/discharge would be. This in turn would yield what capacity the energy storage system should have.

6.6.1 Energy Storage With Inclusion of Renewable Generation

The preceding discussion regarding energy storage was for the case of a fossil fuel based generator as part of a micro-grid. The incorporation of renewable generation and its inherent intermittency changes the energy storage requirements. If historic data regarding the renewable resource were known, a similar methodology could be applied where the following equation would hold:

$$F_{LOAD}(n) - F_{RENEWABLES}(n) = F_{FOSSIL\ FUEL}(n) \tag{6.41}$$

Where *F* represents the forecasted power profile and *n* represents the discrete data points. From this the new cumulative depth of charge/discharge can be evaluated. The only variable in (6.41) that is controllable is the fossil fuel generation. This forecast is the one that will be modified with the inclusion of energy storage on the system. The ideal

objective would be to design a micro-grid that no longer would require fossil fuel generation. It should be noted that the fossil fuel generation term in (6.41) could also be substituted with imported power from a gird interconnection. Due to the uncertainty in both load and renewable generation for a given day, a real time controller would have to be implemented to control the energy storage device and power set point of the fossil fuel generator, given forecasts based upon historic data and real time atmospheric measurements. Given the intermittency of generation, it is hypothesized that to increase the reliability of a renewable energy micro-grid, a diversity of generation would have to be introduced.

6.6.2 Energy Storage Media

The preceding discussions regarding energy storage did not specify what kinds of energy storage could be used. The subsequent sections will discuss the various promising energy storage mediums as well as their present day limitations. Large-scale energy storage is the most limiting factor associated with the transition to renewable power generation. It is very expensive and difficult to store large amounts of energy. This affects the overall cost of the renewable energy system as well as the stability due to the intermittency of the resource. There are many methods of energy storage that are available for use, including the following:

1. Battery energy storage
2. Super capacitor energy storage
3. Flywheel energy storage
4. Pumped hydro energy storage

5. Compressed air energy storage
6. Thermal energy storage
7. Super magnetic energy storage
8. Fuel cell energy storage

It should be noted from this list that some of these energy storage mediums are location specific. Not every location may have a means storing pumped hydro energy or compressed air. Table 6-1 below summarizes the applicability of each of these energy storage mediums.

Table 6-1: Energy Storage Mediums [85,86,87]

Type	Round Trip Efficiency	Power Rating	Energy Density [W-hr/kg]	Discharge Time	Cost [$/kW-hr]	Cycles
Battery	70-90	0-8MW	10-240	Minutes to hours	100-2500	2000
Capacitor	90-95	0-300kW	2.5-15	Seconds	300-2000	Unbounded
Flywheel	85-95	0-250kW	10-30	Seconds	1000-5000	20,000+
Pumped Hydro	65-87	100-5000MW	0.5-1.5	Hours to days	5-100	Unbounded
Compressed Air	50-89	5-300MW	30-60	Hours to days	2-50	Unbounded
Super Magnetic	95-98	0.1-10MW	0.5-5	Seconds	1000-10,000	100,000+
Fuel Cell	20-35	0-50MW	800-10000	Seconds to hours		1000

From this array of energy storage mediums, they can be categorized into three groups: short duration power, medium to long duration power, and availability. Given a diversity of renewable generation, it is most likely that energy storage that can provide power in the minutes to hours range would be desired, which results in battery storage being the suitable medium of energy storage.

Chapter 7: Offshore Power Case Study

In this chapter, the analysis techniques developed in the previous chapters will be applied to a specific case study in Nova Scotia, Canada.

7.1 Introduction

This case study will be based on a study published by the Offshore Energy Research Association (OERA) in Nova Scotia, Canada [88]. The study will be conducted at the Grand Passage tidal power site, which has a potential for 3.6MW of power extraction [88]. This tidal power site location can be seen in Figure 7-1 below.

Figure 7-1: Grand Passage Tidal Site Location [89]

Two options of how to interconnect this turbine with Nova Scotia are immediately observable. These two options would be the following:

1. Connect the turbine to the grid at the rural location. This would require an underwater transmission line length of less than 2km.
2. Connect the turbine to mainland Nova Scotia, presumably to a stronger section of the power grid. This would require approximately 16-18km of underwater power cable.

For this study it will be assumed that this tidal turbine will be used to generate power for the local communities. The pre-existing electrical connection with mainland Nova Scotia will be maintained as a grid tie-in point, resulting in this region of Nova Scotia operating as an offshore power micro-grid. The following list outlines the process for the design of this offshore power system.

1. Determination of the load and generation profile for the renewable resource and the local communities.
2. Determine if AC or DC power transmission is most economic.
3. Determine what transmission line would be most economic. From this, the cables core conductor diameter and insulation thickness can be determined. The line parameters and steady state performance of the cable can then be determined.
4. Analyze the various methods of power conversion that can be applied (if necessary) and how the generated harmonics will propagate through the underwater transmission line.
5. Quantify how much energy storage would be required to smooth the load profile.

A flow chart for this process can be observed in Figure 7-2 below.

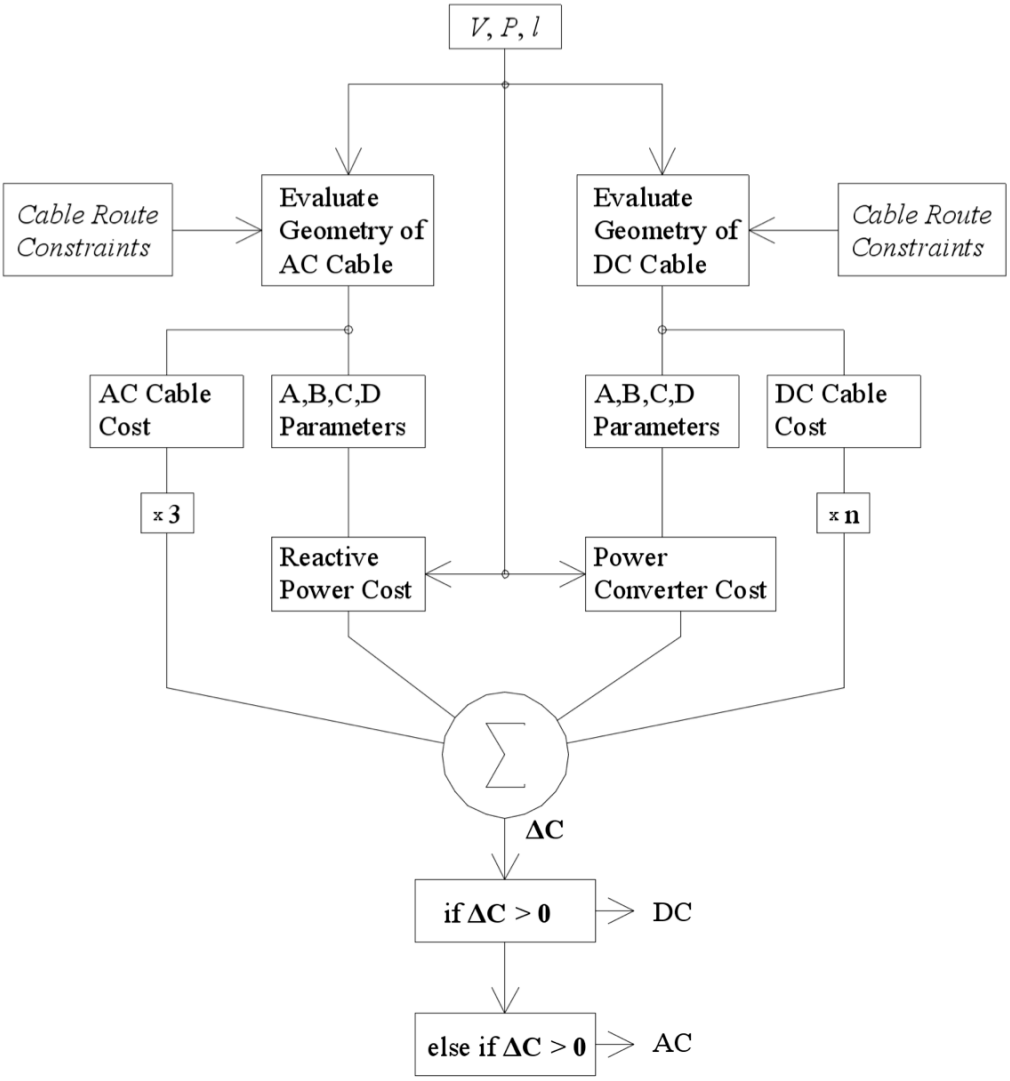

Figure 7-2: Design Flow Chart

7.2 AC or DC Transmission

From the analysis described in Chapter 5, the cost crossover threshold can be determined and is displayed in Figure 7-3 below.

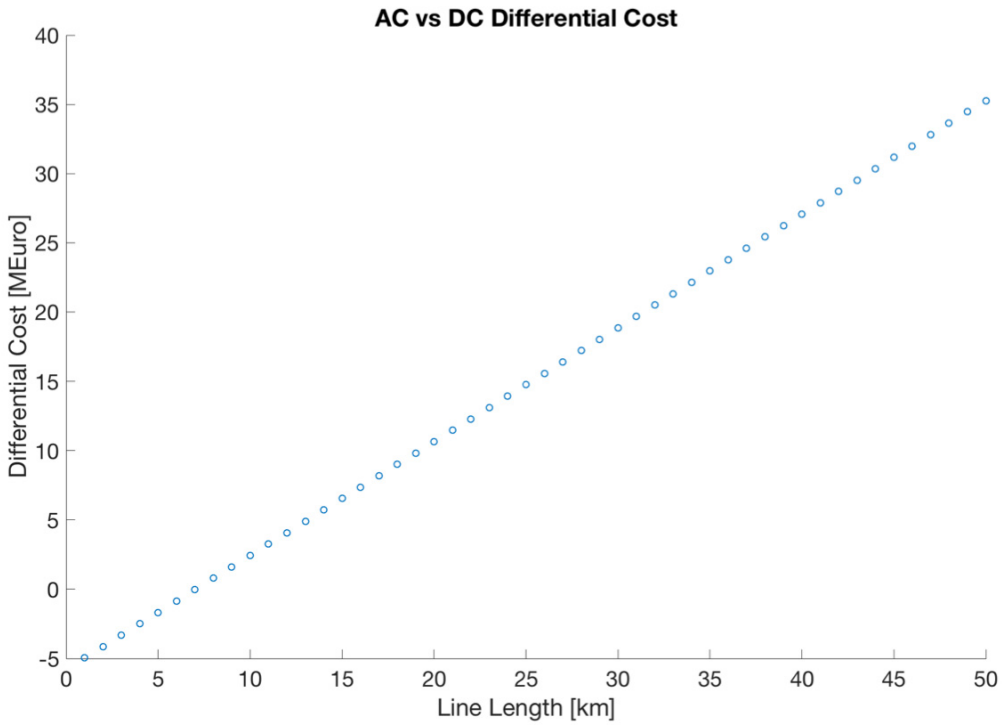

Figure 7-3: Cost Crossover

From Figure 7-3 it can be observed that the cost crossover point for this system is between 7 and 8km. The length of underwater transmission line for this application would be at least 16km in length. Therefore, the most economic transmission medium would be DC.

7.3 Transmission Line Geometry Selection

As discussed in Chapter 5, the most economic transmission line geometry can be determined. This is based upon the cost function for the underwater DC cables as well as the regression equations for voltage/insulation thickness and ampacity/core conductor radius. The cost gradient for underwater power cable can be evaluated from the equations

developed in Chapter 5. The power balance equation for a bipolar DC link can be given by the following equation:

$$\frac{P}{2000I} - R(I)\frac{I}{1000} = V \tag{7.1}$$

From these two equations, the optimal selection of voltage and current can be determined. These can be solved using the method of Lagrange multipliers. The Lagrangian is as follows:

$$\mathcal{L} = C_{Cable}(V, I) + \lambda\left(\frac{P}{2000I} - R(I)\frac{I}{1000} - V\right) \tag{7.3}$$

The partial derivatives of the Lagrangian can be evaluated to be the following:

$$\frac{\partial \mathcal{L}}{\partial \lambda} = 0 = \frac{P}{2000I} - R(I)\frac{I}{1000} - V \tag{7.4}$$

$$\frac{\partial \mathcal{L}}{\partial V} = 0 = \frac{\partial C_{Cable}}{\partial V} - \lambda \tag{7.5}$$

$$\frac{\partial \mathcal{L}}{\partial I} = 0 = \frac{\partial C_{Cable}}{\partial I} + \lambda\left(\frac{-P}{2000I^2} - \frac{dR(I)}{dI}\frac{I}{1000} - \frac{R(I)}{1000}\right) \tag{7.6}$$

Solving equations (7.4) through (7.6) results in a selection of 22kV and 68A as the nominal voltage and ampacity of the cable. From this a cables geometry can be determined to require 5.65mm insulation thickness and a 6.4mm core conductor diameter.

7.4 System Performance

The performance of the system can now be evaluated. The performance will be analyzed for three cases, the steady state performance, transient performance, and harmonic performance. From the cable geometry defined above and using a typical underwater power cable geometry, the two port network parameters can be evaluated. The system that will be analyzed is shown in Figures 7-4 and 7-5 below.

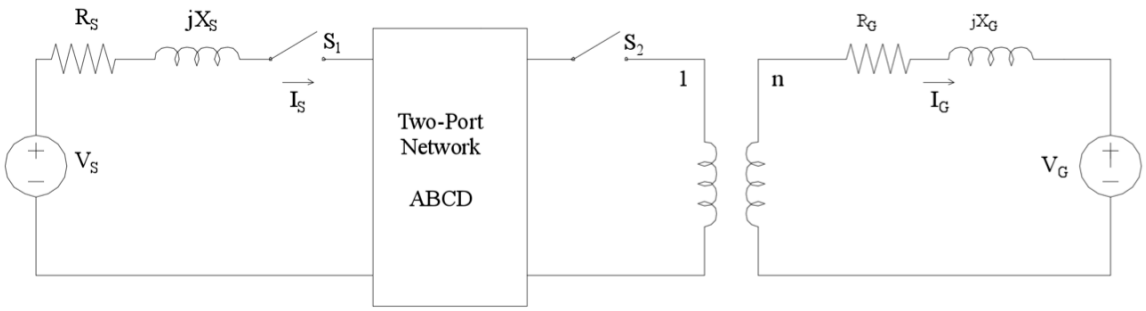

Figure 7-4: Offshore Turbine System Steady State Model

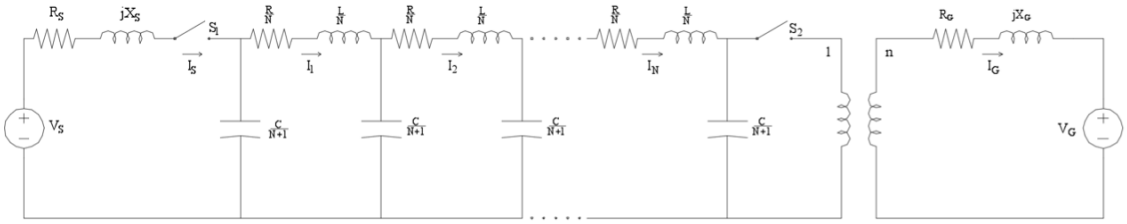

Figure 7-5: Offshore Turbine System Transient

Figure 7-4 represents the system model that will be used for the analysis of the steady state and harmonic performance. Figure 7-5 will be used to evaluate the transient performance of this system. For the transmission line geometry defined previously, the line parameters can be evaluated to be the following at a 60Hz frequency:

- R=897.5 [mΩ/km]
- L=1.654 [mH/km]
- C=0.1595 [μF/km]
- G=61.76 [pS/km]

The steady state analysis of this transmission link, since it will be transmitting DC power is trivial to evaluate. The attenuation of voltage between sending end and receiving end of a bipolar DC link can be evaluated as follows:

$$\frac{V_R}{V_S} = 1 - \frac{\ell P}{2\sigma A^2 {V_S}^2} \tag{7.7}$$

From this, the voltage gain can be evaluated to be 0.974. The harmonic performance of the transmission line can be evaluated as described in Chapter 3. Figure 7-6 and 7-7 below represents the worst-case series of resonances that will occur to this cable in the event of a loss of load (S1 closed and S2 open) in Figure 7-4 above.

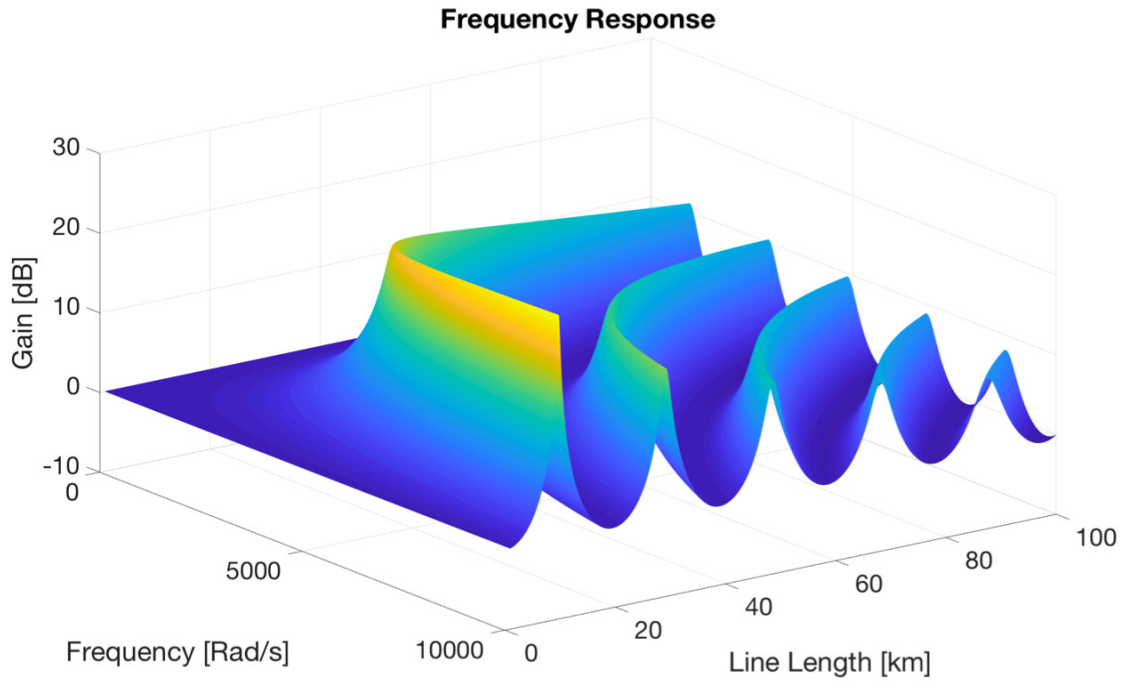

Figure 7-6: Underwater Transmission Line Resonances

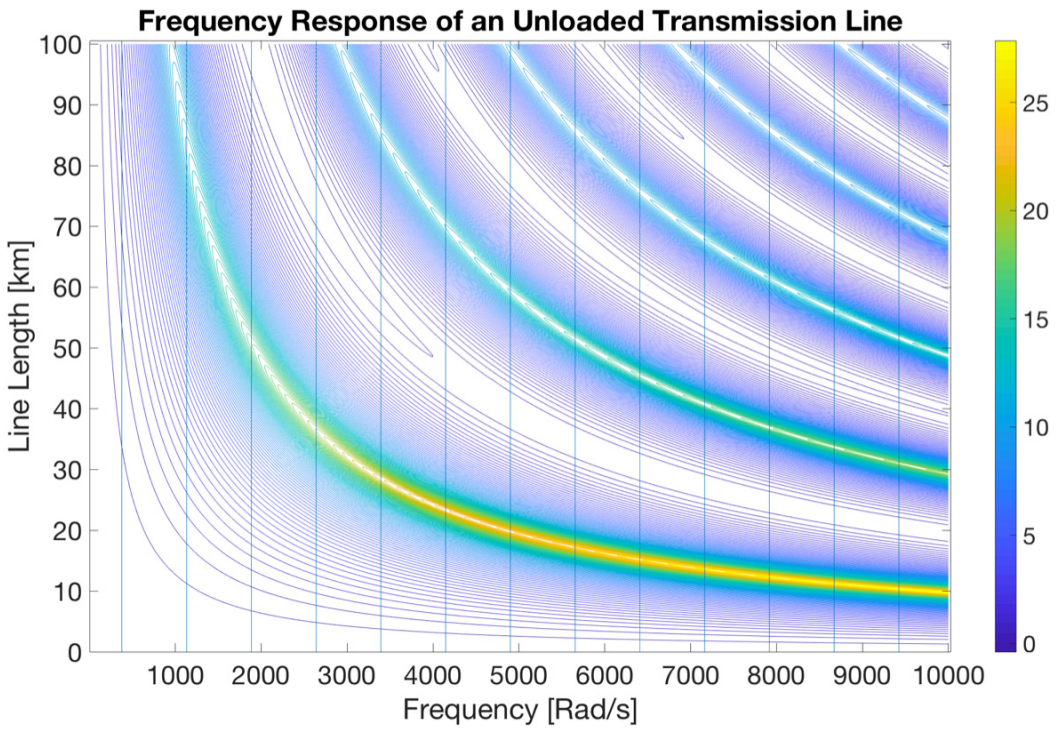

Figure 7-7: Underwater Transmission Line Resonances Contour Plot

From Figures 7-6 and 7-7 above it can be observed that there is a resonant arc that exists for frequencies greater than 800Hz for line lengths of 16km or less. If a three-phase rectifier using a Graetz circuit, or equivalent, is applied then there will be harmonic components at the following frequencies:

$$f_n = 6nf \tag{7.8}$$

Where n is the harmonic number and f is the fundamental frequency of 60Hz. It can be observed that there would be several harmonics with resonances along the length of the transmission line, the most significant being the first harmonic. A different interpretation of this can be observed in Figures 7-8 and 7-9 below.

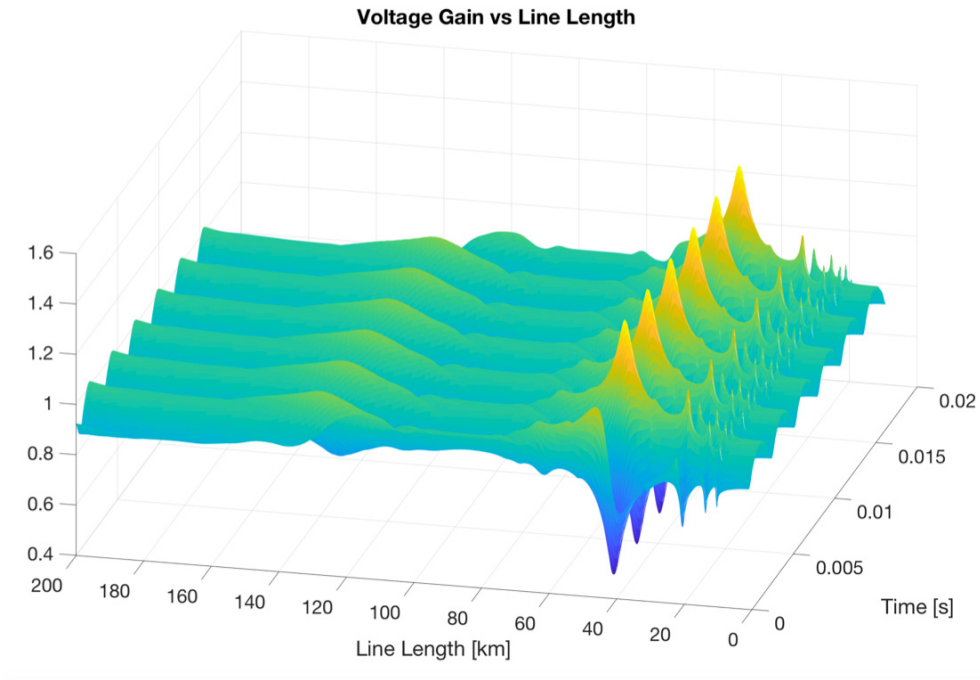

Figure 7-8: Resonances as a Function of Time and Line Length

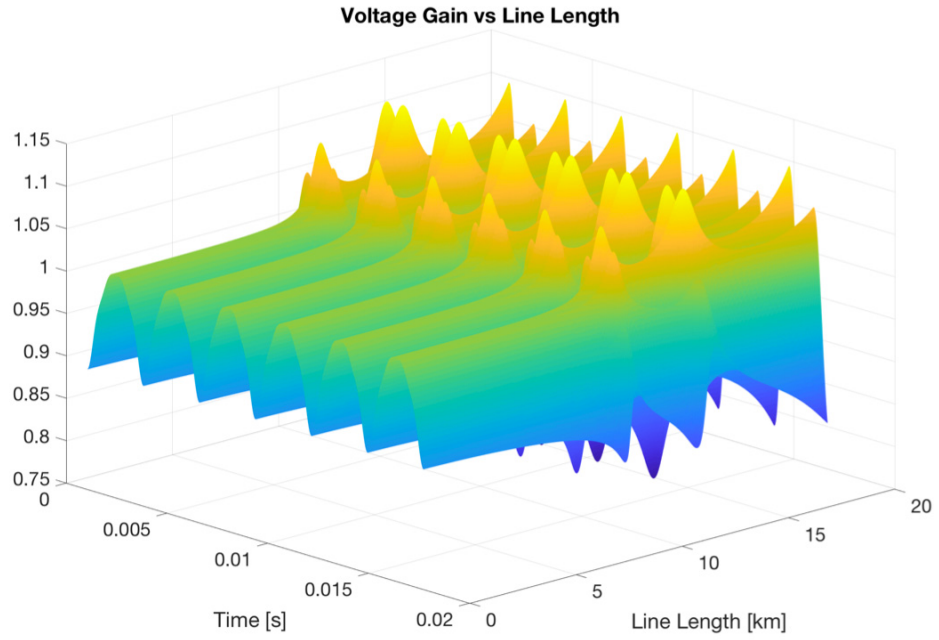

Figure 7-9: Resonances as a Function of Time and Line Length Less Than 20km

These figures show what the resonances will look like as a function of time and transmission line length. Figure 7-8 represents this transmission line for line lengths up to 100km where Figure 7-9 limits itself to line lengths less than 20km. From Figure 7-9 it can be observed that at line lengths less than 5km, the nominal Graetz circuit output is observed. At line lengths between 5 and 20km, higher frequency resonances begin to become quite pronounced with a voltage gain of approximately 1.1. Figure 7-10 below shows a contour plot view of Figure 7-9.

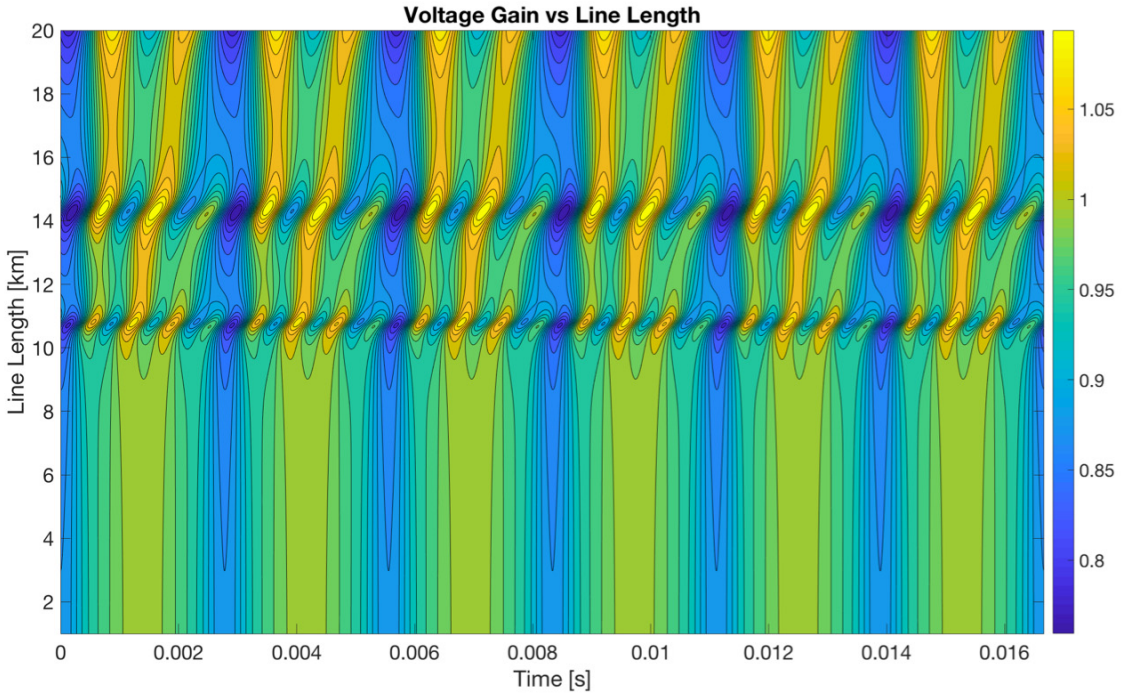

Figure 7-10: Contour Plot of Cable Resonances

The transient performance of this transmission link can be determined by evaluating the step response of the transmission line when the grid connection is translated to an equivalent on the DC bus as described in Appendix A. Figures 7-11 and 7-12 below show what the transient response of this transmission line would be for various cases.

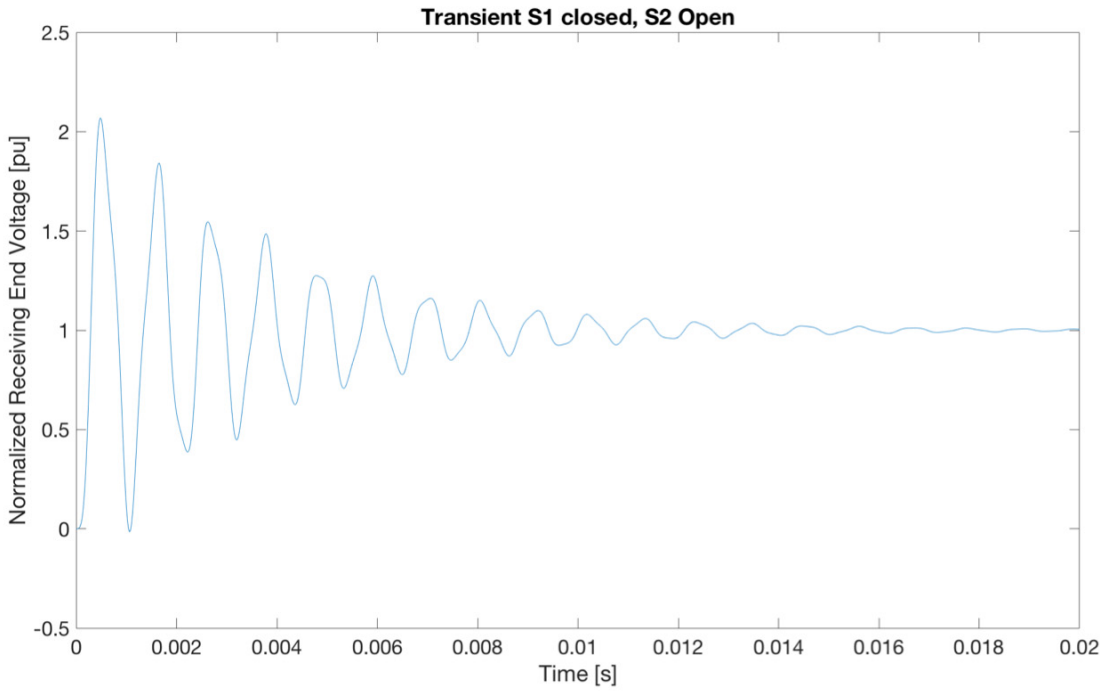

Figure 7-11: Transient Response, S1 Closed, S2 Open

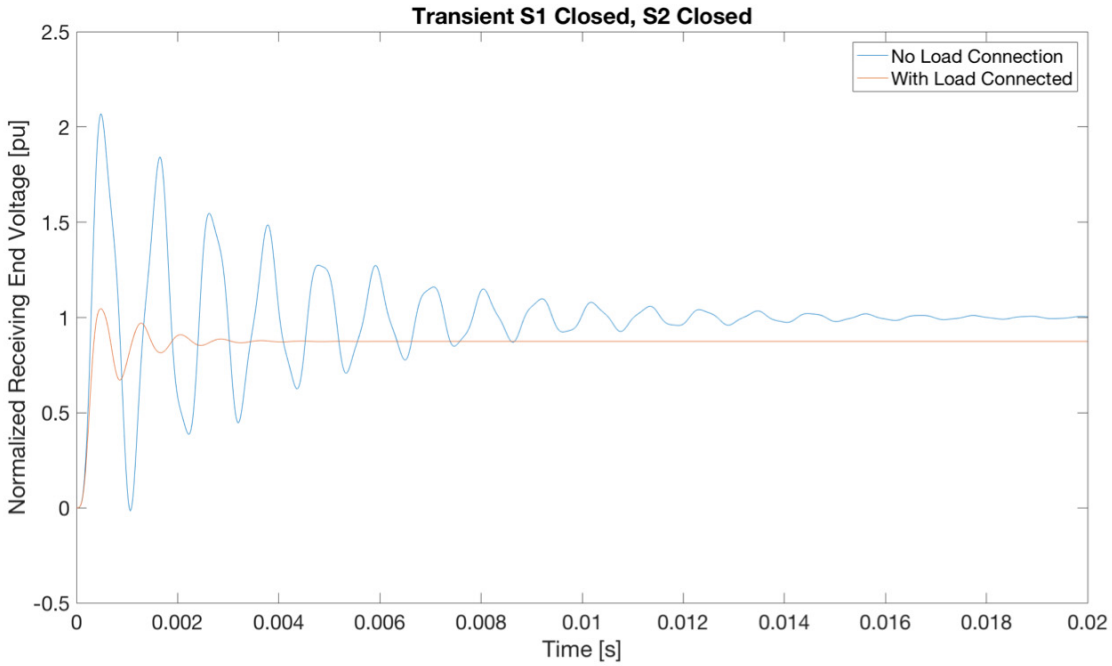

Figure 7-12: Transient Response, S1 Closed, S2 Closed

From Figures 7-11 and 7-12, the following observations can be made:

- When there's no load connected at the receiving end, the voltage will have a percent peak overshoot of approximately 100%. The oscillations will persist for approximately one 60Hz AC cycle.
- The effect that the rest of the system has on the transient effect is that it provides significant damping of the transient oscillations as well as reducing the percent peak overshoot to approximately 20%.

Chapter 8: Conclusion

In this thesis, a review of the state of offshore power and offshore power technology has been conducted. The analysis of various forms of underwater power cables were analyzed and their line parameters determined. The steady state power transmission performance of these various cables has been analyzed and their limitations outlined. Equivalent transmission line models have been developed and the limitations of their validity as the transmission length increased has also been determined. These equivalent models are important for determining the transient response of an offshore transmission line as well as for use in power flow analysis. Harmonic analysis has been conducted for the various transmission lines to determine where resonances or troughs may be located along a transmission line's length. The resonances and troughs have been analyzed for two cases: when the cable is loaded and when it is not loaded. This analysis, along with the review and analysis of modern power electronic systems, allows for the determination of where various harmonics will have a resonance along the length of the transmission line. This allows for the determination of where the cables insulation may be prematurely broken down. The harmonic propagation has been determined for various configurations of power electronic systems.

An economic analysis has been conducted with the objective of determining the cutoff transmission length to determine when it is most economical to transmit DC rather than AC power. This analysis, in conjunction with the previous analysis, resulted in the determination that at a transmission line's length greater than 15km, DC is the preferable medium of transmission. There are multiple economic models presented to represent the

varying situations of communities. The cost functions of underwater cables coupled with underwater cable manufacturer data allow for the determination of the most economic cable geometry.

The analysis of an offshore micro-grid is presented for a general micro-grid topology. The micro-grid is defined as being a potentially autonomous segment of power grid that uses offshore generation to both power an onshore and a potential offshore load. Energy storage techniques are summarized and its applicability for micro-grids is discussed. This offshore micro-grid is modelled using the IEEE 14-bus system where one of the generation units is replaced by offshore generation. The results of this are contrasted with the results of the normal IEEE 14-bus system found in the Appendix.

This thesis provides a methodology of analysis for offshore power system micro-grid design and the results that can be applied and used for modelling of potential offshore power systems. An example case study for a tidal power site in Nova Scotia, Canada, is analyzed to demonstrate the application of the methodology that has been developed.

Future work would include analyzing the effects that energy storage would have on a micro-grid and how to select an energy storage devices energy capacity. This would include analysis on the economics of energy storage devices.

References

[1] “Offshore Wind Energy”, Environmental and Energy Studies Institute, October 2010, [online], Available: http://www.eesi.org/files/offshore_wind_101310.pdf

[2] “London Array”, 4C Offshore, February 24 2015, [online], Available: http://www.4coffshore.com/windfarms/london-array-united-kingdom-uk14.html

[3] Denholm-Hall, R., “World’s second largest offshore wind farm opens off coast of Wales”, Wales Online, June 18 2015, [online], Available: http://www.walesonline.co.uk/business/business-news/worlds-second-largest-offshore-wind-9476670

[4] “UK: Greater Gabbard Offshore Wind Farm Generates Power”, Offshore Wind, September 7 2012, [online], Available: http://www.offshorewind.biz/2012/09/07/uk-greater-gabbard-offshore-wind-farm-generates-power/

[5] “Anholt”, 4C Offshore, October 26, 2015, [online], Available: http://www.4coffshore.com/windfarms/anholt-denmark-dk13.html

[6] “BARD Offshore 1”, 4C Offshore, October 5, 2015, [online], Available: http://www.4coffshore.com/windfarms/bard-offshore-i-germany-de23.html

[7] Odams, R., Benzinger, A., “World’s largest offshore wind farm with 175 Siemens wind turbines inaugurated”, Siemens News Press, 2013, [online], Available: http://www.siemens.co.uk/pool/news_press/news_archive/2013/london-array.jpg

[8] Bray, J.W., Fair, R., Haran, K., “Wind and Ocean Power Generators”, IEEE Transactions on Applied Superconductivity, vol. 24, no. 3, 2013

[9] “The European Offshore Wind Industry – Key Trends and Statistics 2016”, European Wind Energy Association, January 2017, [online], Available: https://windeurope.org/wp-content/uploads/files/about-wind/statistics/WindEurope-Annual-Offshore-Statistics-2016.pdf

[10] “Offshore wind in Europe Walking the tightrope to success”, The European Wind Energy Association, March 2014

[11] Twidell, John, Gaudiosi, Gaetano, “Offshore Wind Power”, Multi-Science Publishing Co. Ltd., UK, ISBN 978-0906522-639

[12] Charlier, R.H., Finkl, C.W., “Ocean Energy Tide and Tidal Power”, Springer, Berlin, 2009

[13] Clark, Robert, H., “Elements of Tidal-Electric Engineering”, IEEE Press, US, 2007

[14] “Industry Vision Paper”, European Ocean Energy, 2013, [online], Available: http://www.oceanenergy-europe.eu/images/Publications/European_Ocean_Energy-Industry_Vision_Paper_2013.pdf

[15] “Tidal giants – the world’s five biggest tidal power plants”, Power Technology, April 11 2014, [online], Available: http://www.power-technology.com/features/featuretidal-giants---the-worlds-five-biggest-tidal-power-plants-4211218/

[16] “Grid-Connected Wave Test Site”, The European Marine Energy Center Ltd., Accessed: October 29, 2015, [online], Available: http://www.emec.org.uk/facilities/wave-test-site/

[17] Odams, R., “Hat trick for SeaGen tidal current turbine”, Siemens News Press, 2012, [online], Available: http://www.siemens.co.uk//en/news_press/index/news_archive/seagen-tidal-currant-turbine-milestone-hat-trick.htm

[18] Barrage de la Rance, June 20 2017, [online], Available: https://upload.wikimedia.org/wikipedia/commons/thumb/e/eb/Barrage_de_la_Rance.jpg/800px-Barrage_de_la_Rance.jpg

[19] Count, B., “Power from Sea Waves”, Academic Press, UK, 1979

[20] Hardisty, Jack, “The Analysis of Tidal Stream Power”, Wiley-Blackwell, UK, 2009

[21] “Hydraulic turbine and electrical generator, cutaway view”, U.S. Army Corps of Engineers, March 4 2012, [online], Available: http://upload.wikimedia.org/wikipedia/commons/thumb/0/09/Water_turbine_(en_2).svg/2000px-Water_turbine_(en_2).svg.png

[22] “Generating Electricity from the Tide”, Murdoch University, [online], Available: http://www.see.murdoch.edu.au/resources/info/Tech/tidal/image007.jpg

[23] “Fundamentals of hydropower. Horizontal Kaplan hydro units”, RusHydro, November 20, 2011, [online], Available: http://blog.rushydro.ru/wp-content/uploads/2011/11/Bulb_Turbine_Cross_Section.jpg

[24] “Outer rim seal a Straflo turbine”, Institute of Hydraulic Fluid Machinery, [online], Available: http://www.hfm.tugraz.at/fileadmin/_migrated/pics/Experimental-investigation-of-the-rim-lip-seal-of-a-double-regulated-STRAFLO-Kaplan-turbine.jpg

[25] “Wind Power”, International Renewable Energy Agency, Renewable Energy Technologies: Cost Analysis Series, Volume 1: Power Sector, Issue 5/5, page 23, [online], Available: http://www.irena.org/DocumentDownloads/Publications/RE_Technologies_Cost_Analysis-WIND_POWER.pdf

[26] Umans, Stephen D., “Fitzgerald & Kingsley’s Electric Machinery”, Seventh Edition, McGraw Hill, New York, NY, 2014

[27] Worzyk, T, “Submarine Power Cables Design, Installation, Repair, Environmental Aspects”, Springer, Heidelberg, Berlin, 2009

[28] “XLPE Submarine Cable Systems Attachment to XLPE Land Cable Systems – User’s Guide”, ABB, 2010

[29] MacNeill, A. M., El-Hawary, M. E., Molloy, S., "Submarine Power Cable Performance Evaluation For Marine Energy Applications", The Journal of Ocean Technology, Volume 8 Number 1, St. Johns, NL, 2013

[30] El-Hawary, M.E, “Electrical Power Systems Design and Analysis”, IEEE Press, New York, NY, 1995

[31] MacNeill, A.M., El-Hawary, M.E., Molloy, S., Ghanashyam, R., “Investigation and Modelling of Cable Performance Characteristics for Marine Energy”, Technical Report Prepared for Natural Resources Canada Marine Energy Technology Group, May 2013

[32] Pieroni, A., Charles, Fellows, W., Bruce, “Life Evaluation of a 35-kV Submarine Power Cable in a Continuous Flexing Environment”, IEEE Journal of Oceanic Engineering, Vol. OE-4 No. 1, 1979

[33] Kirtley Jr., James L., “Class Notes 3: Eddy Currents, Surface Impedances and Loss Mechanisms”, Massachusetts Institute of Technology, September 2005

[34] Sadiku, M.N.O, “Elements of Electromagnetics Fourth Edition”, Oxford University Press, New York, NY, 2007

[35] Hauge, O., Normann, Johnsen, J., Holte, T.A., Bjorlow-Larsen, K., “Performance of The +/-250kV HVDC Skagerrak Submarine Cables. Further Development of the HVDC Paper-Insulated, Mass Impregnated (Solid Type) Submarine Cable”, IEEE Transactions on Power Delivery, 1988

[36] Thue, A., William, “Electrical Power Cable Engineering”, CRC Press, New York, NY, 1998

[37] Westerwell, Th., Price, J., J, "Basslink HVDC Interconnector – System Design Considerations", IEEE AC and DC Power Transmission, 2006

[38] Doyen, H., Eberling, H., Fiss, H. J., Labrenz, M., "Experiences With Different Cable Laying Designs and Laying Methods in Conjunction With the Power Supply of the Islands in the North and Baltic Sea", IEEE Electrical Distribution, 1989

[39] Wolff, C., Elberling, T., "The Kontek HVDC Link between Denmark and Germany", IEEE Power Engineering Society, 2000

[40] Ohman, Marcus C., Sigray, Peter, Wsterberg, Hakan, "Offshore Windmills and the Effects of Electromagnetic Fields on Fish", Royal Swedish Academy of Sciences, 2007

[41] Tricas, Timothy, Gill, Andrew, "Effects of EMFs From Undersea Power Cables On Elasmobranchs and Other Marine Species", Normandeau Associates, Inc., 2011

[42] Schelkunoff, S.A, "The Electromagnetic Theory of Coaxial Transmission Lines and Cylindrical Shields", Bell System Technical Journal, vol. XIII (1934), pp. 532-578

[43] Carson, John R., Gilbert, J.J., "Transmission Characteristics of The Submarine Cable", Bell System Technical Journal, Journal of the Franklin Institute, December 1921

[44] Tranter, C.J, "Bessel Functions With Some Physical Applications", Hart Publishing Company, Inc., New York, NY, 1969

[45] Bianchi, G, Luoni, G, "Induced Currents and Losses In Single-Core Submarine Cables", IEEE Transactions on Power Apparatus and Systems Vol. PAS-95, no. 1, 1976

[46] Ametani, A., "A General Formulation of Impedance and Admittance of Cables", IEEE Transactions on Power Apparatus and Systems, Vol. PAS-99, no.3, 1980

[47] Chien, C.H., Bucknall, R. W. G., "Harmonic Calculations of Proximity Effect on Impedance Characteristics in Subsea Power Transmission Cables", IEEE Transactions on Power Delivery, Vol. 24, No. 4, October 2009

[48] Kane, M., Auriol, P., "Analytical Modelling of Frequency Parameters of Lines", IEE Second Annual Conference on Computation in Electromagnetics, pp. 239-242, May 1994

[49] Ferkal, K., Poloujadoff, M., Dorison, E., "Proximity Effect and Eddy Current Losses in Insulated Cables", IEEE Transactions on Power Delivery, Vol. 11, No. 3, July 1996

[50] Sadiku, M.N.O, "Numerical Techniques in Electromagnetics with MATLAB, Third Edition", Taylor & Francis Group, CRC Press, 2009

[51] McDonald, Kirk T., "An Off-Center "Coaxial" Cable", Joseph Henry Laboratories, Princeton University, 1999

[52] MacNeill, A.M., El-Hawary, M. E., "Underwater Power Cable Approximation Models for Offshore Applications", Oceans 2014

[53] Greenwood, Allan, "Electrical Transients in Power Systems", Wiley-Interscience, United States, 1971

[54] Bickford, J.P., Mullineux, N., Reed, J.R., "Computation of Power System Transients", Peter Peregrinus Ltd., Stevenage, Herts. SG1 1HQ, England, 1976

[55] Hayt, William H. Jr., Kemmerly, Jack E., Durbin, Steven M., "Engineering Circuit Analysis Seventh Edition", Mcgraw Hill, New York, NY, 2007

[56] Arrillaga, J., Bradley, D.A., Bodger, P.S., "Power System Harmonics", Wiley-Interscience, 1985

[57] Chien, C. H., Bucknall, W. G., "Analysis of Harmonics in Subsea Power Transmission Cables Used in VSC-HVDC Transmission Systems Operating Under Steady-State Conditions", IEEE Transactions on Power Delivery, Vol. 22, No. 4, October 2007

[58] Chien, C. H., Bucknall, R. W. G., "Theoretical aspects of the harmonics performance of subsea AC transmission systems for offshore power generation schemes", IEE Proceedings – Generation, Transmission and Distribution, Vol. 153, Issue 5, 2006

[59] Hart, Daniel W., "Power Electronics", McGraw Hill, New York, NY, 2011

[60] Acha, E., Agelidis V. G., Anaya-Lara, O., Miller, T. J. E., "Power Electronics Control in Electrical Systems", Newnes, 2002

[61] "High Voltage Direct Current Transmission – Proven Technology for Power Exchange", Siemens, Siemens AG Energy Sector, 2011

[62] "ABB awarded $400 million order for Maritime Link power project in Canada", ABB, July 9 2014, [online], Available: http://www.abb.ca/cawp/seitp202/d0f4803b261ba8a9c1257d0f0078eb1e.aspx?_ga=1.189912043.1599510773.1473958651

[63] "Maritime Link Connecting remote generation and interconnecting grids", ABB, [online], Available: https://library.e.abb.com/public/f523db335c701667c1257dcf00509242/POW0097%20Rev%201.pdf

[64] Adam, Grain Philip, Williams, Barry W., "Multi-pole voltage source converter HVDC transmission systems", IET Journals & Magazines, IET Generation, Transmission & Distribution, Vol. 10 Issue 2, 2016

[65] IEEE Std 519-2014, "IEEE Recommended Practices and Requirements for Harmonic Control in Electric Power Systems", IEEE, 1993

[66] "ABB wins $900 million order to connect Norwegian and German power grids", ABB, [online], Available: http://www.abb.com/cawp/seitp202/8893afcd95434d02c1257e0d003af5a4.aspx

[67] "Offshore wind energy: TenneT awards "DolWin3" project to Alstom, marking next step in Germany's energy turnaround", Alstom, [online], Available: http://www.alstom.com/press-centre/2013/2/offshore-wind-energy-tennet-awards-dolwin3project-to-alstom-marking-next-step-in-germanys-energy-turnaround/

[68] "ABB positions world's most powerful offshore converter platform in the North Sea", ABB, [online], Available: http://new.abb.com/systems/hvdc/references/dolwin2

[69] "Western HVDC Link", Prysmian, [online], Available: http://www.prysmiangroup.com/en/corporate/about/special_projects/western-HVDC-link/

[70] "South West Link Balancing the power supply between central and southern Sweden with HVDC", Alstom, [online], Available: http://www.gegridsolutions.com/alstomenergy/grid/Global/OneAlstomPlus/Grid/PDF/Supergrid/SouthWest%20link%20HVDC%20project-epslanguage=en-GB.pdf

[71] Dicorato, M., Forte, G., Pisani, M., Trovato, M., "Guidelines for assessment of investment cost for offshore wind generation", Elsevier, Renewable Energy 36, 2011, pp. 2043-2051

[72] Lundberg, Stefan, "Performance comparison of wind park configurations", Chalmers University of Technology, Göteborg Sweden, 2003

[73] De Prada, Mikel, Corchero, Cristina, Gomis-Bellmunt, Oriol, Sumper, Andreas, "Hybrid AC-DC Offshore Wind Power Plant Topology: Optimal Design", IEEE Transactions on Power Systems, Vol. 30 No. 4, July 2015

[74] "Utility rate comparisons", Manitoba Hydro, May 1 2016, [online], Available: https://www.hydro.mb.ca/regulatory_affairs/energy_rates/electricity/utility_rate_comp.shtml

[75] "Electricity Rates by Province", Ontario Hydro, 2013, [online], Available: http://www.ontario-hydro.com/index.php?page=electricity_rates_by_province

[76] "Electricity Power Monthly", U.S Energy Information Administration, June 2016, [online], Available: http://www.eia.gov/electricity/monthly/epm_table_grapher.cfm?t=epmt_5_6_a

[77] "Half-yearly electricity and gas prices, second half of year, 2012-2014 (EUR per kWh)", Eurostat, [online], Available: http://ec.europa.eu/eurostat/statistics-explained/index.php/File:Half-yearly_electricity_and_gas_prices,_second_half_of_year,_2012%E2%80%9314_(EUR_per_kWh)_YB15.png

[78] Debs, Atif S., "Modern Power Systems Control and Operation", Springer US, 1988

[79] Angeles-Camacho, C., Tortelli, O.L., Acha, E., Fuerte-Esquivel, C.R., "Inclusion of a high voltage DC-voltage source converter model in a Newton-Raphson power flow algorithm", IEE Proceedings – Generation, Transmission and Distribution, Vol. 150, Iss. 6, Nov. 2003

[80] Pai, M., A., "Computer Techniques in Power System Analysis", Second Edition, McGraw Hill, 1979

[81] Milano, F., "Power System Modelling and Scripting", Springer, London, 2010

[82] Khan, J., Leon, D., Moshref, A., Arabi, S., Bhuyan, G., "Network Security Assessments for Integrating Large-Scale Tidal Current and Ocean Wave Resources Into Future Electrical Grids", Proceedings of the IEEE, Vol. 101, No. 4, April 2013

[83] Erlich, I., Shewarega, F., Feltes, C., Koch, F., Fortmann, J., "Offshore Wind Power Generation Technologies", Proceedings of the IEEE, Vol. 101, No.4, April 2013

[84] Chen, S.X., Gooi, H.B., Wang, M.Q., "Sizing of Energy Storage for Microgrids", IEEE Transactions on Smart Grid, Vol. 3, No. 1, March 2012

[85] Ter-Gazarian, A., "Energy Storage for Power Systems", Second Edition, IET Power and Energy Series Vol. 63, Herfordshire, U.K, 2011

[86] Luo, X., Wang, J., Dooner, M., Clarke, J., "Overview of current development in electrical energy storage technologies and the application potential in power system operation", Elsevier Applied Energy, Volume 137, p.p 511-536, 2015

[87] Aneke, M., Wang, M., "Energy storage technologies and real life applications – A state of the art review", Elsevier Applied Energy, Volume 179, p.p 360-377, October 2016

[88] Karsten, R., "Tidal Energy Resource Assessment Map for Nova Scotia", Report to OEER/OETR, Acadia Tidal Energy Institute, Acadia University, November 9th 2012

[89] Google Maps, (2017), Grand Passage Nova Scotia, [online], Available: https://www.google.ca/maps/@44.2440711,-66.2602413,11.91z

Appendix A: Power System Model

This chapter provides an overview of power system analysis and methods to analyze the fusion of offshore generation with an onshore power grid. Evaluation of the voltage and phase for each bus in a power system, given a generation set point, provides important information about the power system. Using the power flow equations and appropriate models for components, this analysis can be performed.

A.1 Introduction

The power flow formulation of a power system is a very important analysis tool. It provides a steady state evaluation of the system. For this formulation its assumed that lumped circuit elements can be used to represent the various components of the power system. These components would include transmission lines, transformers, and power converters. Due to the unique properties of offshore power cables, an expanded transmission line model may be required to be used in modelling the offshore system. There exist several standards of power system that can be used as a model for analysis; these are the IEEE bus systems. Using the IEEE 14 bus system, a power flow solution for an onshore power system could be used to contrast the power flow solution when generation is offshore.

A.2 Power flow

The power flow is a method that takes known power system information (voltage, phase, power, reactive power) and the known topology of the network, and solves for the

unknowns in the system [30,78]. The known parameters are defined based upon the bus designations in the power system. A bus is said to be one of the following [30,78]:

- Generator Bus, the voltage and real power are defined
- Load Bus, the real and reactive power requirements are defined
- Slack Bus, the voltage and phase are defined

The power flow generates two equations for every bus in the power system. The equations are based off of the principle that the power incoming to the bus equals the power outgoing. This applies for the real and reactive power. To generalize this concept, two interconnected busses can be analyzed, and the power flow equations developed. Figure A-1 below is a diagram of a two-bus system [78].

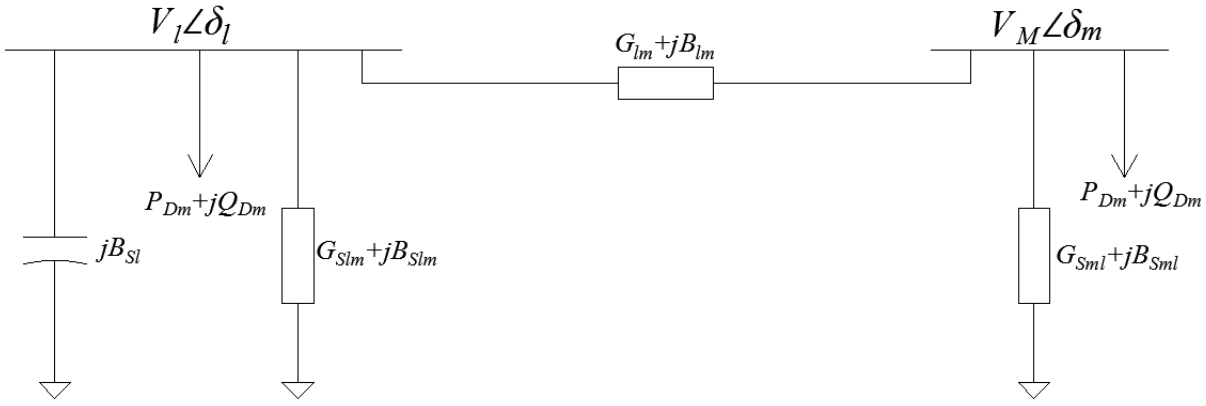

Figure A-1: Two-Bus System

This represents a generalized two-bus connection, where a transmission line, pi model, connects the two busses in this case. Also on bus *l* there is a shunt capacitor, which further

generalizes the model. The general power flow equations can be found to be as follows [78]:

$$P_l = V_l{}^2[\sum(G_{slm} + G_{lm})] - V_l \sum V_m[G_{lm}\cos(\delta_l - \delta_m) + B_{lm}\sin(\delta_l - \delta_m)] \quad \text{(A.1)}$$

$$Q_l = -V_l{}^2[B_{sl} + \sum(B_{slm} + B_{lm})] - V_l \sum V_m[G_{lm}\sin(\delta_l - \delta_m) - B_{lm}\cos(\delta_l - \delta_m)] \quad \text{(A.2)}$$

For any bus in the power system, equations for P_l and Q_l can be written. These equations correspond to the power and reactive power injected to a bus. For generation busses, it is equal to the power injected to the bus from the generator [78]. For load busses, it is equal to the negative of the load [78]. For the slack bus, it is undefined [78]. For intermediate busses the net power and reactive power is zero. It should be noted also that if intermediate busses do exist, busses that are neither load nor generator busses, they can be absorbed by other busses in the system. The system of equations that is generated from the power flow is non linear and requires an iterative solution. There are many methods to iterate a solution. The newton-raphson, fast-decoupled, and the gauss-seidel methods are examples of iteration techniques [30,78]. The general equation that represents the newton-raphson iteration method is shown below [78]:

$$x^{(k+1)} = x^{(k)} + J(x^{(k)})^{-1} \cdot (y - f(x^{(k)})) \quad \text{(A.3)}$$

Where, *x* represents the variables that are required to be solved, *y* represents the constant that the functions being iterated equals, *f(x)* represents the functions evaluated at the current set of iteration values, and *J(x)* represents the Jacobian matrix evaluated at the current set of iteration values. The Jacobian matrix is defined as follows:

$$J = \begin{matrix} \frac{\partial f_1}{\partial x_1} & \cdots & \frac{\partial f_1}{\partial x_n} \\ \vdots & \ddots & \vdots \\ \frac{\partial f_m}{\partial x_1} & \cdots & \frac{\partial f_m}{\partial x_n} \end{matrix} \quad \text{(A.4)}$$

Applying this solution technique, a solution to the power flow equations can be obtained. Depending on the size of the power system, an appropriate iteration method can be applied. The fast-decoupled method provides a faster solution. This is due to assumptions made regarding the effect of voltage or phase angle on the power and reactive power. These assumptions fill the Jacobian matrix with zeros, which makes the matrix inversion faster to compute. This is typically used in larger power system analysis. For the purpose of analysis of the IEEE 14 bus system, the newton-raphson method will prove to be sufficiently capable of solving the system variables.

A.3 Power System Components

In a power system there exist several components that require lumped component modelling such that they can be included into the power flow model. There are four components, transformers, transmission lines, underwater transmission lines, and power converters. These components will be discussed in the subsequent sections.

A.3.1 Transformer Model

To further complete the power flow analysis, a model of a transformer can be developed. This model is necessary to be used with the power flow method described in the previous section. In the current AC power system, transformers are very commonly used. Figure A-2 below shows the equivalent model for a transformer [78].

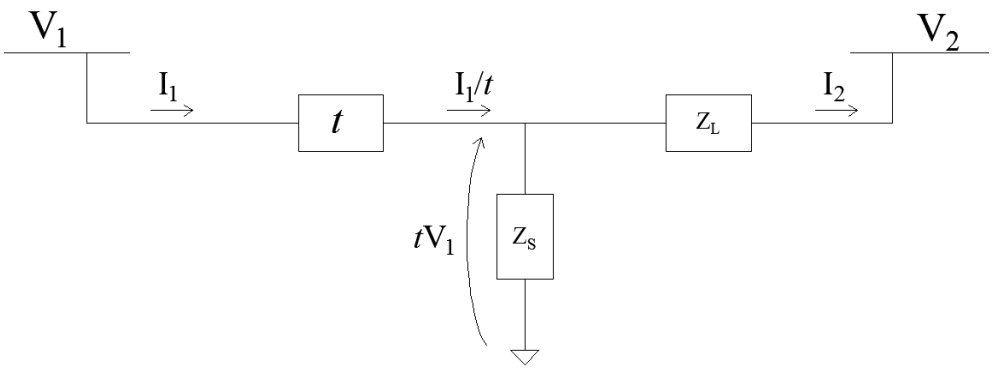

Figure A-2: Transformer Model

Where, t represents the ideal turns ratio, Z_L and Z_S are the in-line and shunt impedances respectively. The relationship between the voltage and current on bus 1 and bus 2 can be found to be as follows [78]:

$$\begin{bmatrix} I_1 \\ I_2 \end{bmatrix} = \begin{bmatrix} t^2(Y_L + Y_S) & -tY_L \\ tY_L & -Y_L \end{bmatrix} \begin{bmatrix} V_1 \\ V_2 \end{bmatrix} \tag{A.5}$$

The model for a transformer can next be represented as a pi equivalent circuit between bus 1 and bus 2. Figure A-3 below shows what this equivalent circuit for the transformer will be.

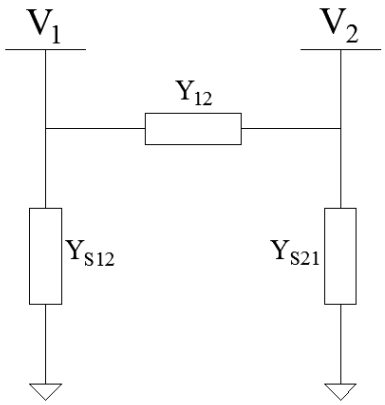

Figure A-3: Transformer Equivalent Circuit

The equivalent circuit in Figure A-3 has the following relationship between the current and voltage on bus 1 and 2 [78]:

$$\begin{bmatrix} I_1 \\ I_2 \end{bmatrix} = \begin{bmatrix} Y_{12} + Y_{s12} & -Y_{12} \\ Y_{12} & -(Y_{12} + Y_{s21}) \end{bmatrix} \begin{bmatrix} V_1 \\ V_2 \end{bmatrix} \tag{A.6}$$

It can then be concluded that the impedance components of the transformer can be transformed into the impedance components in Figure A-3 through the following relationships [78]:

$$Y_{12} = tY_L \tag{A.7}$$

$$Y_{s12} = t(t-1)Y_L + t^2 Y_S \tag{A.8}$$

$$Y_{s21} = (1-t)Y_L \tag{A.9}$$

This equivalent model can be used to represent a transformer. This can further be applied to easily help solve the power flow equations when transformers are present in the power system. It should be noted that this model only characterizes non-phase shifting transformers. An equivalent circuit, as seen previously, cannot be used to model phase shifting transformers.

A.3.2 Overhead Transmission Line Model

There are three transmission line models that can be used to model an overhead transmission line. These models are as follows:

- The short line approximation
- The medium line approximation (nominal pi)
- The exact pi model

As discussed in Chapter 3, transmission lines are accurately represented by distributed components. This cannot be easily analyzed using the power flow equations since this would imply that an infinite number of busses, thus an infinite number of equations be solved. A simplified lumped component model of the transmission line must be used.

A.3.2.1 Short Line Approximation

The series impedance of the transmission line represents the short line approximation. The capacitance and conductance are assumed negligible. This approximation is valid for transmission line lengths up to 80km [30]. Figure A-4 below shows what the lumped component model for this transmission line would be.

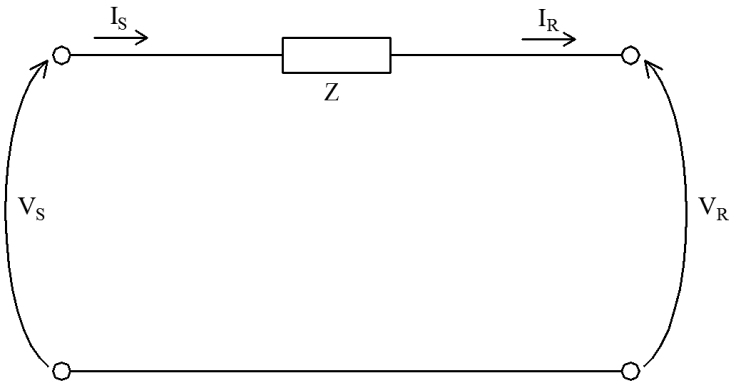

Figure A-4: Short Line

This model has the following two-port network equations:

$$\begin{bmatrix} V_s \\ I_s \end{bmatrix} = \begin{bmatrix} 1 & Z \\ 0 & 1 \end{bmatrix} \begin{bmatrix} V_R \\ I_R \end{bmatrix} \tag{A.10}$$

This corresponds to *A=D=1, C=0, B=Z* as the ABCD parameters for this lumped component transmission line model.

A.3.2.2 Medium Line Approximation

The medium line approximation model of a transmission line is a nominal pi topology. The series impedance has half of the admittance at the input and output. This model is valid for transmission line lengths of up to 250km [30]. Figure A-5 below shows the topology for this nominal pi transmission line model.

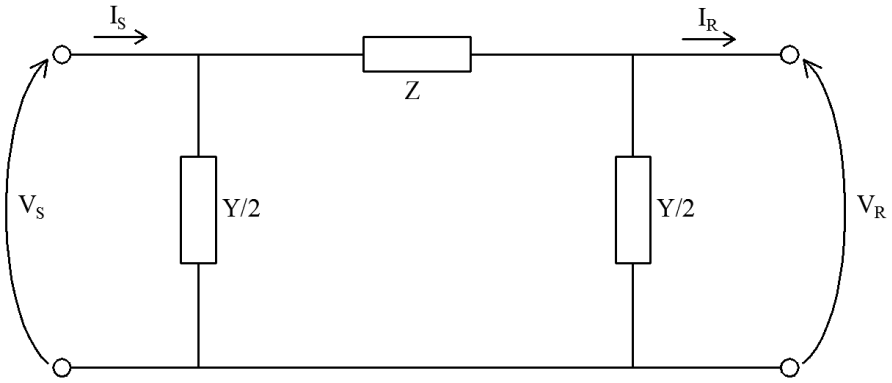

Figure A-5: Medium Line

This model has the same two-port network equations as was found in Chapter 3.

$$\begin{bmatrix} V_s \\ I_s \end{bmatrix} = \begin{bmatrix} 1 + \frac{ZY}{2} & Z \\ Y + \frac{ZY^2}{4} & 1 + \frac{ZY}{2} \end{bmatrix} \begin{bmatrix} V_R \\ I_R \end{bmatrix} \tag{A.11}$$

This is the transmission line model that has been assumed in the power flow model of Figure A-1. Note that if *Y=0*, that (A.11) becomes (A.10).

A.3.2.3 Exact Pi Model

The exact pi model is similar to the nominal pi in terms of the topology. The difference between the two models is that the impedance and admittance values are abstracted and

depend on the actual ABCD parameters, using distributed components, which are discussed in Chapter 3. Figure A-6 below shows the topology for this model.

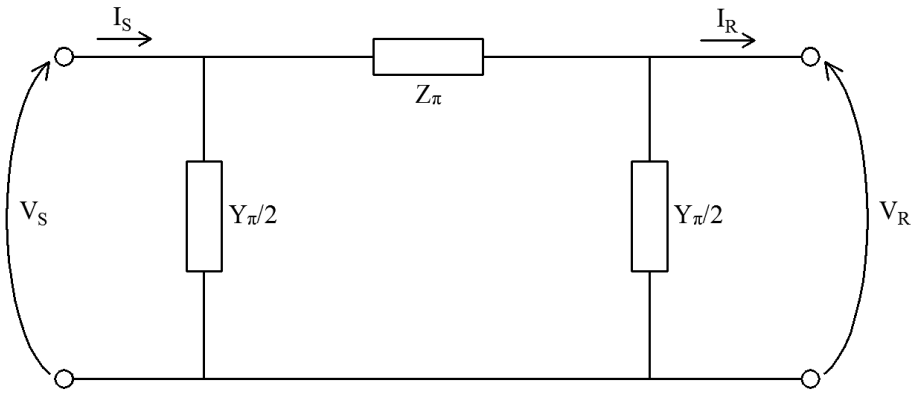

Figure A-6: Exact Pi Model

The equations for this can be determined by making the following relations:

$$A = D = 1 + \frac{Z_\pi Y_\pi}{2} \tag{A.12}$$

$$B = Z_\pi \tag{A.13}$$

$$C = Y_\pi \left(1 + \frac{Z_\pi Y_\pi}{4}\right) \tag{A.14}$$

From equation (A.13) and (A.12) it can be seen that:

$$Y_\pi = \frac{2(A-1)}{B} \tag{A.15}$$

This model of the transmission line is abstracted, however, provides accurate modelling of a longer transmission line lengths.

A.3.3 Underwater Transmission Line Model

Due to the large capacitance associated with underwater power cables, different models are required to be used [52]. Chapter 3 discusses this in detail, the results of which will be reiterated. A nominal pi model as in Figure A-5 above can represent an underwater power

cable if the line lengths do not exceed 10 km [52]. If the transmission line length is greater than 10 km but less than 40 km, then two cascaded nominal pi models are required to model the transmission line [52]. This can be generalized as can be seen in Figure A-7 below.

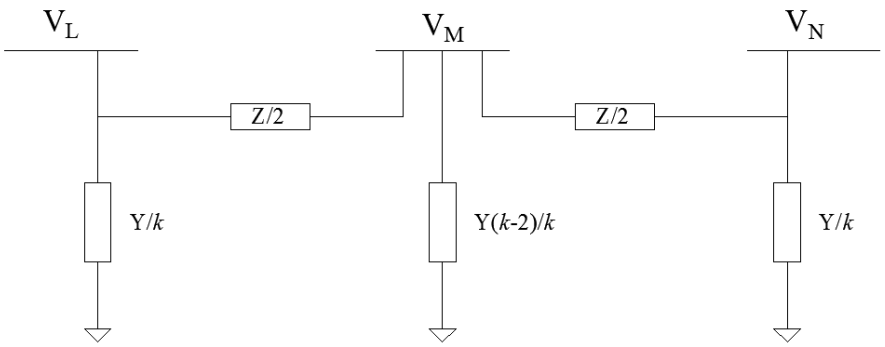

Figure A-7: Underwater Transmission Line General Model

Note that in Figure A-7, if $k=2$, the model reduces to the nominal pi. To use the model in Figure A-7 in the power flow equations, an artificial bus can be inserted midway through the transmission line. The power flow formulation previously discussed assumed that a pi topology was used for the transmission line. This additional bus allows for easy analysis of the underwater transmission lines using the already existing power flow formulation. If transmission lines of length longer than 40 km are used, then multiple artificial busses and more nominal pi models can be used to model the transmission line [52].

A.3.4 Power Converter Model for AC Power Flow Evaluation

A DC power link can be modelled in the AC power flow formulation. The model for this assumes that voltage source converters are being implemented. This model makes the following assumptions regarding the power converters [79].

- The transmission losses and converter losses can be lumped into a single real power loss.
- The fundamental frequency, 60Hz, is the frequency being output of the inverter system. This in reality would not be the case. In reality there would be the super position of odd order harmonics injected into the system. This would require multiple power flow solutions be formulated for each of the harmonics injected into the system by the power converter.
- There are transformers or reactors connected before the rectifier stage and after the inverter stage.

The equivalent network of a DC transmission link, which can be implemented in a classical power flow formulation, can be observed in Figure A-8 below [79].

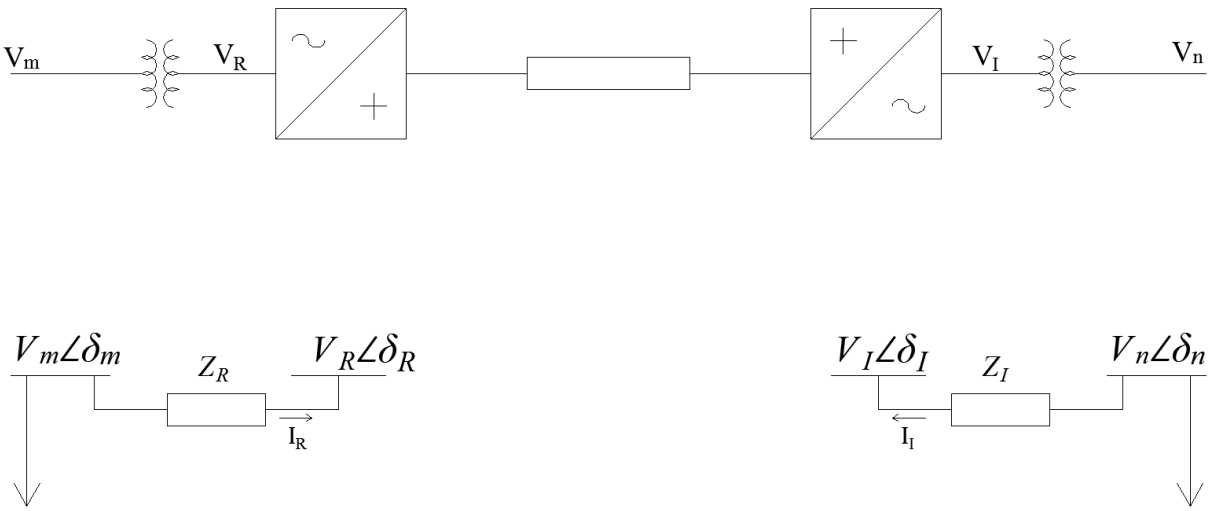

Figure A-8: Power Converter Model

From Figure A-8 the power flow formulation can be written for each of the busses as follows [79]:

$$P_m = |V_m|^2 G_R - |V_m||V_R|(G_R \cos[\delta_m - \delta_R] + B_R \sin[\delta_m - \delta_R]) \quad \text{(A.16)}$$

$$Q_m = -|V_m|^2 B_R - |V_m||V_R|(G_R \sin[\delta_m - \delta_R] + B_R \cos[\delta_m - \delta_R]) \quad \text{(A.17)}$$

$$P_R = |V_R|^2 G_R - |V_m||V_R|(G_R \cos[\delta_R - \delta_m] + B_R \sin[\delta_R - \delta_m]) \quad \text{(A.18)}$$

$$Q_R = -|V_R|^2 B_R - |V_m||V_R|(G_R \sin[\delta_R - \delta_m] + B_R \cos[\delta_R - \delta_m]) \quad \text{(A.19)}$$

$$P_n = |V_n|^2 G_I - |V_I||V_n|(G_I \cos[\delta_n - \delta_I] + B_I \sin[\delta_n - \delta_I]) \quad \text{(A.20)}$$

$$Q_n = -|V_n|^2 B_I - |V_I||V_n|(G_I \sin[\delta_n - \delta_I] + B_I \cos[\delta_n - \delta_I]) \quad \text{(A.21)}$$

$$P_I = |V_I|^2 G_I - |V_I||V_n|(G_I \cos[\delta_I - \delta_n] + B_I \sin[\delta_I - \delta_n]) \quad \text{(A.22)}$$

$$Q_I = -|V_I|^2 B_I - |V_I||V_n|(G_I \sin[\delta_I - \delta_n] + B_I \cos[\delta_I - \delta_n]) \quad \text{(A.23)}$$

There is one additional constraint that must be applied. This constraint is given as follows [79]:

$$RE\{V_R {I_R}^* + V_I {I_I}^* + P_{DC}\} = 0 \quad \text{(A.24)}$$

What this equation implies is that the real power injected into the rectifier equals the output power of the inverter in addition to the power losses of transmission. From this system of equations, a solution can be iterated. This methodology can allow the inclusion of a DC transmission link into the AC power flow formulation.

A.4 IEEE 14 Bus System

A power system that could be used as a modelling tool to see the effects of an offshore power system would be an IEEE Bus System.

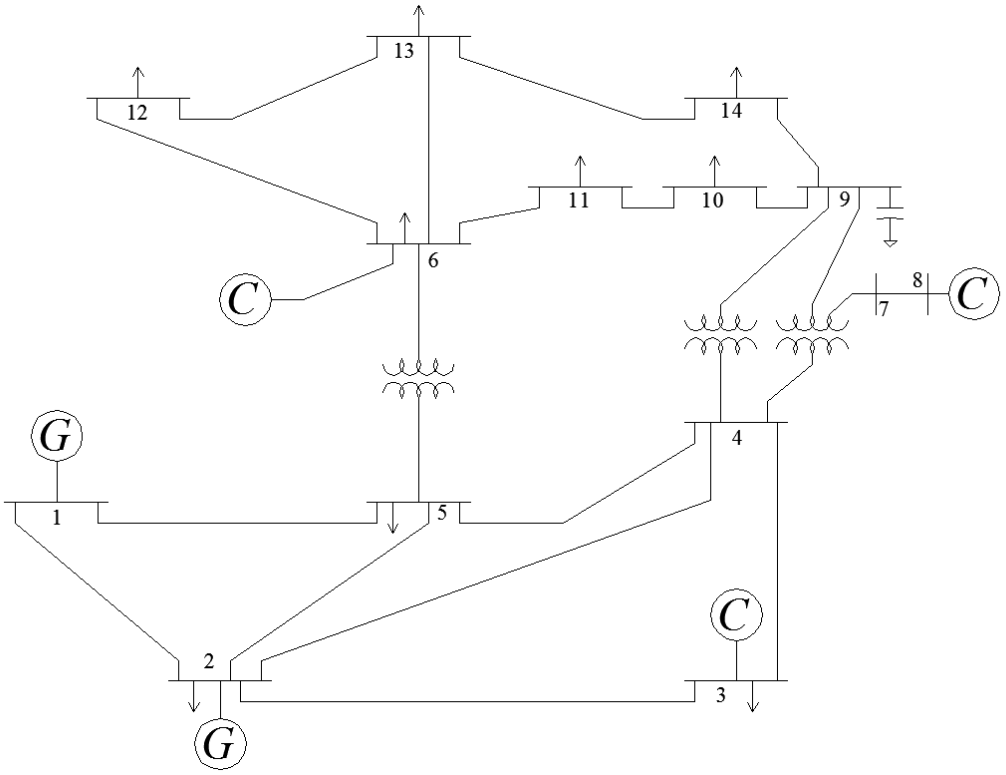

Figure A-9: IEEE 14 Bus System

This model can be used to simulate the effects of having one of the conventional generators replaced by offshore power cables and offshore wind or tidal generators. Power flow analysis of the power system would allow the study of the deviation of system voltage and phase angles, provided that the same power generation is supplied by the offshore power system.

A.4.1 Bus Specifications

For this IEEE 14 bus system, the generation bus voltages and real power must be defined and the load bus real and reactive power requirements must be defined. Table A-1 below provide these specifications:

Table A-1: Bus Specifications [80,81]

Bus	Bus Type	|V|	P_{GEN}	Q_{GEN}	P_{LOAD}	Q_{LOAD}	$Q_{GEN\ MAX}$	$Q_{GEN\ MIN}$
1	Slack	1.06	2.32	-0.1601	0	0	10	-10
2	Gen	1.045	0.4	-0.4541	0.217	0.127	0.5	-0.4
3	Gen	1.01	0	0.2528	0.942	0.19	0.4	0
4	Load	-	0	0	0.478	-0.039	0	0
5	Load	-	0	0	0.076	0.016	0	0
6	Gen	1.07	0	0.1362	0.112	0.075	0.24	-0.06
7	Load	-	0	0	0	0	0	0
8	Gen	1.09	0	0.1824	0	0	0.24	-0.06
9	Load	-	0	0	0.295	0.166	0	0
10	Load	-	0	0	0.09	0.058	0	0
11	Load	-	0	0	0.035	0.018	0	0
12	Load	-	0	0	0.061	0.016	0	0
13	Load	-	0	0	0.135	0.058	0	0
14	Load	-	0	0	0.149	0.05	0	0

From this bus specification it should also be noted that the values in per-unit. The bases for these per-unit values are as follows [80,81]:

- The power base is 100MVA
- The voltage base is 69kV for busses 1-5, 13.8kV for busses 6, 7, 9-14, and 18kV for bus 8

The per-unit system normalizes the numbers such that convenient small numbers can be used to describe voltages and powers.

A.4.2 Impedance Specifications

In addition to the bus information, the impedances of the transmission lines connecting all of the busses in the IEEE 14 bus system must also be defined. Table A-2 below show these impedances as well as the transformer turns ratios.

Table A-2: Impedance Specifications [80,81]

From	To	Resistance (p.u)	Reactance (p.u)	Susceptance (p.u)	Tap Ratio (t_{ij})
1	2	0.01938	0.05917	0.0528	1
1	5	0.05403	0.22304	0.0492	1
2	3	0.04699	0.19797	0.0438	1
2	4	0.05811	0.17632	0.0374	1
2	5	0.05695	0.17388	0.034	1
3	4	0.06701	0.17103	0.0346	1
4	5	0.01335	0.04211	0.0128	1
4	7	0	0.20912	0	0.978
4	9	0	0.55618	0	0.969
5	6	0	0.25202	0	0.932
6	11	0.09498	0.1989	0	1
6	12	0.12291	0.25581	0	1
6	13	0.06615	0.13027	0	1
7	8	0	0.17615	0	1

7	9	0	0.11001	0	1
9	10	0.03181	0.0845	0	1
9	14	0.12711	0.27038	0	1
10	11	0.08205	0.19207	0	1
12	13	0.22092	0.19988	0	1
13	14	0.17093	0.34802	0	1

In addition to this, there is a shunt capacitor connected to bus number 9 in Figure A-9. This shunt capacitor has an admittance of 0.19 per-unit.

The base impedance can be calculated from the voltage and power base values defined in the previous section. The impedance base is equal to the following:

$$Z_{base} = \frac{{V_{base}}^2}{S_{base}} \tag{A.25}$$

It is assumed that the admittance values defined in Table A-2 correspond to each of the shunt components of a pi model transmission line. It is also assumed that the shunt conductance for all transmission lines is negligible.

A.5 IEEE 14 Bus System Model

To generate the power flow equations, the matrices defining what the impedances of the system are must be created. In accordance with the notation used in Figure A-1 for the power flow formulation, and the data in Table A-2, the following impedance matrices can be created:

$G_{lm}[p.u]$

$$=\begin{matrix}
6.017 & -4.99913 & 0 & 0 & -1.0259 & 0 & 0 & 0 & 0 & 0 & 0 & 0 & 0 & 0 \\
-4.99913 & 9.521 & -1.135 & -1.686 & -1.7011 & 0 & 0 & 0 & 0 & 0 & 0 & 0 & 0 & 0 \\
0 & -1.135 & 3.121 & -1.986 & 0 & 0 & 0 & 0 & 0 & 0 & 0 & 0 & 0 & 0 \\
0 & -1.686 & -1.986 & 10.513 & -6.841 & 0 & 0 & 0 & 0 & 0 & 0 & 0 & 0 & 0 \\
-1.0259 & -1.7011 & 0 & -6.841 & 9.568 & 0 & 0 & 0 & 0 & 0 & 0 & 0 & 0 & 0 \\
0 & 0 & 0 & 0 & 0 & 6.58 & 0 & 0 & 0 & 0 & -1.955 & -1.526 & -3.099 & 0 \\
0 & 0 & 0 & 0 & 0 & 0 & 0 & 0 & 0 & 0 & 0 & 0 & 0 & 0 \\
0 & 0 & 0 & 0 & 0 & 0 & 0 & 0 & 0 & 0 & 0 & 0 & 0 & 0 \\
0 & 0 & 0 & 0 & 0 & 0 & 0 & 0 & 5.326 & -3.902 & 0 & 0 & 0 & -1.424 \\
0 & 0 & 0 & 0 & 0 & 0 & 0 & 0 & -3.902 & 5.783 & -1.881 & 0 & 0 & 0 \\
0 & 0 & 0 & 0 & 0 & -1.955 & 0 & 0 & 0 & -1.881 & 3.836 & 0 & 0 & 0 \\
0 & 0 & 0 & 0 & 0 & -1.526 & 0 & 0 & 0 & 0 & 0 & 4.015 & -2.489 & 0 \\
0 & 0 & 0 & 0 & 0 & -3.099 & 0 & 0 & 0 & 0 & 0 & -2.489 & 5.588 & -1.137 \\
0 & 0 & 0 & 0 & 0 & 0 & 0 & 0 & -1.424 & 0 & 0 & 0 & -1.137 & 2.561
\end{matrix}$$

$B_{lm}[p.u]$

$$=\begin{matrix}
-19.498 & 15.263 & 0 & 0 & 4.235 & 0 & 0 & 0 & 0 & 0 & 0 & 0 & 0 & 0 \\
15.263 & -30.355 & 4.782 & 5.116 & 5.194 & 0 & 0 & 0 & 0 & 0 & 0 & 0 & 0 & 0 \\
0 & 4.782 & -9.85 & 5.0688 & 0 & 0 & 0 & 0 & 0 & 0 & 0 & 0 & 0 & 0 \\
0 & 5.116 & 5.0688 & x_4 & 21.58 & 0 & x_2 & 0 & x_3 & 0 & 0 & 0 & 0 & 0 \\
4.235 & 5.194 & 0 & 21.58 & x_5 & x_1 & 0 & 0 & 0 & 0 & 0 & 0 & 0 & 0 \\
0 & 0 & 0 & 0 & x_1 & x_6 & 0 & 0 & 0 & 0 & 4.094 & 3.176 & 6.103 & 0 \\
0 & 0 & 0 & x_2 & 0 & 0 & x_7 & 5.677 & 9.09 & 0 & 0 & 0 & 0 & 0 \\
0 & 0 & 0 & 0 & 0 & 0 & 5.677 & -5.677 & 0 & 0 & 0 & 0 & 0 & 0 \\
0 & 0 & 0 & x_3 & 0 & 0 & 9.09 & 0 & x_8 & 10.365 & 0 & 0 & 0 & 3.029 \\
0 & 0 & 0 & 0 & 0 & 0 & 0 & 0 & 10.365 & -14.768 & 4.403 & 0 & 0 & 0 \\
0 & 0 & 0 & 0 & 0 & 4.094 & 0 & 0 & 0 & 4.403 & -8.497 & 0 & 0 & 0 \\
0 & 0 & 0 & 0 & 0 & 3.176 & 0 & 0 & 0 & 0 & 0 & -5.428 & 2.252 & 0 \\
0 & 0 & 0 & 0 & 0 & 6.103 & 0 & 0 & 0 & 0 & 0 & 2.252 & -10.67 & 2.315 \\
0 & 0 & 0 & 0 & 0 & 0 & 0 & 0 & 3.029 & 0 & 0 & 0 & 2.315 & -5.344
\end{matrix}$$

$$B_{slm}[p.u] = \begin{matrix}
0.102 & 0 & 0 & 0 & 0 & 0 & 0 & 0 & 0 & 0 & 0 & 0 & 0 & 0 \\
0 & 0.168 & 0 & 0 & 0 & 0 & 0 & 0 & 0 & 0 & 0 & 0 & 0 & 0 \\
0 & 0 & 0.0784 & 0 & 0 & 0 & 0 & 0 & 0 & 0 & 0 & 0 & 0 & 0 \\
0 & 0 & 0 & x_9 & 0 & 0 & 0 & 0 & 0 & 0 & 0 & 0 & 0 & 0 \\
0 & 0 & 0 & 0 & x_{10} & 0 & 0 & 0 & 0 & 0 & 0 & 0 & 0 & 0 \\
0 & 0 & 0 & 0 & 0 & x_{11} & 0 & 0 & 0 & 0 & 0 & 0 & 0 & 0 \\
0 & 0 & 0 & 0 & 0 & 0 & x_{12} & 0 & 0 & 0 & 0 & 0 & 0 & 0 \\
0 & 0 & 0 & 0 & 0 & 0 & 0 & 0 & 0 & 0 & 0 & 0 & 0 & 0 \\
0 & 0 & 0 & 0 & 0 & 0 & 0 & 0 & x_{13} & 0 & 0 & 0 & 0 & 0 \\
0 & 0 & 0 & 0 & 0 & 0 & 0 & 0 & 0 & 0 & 0 & 0 & 0 & 0 \\
0 & 0 & 0 & 0 & 0 & 0 & 0 & 0 & 0 & 0 & 0 & 0 & 0 & 0 \\
0 & 0 & 0 & 0 & 0 & 0 & 0 & 0 & 0 & 0 & 0 & 0 & 0 & 0 \\
0 & 0 & 0 & 0 & 0 & 0 & 0 & 0 & 0 & 0 & 0 & 0 & 0 & 0 \\
0 & 0 & 0 & 0 & 0 & 0 & 0 & 0 & 0 & 0 & 0 & 0 & 0 & 0
\end{matrix}$$

$$B_{sl}[p.u] = \begin{bmatrix} 0 & 0 & 0 & 0 & 0 & 0 & 0 & 0 & 0 & 0 & 0 & 0 & 0 & 0 \\ 0 & 0 & 0 & 0 & 0 & 0 & 0 & 0 & 0 & 0 & 0 & 0 & 0 & 0 \\ 0 & 0 & 0 & 0 & 0 & 0 & 0 & 0 & 0 & 0 & 0 & 0 & 0 & 0 \\ 0 & 0 & 0 & 0 & 0 & 0 & 0 & 0 & 0 & 0 & 0 & 0 & 0 & 0 \\ 0 & 0 & 0 & 0 & 0 & 0 & 0 & 0 & 0 & 0 & 0 & 0 & 0 & 0 \\ 0 & 0 & 0 & 0 & 0 & 0 & 0 & 0 & 0 & 0 & 0 & 0 & 0 & 0 \\ 0 & 0 & 0 & 0 & 0 & 0 & 0 & 0 & 0 & 0 & 0 & 0 & 0 & 0 \\ 0 & 0 & 0 & 0 & 0 & 0 & 0 & 0 & 0 & 0 & 0 & 0 & 0 & 0 \\ 0 & 0 & 0 & 0 & 0 & 0 & 0 & 0 & 0.19 & 0 & 0 & 0 & 0 & 0 \\ 0 & 0 & 0 & 0 & 0 & 0 & 0 & 0 & 0 & 0 & 0 & 0 & 0 & 0 \\ 0 & 0 & 0 & 0 & 0 & 0 & 0 & 0 & 0 & 0 & 0 & 0 & 0 & 0 \\ 0 & 0 & 0 & 0 & 0 & 0 & 0 & 0 & 0 & 0 & 0 & 0 & 0 & 0 \\ 0 & 0 & 0 & 0 & 0 & 0 & 0 & 0 & 0 & 0 & 0 & 0 & 0 & 0 \\ 0 & 0 & 0 & 0 & 0 & 0 & 0 & 0 & 0 & 0 & 0 & 0 & 0 & 0 \end{bmatrix}$$

Within these matrices are variables. These variables are defined in Table A-3 below. They account for the sum of shunt impedance components as well as the transformer additional impedance.

Table A-3: Matrix Variables

Name in Matrices	Value for Matrices
$\mathbf{x_1}$	$3.968 \cdot t_{56}$
$\mathbf{x_2}$	$4.782 \cdot t_{47}$
$\mathbf{x_3}$	$1.789 \cdot t_{49}$
$\mathbf{x_4}$	$-31.7546 - 4.782 \cdot t_{47} - 1.798 \cdot t_{49}$
$\mathbf{x_5}$	$-31.009 - 3.968 \cdot t_{56}$
$\mathbf{x_6}$	$-13.372 - 3.968 \cdot t_{56}$
$\mathbf{x_7}$	$-14.767 - 4.782 \cdot t_{47}$
$\mathbf{x_8}$	$-22.484 - 1.798 \cdot t_{49}$
$\mathbf{x_9}$	$0.0848 - (t_{49} - 1) \cdot B_{line}(4,9) - (t_{47} - 1) \cdot B_{line}(4,7)$
$\mathbf{x_{10}}$	$0.096 - (t_{56} - 1) \cdot B_{line}(5,6)$
$\mathbf{x_{11}}$	$-(1 - t_{56}) \cdot \dfrac{B_{line}(5,6)}{t_{56}}$

$\mathbf{x_{12}}$	$-(1 - t_{47}) \cdot \frac{B_{line}(4,7)}{t_{47}}$
$\mathbf{x_{13}}$	$-(1 - t_{49}) \cdot \frac{B_{line}(4,9)}{t_{49}}$

The states of the system can also be defined as well as the net real/reactive power at each bus and the initially assumed state values. The net real/reactive power is equivalent to the load real/reactive power subtracted from the generated real/reactive power.

$$x = \begin{bmatrix} V_4 \\ V_5 \\ V_7 \\ V_9 \\ V_{10} \\ V_{11} \\ V_{12} \\ V_{13} \\ V_{14} \\ \delta_2 \\ \delta_3 \\ \delta_4 \\ \delta_5 \\ \delta_6 \\ \delta_7 \\ \delta_8 \\ \delta_9 \\ \delta_{10} \\ \delta_{11} \\ \delta_{12} \\ \delta_{13} \\ \delta_{14} \end{bmatrix}, x^0 = \begin{bmatrix} 1 \\ 1 \\ 1 \\ 1 \\ 1 \\ 1 \\ 1 \\ 1 \\ 1 \\ 0 \\ 0 \\ 0 \\ 0 \\ 0 \\ 0 \\ 0 \\ 0 \\ 0 \\ 0 \\ 0 \\ 0 \end{bmatrix}, y = \begin{bmatrix} P_2 \\ P_3 \\ P_4 \\ P_5 \\ P_6 \\ P_7 \\ P_8 \\ P_9 \\ P_{10} \\ P_{11} \\ P_{12} \\ P_{13} \\ P_{14} \\ Q_4 \\ Q_5 \\ Q_7 \\ Q_9 \\ Q_{10} \\ Q_{11} \\ Q_{12} \\ Q_{13} \\ Q_{14} \end{bmatrix} = \begin{bmatrix} 0.183 \\ -0.942 \\ -0.478 \\ -0.076 \\ -0.112 \\ 0 \\ 0 \\ -0.295 \\ -0.09 \\ -0.035 \\ -0.061 \\ -0.135 \\ -0.149 \\ 0.039 \\ -0.016 \\ 0 \\ -0.166 \\ -0.058 \\ -0.018 \\ -0.016 \\ -0.058 \\ -0.05 \end{bmatrix}$$

The above vectors are defined as follows: x represents the states of the system, x^0 represents the initial guess of voltages and phase angles for the states, and y is the equality for each

power equation. From the admittance matrices, state vector, defined voltages on busses 1, 2, 3, 6, and 8, and the assumed phase angle of 0 at bus 1, the real and reactive power equations can be determined. From these equations, the Jacobian can be determined and the power flow solution iterated as described in previous sections.

A.6 IEEE 14 Bus System Power Flow Solution

The power flow solutions provided the preceding bus specifications is as follows:

$$x = \begin{bmatrix} V_4 \\ V_5 \\ V_7 \\ V_9 \\ V_{10} \\ V_{11} \\ V_{12} \\ V_{13} \\ V_{14} \\ \delta_2 \\ \delta_3 \\ \delta_4 \\ \delta_5 \\ \delta_6 \\ \delta_7 \\ \delta_8 \\ \delta_9 \\ \delta_{10} \\ \delta_{11} \\ \delta_{12} \\ \delta_{13} \\ \delta_{14} \end{bmatrix} = \begin{bmatrix} 0.9936 \\ 1.0027 \\ 0.992 \\ 0.8671 \\ 0.9933 \\ 0.9939 \\ 0.9855 \\ 1.034 \\ 0.9752 \\ -0.1318 \\ -0.2962 \\ -0.257 \\ -0.2165 \\ -0.3083 \\ -0.3777 \\ -0.3777 \\ -0.4396 \\ -0.4225 \\ -0.3696 \\ -0.2819 \\ -0.2419 \\ -0.3733 \end{bmatrix}$$

This solution can be used as a basis of comparison for when the generation is replaced with offshore generation. It should be noted that this is the steady state solution.